A *Candida auris*-Specific Adhesin, Scf1, Governs Surface Association, Colonization, and Virulence

by

Darian J. Santana

A dissertation submitted in partial fulfillment
of the requirements for the degree of
Doctor of Philosophy
(Microbiology and Immunology)
in the University of Michigan
2024

Doctoral Committee:

Assistant Professor Teresa R. O'Meara, Chair
Associate Professor Michael Bachman
Professor Vern B. Carruthers
Associate Professor Evan Snitkin

Darian J. Santana

santanad@umich.edu

ORCID iD: 0000-0002-5847-8352

Dedication

This dissertation is dedicated to my beautiful family who have always reminded me that perseverance through the marathon of a PhD is not really so burdensome so long as the rest of your life keeps moving forward in wonderful ways. For my amazing and supportive wife, Karyn, who dropped everything else in her life to follow me across the country to this cold and icy place. And for the two cutest kids in the world, Edison and Emery, who have become native Michiganites… Michiganders? Michigonians? All so that their dad could go to work and play science every day.

Acknowledgements

A dissertation feels like a door between two roads of my life: my scientific career ahead and the journey I've taken up to this point. It's humbling to look back and think about all the mentors and colleagues that have guided and shaped my path and my progress. A little over a decade ago this year I held a pipette for the first time as a starry-eyed, inexperienced, and unqualified microbiology analyst at Nelson Laboratories. I still couldn't tell you what possessed my first real scientific mentors, Becky Anderson and Tonya Morris, to give the young and arrogant college dropout who showed up on their doorstep a shot. I remember the orientation trainer making a joke about people who at least knew enough not to "stick their thumbs in the agar" while I awkwardly wondered what agar was. But I put my head down and got to work. My trainer, mentor, and ultimately friend and partner Mindi Thomas patiently (and sometimes impatiently) taught me all the fundamentals of microbiology from culturing bacteria to harvesting filamentous fungal spores to running assays for viral plaques, MICs, or endotoxins. As I fell in love with the microbial world, it was my friend and colleague Lisa Rhees who showed me that I was only scratching the surface and convinced me to return to school. Even only spending a few semesters at Weber State, I had exceptional mentors in the Microbiology Department there: Michele Culumber for always being a sounding board for career and development guidance; Matthew Crook for introducing me to microbial genetics, which has festered into a love that has strongly shaped my PhD direction; and Carie Frantz for helping me realize that microbes own the world and we humans just happen to get in their way sometimes. I

also need to express my appreciation for my research mentor Eric Ruben at Harvard, who sat me down and listed every microbiology graduate program in the country that he respected and who specifically lobbied for me to apply to the University of Michigan in the first place. Without the guidance and contributions of these amazing individuals and others like them, my career and my PhD would look very different today.

My four and a half years at U of M have of course been rife with exceptional mentorship and guidance. Foremost, I've been fortunate to foster an incredible working relationship with my PI and mentor, Teresa O'Meara. Joining the department at the same time, I think we both really took a chance on each other, and it has paid off fabulously. My favorite quote from Teresa is "I can be convinced," which she has said hesitantly every time I've thrown around some insane idea about barnacles or plastic. I don't think this dissertation reflects the project either of us thought was going to develop when we signed our first contract, but Teresa has done extremely well fostering an openminded and creative scientific environment, where the only limitation is the ideas we can imagine. My other committee members have also been exceptional and have all brought diverse perspectives to our conversations, both scientifically and professionally. All have been personally invested in my scientific and professional development, and I have leaned on each of them in turn throughout my doctoral training. Numerous other faculty I've interacted with through rotations, joint lab meetings, courses, my time on the MMMP T32, and my epidemiological training have also contributed greatly to my experience. Furthermore, I have to highlight the exceptional collaborative environment at Michigan and within the fungal community at large. I've named individual collaborators who have directly supported my projects in the following chapters, but I cannot hope to capture every fantastic scientist who has shared insightful and thought-provoking conversations about my science over the past few years.

Table of Contents

List of Tables

List of Figures

Abstract

Since its initial report in 2009, the emerging fungal pathogen *Candida auris* has become an increasingly common source of life-threatening infection, with cases and outbreaks reported in dozens of countries on every major continent. The global prevalence of *C. auris* is characterized by the simultaneous emergence of six distinct clades, separated geographically and genetically on the scale of hundreds of thousands of single nucleotide polymorphisms. *C. auris* is recognized as an urgent and critical public health threat due to its propensity for multidrug resistance and its ability to cause healthcare associated outbreaks, although molecular understanding of the phenotypes underpinning critical clinical behaviors in *C. auris* remains severely limited.

Early functional genetic work in *C. auris* was constrained by poor genetic tractability. Tools and techniques used for manipulating the genomes of other fungal species proved to be unreliable and variably effective in *C. auris*, contributing to the field's limited advances in molecular insights. To address these limitations, I developed forward and reverse genetic tools optimized for *C. auris* and demonstrated their efficiency in promoting genetic tractability in diverse clinical isolates sourced from around the globe. These techniques demonstrated quantifiable improvements in the genetic tractability of diverse *C. auris* isolates over existing methods. I used these tools to identify chitin regulatory pathways as the genetic basis for an enigmatic multicellular phenotype reported in *C. auris* and investigated the implications of this phenotype for virulence and antifungal resistance, demonstrating their utility for characterizing genetic function in *C. auris*.

I next investigated the peculiar ability of *C. auris* to spread between individuals and drive outbreaks, especially in healthcare environments. *C. auris* is frequently reported in association with nosocomial outbreaks, a characteristic rarely described in other *Candida* species. *C. auris* outbreaks are characterized by persistent colonization of patient skin and abiotic surfaces, which can remain positive for extensive lengths of time and serve as a source of horizontal transmission or potentiate invasive infection. Here, I investigated the molecular mechanisms of *C. auris* surface association to understand its colonization and transmission potential. I employed a forward genetic screen to identify *SCF1* (*Surface Colonization Factor*), a cell surface adhesin gene that is necessary and sufficient for *C. auris* surface colonization. *SCF1* is encoded by all *C. auris* clades, but appears to be lineage-specific, as homologs exist only in the *haemulonii* complex members *C. auris* and the closely related *Candida haemulonii*. Despite its conservation within *C. auris*, utilization of *SCF1* and adhesive capacity varies widely among isolates. Among diverse clinical isolates representing the major genetic clades and sourced from cases and outbreaks around the world, *SCF1* transcriptional control is tightly correlated with surface association. This pattern holds both between and within genetic clades, suggesting adaptation around *SCF1* transcriptional control is more recent than the separation of clades. In contrast to established molecular mechanisms in conserved yeast adhesins, which rely on hydrophobic interactions to drive surface association, Scf1 relies on exposed cationic residues for electrostatic association with diverse substrates in a manner reminiscent of bivalve adhesion proteins. *SCF1* is critical for *C. auris* biofilm formation, colonization of central venous catheters *in vivo*, skin colonization, and hematogenous infection, and its differential utilization is explanatory for strain-specific variation in these clinically relevant phenotypes. Together, these findings detail the discovery and characterization of critical virulence and colonization factors in *C. auris*.

Chapter 1 Introduction

1.1 On the emergence of *Candida auris*

In 2009, a clinical report published by Satoh and colleagues detailed the first identification of a novel ascomycetous yeast species in the Metschnikowiaceae clade, isolated from the external ear canal discharge of a 70-year old Japanese woman, dubbing this new organism *Candida auris*[1]. Subsequent clinical investigations in the early years after this initial report found dozens of *C. auris* external ear infections in east Asia, primarily from Korean and Japanese patients, providing preliminary evidence of the emergence of a previously undescribed human pathogen[2,3]. Ensuing surveillance initiatives worldwide began to identify *C. auris* infections across diverse geographies, and in just over a decade since the initial isolation of this pathogen, cases and outbreaks have been reported in dozens of countries on all six major inhabited continents[4–6]. Perplexingly, the global phenomenon of *C. auris* reflects not just a single emergence and dispersion event, but rather the distinct and simultaneous emergence of at least six phylogeographic lineages, separated by hundreds of thousands of single nucleotide polymorphisms (SNPs) and diverse geographical origins[5,7–9]. Phylogenetic dating through molecular clock analysis suggests the time to the most recent common ancestor for each clade occurred within the last 360 years, with the most recent divergence in the South American lineage in the late twentieth century[5]. Retrospective analysis of clinical fungal collections dates the earliest suspected human *C. auris* infection in 1996, suggesting a very recent selective pressure for the simultaneous adaptation of each distinct *C. auris* lineage towards a human-associated and infectious entity[10].

Isolates belonging to the type East Asian (clade II) lineage have historically demonstrated an almost universal proclivity for ear infection, and this pattern of host association is shared by other lineages with low clinical representation[2,7]. The South Asian (clade I), African (clade III), and South American (clade IV) lineages represent the bulk of the reported infectious burden though, and whereas isolates from these lineages can be associated with ear infection, they can also cause severe bloodstream and tissue infection associated with high rates of mortality and poor treatment success[6]. Interestingly, this dichotomy echoes growing examples of phenotypic divergence among *C. auris* lineages, reflecting the isolated nature of each distinct emergence event. There is also no substantial evidence of admixture or recombination since the divergence of clades, despite the different clades encoding different mating type loci, which might be expected to result in mating compatibility: Clades I, IV, and V encode *MTL****a*** and clades II, III, and VI encode *MTL*$\boldsymbol{\alpha}$ at the *MAT* locus[5,9,11]. The absence of evidence for mating may be due to geographic separation of clades or due to biological impediments, such as nucleotide deletions present in the putative pheromone transporter encoded by an *STE6* homolog in clade I[12].

Relatively little is known about *C. auris* environmental reservoirs, and the few isolates characterized outside of human association represent sparse and scattered events rather than a cohesive and compelling model for the niche that may have selected for the emergence of a human pathogen. Most prominently, a survey of the coastal wetlands of the secluded Andaman islands found isolates genetically related to human-associated isolates of the geographically similar South Asian clade[13]. Two isolates were found in water samples collected from Colombian coastal and estuarial environments, geographically linked to the South American clade[14]. In each of these cases the authors described the local environment as free from substantial human activity, suggesting they may represent true environmental niches. These

findings, paired with the notable experimentally determined high halotolerance in *C. auris* compared to related species, have spurred the hypothesis of a marine reservoir for environmental *C. auris*[15,16]. However, the transition from this potential reservoir to human association, and any associated selective pressures, remains poorly understood. A zoonotic host may be possible, as sampling a heterogenous cohort of 87 dogs from a shelter in Delhi, India found a small percentage of animals with chronic skin infections demonstrating evidence of *C. auris* in their ear canal or on their skin[17]. However, this canine isolation is geographically linked to a region with high levels of circulating *C. auris* in human populations, and any directionality between zoonotic and human colonization is unclear. Surveys in this same region have found *C. auris* colonizing the surface of stored fruit, potentially spread from contaminated workers, and it has been suggested that the surface waxing used to preserve the fruit may confer a similar environmental niche to the cerumen lined ear canal[18]. Interestingly, *C. auris* has also been isolated from dairy products during storage and preparation, which may reflect a similar ability to associate with host derived proteins or lipids that could be reflected in its infection and colonization proclivities[19]. More than likely, such an association would reflect an adaptation more ancient than modern food storage practices. Other environmental *Candida* species are often found as colonizers of plant surfaces, and a selective pressure for cutin association or even metabolization could theoretically lead to an advantage for colonization of waxy and fatty human niches[20,21].

The vast majority of interactions with human hosts for *C. auris* represent asymptomatic colonization events. Patient skin is the most common niche for colonization, and affected patients demonstrate high levels of fungal burden in warm and moist body sites that are recalcitrant to effective hygiene, such as axillae, inguinal creases, toe webs, fingernails, nares,

and external ear canals[22]. Other nonsterile body samples such as urine or broncheoalveolar lavage are prominently associated with *C. auris* positivity, though these cases can present asymptomatically and there is debate whether they represent colonization or infection[23,24]. In outbreak settings, colonization can become widespread among medically vulnerable patients and those with prolonged healthcare exposures, but colonization of healthy individuals is extremely rare. While extensive screening of individuals outside healthcare settings has not been performed, some studies have failed to detect persistent colonization among healthy medical workers in outbreak settings, although transient carriage on worker hands is possible[25–27]. Mechanistically, this may be linked to the ability of individuals to mount an effective immune response, as skin colonization in murine models is potentiated by deficient IL-17 signaling, but other potential avenues of immune interaction and skin colonization have not been explored[28]. An intact skin microbiome may also be protective against colonization, as numerous pathogenic colonizers have been correlated with *C. auris* skin colonization, although without clear causality[22]. These observations may explain the essentially exclusive association of *C. auris* with nosocomial occurrence, as at this point there is no compelling evidence that *C. auris* colonizes individuals without prior healthcare exposure[29].

Colonization itself plays a central role in the clinical and public health burden of *C. auris*, and by extension the emergence of this organism as a global health threat. Once colonized, individuals can remain positive for *C. auris* for extensive periods, with some reports documenting persistent colonization for months despite routine antiseptic intervention[30,31]. Colonized patients in turn shed fungal cells into their surrounding environment, resulting in contamination of nearby abiotic surfaces[32,33]. Furniture, medical devices, textiles, doorknobs, wall and ceiling panels, bedding, and the like are commonly reported as contaminated,

presenting a potential secondary reservoir for fomite-mediated transmission. Experimental evidence suggests *C. auris* can remain viable on contaminated surfaces for weeks to months absent nutritional access and under desiccate conditions[16,34]. Multiple case reports have linked outbreak extension to circulation of contaminated objects, and in many cases outbreak resolution is only achieved after identification and removal of contaminated fomites[35–37]. These examples suggest a circularity between colonization of patients and colonization of inert surfaces in clinical settings, where each reservoir propagates the other. In practice, this is typically reflected in high rates of contamination, and for *C. auris*, this leads to persistent and recalcitrant healthcare-associated outbreaks, the most severe of which remain ongoing after multiple years and now essentially represent endemic spread and transmission[30]. Expert recommendations for combatting *C. auris* outbreaks entail extensive screening and surveillance, patient cohorting and practitioner segregation, and intensive decontamination efforts – protocols more consistent with hospital-associated bacterial infectious agents than the usually commensal and opportunistic *Candida* genus[38]. In particular, decontamination can represent a significant burden. Because *C. auris* is readily resistant to many low level disinfectants, often considered the workhorses of healthcare decontamination, sporicidal disinfectants or disinfectants with specific *C. auris* claims are recommended[39]. Even still, the recirculation between contaminated patients and healthcare environment presents challenges, as colonized patients can recolonize their surroundings to high levels within hours after intensive disinfection[33]. Furthermore, the most extensive outbreaks are often in long-term care facilities with lower patient turnover, reducing opportunities for terminal cleaning and disinfection, extending and potentiating outbreak progression[30]. Even where cleaning of patient rooms is possible, circulating objects such as lanyards or temperature probes that may be overlooked by cleaning regimens can still serve as fomites to prolong outbreaks and

cause transmission[35,36]. Some evidence also suggests airborne transmission of viable cells to otherwise inaccessible areas is possible, such that routine disinfection is unlikely to entirely capture every contaminated surface[40]. Together, this patten of outbreak progression can present a substantial challenge of infection prevention. In recent years, outbreaks in the United States and Europe have increased in number and scope exponentially, which has been suggested to be due to healthcare environments overburdened by the COVID-19 pandemic failing to meet the infection prevention standards required for mitigating *C. auris* outbreaks[41,42]. In this way, the global emergence of *C. auris* and *C. auris* outbreaks and nosocomial persistence are interdependent, with healthcare settings being the most apparent reservoir for expanding and propagating *C. auris* populations.

While colonization can be widespread, a relatively small percentage of individuals develop invasive infection of *C. auris*. Infection occurs when fungal cells enter sterile body sites and can become disseminated to diverse tissues, resulting in a pathology that is often indistinguishable from other systemic fungal infections[43]. Asymptomatic colonization may be a precursor for infection, and different reports have reported 5-20% of colonized individuals develop infection over time[44,45]. Potentially, colonization is not a prerequisite for infection though, as invasive infection in individuals with no prior culture positivity is common and some examples have failed to find significant associations between certain colonization sites and infection[45,46]. Like for other *Candida* infections, indwelling medical devices can serve as a portal of entry into the bloodstream, and colonization of these devices in particular represents a strong risk for the development of infection[46]. Upon infection, crude in hospital mortality rates generally range from 30-70%, although very few reports have assigned attributable mortality, which is likely to be much lower for susceptible populations that are often afflicted with diverse

comorbidities[6,47]. *C. auris* encodes genes homologous to classical virulence factor genes in other *Candida* species, such as secreted aspartyl proteases, lipases, oligopeptide transporters, and major facilitator superfamily transporters, which may directly influence clinical outcomes, but experimental evidence of their importance in attributable infection is almost entirely lacking[48]. Perhaps better appreciated scientifically is the high rate of acquired antifungal resistance among *C. auris* isolates. Around 90% of all isolates exhibit acquired resistance to at least one class of antifungal, which is in stark contrast to the next highest rate among *Candida* species at 10-12% in *Candida glabrata*[29,49]. Furthermore, isolates exhibiting multidrug resistance are common, and isolates exhibiting pan resistance are known to remain infectious and transmissible despite any potential fitness costs associated the development of acquired resistance[50]. Interestingly, antifungal resistance itself has also been proposed as a potential driver of the emergence of *C. auris*[29]. Increasing usage of antifungal compounds for human and animal medicine and agriculture may have directly selected for resistant organisms or may have altered human and natural microbiomes to favor the emergence of new organisms, such as *C. auris*[51]. While there remains little evidence to explain why resistance rates are so high in *C. auris*, the potential for treatment failure and lack of therapeutic options upon infection remain foremost concerns for clinical and public health authorities.

Despite the decade and a half emergence since the initial description of *C. auris*, the scientific community has only begun to explore the functional biology underpinning the clinically critical and unique behaviors of this organism. Being an emerging pathogen in the age of modern genomics, the most extensive descriptions of *C. auris* biology have primarily taken the form of surveillance and sequencing data and analysis, while experimental functional genetic annotation has historically been complicated by poor tractability. Areas of major research

interest center around several distinctive and enigmatic traits of *C. auris* with widespread implications: selective pressures and advantages that have accompanied its recent emergence, mechanisms of resistance to antifungal agents and decontamination efforts, and molecular underpinnings for its proclivity towards nosocomial persistence and transmission. In this dissertation, my contributions to this global research effort involve the development of novel techniques for feasible genetic manipulation of *C. auris* to perform functional genomic annotation, exploration of morphogenic mechanisms explaining a multicellular phenotype differentially associated with the emergence of certain strains, and the identification of a lineage-specific adhesin at the center of strain-specific plasticity and adaptation in mediating cellular association with biological and abiotic surfaces, influencing colonization and dissemination dynamics in clinically relevant models.

1.2 On mechanisms of fungal and microbial adhesion

Because *C. auris* outbreaks depend so heavily on colonization, the research in this dissertation culminates in the exploration of the molecular mechanisms of *C. auris* surface contamination. In practice, surface colonization is not one phenotype but the sum of many: cells must physically associate with a substrate, attach to the substrate in a manner that is functionally irreversible upon relevant physical stresses, tolerate electrostatic stresses conveyed by the substrate, maintain viability under conditions often consisting of desiccation and nutrient deprivation, and potentially achieve an active metabolic state to propagate colonization. Furthermore, for transmission to occur, a subpopulation must be released either actively through biological mechanisms or passively through adhesive or cohesive failure upon physical stress, and this subpopulation must remain capable of establishing colonization of a new substrate. In modeling this myriad phenotype experimentally, it can be challenging to attribute behaviors to one specific

function in the colonization process. In this dissertation, I have approached this problem by specifically modeling the initial and predicating step in colonization: surface association and adhesion, then extending my findings to long term colonization models to understand the ultimate implications of molecular perturbations in this initial step.

At the most fundamental level, adhesion to an abiotic substrate can be thought of as the product of physiochemical interactions between two entities on a molecular or even atomic scale[52,53]. One model for explaining these interactions in a theoretical framework is the DLVO theory (named after Boris Derjaguin and Lev Landau, Evert Verwey and Theodoor Overbreek), which is most frequently applied to uniform particles but has also been used to approximate microbial adhesion dymanics[54,55]. As two particles approach one another, their ionic atmospheres begin to overlap and electric double layer forces produce a repulsive interference that increases with reduced distance. However, van der Waals forces, attractive in nature, increase as the particles approach one another. At any given distance, there is a total potential energy between the two particles that is the sum of the attraction and repulsion potential from these competing forces. For a symmetrical situation where two particles have similar electric double layer and van der Waals potentials, double layer forces dominate at intermediate distances, but increasing van der Waals forces at very small separation distances overcome repulsive forces to dictate the adhesive profile. The precipitous increase in attractive forces near contact, balanced against the maximal repulsive forces at very short distances, results in a deep energy well called the primary minimum. Ultimately, two symmetrical particles approaching one another with enough kinetic energy to reach the primary minimum achieve a functionally irreversible aggregation as the energy required to overcome the balance between attractive and repulsive forces approaches a theoretically infinite binding affinity. Importantly, local ionic strength, shear forces, kinetic

energy, and myriad other physical constraints can influence the dynamics of particulate aggregation, so the reality often proves more complicated than the theoretical potential energy upon approach. These same principles can also be applied to explain either the net deposition or repulsion of a particle with a given electric charge and Van der Waals potential against a surface, resulting in the phenomenon of adhesion.

In the context of biological systems, interpretation of the impacts of these forces becomes prohibitively complex to model mathematically. Unlike our theoretical particles with defined physical parameters, the cell surface can be dynamic and highly variable, and surface appendages can influence local interactions at a molecular scale with consequences for the fate of the entire cell[52,54]. Still, in many cases, the combination of electrostatic repulsion and Van der Waals attraction can be interpreted to approximate nonspecific adhesion to substrates. In this case, electrostatic forces might mediate initial but reversible interactions between cell and substrate, followed by irreversible van der Waals interactions at the energetic primary minimum[52]. One prominent example in experimental modeling of cell adhesion: many polymer substrates of medical importance are strongly hydrophobic. In aqueous environments, the attractive forces between symmetrical hydrophobic entities can be entirely explained by van der Waals forces[56]. Numerous examples exist of microbial cell surface adhesins either modulating the entire cell surface towards a globally more hydrophobic state or comprising local, critical clusters of hydrophobic residues that mediate functional interactions with a substrate resulting in microbial adhesion[52,57,58]. For this reason, increasing the hydrophilicity of polymer surfaces is commonly proposed as a method of anti-fouling in medical device design[59]. The electric double layer potentials of surfaces can vary widely, but under aqueous conditions, many solid surfaces acquire a slight negative charge[60]. In theory, this should be repulsive against a negatively

charged microbial membrane, although local interactions can dominate repulsive effects at larger distances, which may explain why alterations in cellular zeta potentials (one measure of the electric double layer strength of individual particles) can be associated with adhesion[61,62]. A prominent example of biological electrostatic adhesion comes from the adhesion systems of bivalves, which rely on clustered cationic-aromatic amino acid groups to mediate an irreversible adhesion or cohesion to substrates[63–65]. This may be directly mediated by local cation-pi interactions between adhesion proteins and the substrate to overcome electrostatic repulsion, but a more complex interaction has also been proposed involving competitive displacement of hydrated ions at the surface microenvironment by strongly basic arginine and lysine residues[63]. In the case of bivalve adhesion, proximity to the aromatic residue Dopa appears to be functionally important, but traditional bulky, hydrophobic aromatic residues also potentiate cation-mediated adhesion and cohesion in synthetic systems, perhaps by sterically inhibiting competitive replacement of hydrated cations[66]. This adhesion mechanism has only recently been proposed in microbial life for the *Vibrio cholerae* biofilm adhesion Bap1, although I will present evidence in Chapter 4 supporting this mechanism for the lineage specific *C. auris* adhesin Scf1 as well[67].

In yeast, the best characterized biological mechanisms affecting adhesion are through cell-surface exposed proteins known as adhesins. Many canonical adhesins in *Candida* and other yeast species contain a three domain architecture[68]. The N-terminal region follows a secretion signal peptide and consists of an ordered domain, generally thought to be apical and most likely to confer interactive functions with external substrates. The second, internal domain commonly contains a disordered region comprising tandem satellite repeats rich in serine and threonine residues and of lengths that vary substantially from adhesin to adhesin. The primary function of

this domain is widely considered to be extension of the apical N-terminal domain, although there are examples providing evidence that the low complexity repeat region is sufficient for directly mediating adhesion, and variation in repeat length can directly influence adhesive behavior[69–71]. The length and structure of repeats can also confer tensile strength upon adhesin binding[72]. Some adhesins also contain other functionally relevant subdomains in this region, such as the 13-residue amyloid spines present in *C. albicans* Als5 and Als1[73]. The C-terminal domain is responsible for anchoring the adhesin to the cell surface, and for the adhesins discussed in this dissertation, this is accomplished through a glycosylphosphatidylinositol (GPI) linkage, which in *Candida* species ultimately forms a covalent bond between the adhesin and glycans on the fungal cell wall[68]. Interestingly, there are cases where removal of the C-terminal domain does not disrupt cell surface localization, suggesting the GPI linkage may not be required for surface exposure of every individual adhesin molecule. Other functions of the C-terminal domain have not been described well, but there is often ample protein sequence beyond the GPI omega site with unclear functional relevance. The *C. auris* adhesin Scf1 described in Chapter 4 contains a secondary tandem repeat region comprising a trimeric repeat with a glycine every third residue and commonly neighboring prolines. This pattern is the hallmark of collagen folds, suggesting the possibility of trimerization of this domain[74]. Collagen trimerization requires initiating interactions upstream or downstream of the collagen repeat, which may indicate an additional function for the C-terminal domain.

Based on primary sequence and domain architecture, yeast adhesins have been grouped into families and superfamilies[75]. The Als family of adhesins comprises 8 well characterized members in the model *C. albicans* sharing highly similar tandem immunoglobulin-like N-terminal domains[76]. In *C. albicans*, Als adhesins are often studied as virulence factors mediating

pathogenic interactions with host cells and surfaces. The Als N-terminal domain features both peptide-binding and lectin activity which are thought to play critical roles in host association[77,78]. Several Als proteins are also prominently implicated in biofilm formation, and some members but not all have been directly linked to nonspecific adhesion to abiotic surfaces[79,80]. The mechanism of this nonspecific adhesion is unclear for Als proteins, but one proposed model holds that the observed surface association is result of promiscuous binding of immobilized peptide or glycan moieties at the surface interface[68]. Another hypothesis holds that the surface adhesion is mediated by the low complexity repeat regions rather than the N-terminal domain, as modeling suggests these domains contain exposed hydrophobic surfaces surrounded by glycosylation sites, and purified tandem repeat domains demonstrated plastic binding activity[70]. Interestingly, other adhesive functions have been described for some members of the family. Als1, Als3, and Als5 in *C. albicans* contain an occult amyloid-forming region that becomes exposed following a conformational change from shear stress and mediates cross-β aggregation, promoting surface clustering and cell to cell adhesion[73,81]. Despite the similarity in the family and the potential for redundancy, specific adhesive functions have been attributed to specific members, and even allelic variants of the same member[71,80]. This variation suggests potential selective mechanisms for expanding, maintaining, and regulating different Als proteins even among a large family of highly similar members. The implications of this become evident when exploring the functional relevance of this family in different species. While the Als family itself is widely conserved across *Candida* species, phylogenetic evidence suggests a common ancestor has expanded independently in multiple lineages, such that the three Als proteins encoded by *C. auris* do not have clear or direct homologues to any of the eight in *C. albicans* and require independent characterization to determine function[82]. Many *ALS* genes and genes encoding other

adhesins are enriched at chromosomal ends, likely contributing to expansion and rapid evolution as a result of ectopic recombination and break-induced replication[83].

Similarly, the Iff/Hyr family of adhesins has independently expanded in multiple pathogenic *Candida* lineages, including *C. auris*[83]. These adhesins follow the canonical three domain architecture with a shared N-Terminal Hyr (Hyphal_reg_CWP) domain comprising a Beta-helix followed by an alpha-crystallin domain, similar in structure to the Awp1 adhesin in *C. glabrata* or numerous bacterial adhesins from *Haemophilus influenzae*, enterotoxigenic *E. coli*, *Caldicellulosiruptor hydrothermalis*, *Limosilactobacillus reuteri*, and others[83]. *C. auris* encodes eight Iff/Hyr proteins that exhibit remarkable variability in length and β-aggregation potential in their highly divergent central domains as a result of rapid diversification following duplication[83,84]. Most of the characterization of this family in *C. albicans* has been phenotypic such that little is known regarding the molecular basis for adhesion. Several members have been linked to adhesion to mammalian cells or plastics, while others have been tied to cell wall integrity and virulence[85–87]. Iff4109 appears to have a dominant effect on inert surface adhesion in *C. auris*, and I will present data in Chapter 4 suggesting this nonspecific association is directly related to modulation of cell surface hydrophobicity and increased van der Waals attraction towards hydrophobic substrates. This is a known mechanism for the widely expanded Epa family of adhesins in *Candida glabrata*, many of which have strong experimental links to cell surface hydrophobicity and hydrophobic substrate interactions, so it is notable to see this mechanism appearing independently in a different adhesin family in *C. auris*[57,58]. Local hydrophobic interactions also dominate in the flocculin Flo11 from *Saccharomyces cerevisiae* and its homologs across Ascomycota[88,89]. In this case, critical clusters of aromatic residues in the apical domain mediate homotypic interactions and kin discrimination by extension. Interestingly, there

is only weak evidence that Flo11 can mediate adhesion to inert surfaces, and in our hands, it did not affect adhesion to hydrophobic substrates, suggesting differences in selective advantages between the localized hydrophobic effect of the flocculin and the global hydrophobic effects of Iff4109 and Epa proteins, for instance.

1.3 Brief summary and chapter outline

The goal of the research in this dissertation was to explore the selective advantages that have allowed *C. auris* to emerge as a global nosocomial pathogen. In Chapter 2, I discuss experimental, clinical, and epidemiological evidence of medically relevant phenotypic and strain variation, highlighting the reality that understanding a globally distributed pathogen requires understanding the patterns that have driven distinct lineages to pathobiological success. In Chapter 3, I detail the development and optimization of forward and reverse genetic techniques suitable for manipulation of clinical isolates of *C. auris* from distinct genetic backgrounds and leverage these techniques to explore the molecular basis behind multicellularity and aggregation in *C. auris*. In Chapter 4, I survey the molecular basis for *C. auris* association with abiotic and biotic surfaces to identify two dominant adhesins: the conserved Iff4109 and the lineage specific Scf1. I further explore the natural variation in adhesin utilization amongst isolates of distinct geographic origin and model the impact of such variation in long term colonization and host association experiments. In Chapter 5, I offer a discussion to place these findings in the greater context of *C. auris* emergence, arguing the source of adaptations, selective pressures, and evolutionary advantages for adhesive regulation and plasticity.

Chapter 2 On Phenotypic and Strain Variation in *Candida auris*[1]

2.1 Abstract

Candida auris is an emerging fungal pathogen with an unusual evolutionary history—there are multiple distinct phylogeographic clades showing a near simultaneous transition from a currently unknown reservoir to nosocomial pathogen. Each of these clades has experienced different selective pressures over time, likely resulting in selection for genotypes with differential fitness or phenotypic consequences when introduced to new environments. We also observe diversification within clades, providing additional opportunities for phenotypic differences. These differences can have large impacts on pathogenic potential, drug resistance profile, evolutionary trajectory, and transmissibility. In recent years, there have been significant advances in our understanding of strain-specific behavior in other microbes, including bacterial and fungal pathogens, and we have an opportunity to take this strain variation into account when describing aspects of *C. auris* biology. Here, we critically review the literature to gain insight into differences at both the strain and clade level in *C. auris,* focusing on phenotypes associated with clinical disease or transmission. Identifying differences between strains and understanding which phenotypes are strain specific will be crucial for understanding this emerging pathogen, and an important caveat when describing the analysis of a singular isolate.

[1] The data in this chapter has been published in *PLOS Pathogens*.

Santana, D.J., Zhao, G., O'Meara, T.R. (2024). The many faces of *Candida auris*: Phenotypic and strain variation in an emerging pathogen. PLoS Pathog *20*(3): e1012011.

2.2 Introduction

Fungal diseases account for over 6.5 million invasive infections annually, with nearly one quarter of these attributed to members of the *Candida* genus[90]. In 2009, a clinical report detailed the isolation of a previously uncharacterized pathogenic member of this genus, *Candida auris*, from the ear canal of an inpatient in a Japanese hospital[1]. This report marked the beginning of the emergence of a globally distributed, often multidrug resistant, outbreak-capable pathogen, ultimately recognized by the US Centers for Disease Control and Prevention and the World Health Organization as an urgent and critical public health threat[1,91]. Within a decade of its initial characterization, surveillance initiatives defined the nearly simultaneous emergence from a currently unknown reservoir of distinct *C. auris* genetic lineages in dozens of countries across all six major continents[4,5], driven both by multiple geographic origins and carriage through patient travel[5]. *C. auris* infection presents similarly to candidiasis caused by other *Candida* species, with the most severe cases attributed to candidemia and subsequent organ dissemination[92]. Unlike related *Candida* species however, *C. auris* is frequently reported in association with nosocomial transmission, leading to clonally disseminated outbreaks in healthcare settings and in some circumstances, multi-year and regionally endemic spread[30,46]. Surveillance efforts in the United States and Europe have recognized exponentially increasing rates of outbreaks since the introduction of *C. auris* into these regions, highlighting the difficulty in containing this organism[41,42]. In outbreak settings, *C. auris* persistently colonizes patient skin, hospital surfaces, and medical devices, demonstrates contaminative and fomite transmission between individuals, and causes invasive infections, often with high rates of mortality and widespread acquired antifungal resistance[5,6,22,32,35,36,46]. For these reasons, *C. auris* is recognized as a critical public health threat and represents a substantial challenge to prevent infection and disease.

Four major genetic lineages of *C. auris* have been extensively described, with origins clustering geographically in South Asian (I), East Asian (II), African (III), and South American (IV) clades[5]. Sparse reports of isolates that are genetically distinct from the four major clades suggest at least two additional lineages, with isolates having geographic links to Iran (V) or Singapore and Bangladesh (VI)[7–9]. Notably, the clades are genetically well-separated, differing by tens of thousands to hundreds of thousands of single nucleotide polymorphisms (SNPs)[9,11,48]. Even within clades, individual strains can differ by thousands of SNPs, exhibit karyotypic diversification, and have stable chromosomal rearrangements[5,11,48,93,94]. Increasing evidence even suggests isolates collected from clonal outbreaks, differing only by small numbers of SNPs, can exhibit clinically meaningful phenotypic variation, suggesting the possibility of adaptation within the timescale of outbreak settings[95–97]. The result is the emergence of at least six highly divergent genetic lineages of *C. auris* and within-lineage variation, ultimately associated with divergent clinically relevant phenotypes such as antifungal resistance[5], virulence and pathogenesis in infection models[98–100], body site tropism[3,7], outbreak potential[2,3], morphogenesis[101], host colonization[28], disinfection resistance[39,102,103], and metabolite utilization[104].

In this review, we explore experimental, surveillance, and clinical data to synthesize evidence of clinically impactful variation between strains and between clades of *C. auris*. We perform a systematic analysis of the most extensively described examples of variation and propose mechanistic models to understand the basis and scope of such variation and to clarify ambiguity present in isolated reports. Finally, we offer hypotheses to promote further research pertaining to the mechanistic and molecular bases for medically relevant behavior in *C. auris* and perspectives around studying a global, emerging, divergent pathogen.

2.2.1 Topical Focus

We performed a systematic search of Pubmed, Web of Science, and Scopus databases with the only search term “Candida auris” to identify all records from inception until August 4, 2023. Search results were deduplicated using the Systematic Review Accelerator[105] to yield 1945 unique reports. Titles and abstracts for all reports were reviewed and each study was categorized thematically. A weekly recurring automated Pubmed search for “Candida auris” was performed to identify and categorize new reports as appropriate during manuscript preparation. Based on categorical representation, topics were selected that were most likely to encompass characterization of clinically relevant strain variation.

Among clinical reports, 192 included more than 1 patient. The full text of each of these reports was reviewed and data was systematically extracted using a standardized form to record relevant findings. To perform a meta-analysis of crude mortality, 39 reports[4,25,26,36,44–46,92,106–140] were selected that met the acceptance criteria of having 1) At least 5 infection cases, 2) Determination of clade made by the authors or identifiable through publicly available analyses through one or more molecular typing techniques, and 3) Crude in-hospital mortality reported. Meta-analysis with subgroup analysis was performed using the meta R package (version 6.5-0) using a random intercept logistic regression model with logit-transformation, maximum-likelihood estimator for τ^2 without a common estimate across subgroups, and the Clopper-Pearson confidence interval for individual studies with a continuity correction of 0.5 for studies with zero cell frequencies.

For experimental virulence models, 11 reports of invertebrate or murine infection models[96,97,100,141–148] were identified that met the acceptance criteria of having 1) Multiple isolates with clade or body site origin indicated, 2) Identical infection protocol between isolates,

and 3) Survival data available. Because of the small number of studies available, an acceptance criteria including any study that compared more than 1 isolate from different groups was established, with the anticipated limitation that studies with small sample sizes might exhibit greater variation from a true effect. For each study, isolates were ranked by virulence score: first by overall mortality (number of mortality events or time to 100% mortality, whichever was more appropriate) then by median survival time. Survival results for individual isolates were plotted by within-study ranks, colored by clade or origin.

To evaluate outbreak sizes, 109 clinical reports were selected that met the acceptance criteria of having 1) At least two linked cases, 2) Single center or clustered multi-center outbreak, 3) Dates of the outbreak or data collection reported, and 4) Location of the outbreak reported. Outbreak size was determined as the total number of affected patients (colonized or infected) and average rate was determined by dividing the total number of affected patients by the length of time sampling was performed.

2.3 *C. auris* Association With Human Hosts

While limited evidence supports the possibility of environmental, zoonotic, or foodborne reservoirs of *C. auris*[13,14,17–19,149], the best understood reservoir for carriage, transmission, and dispersal is the human body. *C. auris* exhibits both asymptomatic and infectious associations with susceptible hosts, and understanding the dynamics of these associations has been a topical focus for much of the clinical and experimental literature. Critically, decontamination of colonized or infected patients with antiseptics or antifungals has presented substantial clinical challenges, and recent work has highlighted some of the biological underpinnings exacerbating these difficulties.

2.3.1 Virulence

C. auris persistently colonizes multiple body sites. Most prominently, skin sites such as the nares, palms, fingertips, axillae, inguinal creases, and toe webs show high positivity, but asymptomatic isolation from other non-sterile body sites such as lungs and urine is not uncommon[22,150]. Unlike for some other human-associated *Candida* species, colonization is likely a rare event specific to individuals with healthcare exposures. For instance, a recent search of ~300,000 publicly available metagenomic runs found only 20 runs from five projects likely containing *C. auris* genomic information, most of which were specifically linked to surveillance initiatives in *C. auris* outbreak settings[151]. Colonization can increase the risk for disseminated infection, especially candidemia[152,153]. One report found that approximately 5-10% of colonized patients develop bloodstream infections[44], while another estimated a 25% cumulative risk of candidemia 60 days after initial detection of colonization[45]. In addition, urinary tract infections, wound infections, otitis, and skin abscesses are common, but *C. auris* is not prominently associated with other common types of candidiasis such as oral thrush or vulvovaginal candidiasis[29]. The clinical presentation of invasive disease is often nonspecific and indistinguishable from other types of systemic microbial infection, and reported in-hospital crude mortality rates for *C. auris* infection range from 25% to 70%[47,154].

Multiple mammalian and invertebrate infection models have been employed to characterize *C. auris* virulence, with some reports directly comparing isolates of distinct genetic lineages or origins[96,97,99,100,141–148]. Independently, two separate reports concluded that isolates from clade IV showed the highest virulence of the four major clades in either murine or silkworm infection models[99,100]. We found this to be consistent across multiple reports, with clade IV and clade I isolates generally exhibiting virulence greater than the median of all comparators and clade II and clade III generally exhibiting virulence below the median (Fig. 2-

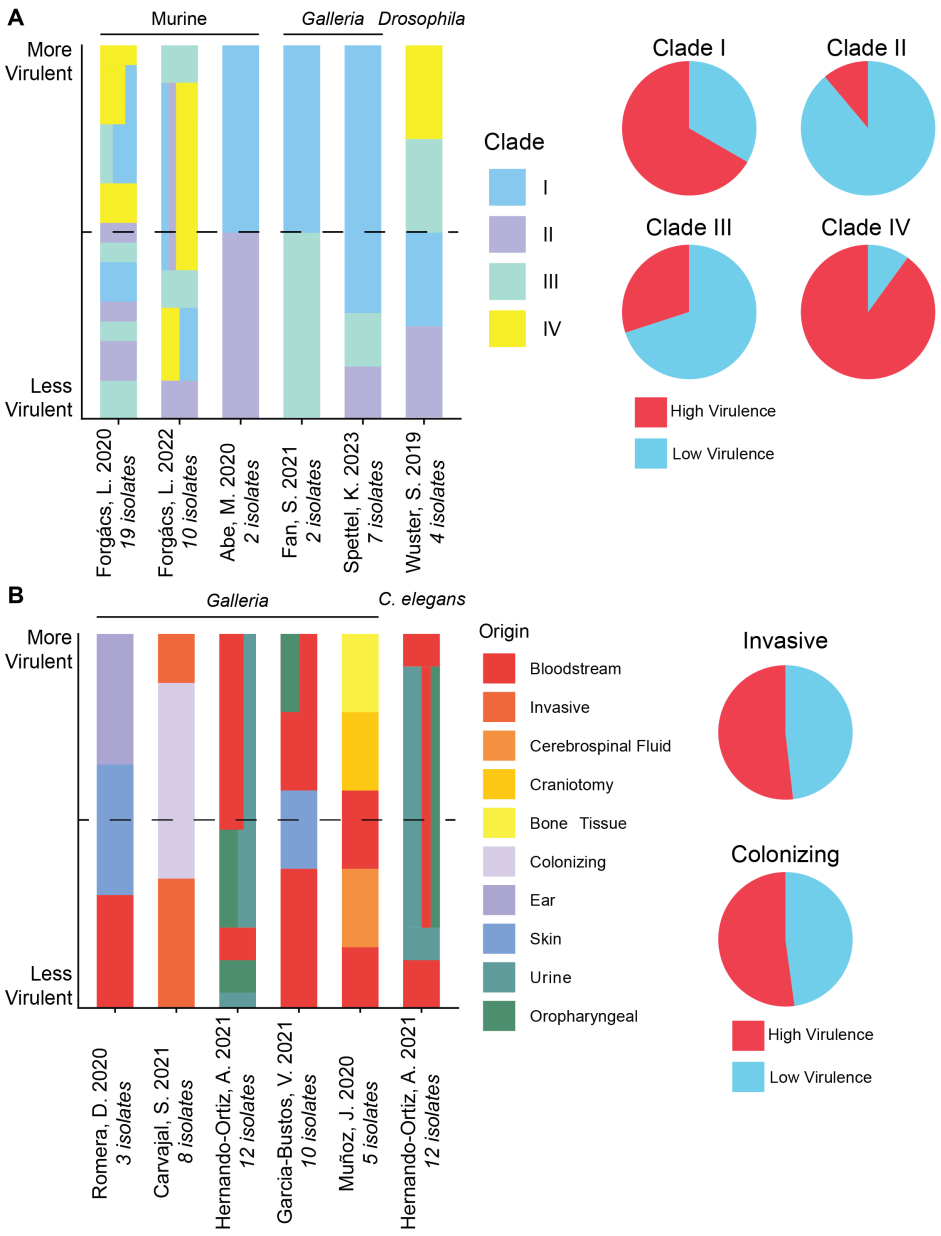

Figure 2-1 Experimental infection models suggest *C. auris* exhibits clade-specific but not body site specific virulence. Survival data was extracted from studies directly comparing virulence between isolates of different clades **(A)** or body site origins **(B)** in animal infection models. For each study, the virulence of each isolate was ranked by mortality and median survival. Stacked bars plot the virulence rank of each isolate per study, with higher virulence rankings plotted at the top. The horizontal dashed line corresponds to the average virulence rank for each study. Because isolates were ranked on survival by time to mortality and median survival time, isolates with tied ranks are plotted at the same height on the y-axis. Where isolates from multiple groups share a tied rank, the width of bars grouped horizontally corresponds to the proportion of isolates of that rank attributable to a given group. Pie charts summarize the survival rankings by bisecting all isolates into high or low virulence scores, corresponding to a virulence rank greater than the median of within study comparators (High Virulence) or less than the median (Low Virulence). For panel (B), hot colors indicate invasive origins and cool colors indicate colonizing origins.

1A). Notably, of the four major clades, only clade II is not associated with human invasive infection or outbreaks, consistent with its poorer pathogenicity in infection models[2,3,99,100]. One possible mechanism of this phenotypic diversity is adaptation in response to host association. Based on reports comparing the virulence of isolates recovered from different body sites, however, we found no evidence of

differential pathogenicity associated with strains originating from either invasive or colonizing sites (Fig. 2-1B). Together, this analysis suggests genetic lineage, but not within host adaptation, predicts *C. auris* virulence in infection models.

To investigate whether the clade-specific virulence was reflected in human infection, we performed a meta-analysis of crude mortality after *C. auris* infection for all case reports comprising at least 5 infected individuals and for which *C. auris* clade was reported based on molecular typing. As clades II, V, and VI have not yet been associated with outbreaks, no case reports met the selection criteria for number of infected individuals. For the remaining reports comprising isolates from clades I, III, and IV, pooled crude mortality was 41% (95% CI:

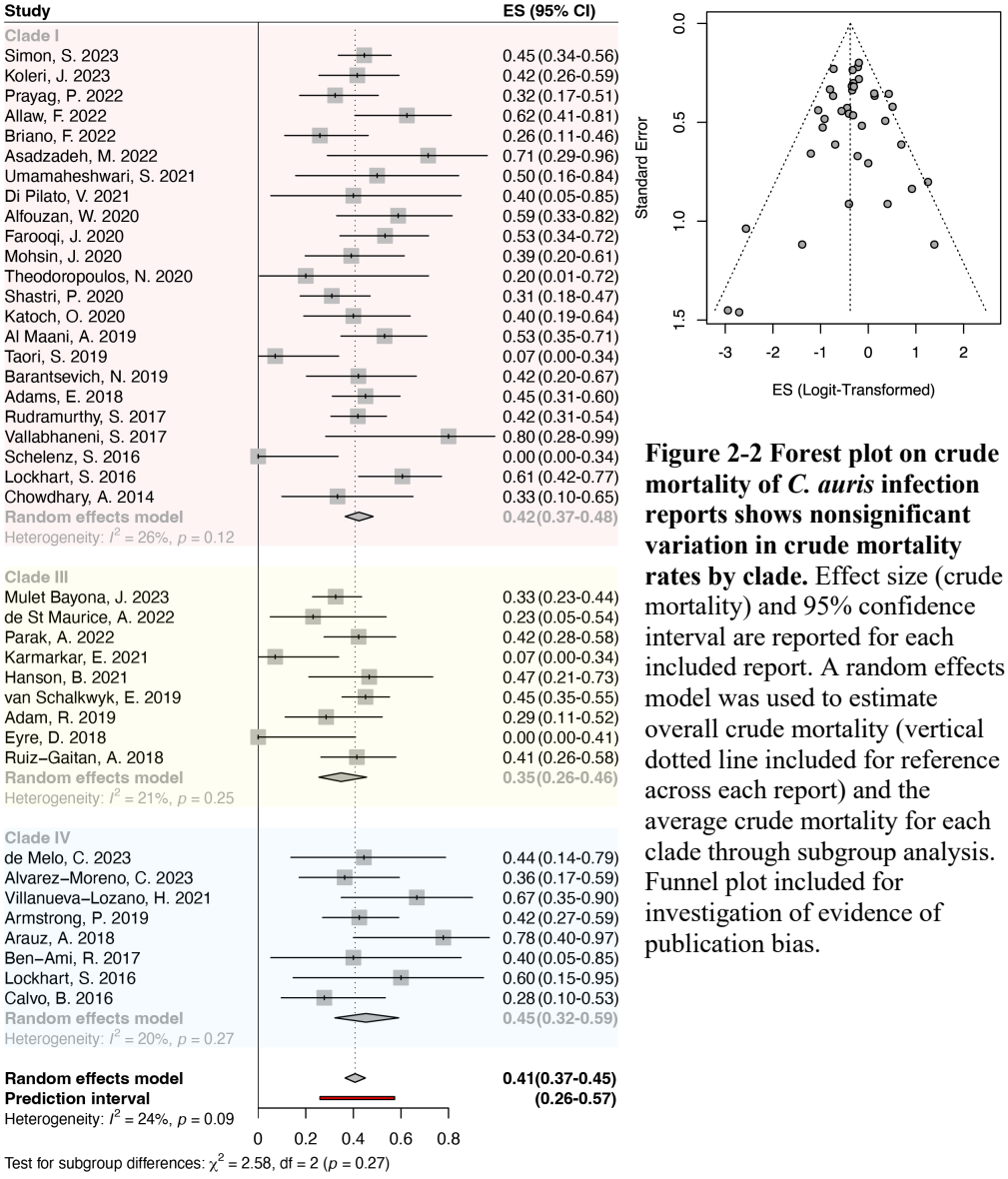

Figure 2-2 Forest plot on crude mortality of *C. auris* infection reports shows nonsignificant variation in crude mortality rates by clade. Effect size (crude mortality) and 95% confidence interval are reported for each included report. A random effects model was used to estimate overall crude mortality (vertical dotted line included for reference across each report) and the average crude mortality for each clade through subgroup analysis. Funnel plot included for investigation of evidence of publication bias.

37-45%) with a prediction interval of 26-57%, which aligns well with previous reports of crude mortality for *C. auris* infection (Fig. 2-2). Egger's test gave a p-value of 0.4095, indicating no evidence of publication bias (Fig. 2-2), and heterogeneity among reports was marginal and nonsignificant ($I^2 = 24\%$, $p = 0.09$). Subgroup analysis indicated nonsignificant differences between *C. auris* clades ($\chi^2 = 2.58$, $df = 2$, $p = 0.27$). However, clade IV showed the highest effect size (45% mortality, 95% CI: 32-59%), followed by clade I (42% mortality, 95% CI: 37-48%), then clade III (35% mortality, 95% CI: 26-46%). While these differences do not reach statistical significance, the trend agrees with the attributable mortality data demonstrated by the experimental virulence models, suggesting clade IV and potentially clade I may truly exhibit greater pathogenicity during infection. Importantly, our meta-analysis only included crude mortality and so is likely underpowered to describe attributable differences by *C. auris* clade. Moreover, because the genetic lineages have historically clustered geographically, it is difficult to uncouple strain-specific virulence from regionally differential healthcare practices. However, our analysis suggests the possibility that clade IV is more virulent than other clades.

2.3.2 Host Colonization

In vitro and *in vivo* models have been developed to study skin colonization by *C. auris*. In an *in vitro* model using an artificial human axillary sweat medium and *ex vivo* porcine skin as a substrate, *C. auris* was able to produce dense, multilayered accumulations[155]. Interestingly, *C. auris* exhibited a fungal burden ten-fold greater than that of *C. albicans* in the artificial sweat medium but not RPMI-MOPS, along with an apparent persistence of *C. auris* in concentrated sweat medium designed to mimic the evaporation of sweat even after fourteen days, where the *C. albicans* formations were not viable[155]. This finding suggests a distinct capacity for growth in a physiological environment that might be encountered during colonization of high-sweat body

sites such as the axillae or inguinal crease. The salt concentration in this synthetic sweat medium is around 3%, and other reports have found this level of salinity to be well tolerated *by C. albicans*, suggesting the differential growth capacities in this media between *C. albicans* and *C. auris* may not be attributed to differences in halotolerance alone, despite increased halotolerance in *C. auris* compared to other clinically relevant *Candida* species[37,156]. In this same model, the observed substantial biofilm burden was achieved by clinical isolates of all four major clades of *C. auris* without notable differences[157]. This behavior likely reflects an advantage for *C. auris* in human skin colonization, which serves as a source for nosocomial transmission between patients. Notably, in this model, fungal burden was extensive on the skin surface but there was no evidence of invasive growth into the dermis.

Another study, using an *in vivo* murine model of skin colonization, observed varying levels of fungal burden following colonization with individual isolates from each of the four major clades[28]. In this model, *C. auris* was applied onto the shaved mouse skin. A clade III isolate showed the greatest fungal burden fourteen days after infection, followed by clade IV, then clade I, and a clade II isolate exhibited the lowest fungal burden. Notably, histopathological evidence suggested *C. auris* cells invaded deeper into the skin tissue and resided within the hair follicle[28]. Furthermore, *C. auris* cells were recovered from skin tissues for up to four months, even after surface swabbing resulted in negative cultures, perhaps suggesting that such prolonged persistence could be attributed to its potential to survive deeper within the skin tissue.

The fungal factors contributing to strain or clade-specific advantages in skin colonization have only begun to be explored. Utilizing both an *ex vivo* human skin model and an *in vivo* murine epicutaneous model, we specifically investigated the role of adhesins in skin colonization in two Clade I isolates, AR0382 and AR0387, finding greater skin bioburden from the more

adhesive AR0382[95]. The variation in skin colonization potential could be partly attributed to the differential expression of two adhesins: the canonical adhesin Iff4109 and the *C. auris*-specific adhesin Scf1[95]. Notably, the deletion of *SCF1* and *IFF4109* in AR0382 led to a reduced ability to colonize both *ex vivo* human skin explants and *in vivo* murine skin. Conversely, overexpressing *SCF1* in AR0387 significantly enhanced its skin colonization capacity. Another report found increased bioburden in skin colonization models associated with strain-specific increased expression of the adhesin Als4112[158]. Expression of these adhesins may directly mediate surface association with the skin substrate. As adhesin expression varies widely among *C. auris* isolates, this may substantially explain variability in strain colonization potentials[95,158]. Interestingly, a study using an intradermal infection model observed nearly equivalent fungal burdens among four strains from the four major clades, suggesting the source of strain-specific variation may have been bypassed by intradermal inoculation in this case[159]. Natural variation observed in colonization potential then likely predominantly reflects variation in skin surface association.

In humans, patients colonized with *C. auris* can remain positive for extensive periods of time[30,44]. The observation that *C. auris* can reside in the hair follicle and persist for months in murine colonization model may in part explain the prolonged colonization of *C. auris* on patient skin[28]. In addition, the recovery of *C. auris* cells from skin tissues even after negative cultures from surface swabs could explain challenges in identifying *C. auris* colonization during patient screening. Proctor et al. reported that taking swab samples from at least six body sites, including nares, palm and fingertips, toe webs, perianal skin, inguinal crease, and axilla, maximizes the sensitivity of colonization screening[22]. However, for routine screening and practicality, the authors recommended focusing on high-yield areas such as the armpits, inguinal creases, and anterior nostrils[22]. Antiseptic agents such as chlorhexidine gluconate (CHG) are routinely

utilized for skin care and decontamination in long term care patients. Using an *in vivo* murine model, Huang et al. showed that treating mice with CHG prior to or post *C. auris* colonization significantly reduced fungal burden on the skin[28]. However, some reports suggest *C. auris* can continue to spread even after the introduction of unit-wide CHG bathing[30], indicating the effectiveness of CHG bathing in reducing *C. auris* skin colonization in clinical settings requires additional investigation.

Despite the advancements in our understanding of *C. auris* colonization dynamics, the ability of available colonization models to recapitulate human data is largely unexplored. First, it is unclear whether critical interactions between *C. auris* and the human skin microbiome would be recapitulated by the *in vivo* murine models. One study showed distinct microbiome compositions associated with healthy patients compared to *C. auris* colonized patients[22]. The microbiome of *C. auris* negative samples were dominated by *Malassezia* species and skin commensal bacteria species: *Staphylococcus hominis*, *Corynebacterium tuberculostearicum*, *Staphylococcus epidermidis*, *Staphylococcus caprae*, and *Corynebacterium striatum*. However, *C. auris* positive samples were associated with various *Candida* species along with bacteria such as *Pseudomonas aeruginosa*, *Klebsiella pneumoniae*, *Providencia stuartii*, and *Proteus mirabilis*. Whether this association has a causal influence on *C. auris* colonization remains unclear. However, the authors proposed an example mechanism that could directly link the *C. auris*-associated microbiome with *C. auris* colonization, pointing to reports demonstrating that the skin commensal *S. epidermidis* induces the expression of the antimicrobial peptide LL-37 in human keratinocytes[160], which could in turn inhibit *C. auris* growth and skin colonization[161].

Furthermore, the physiological conditions present in distinct body sites favored by *C. auris* for skin colonization may not be fully captured in existing models. Common colonization

sites like the axilla, groin, nostrils, and fingertips contribute to both persistent infections and transmission risks, although each body site presents a unique colonization environment[22,162]. For instance, differing from the epidermal cells found in other areas, the nares are lined with mucosal epithelium, which secretes mucus, contributing to the nares' moist environment. Alternatively, the axillae are home to a higher concentration of sweat glands and typically exhibits a pH of 6.5, in contrast to the more acidic pH of 5.5 found in other skin areas[163]. This reduction in acidity is associated with altered bacterial growth, resulting in a distinct microbiome compared to other body sites[164]. Where *C. auris* robustly colonizes diverse skin niches, adaptations to distinct environmental pressures are likely to inform differential colonization dynamics.

2.3.3 Antifungal Resistance

The high rate of acquired antifungal resistance in *C. auris* poses a substantial threat to treatment efficacy. While antifungal susceptibility cutoff values have not been established for *C. auris*, the US CDC has proposed tentative breakpoints. Based on these values, it is estimated that 80-90% of isolates exhibit fluconazole resistance, 20-50% of isolates exhibit amphotericin B resistance, and 5-7% are resistant to echinocandins[5,165]. The rate of antifungal resistance in non-*auris* *Candida* species overall is estimated at only 7%, demonstrating remarkable plasticity and adaptation in *C. auris* by comparison[29]. Notably, resistance rates vary by clade, with isolates of clade I and III demonstrating almost universal resistance to fluconazole, isolates of clade II being widely susceptible, and isolates of clade IV demonstrating variable resistance[5]. These trends are largely associated with acquired and lineage specific mutations in genes encoding drug targets or efflux regulators, highlighting stable adaptability in *C. auris* even around cellular processes with potentially impactful fitness implications. Multidrug and even pan-resistant isolates have demonstrated the capacity to spread and transmit between individuals, despite any fitness costs

potentially associated with the development of high levels of resistance, and resistance is known to emerge upon therapy, limiting viable treatment options[50]. Specific mutations and mechanisms leading to acquired resistance have been extensively analyzed elsewhere, and we direct the reader to other excellent reviews for detailed discussion[29,165]. Briefly, characterized resistance mutations largely accumulate in genes encoding drug targets or regulators of efflux, in line with classical mechanisms of antifungal resistance. Somewhat enigmatically, however, *C. auris* also exhibits high rates of resistance to amphotericin B, a polyene antifungal rarely associated with resistance in other pathogenic fungi, and the vast majority of resistant isolates lack canonical resistance mutations[165,166] One recent report found experimentally evolved amphotericin B resistance most commonly emerged in association with membrane sterol modulation through mutation in *ERG* pathway genes, though high level resistance frequently arose at the cost of growth rate or infection potential[167]. Using wild type isolates from four different clades, the authors observed strain-specific variability in both resistance development and resistance-associated fitness loss, suggesting the importance of differential genetic backgrounds for the emergence of acquired resistance. Mechanistically, the authors noted an evolved mutant with a compensatory mutation in the cAMP/PKA signaling pathway responsible for rescuing the fitness tradeoff associated with sterol modulation, and a similar mutation has been reported in one case of clinically acquired amphotericin B resistance[167,168]. This finding suggests a broader crosstalk between stress response and drug resistance, which may prove critical in understanding the development of antifungal resistance and variations in acquired resistance in divergent *C. auris* lineages.

2.4 Aggregation

Filamentation and morphogenic plasticity are critical virulence traits in many fungal pathogens, including the model pathogenic yeast *Candida albicans*. While morphogenic transitions in *C. auris* are less apparent in response to canonical filamentation cues described in model species, numerous reports have documented cases of isolates exhibiting an alternative aggregative morphological state, with cells growing in multicellular conjoined structures. While some experimental evidence has suggested aggregation can influence host association[148,169,170], and while similar multicellular phenotypes have been argued to convey environmental advantages in nonpathogenic settings in other species[171,172], selective advantages for aggregation in *C. auris* remain largely speculative. Efforts to characterize this behavior suggests *C. auris* aggregation is the result of one of a multitude of phenotypes rather than a single phenomenon. Aggregative states have been reported as either a constitutive and heritable characteristic or as an inducible response to environmental conditions[169,173–175]. Some reports suggest aggregation as a phenotype is strain or clade specific, while others suggest any representative isolate from diverse clades can grow in aggregates[100,169,175]. Isolates from other closely related species exhibit similar heritable multicellular phenotypes, suggesting the evolution of aggregation is not specific to any *C. auris* lineage[176]. With aggregation being a largely qualitative phenotype with an observational but not always biological definition, the broad umbrella term of aggregation may encompass multiple molecular underpinnings. Aggregates may exhibit common selective advantages, such as those conferred by their physical multicellular structure, but may also exhibit distinct phenotypes specific to the molecular mechanisms associated with the aggregative state.

Three distinct mechanisms of aggregation have been described: 1) Adhesin-mediated aggregation, 2) Cell separation defects, and 3) Extracellular matrix aggregation (Fig. 2-3).

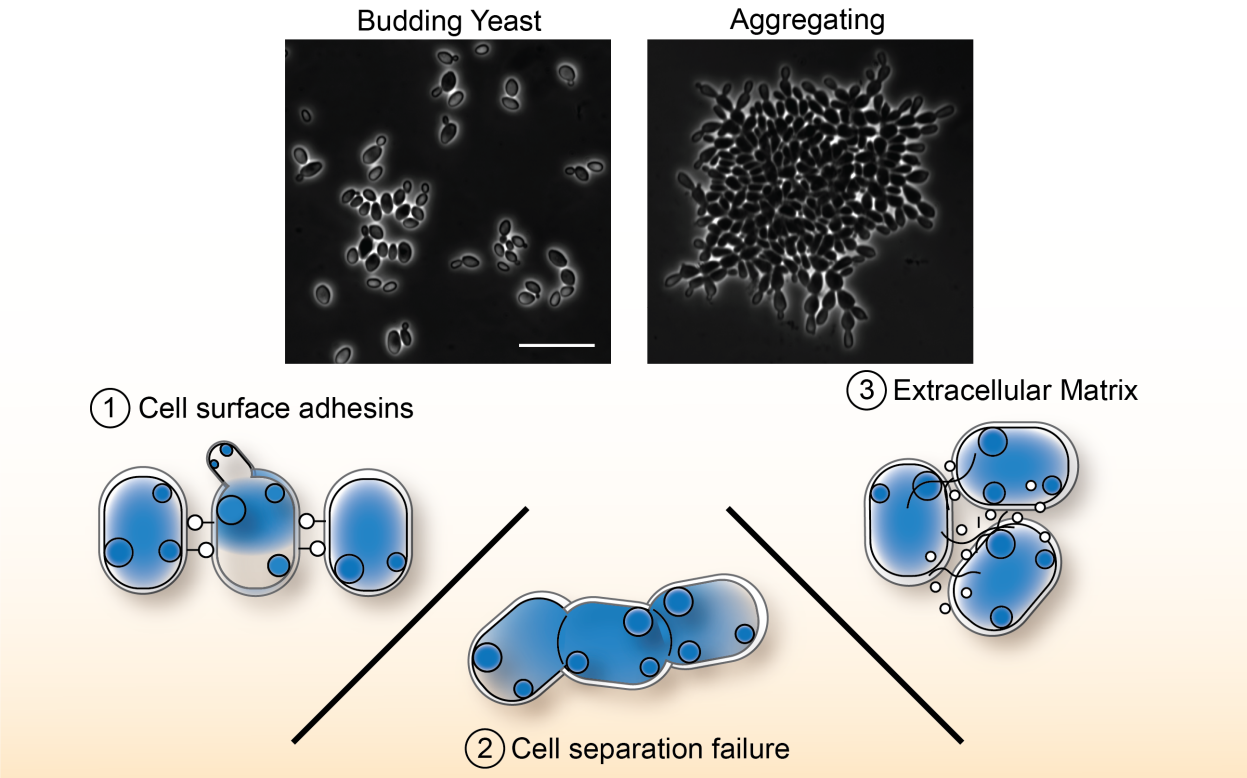

Figure 2-3 Three distinct molecular mechanisms of *C. auris* aggregation. *C. auris* can exist in either a unicellular, budding yeast morphology or in multicellular aggregates (phase contrast microscopy, top; scale bar = 20 μm). Three distinct mechanisms of aggregation have been reported: 1) Cell-cell adhesion mediated by cell surface bound proteins, with strong evidence for a prominent role by the adhesin Als4112, 2) Failure of daughter cells to separate from parent cells after budding, often due to incomplete septum degradation, 3) Cohesive multicellular clusters conjoined by secreted extracellular components.

Adhesin-mediated aggregation appears to be the result of cell-cell adhesion driven by cell surface proteins. For *C. auris*, the *ALS* family adhesin encoded by the reference locus B9J08_004112 (*ALS4112*) is frequently reported in association with cellular aggregation. In *C. albicans*, Als5 and other cell wall proteins promote cell-cell adhesion through the formation of amyloid aggregates[81,177]. The mechanism for Als4112 aggregation in *C. auris* may be similar, as treatment of aggregating isolates with amyloid-inhibiting compounds Thioflavin-T or Congo Red partially suppresses aggregation[175]. Interestingly, one report detailed an isolate exhibiting reversible aggregation when suspended in PBS that could be suppressed by suspension in pure water, which could potentially be explained by electrostatic requirements for amyloid

formation[174]. Disruption of some forms of aggregation by Proteinase K also suggests a cell surface proteinaceous mechanism[158,174]. A similar mechanism may be responsible for aggregation in other *C. haemulonii* complex members, which can be disrupted by treatment with Proteinase K, trypsin, or SDS[176].

Transcriptional control of Als4112 specifically has been demonstrated as a mechanism for development of an aggregative state. Numerous reports have detailed aggregation in response to subinhibitory concentrations of triazoles and echinocandins[101,178,179]. One study found overexpression of *ALS4112* associated with aggregation in a strain grown for multiple generations under subinhibitory concentrations of caspofungin[178]. In this case, removal of the caspofungin stress resulted in loss of aggregation and reduced *ALS4112* expression. This behavior is reminiscent of *ALS*-mediated echinocandin-induced aggregation described in *C. albicans*[180]. In another case, Bing et al. identified naturally aggregating isolates that exhibited substantial copy number increases in the *ALS4112* locus[158]. Similarly, a clade III isolate that exhibited aggregation when grown in sabouraud dextrose media but not RPMI demonstrated transcriptional overexpression of *ALS4112* under aggregation-growth conditions but failed to aggregate when *ALS4112* was deleted[174]. Interestingly, the media-inducible expression of *ALS4112* and associated aggregation was not observed in a clade I isolate[174], although in our recent work we found that overexpression of *ALS4112* in a clade I isolate by promoter replacement was sufficient to drive aggregation, suggesting the strain-specific phenotypes reported in association with *ALS4112* aggregation are likely due to regulation of the gene rather than clade-specific adhesin sequence variation[95].

As an alternative mechanism of aggregate formation, isolates exhibiting defects in cell separation after budding have been described. Mechanistically, this can result from a failure of

septum degradation. Through genetic screening, we identified aggregative mutants associated with defects in the Regulation of *ACE2* and Morphogenesis (RAM) pathway[170]. The RAM pathway is a conserved regulatory network that controls daughter cell localization of the terminal transcription factor Ace2, which in turn regulates transcription of a suite of septum-degrading enzymes, including chitinases and glucanases[181]. The aggregative phenotype associated with defects in *ACE2* or upstream members of the RAM pathway is conserved in other *Candida* species and *Saccharomyces*[182,183]. Interestingly, cultivation under conditions that favor multicellularity can select for spontaneous RAM pathway mutants in model species[171], which may explain some instances of aggregation in *C. auris*. One report identified two urinary tract *C. auris* patient isolates exhibiting rugose colony morphology and strong cellular aggregation associated with a nonsense mutation in *ACE2* that was heritable over 30 passages over the course of 6 months[173]. This spontaneous emergence of heritable and constitutive aggregation may be mechanistically similar to aggregative or elongated isolates recovered in rare events after passage of non-aggregative parent strains through animal hosts, though the genetic bases for these reports remain unexplored[184,185]. Other reports have detailed transcriptional downregulation of chitinase genes in naturally aggregating isolates, but it is unclear whether this is responsible for the aggregative phenotype or whether this downregulation is the result of defects in the RAM pathway[175,186]. Interestingly, one report suggested cell separation defects may also contribute to echinocandin-induced aggregation[174].

A third proposed mechanism for aggregation relies on extracellular matrix (ECM) connecting cells together. In this case, aggregation is the result of an inducible response associated with production of ECM. Through SEM, Malavia-Jones et al. observed aggregates connected by ECM in cells cultured at 37°C[175]. This inducible aggregation was observed in

isolates from all four major clades, even for isolates that exhibited no aggregation or notable ECM production when cultured at 30°C[175]. This finding may be consistent with an observation that all isolates from a panel of 19 strains, representing aggregative and non-aggregative phenotypes *in vitro* from all four major clades, formed aggregates in infected organs in a murine model[100]. Importantly, these reports suggest all *C. auris* isolates have the potential for aggregation under specific conditions.

Morphological variation is a critical pathogenic feature in *C. albicans* and other related fungi, so it is reasonable to examine aggregation in *C. auris* from a clinical perspective. Aggregating isolates are often found to be less virulent in experimental models compared to non-aggregating isolates (e.g. Refs.[148,169,170]), although exceptions are common, with reports that strain-specific virulence differences are independent of aggregation (e.g. Refs.[97,100,174]). Importantly, quantitative comparisons in virulence models should be examined carefully, as standardization of infectious units in inocula between single-celled yeast and multicellular aggregates is unrealistic, and colony forming unit recovery can be unreliable for aggregating isolates[100]. Still, physical or biological variation may meaningfully contribute to virulence. One report found that phagocytic uptake by THP-1 cells was minimal for aggregating isolates, and it has been suggested that aggregation may be a mechanism of immune evasion *in vivo*[139,174]. In the same experiment, stray single *C. auris* cells were efficiently recognized by the immune cells, suggesting the physical bulk of aggregates may hinder phagocytosis[174]. This model is difficult to reconcile as an explanation for differential virulence between aggregative and non-aggregative strains, though, given the propensity of even non-aggregative strains to form aggregates *in vivo*[100,139]. It has also been suggested that aggregation may hinder dissemination *in vivo*, but this idea is inconsistent with observations that both aggregating and non-aggregating isolates exhibit

similar capacities for tissue invasion in murine models[100,175]. Differences in virulence, then, likely arise from strain-specific biological variation beyond aggregation in and of itself.

2.5 Outbreak Potential

Clonally distributed outbreaks in healthcare settings remain a substantial driver of public health and clinical concern for *C. auris*. While carriage by an index patient represents the most likely primary reservoir in these settings, viable *C. auris* cells are rapidly and extensively shed to surrounding areas, and colonization of inert substrates in the nearby clinical environment can provide a secondary reservoir to potentiate outbreak progression. Here, we highlight biological observations exploring the persistence of *C. auris* nosocomially on abiotic reservoirs and its recalcitrance to decontamination efforts in these environments.

2.5.1 Disinfection Resistance

While high level and sporicidal disinfectants have widely been observed to be effective against *C. auris*, other disinfectants demonstrate unreliable and often unpredictable efficacy. Recommendations from the CDC and other authorities particularly caution against the use of water-based quaternary ammonium compounds (QACs)[38,187]. This places an additional burden on infection prevention efforts, as QACs are used extensively in healthcare settings for disinfection of noncritical patient care items and surfaces. Accordingly, the Environmental Protection Agency established the List P Registry to validate disinfectants against *C. auris* specifically, as experimental data suggests even QACs with *C. albicans* claims can exhibit poor efficacy against *C. auris*[187]. While these observations might give the impression that *C. auris* is inherently less susceptible to killing by QACs than *C. albicans*, the reality appears to be more complex. Disinfectant efficacy testing suggests the susceptibility of *C. auris* is dependent on the

genetic background of the isolate tested as well as the formulation of the QAC. For instance, compared to clade I, III, and IV isolates, the clade II isolate type strain consistently shows increased susceptibility to killing by diverse QAC formulations[39,102], including to a benzalkonium chloride QAC that demonstrated poor efficacy against *C. albicans*[103]. Bacterial acquired resistance to QACs most often stems from efflux activity[188]. The strain-specific resistance exhibited by *C. auris* may follow similar principles. Dire et al. found that pulsing a *C. auris* isolate with a subinhibitory concentration of benzalkonium chloride for 15 days increased its MIC to the QAC four-fold[34]. This increase was associated with increased rhodamine-6G efflux activity, suggesting increased efflux may be related to reduced QAC susceptibility[34]. This finding suggests *C. auris* isolates with low susceptibility to QACs may be adapted to increased efflux activity. In practice, this adaptation may even occur upon exposure to subinhibitory concentrations of disinfectant in clinical settings.

While consensus guidelines generally recommend against QAC usage for *C. auris* disinfection, susceptibility data is more complicated, with evidence of both strain-specific tolerance to certain formulations and specific activity of different formulations against different isolates, often in unpredictable associations. For instance, two Kinzua disinfectants with QAC blends as active ingredients showed strong efficacy (approximately 4-log reduction or greater) against *C. albicans* and clade I and II isolates of *C. auris*, while exhibiting only minor efficacy against clade III and IV isolates[39]. Meanwhile, another QAC-based disinfectant exhibited strong efficacy against *C. albicans* and a clade I *C. auris* isolate, while isolates from clades II, III, and IV were largely nonsusceptible[39]. Combinatorial formulations of QACs with other disinfectant classes has shown promise of increased efficacy, such as a QAC/polyhexanide blend that prevented growth and demonstrated a >5-log reduction against a panel of isolates from 3

clades[189] or QAC disinfectants supplemented with varying concentrations of isopropanol or ethanol demonstrating consistent efficacy against diverse isolates[39,102]. Interestingly, some formulations highlight further strain specificity in susceptibility, such as a QAC disinfectant containing 17.2% isopropanol only exhibiting strong efficacy against clade II and clade IV isolates, but not others[102]. With understanding of disinfectant resistance mechanisms being largely incomplete, explaining strain-specific susceptibility to different active ingredients and formulations remains challenging. Efflux potential represents a promising explanation, but lineage specific physiological differences, such as cell surface and membrane profiles, may also be relevant, especially given the differential activity of diverse QAC chemistries.

Ultraviolet-C (UV-C) devices are increasingly used to supplement chemical disinfection regimes. While protocols and devices vary considerably, several reports have examined the disinfectant efficacy of UV-C treatment on *C. auris* isolates from diverse backgrounds. Again, clade II isolates are frequently reported to exhibit greater susceptibility to UV-C killing than isolates from other clades[190,191]. Still, sensitivity to UV-C varies widely among isolates, though increasing exposure time and reducing distance from the UV source can sometimes improve killing of less susceptible isolates[191–194]. Interestingly, several direct comparisons have found *C. albicans* sensitivity in line with clade II and other highly susceptible *C. auris* isolates, while resistant isolates exhibit greater resistance to UV-C than *C. albicans*[190,191,193]. This variation suggests some *C. auris* isolates exhibit an adaptation that is protective against UV killing, though it is unclear whether such an adaptation would be selected for by UV pressure. One possible resistance mechanism is cellular aggregation. Chatterjee et al. observed UV susceptibility among isolates was qualitatively associated with aggregation potential, where non-aggregative isolates were more commonly susceptible[195]. In this case, 2 aggregative clade III isolates exhibited very

little susceptibility, and killing could not be improved by increased exposure time[195]. As is typical of UV disinfectant efficacy, killing is most effective when the cells are directly exposed to the light source[193,196]. It is perhaps possible that exposed cells in large aggregates absorb UV radiation and protect internal cells, offering a resistance strategy implicit to the physical multicellular structure in aggregates that may explain strain-specific UV susceptibility.

2.5.2 Nosocomial Persistence

The frequent association of *C. auris* with healthcare outbreaks is often accompanied by widespread persistence in clinical environments. Inert surfaces near colonized patients show associated high rates of positivity[30,32], and colonized objects have been linked to transmission events between individuals and outbreak persistence[35,36,112,197]. Spread and transmission through contact-independent mechanisms are also possible, as air dispersal of *C. auris* cells to patient-inaccessible areas has been observed[40]. The contaminated environment in turn likely serves as a secondary reservoir to potentiate transmission, and examples of patients acquiring *C. auris* infection after being moved to rooms previously inhabited by colonized individuals have been reported[198]. The ability of *C. auris* to tenaciously colonize surfaces further extends to invasive medical devices, and, like for other *Candida* pathogens, colonization of indwelling equipment poses a substantial risk for the development of invasive infection[46,199]. Considering these and similar observations, *C. auris* outbreaks are met with extensive infection prevention responses, more so than other *Candida* species and in similar force as for classically hospital-associated bacterial infectious agents[38,41,200]. Challenges in adhering to such responses are thought to contribute to the continuingly increasing rate of *C. auris* outbreak[41].

As is the theme of this review, we questioned whether this one size-fits all mentality fully captures the diversity of *C. auris* outbreaks. Examination of reports from single center or

clustered multi-center outbreaks demonstrates widespread variability in both transmission rate and associated outbreak size, ranging from localized outbreaks involving single transmission events to major outbreaks involving rampant contamination of dozens of patients each month, leading to hundreds of affected individuals, with the caveat that variation in surveillance efficiency may be reflected in differences in reported outbreak sizes (Fig. 2-4). Mapping of outbreak size and transmission rate failed to reveal obvious geographic associations between outbreak discrepancies, suggesting varying outbreak scenarios are possible despite differential infection control practices and recommendations from regional authorities.

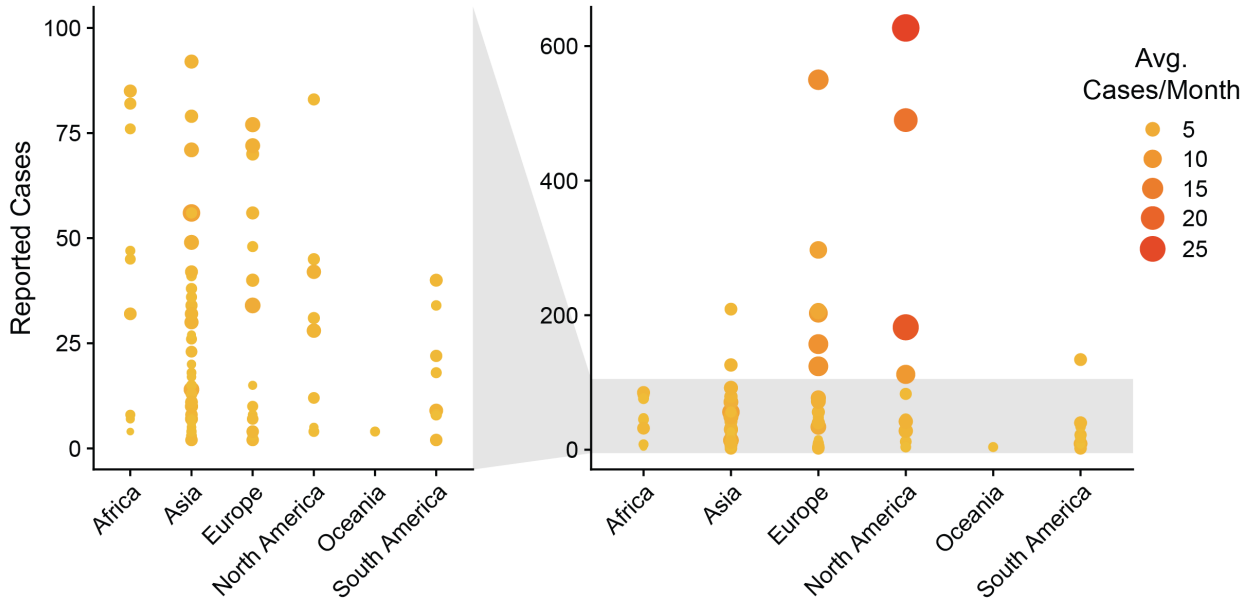

Figure 2-4 Size and transmission dynamics of single center or clustered multi-center *C. auris* outbreaks. Each point represents an individual outbreak report. Outbreaks are represented by total number of affected patients identified (colonized or infected) and by the rate of outbreak progression, defined by the average number of new cases identified per month. Inset (left panel) recapitulates all outbreaks comprising less than 100 affected individuals.

In the most expansive outbreaks, hundreds of patients are affected across several years, resulting in near-endemic spread in multiple clustered facilities. For example, surveillance covering a 2.5-year period of a regional *C. auris* outbreak in the Chicago metropolitan area identified 490 clinical or colonized patients among multiple facilities, with within-facility

prevalence as high as 71%[30]. Environmental sampling of an affected facility during four point prevalence surveys found 38% (73/191) of sampled objects and surfaces were colonized, even after routine cleaning and disinfection[30]. Contaminated objects included reusable and noninvasive patient care items, high touch surfaces such as bedrails and doorknobs, and mobile objects such as nursing carts and mobile ultrasounds, providing a widespread reservoir for persistence and dissemination. Importantly, this example, as is representative of other large outbreaks, has largely been associated with long-term care facilities involving multiple-occupancy rooms filled with furnishings, care equipment, and personal items. These circumstances can promote persistent and prolonged colonization of patients as well as reduced opportunities for terminal and extensive room cleaning, likely substantially influencing outbreak progression.

A pattern of smaller outbreaks can also often be linked to *C. auris* persistence on abiotic substrates, demonstrating multiple acquisition events linked to a contaminated reservoir, but with much lower prevalence and transmission rates. One example of this is a single center observational study in the U.K. encompassing two general adult ICUs affected by a *C. auris* outbreak where a single index case lead to six transmission events over six months[35]. In this case, positivity was lower, with only 2.5% (6/236) of sampled objects collected over three environmental screens exhibiting *C. auris* contamination[35]. A single cloth lanyard (one out of 100 sampled) attached to a controlled drug locker key was found to be contaminated, and removal of the cloth lanyards temporally correlated with termination of the outbreak[35]. Presumably, the contaminated lanyard represented a persistent reservoir, especially being a mobile object handled by numerous healthcare personnel and, importantly, not being subject to routine disinfection, leading to intermittent transmission events. This pattern may be common, as

colonized medical devices such as temperature probes or surgical knives have similarly been linked to outbreak progression, and in some cases exposure to colonized equipment has been demonstrated as an independent risk factor for development of colonization or infection[36,112,197].

Curiously, a contrasting scenario is not uncommon: a single index case with limited environmental persistence and no identified transmission events, despite high occupancy and room sharing. In one example, one patient demonstrating both skin and invasive *C. auris* culture was identified in an oncology ward at a New York hospital, prompting surveillance and deep hospital sampling over the course of three weeks[201]. In total, 48 samples from 18 patients and 132 samples from environmental surfaces throughout the patient room and ward were screened[201]. In this case, no other patients were affected, including one who shared a room with the index patient[201]. From environmental sampling, 2.3% (3/132) of samples demonstrated positivity, with two sequential positive samples taken between cleanings from a single reclining chair in the patient's room[201]. Thirty other samples from the patient's room were negative, as were the remaining samples from throughout the ward[201]. The stark contrast in colonization and dissemination rate in such examples raises the question as to whether the failure of *C. auris* to spread and persistently colonize the environment in these circumstances could be attributed to intrinsic and strain-specific colonization potential.

Efforts to describe colonization dynamics experimentally have largely focused on measuring persistence under desiccation and biofilm formation, and there is evidence in each case of differential behavior between strains. Welsh *et al.* measured the persistence of a clade I isolate dried onto a plastic surface and found recoverable CFU up to 14 days after inoculation and detectable esterase activity for up to 28 days[16]. Similar results were reported in a study that modeled surface contamination by suspending cells in PBS, artificial saliva, or fetal calf serum

before drying cells on a plastic surface, in this case finding recoverable cells 14 days after inoculation[202]. The surface being colonized appears to be important for persistence as well; Dire *et al.* found that fabric, plastic, steel, and wood sustained colonizing cells for at least 21 days under wet or dry conditions, and at times even supported growth, while viability for wet or dry cells on glass decreased significantly by 14 or 21 days[34]. Another report observed survival of *C. auris* cells on latex or nitrile gloves up to 3 minutes but could not detect viable cells by 5 minutes[203]. These initial evaluations suggest survival for minutes to weeks in dry, nutrient poor conditions is plausible. Longer timeframes are likely; for instance, in the case described above, the fomite cloth lanyard that was potentially colonized for several months[35]. Careful quantitative comparison between related and unrelated isolates under consistent experimental conditions is needed, however, to understand the molecular basis for *C. auris* persistence on inert surfaces and to examine strain-specific adaptations. One report examined persistence of two distinct isolates after drying on a plastic surface[202]. While both isolates exhibited viability after 14 days, the recoverable CFU differed by 2-4 orders of magnitude depending on experimental conditions, suggesting strain specific tolerance for desiccated survival[202].

As an alternative model for surface colonization and persistence, several studies have characterized the ability of *C. auris* to form biofilms. Experimentally, biofilm-grown cells exhibit increased persistence and tolerance to decontamination[34,204,205], but it is not well understood where *C. auris* would exist in a biofilm state during a nosocomial outbreak. Colonized sinks and catheters are likely to support biofilm growth given liquid flow and nutrient access, and experimental models suggest cells adopt biofilm characteristics when grown on skin, but individual cells transmitted to dry, nutrient poor surfaces are perhaps less likely to be found in biofilm states[46,135,155,206]. Several reports have demonstrated substantial quantifiable variability

in biomass from biofilm formation between isolates[95,98,158,202,207,208]. Mechanistically, strain specific variation in biofilm formation has been linked to differential expression of specific adhesins: either Scf1 or Iff4109, which mediate the attachment of cells to colonized surfaces, or Als4112, which mediates cell-cell attachment[95,158]. *SCF1* exhibits strain-specific transcriptional variation across isolates from every major clade, and differences in its expression are associated with differences in bioburden in colonization and biofilm formation on surfaces such as catheters or skin[95]. Expression variation in *ALS4112* may be common as well, as genotypic evidence suggests duplication and copy number variation around the *ALS4112* locus has occurred in numerous isolates, and associated overexpression correlates with colonization phenotypes[158]. Interestingly, some reports fail to find strain-specific variation in biofilm formation or colonization under certain experimental models, suggesting differential biofilm phenotypes may be the result specific environmental conditions[98,209,210]. Understanding the appropriate experimental conditions to accurately model nosocomial colonization then will be key to accurately characterizing outbreak dynamics.

Beyond surface association, persistence, and biofilm formation, transmissibility from colonized substrates plays a major role in outbreak settings, but the mechanisms are still unclear. Strain specific adhesin expression results in strains with reduced capacity for surface association and tenacity against shear force[95]. This phenotype may be associated with greater rates of dissemination from surfaces at the expense of reduced colonizing biomass. Similarly, in skin colonization models, different isolates produce varying bioburden[28,95], but the associated consequences on differential levels of shedding from colonized skin, transmission upon contact, or rates of environmental dissemination are unknown. *C. auris* has also been found to disperse across long distances through air transmission, but the dynamics of this mode of dissemination

have not been explored[40]. Understanding the molecular mechanisms underpinning *C. auris* outbreak spread will require experimental modeling of transmission in addition to colonization and persistence and may ultimately yield critical insights into intrinsic fungal factors driving outbreak development.

2.6 Conclusions

In this review, we have focused on virulence and other clinical phenotypic differences between strains and clades of *C. auris,* although there are many phenotypic differences that we have not discussed. It is likely that these differences in core biology will also impact the ability of *C. auris* to cause disease and transmit, and future work on the connections between genotype and phenotype in these different strains will be needed to fully understand this emerging pathogen. From our analyses, we see a few critical points to consider for future research. It appears that Clade IV isolates have a higher pathogenic potential than isolates from other clades; however, the molecular underpinnings of this are currently unknown. On the other hand, Clade I isolates appear to tolerate acquisition of drug resistance mutations more than other clades. The relative impact of these two features on disease outcomes is still unknown. We also observe multiple different modes of aggregation, including some that are strain specific and others that appear to be generalizable across *C. auris.* The importance of these different modes of aggregation during infection still needs to be determined. Lastly, the potential strain-specific differences in outbreak potential is of critical importance, and in this case, we do not observe clade-level trends beyond the lack of outbreaks that can be attributed to Clade II strains.

Going forward, it will be important to clarify which strain of *C. auris* is being investigated for each research question. The differences between strains also provides an opportunity to leverage comparative genomics approaches to map out specific genotypic variants

associated with a phenotype of interest. Variation between strains within a clade provide an opportunity to understand specific evolutionary selective pressures. Importantly, this variation should be considered when deciding which strain is an appropriate wild-type strain for molecular analyses. Recent work in the model fungal pathogen *C. albicans* has identified that the reference SC5314 strain, in many cases, behaves differently than other isolates of *C. albicans* for clinically-relevant phenotypes including induction of host inflammation, degree of filamentation, and level of commensal colonization[211–215]. For *C. auris,* as a field, we have the opportunity to perform analyses across clades that will then allow us to define both species-level and strain-level differences and chose an appropriate strain for laboratory experiments to define mechanisms.

2.7 Notable Contributions

Author contributions are as follows: Guolei Zhao drafted the subsection on host colonization and collaborated on research, discussion, and revisions for this subsection. Teresa O'Meara drafted the abstract and conclusions sections and collaborated on revisions of these sections.

Chapter 3 Development of Forward and Reverse Genetic Systems for *Candida auris* and Molecular Evaluation of Morphogenesis

3.1 Abstract

Candida auris is an emerging healthcare-associated pathogen of global concern. Recent reports have identified *C. auris* isolates that grow in cellular aggregates or filaments, often without a clear genetic explanation. To investigate the regulation of *C. auris* morphogenesis, we applied an *Agrobacterium*-mediated transformation system to all four *C. auris* clades. We identified aggregating mutants associated with disruption of chitin regulation, while disruption of *ELM1* produced a polarized, filamentous growth morphology. We developed a transiently expressed Cas9 and sgRNA system for *C. auris* that significantly increased targeted transformation efficiency across the four *C. auris* clades. Using this system, we confirmed the roles of *C. auris* morphogenesis regulators. Morphogenic mutants showed dysregulated chitinase expression, attenuated virulence, and altered antifungal susceptibility. Our findings provide insights into the genetic regulation of aggregating and filamentous morphogenesis in *C. auris*. Furthermore, the genetic tools described here will allow for efficient manipulation of the *C. auris* genome.

The data in this chapter has been published in *Nature Communications*.

Santana, D.J., and O'Meara, T.R. (2021). Forward and reverse genetic dissection of morphogenesis identifies filament-competent *Candida auris* strains. Nat. Commun. *12*, 7197.

3.2 Introduction

Since its 2009 isolation from the ear canal of a patient in Japan, the emerging fungal pathogen *Candida auris* has caused infections and outbreaks in at least 44 countries on 6 continents[216]. The global prevalence of *C. auris* is characterized by the seemingly simultaneous emergence of four distinct genetic clades, differing on the scale of hundreds of thousands of single nucleotide polymorphisms (SNPs), with a potential fifth clade recently identified[5,7]. Individual isolates exhibit significant heterogeneity both within and between clades, including in murine models of infection and colonization[28,100]. The continually increasing understanding of biologically and clinically relevant phenotypic variation among *C. auris* isolates, and the variation between *C. auris* and other well-studied model organisms, emphasizes the need for facile genetic manipulation approaches to allow for mechanistic characterization of this organism.

Although *C. auris* does not form filaments under many of the same environmental cues that induce hyphal growth in *Candida albicans*[217], numerous reports of irregular or multicellular growth indicate *C. auris* does exhibit cellular polymorphism. Depletion of the essential molecular chaperone *HSP90* results in elongated cell growth[217]. Genotoxic stress induced by hydroxyurea or deletion of the DNA damage responsive long non-coding RNA DINOR similarly result in pseudo-hyphal elongated cells[218,219]. Other stressors such as growth in high salt concentrations induce cell elongation[15]. Strains exhibiting filamentous, elongated, or aggregating morphologies have been isolated from populations of *C. auris* cells following murine infection[184,185]. Furthermore, numerous reports detail patient isolates with multicellular aggregating phenotypes, often described by a failure of cell aggregates to disperse upon mixing or vortexing[101,169,186,202]. Aggregating isolates exhibit reduced biomass in biofilm formation and lower virulence in *Galleria mellonella* infection models compared to non-aggregating

counterparts[169,208]. Still, the genetic determinants of irregular morphogenesis in *C. auris* remain largely unexplored due in part to difficulties in performing genetic manipulation in this organism.

Transformation of *C. auris* is complicated by low rates of targeted integration and variable transformation efficiency among isolates and clades[218,220]. The use of RNA-protein complexes of purified Cas9 and gene-specific guide RNAs, referred to as Cas9-ribonucleoproteins (RNPs), to promote homology directed repair demonstrably increases transformation efficiency and targeted integration rates[221]. Transformation incorporating RNPs is often the method of choice for manipulating the *C. auris* genome, and variations exist using multiple gRNA target sites to further improve targeted integration efficiency[222]. The use of RNPs in transformation, however, comes with increased expense and additional technical considerations during transformation. In *C. albicans*, transformation with linearized gene cassettes encoding Cas9 and sgRNA promote homozygous gene deletion; these cassettes cannot be detected in the genome of transformants, suggesting they are transiently expressed and not stably integrated[223]. A similar transiently expressed CRISPR-Cas9 system promotes targeted genetic manipulation in *Cryptococcus neoformans*[224]. We hypothesized that specific adaptation of the transiently expressed CRISPR-Cas9 system to use *C. auris*-recognized promoters would increase the rates of targeted transformation efficiency.

A forward genetics system represents an alternative approach for manipulating the genome. The piggyBac transposon mutagenesis system has proven successful for performing insertional mutagenesis at saturating levels in a Clade II *C. auris* isolate[219]. This represents a significant advance in the technical ability to genetically manipulate *C. auris*. However, one potential limitation of the piggyBac system is that it requires initial engineering of the strain of

interest to encode the transposon machinery prior to performing genome-scale mutagenesis. To develop a forward genetics system suitable for performing mutagenesis in any *C. auris* clinical isolate without prior engineering, we turned to *Agrobacterium tumefaciens*-mediated transformation (AtMT), an insertional mutagenesis approach with a history of proven success in fungal species[225]. *A. tumefaciens* is a plant pathogen that causes crown gall in dicotyledonous plants through genetic transformation[226]. Its capacity for transformation is not limited to plants, however, and can be taken advantage of to perform insertional transformation in a variety of eukaryotic species, including *C. albicans*, *Candida glabrata*, and *Saccharomyces cerevisiae*[227]. In practice, mobilization of a DNA sequence flanked by left and right direct repeats (T-DNA) is accomplished by induction of *A. tumefaciens* virulence genes during co-culture with a recipient organism using acetosyringone[228]. This T-DNA sequence is encoded on the Ti Plasmid harbored by *A. tumefaciens* and can be manipulated to contain fungal selectable markers.

We used AtMT to generate an insertional mutant library in *C. auris* and identified morphogenic mutants exhibiting aggregating or filamentous growth. Insertions in genes orthologous to regulators of chitinase and chitin synthase in *S. cerevisiae* were associated with defects in daughter cell separation in *C. auris*, leading to aggregating growth, while an insertion in an ortholog of *ScELM1* resulted in constitutive filamentous growth in *C. auris*. We developed a robust transient CRISPR-Cas9 expression system for *C. auris* and demonstrated its ability to significantly increase targeted transformation in isolates from all four major clades. Using this system, we performed deletions in key regulators of cell separation to demonstrate functional conservation of *ELM1* and chitin regulatory genes as morphogenic regulators in *C. auris*. The morphogenic mutants we identified exhibited attenuated virulence in a *G. mellonella* infection model and altered antifungal susceptibility profiles. The tools presented here allowed for detailed

analyses of the genetic circuitry required for morphogenesis in the emerging pathogen *C. auris* and will serve as a resource to the community for future molecular genetic manipulation of this pathogen.

3.3 Results

3.3.1 *Agrobacterium*-mediated transformation identifies *C. auris* morphogenic mutants.

While aggregating and filamentous strains of *C. auris* have been recovered from human and murine hosts, the genetic circuitry governing *C. auris* morphogenesis remains largely uncharacterized. Therefore, we set out to apply a forward genetic approach to identify regulators of morphogenesis in *C. auris*. To accomplish this, we developed an *Agrobacterium tumefaciens*-mediated transformation (AtMT) system for *C. auris*. We cloned the CaNAT1 nourseothricin resistance cassette into the pPZP Ti plasmid backbone between the T-DNA left and right borders to generate pTO128 (pPZP-NATca) and transformed the resulting vector into *A. tumefaciens* strain EHA105, which also harbors the virulence genes necessary for mobilization of the T-DNA. We used representative *C. auris* clinical isolates from the FDA-CDC Antimicrobial Resistance Isolate Bank[229] to measure the transformation efficiency of AtMT in each of the four major *C. auris* clades (Fig. 3-1A). By comparing the number of recovered nourseothricin-resistant transformants to the number of input cells, we observed successful transformation in isolates from all four clades with variable transformation efficiency. Of the isolates tested, we observed the highest transformation efficiency in the Clade I isolate AR0382, with an average

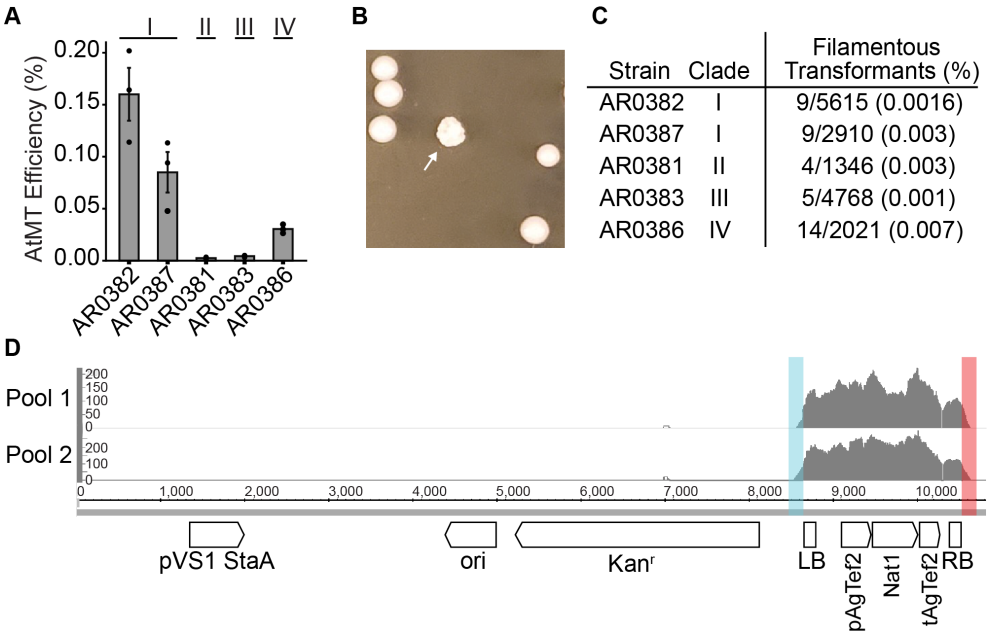

Figure 3-1 *Agrobacterium tumefaciens*-mediated transformation (AtMT) identifies regulators of colony morphology in *C. auris*. (A) AtMT transformation efficiency of *C. auris* was measured after 2, 4, and 7 days of coculture with three different combinations of *C. auris* to *A. tumefaciens* inocula. Maximum transformation efficiency is expressed as the ratio of recovered *C. auris* transformants to the total number of input *C. auris* cells. **(B, C)** Morphogenic mutants were identified in *C. auris* AtMT transformants through irregular colony morphologies (arrow). **(D)** Genomic DNA was extracted from 6 morphogenic mutants and pooled into two pools of 3 for Illumina sequencing. Reads were mapped to the TI Plasmid (pTO128). Highlighted regions in blue and red indicate read sequence that extended beyond the T-DNA left and right borders, respectively, used to identify transgene insertion sites in the *C. auris* genome.

efficiency of 0.16% (1 in 625 *C. auris* cells) (Fig. 3-1A). The Clade II isolate AR0381 showed the lowest transformation efficiency at 0.0025% (1 in 40,000 *C. auris* cells) under the same growth conditions, though even this rate is consistent with the range of transformation efficiencies exhibited in integrative AtMT of other yeast species (Fig. 3-1A)[230,231]. We visually screened recovered transformants for those with altered colony morphology, suggestive of an alteration in cellular morphology (Fig. 3-1B). In this manner, we identified morphological mutants in isolates from all four major clades. The rate at which we recovered morphological mutants differed significantly among the clades (Chi sq. = 22.42, $p = 1.66 \times 10^{-4}$), with the highest rate in the Clade IV isolate AR0386 (Fig. 3-1C). These findings demonstrate the utility of AtMT as a forward genetics system to discover mutant phenotypes in all four major clades of *C. auris*.

Transgene insertion sites can be defined by identifying the genomic regions flanking the insertions using whole-genome sequencing[232]. We reasoned a similar approach could identify transgene insertion sites from multiple mutants sequenced in pools. We mapped Illumina sequencing reads from two pools of three morphogenic mutants selected from AtMT of AR0382 (Clade I) to the sequence of the TI plasmid pTO128 (pPZP-NATca). The sequencing reads mapped exclusively to the T-DNA region of the plasmid, demonstrating the specificity of the integration, with additional read length spanning either junction at the T-DNA left and right borders (Fig. 3-1D). The sequence extending beyond the left and right borders corresponded to *C. auris* genomic regions flanking the transgene insertions. We deconvoluted the pools using standard PCR and Sanger sequencing with insertion site-specific primers.

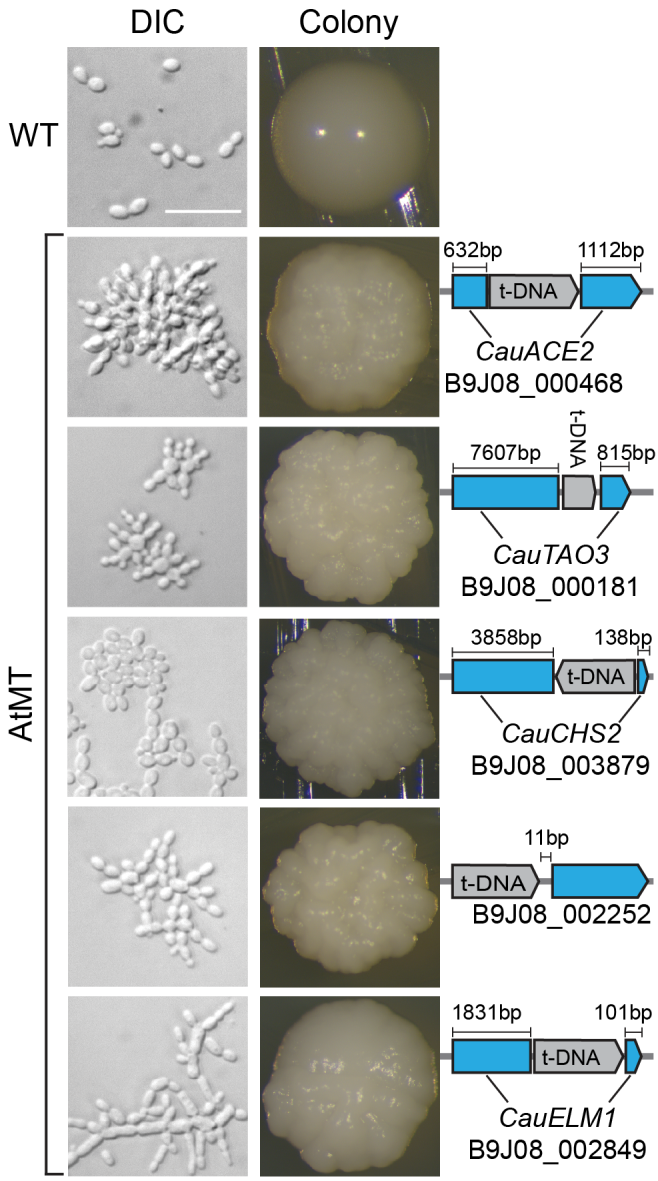

Figure 3-2 Transgene insertion sites associated with C. auris morphogenic mutants. Cell (DIC microscopy, Differential Interference Contrast) and colony morphologies demonstrate distinct morphogenic defects in five AtMT (*Agrobacterium tumefaciens*-mediated transformation) insertional mutants (bottom) compared to wild-type *C. auris* AR0382 (top). Identified transgene insertion sites were confirmed using Sanger sequencing (right). In all five cases, T-DNA insertion events were not accompanied by any additional insertions or deletions in the insertion locus. Scale bar = 20 μm.

Among the mutants identified by irregular colony morphologies, four exhibited a similar aggregating cellular phenotype, with

individual cells connected into clusters that could not be disrupted by vortexing (Fig. 3-2). Insertion events in *CauACE2* (B9J08_000468), orthologous to *S. cerevisiae ACE2* (YLR131C), as well as in *CauTAO3* (B9J08_000181), orthologous to *S. cerevisiae TAO3* (YIL129C), were associated with this aggregatory phenotype. A similar aggregating phenotype resulted from an insertion near the C-terminus of *CauCHS2* (B9J08_003879), an ortholog of *CHS2* (YBR038W) in *S. cerevisiae*. A fourth aggregating strain was associated with an insertion in the upstream region of *B9J08_002252*; however, orthologs of this gene in related species are poorly characterized. To predict a potential function for this gene, we analyzed the *C. albicans* ortholog *C7_00260C* using the CalCEN Co-expression network[233]. GO term analysis revealed that 43 of 50 co-expressed genes fall under the "piecemeal microautophagy of the nucleus" term (Fig. 3-3).

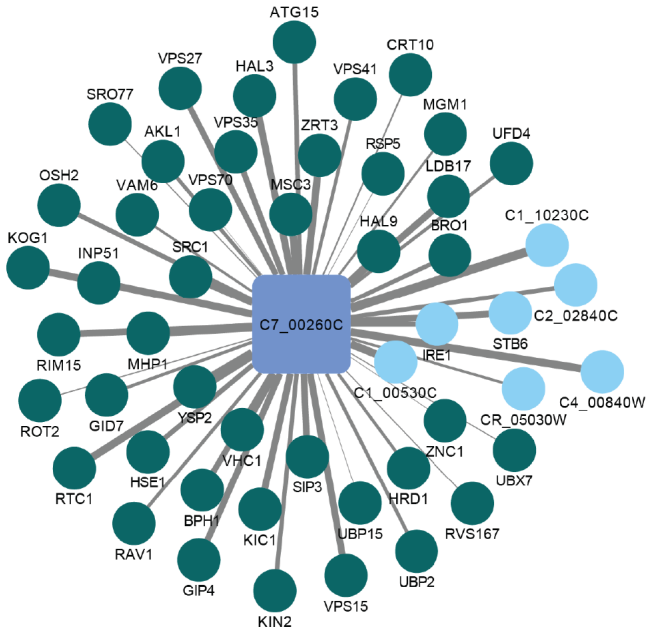

Figure 3-3 A *C. albicans* ortholog of B9J08_002252 is coexpressed with genes involved in piecemeal autophagy of the nucleus. For the *C. albicans* gene *C7_00260C*, a putative ortholog of the *C. auris* gene *B9J08_002252*, coexpressed genes were identified and analyzed for GO term association using the CalCEN coexpression network. Each node represents an individual gene and each edge corresponds to the relative degree of coexpression. 43 of 50 coexpressed genes fall under the "Piecemeal autophagy of the nucleus" GO term (dark green) and 7 fall under "GO term unknown, no annotation available" (light blue).

We also observed pseudohyphae-like filaments characterized by elongated cells with constricted separations between compartments in a mutant with an insertion in *CauELM1* (B9J08_002849), an ortholog of *S. cerevisiae ELM1* (YKL048C) (Fig. 3-2).

A sixth insertional mutant identified by its irregular colony morphology exhibited similar aggregating growth. For this mutant, we identified T-DNA sequence both in the intergenic space upstream of the B9J08_002954 ORF and in the intergenic

region upstream of the B9J08_002667 ORF from the B8441 reference sequence, but we were unable to amplify the complete insertion locus of either site from genomic DNA of the mutant. We hypothesize that a recombination event or other chromosomal rearrangement may have occurred following one or multiple T-DNA insertion events in this mutant, though further investigation is required to confirm this. Together, these findings identify key components of the regulation of cell separation in *C. auris*.

3.3.2 Expression of Cas9 and sgRNA increases targeted recombination in *C. auris*.

To validate the insertional mutagenesis and confirm the role of identified genes in regulating the multicellular phenotypes we observed, we sought to recapitulate the phenotypes via clean deletions of the target genes. However, targeted homologous recombination has low efficiency in *C. auris*, adding considerable technical challenge to performing genetic manipulation[218,220]. Transformation in *C. auris* can be facilitated by the use of Cas9 and sgRNA ribonucleoproteins; however, a previous DNA-based transient CRISPR-Cas9 expression approach used in *C. albicans* does not substantially improve targeted transformation efficacy in *C. auris* (Ref.[217] and personal communication, Sang Hu Kim). Recently, Ng and Dean reported variable increases in targeted transformation efficiency in *C. albicans* when using different promoters to drive the transcription of the sgRNA in a similar system[234]. We hypothesized that the low efficiency of the transient CRISPR system in *C. auris* may be due to poor recognition of the *SNR52* promoter from *C. albicans*. Therefore, we sought to develop a transient Cas9 and sgRNA expression system that can be used for efficient transformation in *C. auris*[223,234]. First, we generated expression cassettes for Cas9 and sgRNA using *C. auris*-specific promoters (Fig. 3-4A). We placed the Cas9 cassette, which has been codon-optimized for expression in CTG clade fungi, under control of the *C. auris ENO1* promoter and the sgRNA cassette under control of the *C.*

auris ADH1 promoter. However, because this RNA Polymerase II promoter would generate a transcript with a 5' cap and 3' polyA tail, ultimately detrimental to the gRNA targeting efficiency, we included the *C. auris tRNA-ALA* sequence immediately upstream of the sgRNA and the hepatitis delta virus (HDV) ribozyme sequence immediately downstream of the sgRNA.

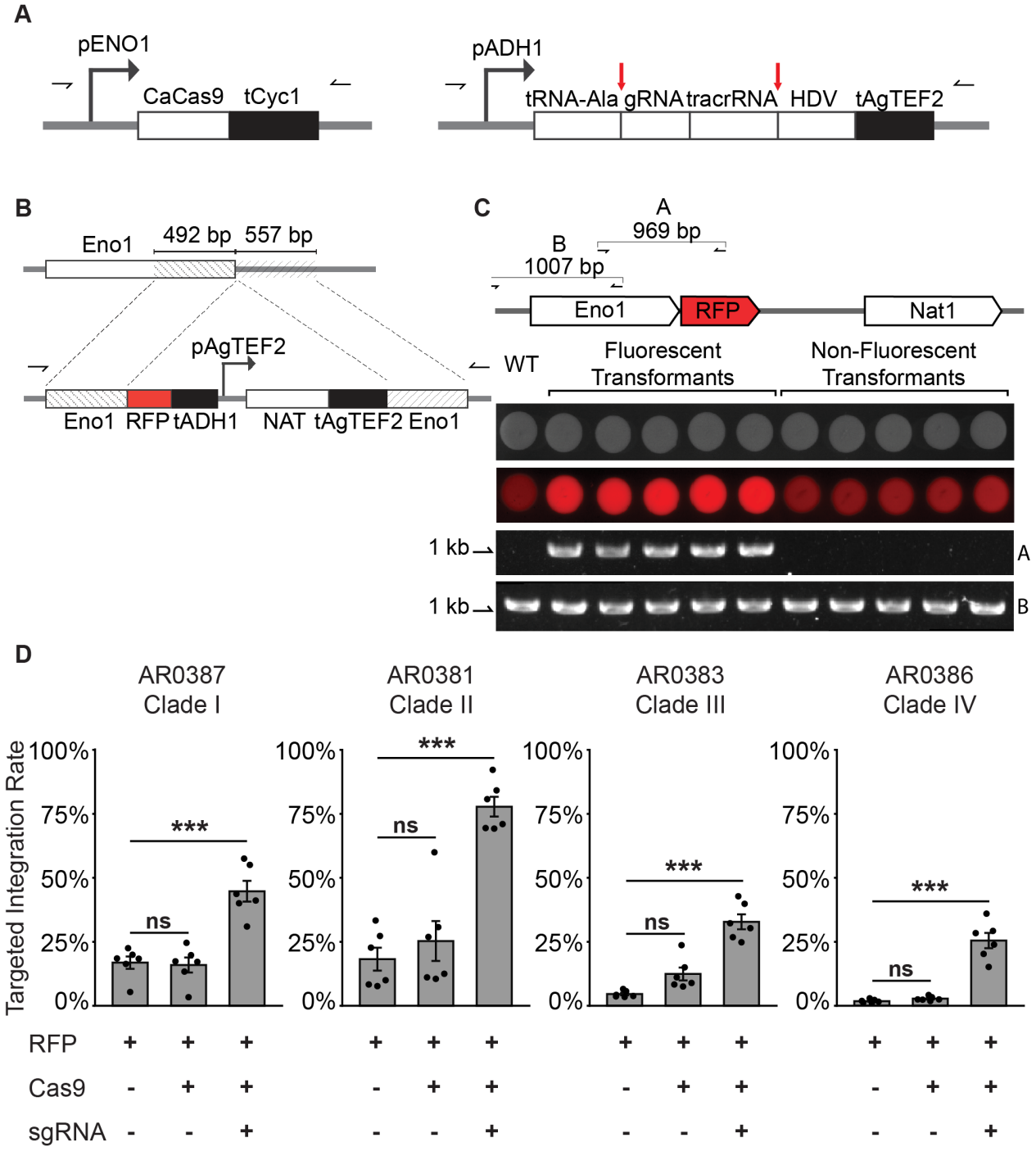

Figure 3-4 A CRISPR-Cas9 expression system promotes targeted transformation in four C. auris clades. **(A)** Structures of the Cas9 and sgRNA expression cassettes. *CAS9* is driven by the *C. auris ENO1* promoter and followed by the *CYC1* terminator. The sgRNA cassette is driven by the *C. auris ADH1* promoter and contains *C. auris* tRNA-Ala immediately upstream of the 20-bp gRNA sequence and hepatitis delta virus (HDV) ribozyme immediately downstream of the tracrRNA sequence. Predicted post-transcriptional cleavage sites are indicated by red vertical arrows. Primer sites to generate linear transformation cassettes are indicated by horizontal arrows. **(B)** Design of the reporter cassette for measuring targeted integration. The cassette is flanked by approximately 500-bp homology to the *C. auris ENO1* C-terminus minus the stop codon and the region immediately downstream of *C. auris ENO1*. *RFP* and the *C. auris ADH1* terminator tag the *ENO1* gene at the C-terminus via a glycine linker to generate *ENO1-RFP* in targeted transformants. An independently-driven nourseothricin resistance cassette (NAT) allows identification of total transformants, regardless of integration site, by selection with nourseothricin. **(C)** Targeted integration events are identifiable by colony fluorescence. Transformation of AR0387 was performed using the reporter cassette described in panel (B). Representative fluorescent transformants and non-fluorescent transformants were spotted onto YPD. Primer set A, spanning the *ENO1-RFP* junction, shows amplification only from fluorescent transformants. Primer set B, spanning a neighboring wild-type locus, shows amplification from all transformants and the wild type. **(D)** Expression of Cas9 and sgRNA promotes targeted integration rate. Transformation was performed in representative isolates from all four major *C. auris* clades with the linear transformation cassettes described in panels (A) and (B). Transformations were performed with and without Cas9 and sgRNA elements; when absent, the cassettes were replaced with an equivalent volume of buffer. Targeted integration rate is expressed as the ratio of fluorescent colonies recovered to total nourseothricin resistant colonies recovered. Each point represents an individual transformation. Shown are the mean ± standard error of the mean from three individual experiments, each performed in duplicate. Statistical differences were determined using one-way ANOVA with Tukey's post hoc test for multiple comparisons: AR0387: ***: $p = 5.4 \times 10^{-5}$, ns: $p = 0.98$; AR0381: ***, $p = 5.8 \times 10^{-6}$, ns: $p = 0.66$; AR0383: ***: $p = 6.0 \times 10^{-7}$, ns: $p = 0.063$; AR0386: ***, $p = 3.0 \times 10^{-7}$, ns: $p = 0.92$.

With this design, we anticipated cleavage at the 3' end of the tRNA sequence by endogenous RNase A and self-catalyzed cleavage at the 5' end of the HDV ribozyme[235,236].

To assess the functional capacity of the Cas9 and sgRNA expression system to increase the efficiency of targeted integration in *C. auris*, we designed a reporter cassette that would allow for rapid and specific identification of targeted integration events (Fig. 3-4B). The reporter cassette contained approximately 500 bp of homology to the C-terminus of *C. auris ENO1* and genomic sequence immediately downstream of *ENO1*. We removed the stop codon from the *ENO1* C-terminus homologous sequence and fused *RFP* to the *ENO1* C-terminus with a glycine linker. Because the *RFP* gene had no promoter element, we anticipated transformants would only demonstrate robust fluorescence if the reporter cassette integrated precisely in frame to tag the Eno1 protein and be driven by the endogenous *ENO1* promoter. The reporter cassette also included an independently-driven nourseothricin resistance (NAT) cassette to allow

identification of the total transformant population by selection on nourseothricin, regardless of integration site. To confirm that the reporter cassette specifically identified targeted integration events, we designed a PCR primer set spanning the *ENO1-RFP* junction and a primer set spanning a region of the *ENO1* locus native to the wild type. We performed transformation with the reporter cassette and recovered a representative sample of nourseothricin-resistant transformants that were either fluorescent or non-fluorescent. Amplification of the region spanning the *ENO1-RFP* junction was only exhibited by the fluorescent transformants and not by the wild type or non-fluorescent transformants, while amplification of the wild-type sequence was exhibited by all the transformants and the wild-type strain (Fig. 3-4C). This demonstrates that the ratio of fluorescent to non-fluorescent colonies is a reliable measure of the efficiency of targeted integration.

We observed variable targeted transformation efficiency among *C. auris* isolates of different genetic backgrounds (Fig. 3-4D). We therefore sought to determine whether the Cas9 and sgRNA expression system promoted targeted transformation in multiple genetically diverse *C. auris* isolates (Fig. 3-4D). The targeted integration rate under each transformation condition was determined by dividing the number of fluorescent colonies by the total number of nourseothricin-resistant transformant colonies. For AR0387, a Clade I isolate, inclusion of the Cas9 and sgRNA expression cassettes increased the targeted integration rate to 44.7% of transformants from an average of 16.9% using only the reporter cassette. We observed similar trends for isolates from each clade. Targeted integration increased from 18.2% to 77.8% in AR0381 (Clade II), from 4.6% to 32.8% in AR0383 (Clade III), and from 1.8% to 25.5% in AR0386 (Clade IV) with the addition of the Cas9 and sgRNA expression cassettes compared to the reporter cassette alone (Fig. 3-4D). The *ENO1* C-terminus homologous arm encoded by the

reporter cassette showed 100% sequence identity in all four isolates, while AR0381 and AR0383 shared 4 nucleotide variants out of 557 bp in the downstream homologous arm and AR0386 showed a single nucleotide variant in the same region. Therefore, differences in the targeted integration efficiency could not be explained by differential homology to the reporter cassette. Moreover, we were unable to detect integration of the *CAS9* cassette in a majority of recovered fluorescent transformants across all four clades (Fig. 3-5), suggesting the Cas9 system is transient as designed, with rare integration events, consistent with previous observations from a similar system in *C. albicans*[223]. Taken together, these observations indicate the Cas9 and sgRNA expression cassettes successfully promote targeted transformation in all four major *C. auris* clades.

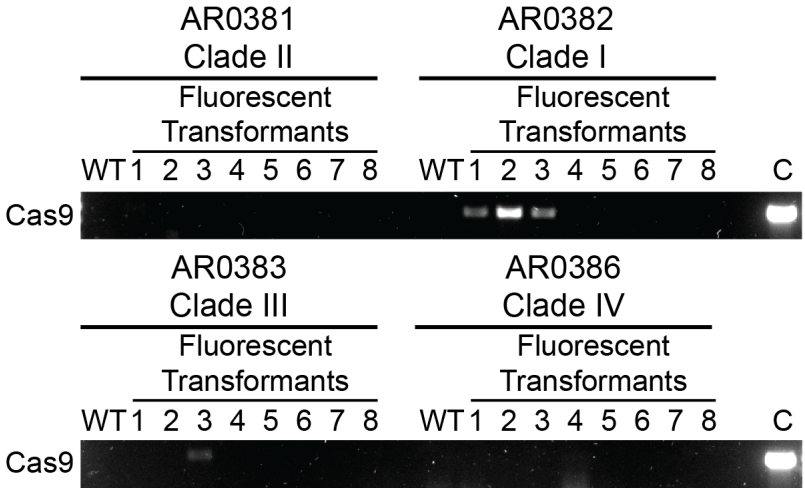

Figure 3-5 Detection of integration of the Cas9 expression cassette in *C. auris* following transformation. Transformation was performed in *C. auris* isolates from each of the four major clades using the Cas9 and sgRNA expression cassettes and the Eno1-RFP reporter cassette. Eight representative transformants were recovered from among those that exhibited robust fluorescence, indicating targeted integration, for each isolate. Detection of stable integration of *CAS9* was measured using PCR primers specific to the *CAS9* expression cassette. C: pTO135 was used as template in this reaction.

3.3.3 Ace2 and Tao3 are regulators of *C. auris* morphogenesis.

Using these tools, we were able to investigate the function of the genes implicated in *C. auris* morphogenic regulation by AtMT. Deletion of *ACE2* or *TAO3* in AR0382 (Clade I) resulted in constitutively aggregating cells with individual cells connected at septa, suggestive of a failure of budding daughter cells to separate from mother cells (Fig. 3-6A). We then codon-optimized a G418 resistance gene for CTG-clade expression and found its expression allowed for selection of

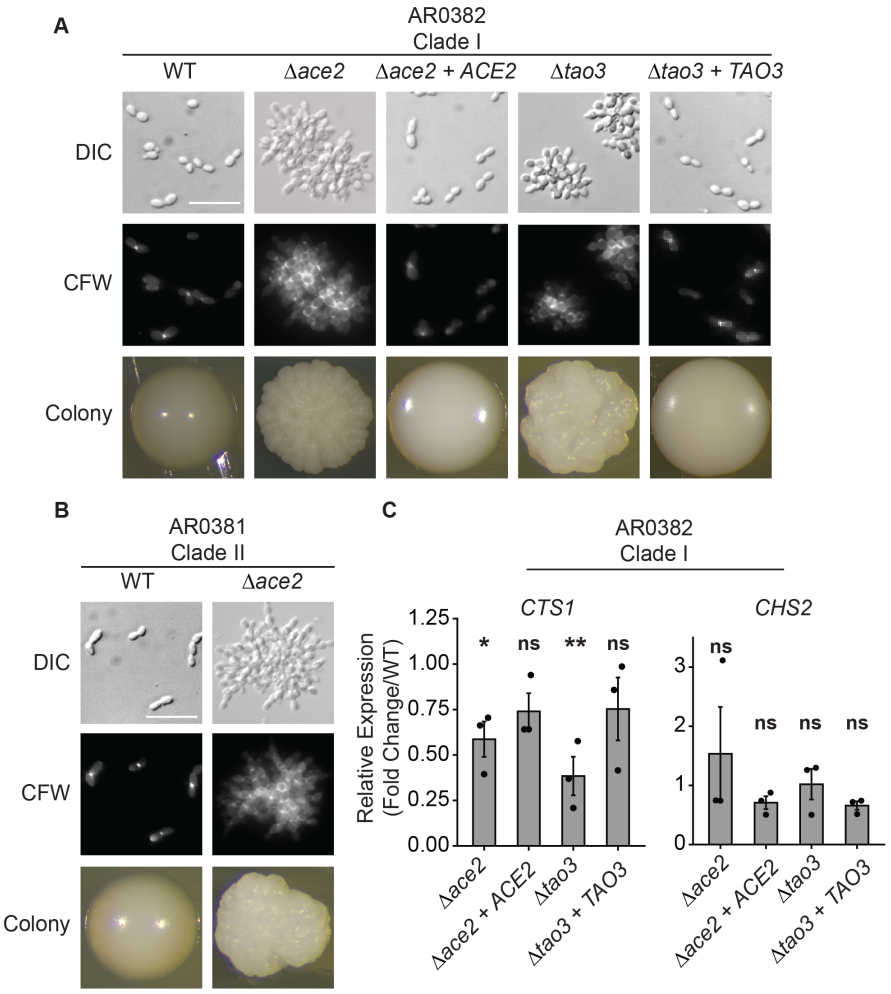

Figure 3-6 Ace2 and Tao3 are regulators of *C. auris* morphogenesis. (A) Microscopy of *Δace2*, *Δtao3*, and complemented strains in the AR0382 (Clade I) genetic background. Representative images shown for DIC (Differential Interference Contrast), cells stained with calcofluor white (CFW), and colonies formed on YPD agar. Scale bar = 20 µm **(B)** *ACE2* regulates morphogenesis across *C. auris* clades. Microscopy of *Δace2* and in the AR0381 (Clade II) genetic background. Representative images shown for DIC, cells stained with calcofluor white, and colonies formed on YPD agar. Scale bar = 20 µm **(C)** *ACE2* and *TAO3* regulate putative chitinase *CTS1* but not *CHS2* transcription. Wild-type (AR0382), *Δace2*, *Δtao3*, and complemented strains were grown to exponential phase in YPD at 30°C prior to RNA extraction and RT-qPCR analysis of upregulated and downregulated genes. Shown are the relative expression of *CTS1* and *CHS2* for each mutant strain compared to the wild type and normalized to *ACT1* gene expression. Mean ± standard error of the mean from three biological replicates, each with three technical replicates. Strains that showed significantly different expression compared to the wild type are indicated. Statistical differences were determined using one-way ANOVA with Dunnett's post hoc test for multiple comparisons. *CTS1*: *Δace2,* *: p = 0.046; *Δace2 + ACE2*, ns: p = 0.25; *Δtao3,* **: p = 0.004; *Δtao3 + TAO3*, ns: p = 0.32. *CHS2*: *Δace2,* ns: p = 0.87; *Δace2 + ACE2*, ns: p = 0.60; *Δtao3,* ns: p = 0.93; *Δtao3 + TAO3*, ns: p = 0.10.

C. auris on media containing 1 mg/L G418. Using this new dominant selectable marker, we were able to complement *Δace2* and *Δtao3* mutants with reconstituted versions of the deleted genes replaced in the endogenous loci. The complemented strains *Δace2 + ACE2* and *Δtao3 + TAO3* restored the wild type cellular and colony morphologies (Fig. 3-6A). In *S. cerevisiae*, Tao3 associates with kinases Kic1 and Cbk1 as part of the Regulation of *ACE2* Morphogenesis (RAM) pathway. Phosphorylation of Ace2 by Cbk1 results in its

accumulation in daughter cell nuclei, where it regulates the expression of enzymes that mediate septum degradation[181]. Mutations in *ACE2* or upstream components of the RAM pathway in *S. cerevisiae* or in *C. albicans* result in a aggregating, multicellular phenotypes similar to those exhibited by *C. auris Δace2* and *Δtao3* mutants, suggesting that *C. auris* has maintained conservation of the RAM pathway in regulating morphogenesis[171,237,238]. An *Δace2* mutant in AR0381 (Clade II) showed a similar aggregating phenotype, suggesting this role is conserved across *C. auris* clades as well (Fig. 3-6B). To assess whether the regulation of cell wall maintenance genes was also conserved in *C. auris,* we investigated the transcriptional change in the chitinase gene *CTS1* (B9J08_002761), which is homologous to a key enzyme regulated by Ace2 and responsible for the degradation of the primary septum during daughter cell separation in *S. cerevisiae*[182]. We observed significant downregulation of *CTS1* expression in *Δace2* and *Δtao3* mutants compared to wild type AR0382, while *Δace2 + ACE2* and *Δtao3 + TAO3* mutants showed no significant change in *CTS1* expression (Fig. 3-6C). Because our forward genetics screen suggested disruption of the chitin synthase gene *CHS2* could also confer an aggregating phenotype, we asked whether *CHS2* expression was altered by deletion of *ACE2* or *TAO3.* However, we observed no significant difference in the expression of *CHS2* in *Δace2* or *Δtao3* mutants compared to the wild type (Fig. 3-6C). Together, these findings demonstrate that *ACE2* and *TAO3* are key regulators of *C. auris* morphogenesis and deletion of either leads to an aggregating phenotype associated with decreased expression of the chitinase gene *CTS1*.

3.3.4 Elm1 is a regulator of *C. auris* filamentous growth.

Next we investigated *ELM1,* disruption of which resulted in both an aggregating and elongated cellular phenotype in our AtMT screen. Deletion of *ELM1* in AR0382 (Clade I) resulted in a polarized growth phenotype resembling filaments (Fig. 3-7A). Individual cells remained

conjoined at invaginated junctions, forming elongated compartments with similar widths to the wild type yeast cells. Complementation with the wild type *ELM1* gene restored the wild type budding yeast morphology (Fig. 3-6A). Deletion of *ELM1* in AR0381 (Clade II) resulted in a similar phenotype as deletion in AR0381 (Clade I), suggesting that its role in regulating polarized growth is conserved across clades (Fig. 3-7B).

Because filamentous growth has

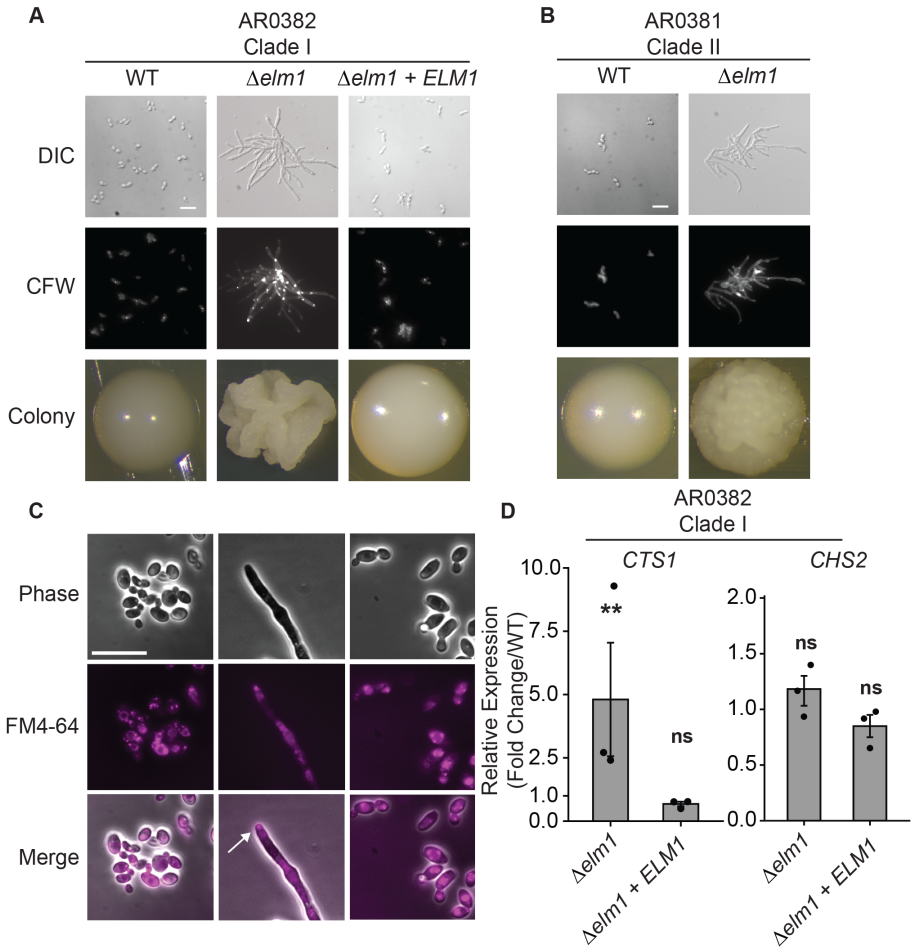

Figure 3-7 Elm1 is a regulator of *C. auris* filamentous growth. (A) Microscopy of wild type AR0382, *Δelm1,* and complemented *Δelm1 + ELM1* strains. DIC (Differential Interference Contrast), cells stained with calcofluor white (CFW), and colonies formed on YPD agar are shown. Scale bar = 10 µm. **(B)** *ELM1* regulates filamentous growth across *C. auris* clades. Microscopy of DIC, cells stained with calcofluor white, and colonies formed on YPD agar for wild type AR0381 (Clade II) and *Δelm1* in the AR0381 background. Scale bar = 10 um. **(C)** *C. auris Δelm1* filaments form a Spitzenkörper-like structure at the filament apex. AR0382 (Clade I) wild type, *Δelm1*, and *Δelm1 + ELM1* strains shown with phase contrast microscopy, stained with the lipophilic dye FM 4-64. Arrow indicates the location of a putative Spitzenkörper where dye has accumulated at the growing filament tip. Scale bar = 10 µm. **(D)** *ELM1* negatively regulates *CTS1* but not *CHS2* expression. Wild-type (AR0382), *Δelm1*, and *Δelm1 + ELM1* were grown to exponential phase in YPD at 30 °C prior to RNA extraction and RT-qPCR analysis of upregulated and downregulated genes. Shown are the relative expression of *CTS1* and *CHS2* for each mutant strain compared to the wild type and normalized to *ACT1* gene expression. Mean ± standard error of the mean from three biological replicates, each with three technical replicates. Strains that showed significantly different expression compared to the wild type are indicated. Statistical differences were determined using one-way ANOVA with Dunnett's post hoc test for multiple comparisons. *CTS1*: *Δelm1,* **: p = 0.0014; *Δelm1 + ELM1*, ns: p = 0.35. *CHS2*: *Δelm1,* ns: p = 0.98; *Δelm1 + ELM1*, ns: p = 0.24.

not been shown to be a natural phenotype in *C. auris*, we asked whether the filamentous growth exhibited by *Δelm1 C. auris* was driven by mechanisms consistent with natural filamentous growth in other fungal species. Maintenance of filamentous growth in other fungal species is achieved through the formation of a Spitzenkörper, a complex of vesicles that coordinates cell wall synthetic enzymes and actin cytoskeleton and related proteins at the apical tip of the growing filament[239]. We observed a structure at the apex of the growing *Δelm1* cells that took up the lipophilic dye FM 4-64, consistent with the formation of a Spitzenkörper (Fig. 3-7C). This structure appeared to be unique to the filamentous form of AR0382, as no similar polar structure was observed in the budding yeast wild type or *Δelm1 + ELM1* strains (Fig. 3-7C).

We next investigated whether the conjoined cell phenotype in AR0382 *Δelm1* was associated with alterations in *CTS1* or *CHS2* regulation like the aggregating mutants. We found the chitinase gene *CTS1* to be significantly upregulated in *Δelm1* compared to wild type AR0382, while the chitin synthase gene *CHS2* was not significantly differentially expressed (Fig. 3-7D). The complemented strain *Δelm1 + ELM1* showed no significant variation in the expression of *CTS1* or *CHS2* compared to wild type AR0382 (Fig. 3-7D). Together, these findings implicate *ELM1* as a regulator of *C. auris* pseudohyphal growth.

3.3.5 *C. auris* morphogenic mutants exhibit attenuated virulence and altered antifungal susceptibility.

Reports of *C. auris* isolates that exhibit aggregating or elongated cell morphologies have largely suggested these morphogenic variants show reduced virulence in infection models compared to budding yeast wild type isolates[169,184,219]. We therefore investigated the pathogenic potential of the *Δace2, Δtao3,* and *Δelm1* mutants in a *Galleria mellonella* model of infection. The *Δelm1* strain exhibited the strongest attenuation of virulence compared to the parental AR0382 strain,

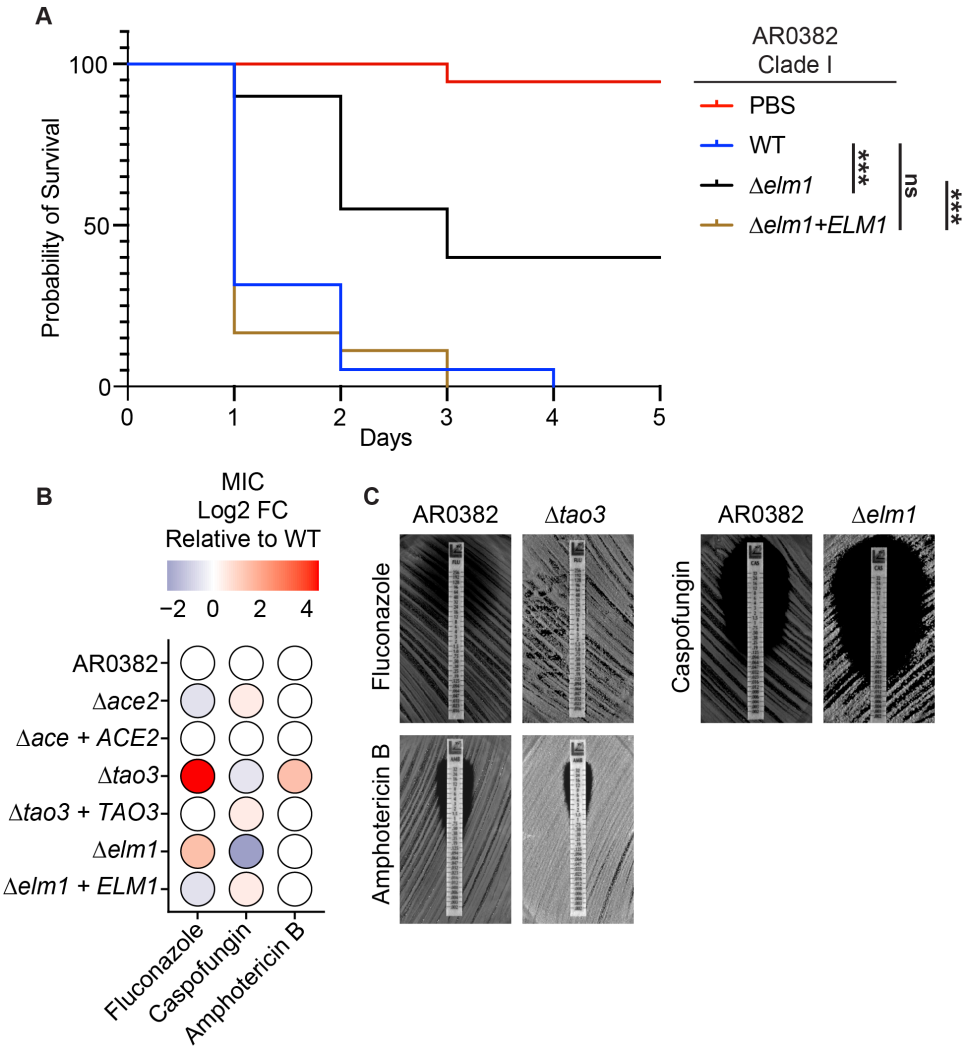

Figure 3-8 *C. auris* morphogenic mutants show attenuated virulence and altered antifungal susceptibility. (A) Wild type AR0382 (Clade I), *Δelm1*, and *Δelm1 + ELM1* strains in the AR0382 background were standardized to an optical density of OD_{600} = 1.0 in PBS before inoculating 20 *Galleria mellonella* larvae per *C. auris* strain with 50 µL of prepared inoculum. Larvae were maintained at 37 °C and monitored daily for survival for 5 days. Statistical differences were determined using a Mantel-Cox log rank test. WT-*Δelm1*, ***: $p < 0.0001$; WT-*Δelm1 + ELM1*, ns: $p = 0.51$; *Δelm1*-*Δelm1 + ELM1,* ***: $p < 0.0001$ **(B)** Gradient MIC test strips were used to determine the susceptibility of wild type AR0382, morphogenic mutants, and complemented strains in the AR0382 background to fluconazole, caspofungin, and amphotericin B. The color and intensity of each point corresponds to the Log_2 fold change in MIC for each strain relative to the wild type. A complete list of MICs is available in Table 3-1. **(C)** MIC test strips with zones of inhibition for mutants with substantially altered antifungal susceptibilities. *Δtao3* exhibited reduced susceptibility to fluconazole and amphotericin B compared to the wild type. *Δelm1* exhibited increased susceptibility to caspofungin.

with mortality rates recapitulating wild type levels in the complemented *Δelm1 + ELM1* strain (Fig. 3-8A). The *Δtao3* mutant did not exhibit significantly attenuated virulence compared to the parental AR0382 ($p = 0.0563$, Log-rank Mantel-cox test), but the *Δace2* mutant showed a modest decrease in virulence (Fig. 3-9). Complemented

strains encoding *ACE2* or *TAO3* genes showed similar mortality profiles to wild type AR0382 (Fig. 3-9).

We also investigated whether mutations in *ACE2, TAO3, or ELM1* were associated with altered antifungal susceptibility profiles. While the *Δace2* mutant did not exhibit a large difference in susceptibility to fluconazole, caspofungin, or amphotericin B compared to wild type AR0382, the *Δtao3* and *Δelm1* mutants showed differential susceptibility profiles (Fig. 3-8B). The *Δtao3* mutant exhibited reduced sensitivity to fluconazole (MIC >256 mg/L compared to 12 mg/L for WT AR0382) and amphotericin B (MIC 1mg/L compared to 0.38 mg/L for WT AR0382) (Fig. 3-8C). The *Δelm1* mutant exhibited increased sensitivity to caspofungin (MIC 0.023 mg/L compared to 0.094 mg/L for WT AR0382) (Fig. 3-8C). In general, the complemented strains closely mimicked the susceptibility profile of the wild type (Fig. 3-8B). A complete list of MICs for each strain against fluconazole, caspofungin, and amphotericin B is available in Table 3-1. Together, these findings demonstrate

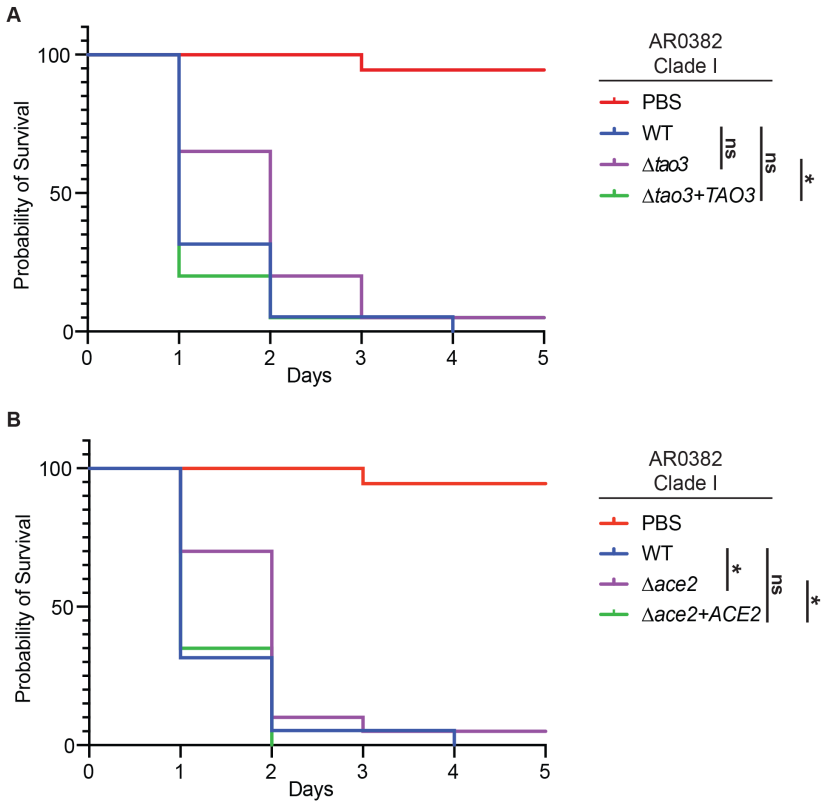

Figure 3-9 *C. auris* morphogenic mutants virulence profiles in *G. mellonella* infection model. Wild type AR0382 (Clade I), *Δtao3* and *Δtao3 + TAO3* strains **(A)** or *Δace2* and *Δace2 + ACE2* strains **(B)** in the AR0382 background were standardized to an optical density of OD_{600} = 1.0 in PBS before inoculating 20 *Galleria mellonella* larvae per *C. auris* strain with 50 µL of prepared inoculum. Larvae were maintained at 37 °C and monitored daily for survival for 5 days. Statistical differences were determined between survival curves using a Mantel-Cox log-rank test: (A) WT- *Δtao3*, ns: p = 0.0563; WT-*Δtao3 + TAO3,* ns: p = 0.7899; *Δtao3-Δtao3 + TAO3*, *: p = 0.0275 (B) WT-*Δace2*, *: p = 0.0427; WT-*Δace2 + ACE2,* ns: p = 0.8962; *Δace2-Δace2 + ACE2,* *: p = 0.0158.

mutations in *C. auris ACE2, TAO3,* and *ELM1* are associated with altered virulence and antifungal susceptibility profiles in addition to altered morphogenesis.

	MIC (mg/L)		
	Fluconazole	Caspofungin	Amphotericin B
AR0382	12	0.094	0.38
Δace2	8	0.125	0.38
Δace2 + ACE2	12	0.094	0.38
Δtao3	>256	0.064	1
Δtao3 + TAO3	12	0.125	0.38
Δelm1	32	0.023	0.38
Δelm1 + ELM1	8	0.125	0.38

Table 3-1 MIC values for AR0382, morphogenic mutants, and complemented strains.

3.4 Conclusions

We have developed approaches to performing facile, cost-effective forward and reverse genetic manipulation in *C. auris*. Using these tools, we identified functional conservation of chitinase regulatory pathways, disruption of which results in aggregating, multicellular growth in *C. auris*. We also uncovered a *C. auris* filamentous mutant, *Δelm1*, demonstrating the ability of *C. auris* to sustain filamentous growth. Our work represents part of a growing global effort to understand the biology of this emerging pathogen by offering alternative methods of improving its genetic tractability. We demonstrated the utility of AtMT for performing insertional mutagenesis in all four major *C. auris* clades without any prior engineering of the *C. auris* strain. We also demonstrated the ability of a *C. auris* CRISPR-Cas9 expression system to consistently and significantly improve targeted integration of a transformation cassette in representative isolates from all four major *C. auris* clades. Targeted integration rates were increased to levels at which mutants of interest can readily be identified by PCR or phenotypic screening. While this level of efficiency was associated with approximately 500 bp arms of homology, we successfully performed deletion of *TAO3* using a transformation cassette with only 50-70 bp of homology,

albeit with reduced targeted transformation efficiency. Furthermore, we developed a new, codon-optimized G418 selectable marker for use in *C. auris*. Our work, in concert with similar advancements such as successful resistance marker recycling and piggyBac genome-wide transposon mutagenesis in *C. auris*[219,222,240], will promote improved accessibility to mechanistic understanding of the genetic machinery in *C. auris*.

From our work, we identified *CauACE2* to be a key regulator of morphogenesis. In *S. cerevisiae*, *ACE2* daughter cell nuclear localization is regulated by the RAM pathway Kic1-Cbk1 kinase complex[181]. *ScTAO3*, sometimes called *PAG1*, physically associates with both *Sc*Kic1 and *Sc*Cbk1 and may mediate activation of Cbk1 by Kic1[183,241]. Disruption of *ScTAO3* or downstream *ScACE2* results in cellular aggregates and a failure of daughter cells to separate from mother cells during budding[182,183,241]. We observed similar aggregating phenotypes in *Δace2* and *Δtao3* mutants in *C. auris*. We therefore propose functional conservation of *ACE2* and the RAM regulatory pathway in *C. auris*. Downstream of this pathway, we identified a putative chitinase, *CauCTS1* (B9J08_002761), that was downregulated in *ΔCauace2* and *ΔCautao3* compared to the wild type. The sequence of *CauCTS1* contains no GPI-anchor signal sequence, and so is likely more closely related functionally to the secreted chitinases *ScCTS1* in *S. cerevisiae* and its functional homolog *CaCHT3* in *C. albicans* than to *CaCHT2* in *C. albicans*[242]. The regulation of *CauCTS1* by *CauACE2* is consistent with homologous pathways in *S. cerevisiae* and *C. albicans*, in which chitin degradation in the primary septum is mediated by the *ACE2*-regulated *Sc*Cts1 or *Ca*Cht3 proteins[237,243]. Interestingly, an experiment performing laboratory evolution of *S. cerevisiae* in a bioreactor resulted in multicellular, fast-sedimenting strains that were associated with mutations in *ACE2*[171]. The design of the bioreactors in this example may have provided a selective advantage for multicellular growth due to increased

sedimentation rate of cell aggregates compared to planktonic cells. An environmental niche may exist that produces a similar selective pressure against the regulatory network upstream of *CTS1* by offering a selective advantage for aggregating cells. Constitutively aggregating strains of *C. auris* have been isolated from clinical samples[101,169,186,202]. Based on publicly available RNA-seq data investigating this natural aggregating phenotype, we found that one such aggregating *C. auris* isolate exhibited significantly downregulated expression of *CTS1* compared to a non-aggregating counterpart when grown planktonically ($log_2FC = -1.3221$, $p = 6e\text{-}13$)[186]. This observation is consistent with the mechanism of aggregation observed in the *Δace2* and *Δtao3* mutants, though we could not find evidence based on the RNA-seq data that the change in *CTS1* regulation of the natural aggregating isolate was directly related to the RAM pathway. Further characterization of the environmental reservoirs for *C. auris* may offer additional insight regarding the selective pressures driving similar phenotypes.

While the role of the serine-threonine kinase *ELM1* in regulating polar bud growth and morphogenic differentiation in *S. cerevisiae* has been long understood, its role in pathogenic fungi is largely unexplored[244,245]. One report demonstrated that deletion of *CgELM1* in *C. glabrata* results in moderately elongated cell growth, though this strain fails to recapitulate the fully pseudohyphal phenotype exhibited by *S. cerevisiae* or *C. auris*[246]. We observed elongated cells growing in pseudohyphal chains associated with an insertion event near the C-terminus of *CauELM1*. However, the full *Δelm1 C. auris* strains exhibited a more filamentous cell morphology. This discrepancy in cell morphologies between insertional disruption and clean deletion of *elm1* in *C. auris* may be explained by similar observations in *S. cerevisiae*. In *S. cerevisiae*, deletion of the C-terminal domain (aa 421-640 of 640) of *ELM1* results in increased Elm1 kinase activity, suggesting this domain may have autoinhibitory functions[247]. This

phenotype is associated with pseudohyphal growth with a cell morphology distinct from that demonstrated by *ΔScelm1*[247]. The distinct but similarly pseudohyphal phenotypes associated with the *C. auris ELM1* insertional mutant encoding a T-DNA insertion 101 base-pairs upstream of the *ELM1* C-terminus, but putatively encoding an intact kinase domain, and *ΔCauelm1* suggests similar *ELM1* regulation may exist in *C. auris*, though the extent to which the *ELM1* protein structure is altered for the insertion mutant is unclear. Intriguingly, the filamentous *Δelm1 C. auris* mutant exhibited a significant increase in the expression of the chitinase gene *CTS1* compared to the wild type. This is in contrast to *Δelm1* in *C. glabrata*, which exhibited decreased expression of *CgCTS1* compared to wild type[246]. Further characterization of Elm1 in diverse fungal species may yet reveal substantial variation in its function. The role that increased *CTS1* expression in *ΔCauelm1* plays in contributing to filamentous growth is unclear. One report indicated reduced expression of the *CTS1* homolog *CaCHT3* in hyphal *C. albicans* compared to *C. albicans* grown in the yeast form[248]. However, total chitinase activity was increased in *C. albicans* hyphae compared to yeast[249]. Whether *C. auris* filamentous growth is controlled by a similar chitinase function as *C. albicans* hyphal growth remains to be determined.

In phenotypic analysis, we observed alterations in virulence for the morphogenic mutants, consistent with other published reports[169,184,219]. We were also interested to observe altered antifungal susceptibility profiles associated with these mutants which may hint at larger roles for the genes of interest. In particular, the *Δtao3* mutant showed markedly reduced susceptibility to fluconazole and amphotericin B that appeared to be independent of *ACE2*, as the *Δace2* mutant did not show the same altered susceptibilities. The resistance to fluconazole conferred by deletion of *TAO3* may indicate the *C. auris* RAM pathway upstream of *ACE2* has divergent regulatory roles from the same pathway in *C. albicans*, mutation of which confers

hypersensitivity to fluconazole[250]. Similarly, *C. albicans ace2Δ/ace2Δ* cells exhibit increased resistance to fluconazole that was not observed for *C. auris Δace2* cells[251]. While the full mechanistic contribution of the *C. auris* RAM pathway to antifungal susceptibility remains unclear, these observations highlight the possibility of regulatory network rewiring in *C. auris* and the importance of specifically investigating how *C. auris* has adapted regulatory pathways that may have well-established mechanisms in related model fungal species.

In sum, our work demonstrates an accessible approach to genetic engineering of *C. auris*, facilitating further understanding of the biology of this emerging pathogen. Using new forward and reverse genetic approaches, we characterized conserved and divergent key regulators of morphogenesis, virulence, and antifungal resistance in *C. auris*.

3.5 Methods

3.5.1 Strains and growth conditions

A list of *C. auris* and *A. tumefaciens* strains used in this study are listed in Table 3-2. Unless specified otherwise, *C. auris* cells were grown at 30°C in YPD liquid media (1% yeast extract, 2% peptone, 2% dextrose) with constant agitation. All strains were maintained in frozen stocks of 25% glycerol at -80°C.

3.5.2 Plasmids

A list of all plasmids used in this study is included in Table 3-3. Constructs and sequences for pTO128, pTO135, pTO136, and pTO149 are available through Addgene (Watertown, MA, USA) under catalog #171105, #171103, #171104, and #177277.

A list of all primers used in this study is included in Table 3-4.

pTO128: An *Agrobacterium* Ti-plamid was constructed to include the CaNAT1 nourseothricin resistance cassette[252] in the pPZP-NEO1 backbone[253]. The CaNAT1 cassette was excised at the SacI and SalI restriction sites from pLC49[254] and ligated between the SacI and SalI restriction sites of pPZP-NEO1, replacing the G418 resistance cassette with CaNAT1 to form pTO128 (pPZP-NATca). pTO128 was subsequently electroporated into *A. tumefaciens* strain EHA 105[255] using a Bio-Rad MicroPulser Electroporator.

All other transformation cassettes were maintained in the multiple cloning site of the pUC19 cloning vector[256] and assembled from fragments as described below using the NEBuilder HIFI DNA Assembly master mix (NEB #E2621) according to the manufacturer's instructions.

pTO135: To assemble pTO135 (pCauCas9), the Cas9 expression cassette minus the promoter sequence was PCR amplified from pLC963[257] using primers oTO114-oTO115. A promoter region consisting of 1000 bp upstream of the *C. auris ENO1* gene (B9J08_000274) was PCR amplified from genomic DNA isolated from *C. auris* strain AR0387 using primers oTO112-oTO113. The pUC19 vector backbone was amplified using primers oTO116-oTO117.

pTO136: To assemble pTO136 (pCausgRNA), a promoter region consisting of 901 bp upstream of the *C. auris ADH1* gene (B9J08_004331) was PCR amplified using primers oTO118-oTO119 and assembled along with a synthesized DNA fragment (Genscript, Piscataway, NJ, USA) containing sequence from *C. auris* tRNA-Ala (B9J08_003096), a 20-bp gRNA sequence targeting the *ENO1* locus, a tracrRNA sequence, and an HDV ribozyme[234]. The pUC19 vector backbone was amplified using primers oTO120-oTO121.

pTO137: To assemble pTO137, containing the *ENO1-RFP* reporter cassette, the *RFP* construct was PCR amplified from pLC1047[258] using primers oTO124-oTO125; a terminator sequence consisting of 933 bp downstream of the *C. auris ADH1* gene was PCR amplified from *C. auris*

AR0387 genomic DNA using primers oTO126-oTO127; the CaNAT1 expression cassette including *TEF* promoter and terminator sequence was amplified from pLC49 using primers oTO128-oTO129; flanking regions containing homology to 492 bp at the C-terminal end of the *C. auris ENO1* gene minus the stop codon and 557 bp immediately 3' of the *C. auris ENO1* gene were amplified from genomic DNA isolated from *C. auris* strain AR0387 genomic DNA using primers oTO122-oTO123 and oTO130-oTO131 respectively; the pUC19 vector backbone was amplified using primers oTO132-oTO133.

pTO154: To assemble pTO154 (p*ELM1::NAT*), 501 bp immediately 5' of *ELM1* (B9J08_002849) and 502 bp immediately 3' of *ELM1* were amplified from AR0387 genomic DNA using primers oTO317-oTO318 and oTO321-oTO337 respectively; the *CaNAT1* expression cassette was amplified from pLC49 using primers oTO319-oTO320; the pUC19 vector backbone was amplified using primers oTO323-oTO324.

pTO155: To assemble pTO155 (p*ACE2::NAT)*, 500 bp immediately 5' of *ACE2* (B9J08_000468) and 498 bp immediately 3' of *ACE2* were amplified from AR0387 genomic DNA using primers oTO325-oTO326 and oTO329-oTO330 respectively; the *CaNAT1* expression cassette was amplified from pLC49 using primers oTO327-oTO328; the pUC19 vector backbone was amplified using primers oTO331-oTO332.

pTO149: pTO149 was assembled to maintain the *NEO* (G418) resistance cassette. A codon optimized *NEO* resistance gene was synthesized with every CUG codon replaced by the synonymous CUC leucine codon. This was assembled into pTO137 in place of the *NAT* resistance cassette, the backbone amplified with oTO272-oTO273. The codon-optimized *NEO* resistance gene was amplified including the *TEF* promoter and terminator sequence for assembly into complementation cassettes.

pTO169: To assemble pTO169 (p*ace2* + *ACE2*), the full length *ACE2* gene along with 1001 bp upstream was amplified from AR0382 genomic DNA using oTO566-oTO567, the *ADH1* terminator sequence and the *NEO* resistance cassette were amplified from pTO149 with oTO568-oTO569, 832 bp downstream of *ACE2* was amplified from AR0382 genomic DNA using oTO570-oTO571, and the pUC19 backbone was amplified using oTO564-oTO565.
pTO174: To assemble pTO174 (p*tao3* + *TAO3*), the full length *TAO3* gene along with 869 bp upstream was amplified from AR0382 genomic DNA using oTO584-oTO585, the *ADH1* terminator sequence and the *NEO* resistance cassette were amplified from pTO149 with oTO586-oTO587, 503 bp downstream of *TAO3* was amplified from AR0382 genomic DNA using oTO588-oTO589, and the pUC19 backbone was amplified using oTO582-oTO583.
pTO175: To assemble pTO175 (p*elm1* + *ELM1*), the full length *ELM1* gene along with 997 bp upstream was amplified from AR0382 genomic DNA using oTO592-oTO593, the *ADH1* terminator sequence and the *NEO* resistance cassette were amplified from pTO149 with oTO594-oTO595, 582 bp downstream of *ELM1* was amplified from AR0382 genomic DNA using oTO596-oTO597, and the pUC19 backbone was amplified using oTO590-oTO591.

All *C. auris* genomic sequence data was obtained from the *C. auris* B8441 reference genome on *fungidb.org*[259]. All plasmid assemblies were verified by restriction digest and sanger sequencing.

3.5.3 *Agrobacterium tumefaciens*-mediated transformation (AtMT)

AtMT was performed as previously described with minor modifications[260]. Briefly, *A. tumefaciens* strain EHA 105 harboring the pTO128 (pPZP-NATca) plasmid was cultured overnight at 30°C in liquid Luria-Bertani (LB) media containing kanamycin. *A. tumefaciens* cells were harvested by centrifugation, washed once with sterile, ultrapure water, then resuspended at

a final OD_{600} of 0.15 in liquid Induction Medium (IM) supplemented with 100 μM Acetosyringone 3',5'-dimethoxy-4-hydroxyacetophenone (AS)[231] and incubated at room temperature for 6 h with constant agitation. Recipient *C. auris* cells were harvested from an overnight culture grown at 30°C in YPD by centrifugation then resuspended in sterile, ultrapure water at a final OD_{600} of 1.0. Equal volumes of prepared *A. tumefaciens* and *C. auris* were combined and the mixed culture was incubated on IM with AS agar at 23°C for 4 days. Cells were then harvested into liquid YPD, washed three times with fresh YPD, then spread-plated onto YPD agar containing 200 μg/mL nourseothricin and 200 μg/mL cefotaxime. Plates were incubated at 30°C for 2 days. Transformation efficiency was determined by dividing the total number of recovered *C. auris* CFU by the total input number of *C. auris* cells. To identify morphogenic mutants, colonies were screened visually for those exhibiting a wrinkled colony morphology then confirmed to exhibit aggregating or filamentous phenotypes using light microscopy.

3.5.4 Genomic DNA isolation

Genomic DNA was isolated from *C. auris* morphological mutants to be used for downstream sequencing and insertion site mapping using a phenol-chloroform extraction. Briefly, cells were incubated overnight at 30°C in liquid YPD then harvested by centrifugation and resuspended in breaking buffer (2% (v/v) Triton X-100, 1% (w/v) SDS, 100 mM NaCl, 10mM Tris-Cl, 1mM EDTA). DNA was extracted by bead beating into PCA then extracted into Chloroform. Following precipitation by ethanol, extracted DNA was resuspended in TE buffer and treated with RNase A. Genomic DNA quality was assessed by 1% agarose gel electrophoresis.

3.5.5 AtMT transgene insertion site mapping

Mapping of T-DNA insertion sites was performed similarly to methods previously described[232]. Genomic DNA isolated from six morphogenic mutants was collected and divided into two pools, each containing equal amounts by mass of genomic DNA from three individual mutants. Library preparation, quality control, and Whole Genome Sequencing were performed by Microbial Genome Sequencing Center (MIGS, Pittsburg, PA, USA). Library preparation was performed based on the Illumina Nextera kit and sequencing performed on the Nextseq 550 platform, generating 150 bp paired-end reads for each pool. Sequencing data was analyzed using the Galaxy web platform public server at *usegalaxy.org*[62]. Read quality was assessed using FASTQC and reads were trimmed using CutAdapt[63] with a Phred quality cutoff of 20. A linearized vector reference sequence of pTO128 (pPZP-Natca) was generated from the circular vector sequence and 150 bp of sequence from the opposite border was added to each border of the linearized sequence. Reads were mapped to the linear pTO128 (pPZP-NATca) reference sequence using the Burrows-Wheeler Aligner with maximum exact matches (BWA-MEM)[64] configured with default parameters except for minimum seed length = 50 and band width = 2. Mapped reads were visualized using IGV[261] and sorted based on position and sequences that extended beyond the left and right boundaries of the tDNA was extracted. Consensus sequences of the extracted reads were mapped to the *C. auris* B8441 reference genome (GCA_002759435.2) using NCBI Blast. Primers specific to each identified insertion site were designed: oTO310 and oTO340 for *B9J08_002252*, oTO311 and oTO344 for *B9J08_003879*, oTO312 and oTO342 for *B9J08_002849*, oTO313 and oTO338 for *B9J08_000181*, oTO314 and oTO339 for *B9J08_000468*, oTO315 and oTO341 for *B9J08_002667*, and oTO316 and oTO343 for *B9J08_002954*. These were used to amplify the identified insertion regions in conjunction with T-DNA specific primers oTO6 and oTO90 using the genomic DNA from each of the six mutants

as templates. Individual insertions were attributed to individual mutants based on amplicon length. Amplicons containing T-DNA insertions were Sanger Sequenced to generate insertion maps for each mutant.

3.5.6 *C. auris* transformation

Transformation of *C. auris* was performed as described previously, with minor modifications[221]. To generate *ENO1-RFP* strains, linear transformation cassettes encoding Cas9, sgRNA, and the RFP repair cassette were PCR amplified from pTO135, pTO136, and pTO137, respectively, using primers oTO18-oTO19. To generate *Δace2, Δelm1*, *Δace2 + ACE2, Δtao3 + TAO3*, and *Δelm1 + ELM1* strains, a linear Cas9 cassette was amplified from pTO135 using primers oTO18-oTO19, linear repair cassettes were amplified from pTO155 for *ACE2::NAT,* pTO154 for *ELM1::NAT*, pTO169 for *Δace2 + ACE2*, pTO174 for *Δtao3 + TAO3*, and pTO175 for *Δelm1 + ELM1* using primers oTO18-oTO19. To generate *Δtao3*, a linear repair cassette incorporating 50-70 bp homology to either end of the target gene flanking the NAT cassette was amplified from pTO137 using primers oTO353-oTO354. Linear sgRNA cassettes were amplified from pTO136 using fusion PCR as described previously to replace the gRNA sequence with gRNA targeting each gene for deletion[223]. Fusion fragments were amplified using primers oTO333-oTO225 and oTO224-oTO334 to target *ELM1*, oTO335-oTO225 and oTO224-oTO336 to target *ACE2*, oTO356-oTO224 and oTO355-oTO225 to target *TAO3,* and oTO224-oTO519 and oTO225-oTO518 to target *NAT*. Each pair of fragments with overlapping sequences were spliced on extension using oTO18-oTO19. PCR products were purified with a Zymo DNA Clean & Concentrator kit (Cat no. D4034, Zymo Research) according to the manufacturer's instructions. *C. auris* cells were incubated overnight at 30°C in YPD to exponential phase, not exceeding OD_{600} of 2.2. Cells were harvested by centrifugation and resuspended in TE buffer with 100 mM

Lithium Acetate then incubated with constant shaking at 30°C for 1 h. DTT was added to the cells at a final concentration of 25 mM and incubation was continued for 30 min at 30°C with constant shaking. The cells were harvested by centrifugation; washed once with ice-cold, sterile, ultrapure water; washed once with ice-cold 1 M Sorbitol; then resuspended in ice-cold 1 M Sorbitol. 40 µL of competent cells was added to a pre-chilled 2 mm-gap electro-cuvette along with 1 µg each of the PCR-amplified linear transformation cassettes encoding Cas9, sgRNA, and the repair cassette. Alternatively, to compare targeted integration efficiency, an equal volume of Zymo elution buffer was added instead of Cas9 or sgRNA cassettes. Cells were electroporated using a Bio-Rad MicroPulser Electroporator set to the programmed *P. pastoris* (PIC) protocol (2.0 kV, 1 pulse), recovered in 1 M Sorbitol, then resuspended in YPD and allowed 2 hrs of outgrowth at 30°C with shaking. The cells were then spread-plated on YPD with 200 µg/mL nourseothricin and incubated at 30°C or 1000 µg/mL G418 and incubated at 23°C. Mutant strains were confirmed with PCR and Sanger sequencing and were confirmed to not exhibit stable integration of the *CAS9* cassette using *CAS9* specific PCR primers oTO514-oTO515.

To estimate the efficiency of targeted RFP integration among transformant colonies, transformation plates were imaged using a Typhoon FLA 9500 Bioimager fitted with a 532 nm filter. Fluorescent images were visualized using Fiji Software[262]. An intensity threshold was set to identify transformant colonies exhibiting fluorescence. Five representative fluorescent colonies and five representative non-fluorescent colonies from transformations performed in AR0387 were spotted onto YPD agar and grown at 30°C for 2 days. A sample of the colony growth was collected from each colony and suspended in 15 µL water. An aliquot of this suspension was used as a template in PCR reactions with primers overlapping the junction of the predicted *ENO1-RFP* insertion site or a genomic region upstream of the junction present in the

wild-type locus. Colony PCR was performed using Phire Plant Direct PCR Master Mix (F160S; Thermo Fisher Scientific) according to the manufacturer's instructions. The proportion of transformant colonies with targeted integration was determined by dividing the number of colonies exhibiting fluorescence by the total number of transformant colonies.

3.5.7 Live cell microscopy

Cells were grown to mid-exponential phase at 30°C in YPD and pelleted by centrifugation for 1 min at 4000 rpm (1500 x g) then resuspended in PBS. 5 µL cell suspension was combined with 1 µL of 0.1 g/L Calcofluor White stain and applied to a glass microscope slide. Alternatively, overnight cultures were prepared for each isolate and wildtype strain in yeast extract peptone dextrose (YPD) at 30°C, with rotation, and then subcultured to mid-log phase before washing twice in 1X PBS and staining with FM4-64 (BioTracker 640 Red C2(FM4-64) Synaptic Dye, Millipore Sigma) at 10 µM for 10 minutes. Cells were visualized using an Olympus IX70 Epifluorescent Microscope fitted with a Hamamatsu C11440 camera and taken with Olympus CellSens v. 3.2 software.

3.5.8 Stereomicroscopy

C. auris cells were grown on YPD agar at 30°C for 2-7 days to form colonies. Colonies were visualized using a Leica KL300 LED stereomicroscope.

3.5.9 RNA extraction

RNA extraction was performed as described previously[263]. Briefly, cells were grown to mid-exponential phase at 30°C in YPD and harvested by centrifugation. Cells were washed in PBS, then centrifuged and all liquid removed. Dry cell pellets were frozen on dry ice then stored at -80°C overnight. Cell pellets were thawed and resuspended in 100 µL FE Buffer (98%

formamide, 0.01M EDTA) at room temperature. 50 µL of 500 µm RNAse-free glass beads was added and the cell suspension was ground in 3 cycles of 30 sec using a BioSpec Mini-Beadbeater-16 (Biospec Products Inc., Bartlesville, OK, USA). The cell lysate was centrifuged to remove cell debris and the crude RNA extract collected from the supernatant. The extract was DNAse-treated and purified using a Qiagen RNeasy mini kit (ref. 74104, Qiagen) as per the manufacturer's instructions. RNA integrity was confirmed through agarose gel electrophoresis using the bleach gel method[264].

3.5.10 RT-qPCR

cDNA was synthesized from isolated RNA using the AffinityScript qPCR cDNA Synthesis Kit (ref. 600559, Agilent Technologies) according to the manufacturer's instructions and used as a template for qPCR. qPCR was performed in three biological replicates, each with three technical replicates using a BioRad CFXConnect Real Time System. Fold changes were calculated using the double-delta CT method with expression normalized to that of *ACT1* and compared to wild type. Amplification was measured for *ACT1* using primers oTO359-oTO360, for *CHS2* using primers oTO361-oTO362, and for *CTS1* using primers oTO363-oTO364.

3.5.11 Co-expression genetic interaction analysis

The *C. albicans* ortholog of *B9J08_002252* was identified through orthology on the Candida Genome Database as C7_00260C_A. This was used as a query in CalCEN and the top 50 most co-expressed neighbors were identified. This set was then examined for putative function through GO term enrichment in the Candida Genome database. The network was visualized using Cytoscape.

3.5.12 *Galleria mellonella* infection

Infections were performed as previously described[265], with minor modifications. Briefly, *G. mellonella* larvae were purchased from *speedyworm.com* and maintained in sawdust at room temperature. Overnight *C. auris* cultures were prepared for each isolate and wildtype strain in yeast extract peptone dextrose (YPD) at 30°C, with rotation. We were unable to standardize inoculum by direct cell count between aggregating and non-aggregating strains, so we standardized each inoculum to a consistent optical density. Cells were washed twice in PBS and diluted to an OD600 of 1 in 1X PBS, and 50 µL was inoculated into the larvae using an exel veterinary U-40 diabetic syringe (0.5CC X 29G X ½). 20 larvae were infected per *C. auris* strain. After injection, larvae were maintained at 37°C and monitored daily for survival. Virulence was analyzed using Kaplan Meier survival curves in GraphPad Prism (version 9).

3.5.13 Antifungal susceptibility assays

C. auris colonies were suspended in PBS to OD_{600} = 1.0. A sterile cotton applicator was saturated with the cell suspension and used to inoculate the entire surface of a YPD plate three times, rotating the plate approximately 60 degrees each time. The surface of the agar was allowed to dry at room temperature. MIC test strips containing 0.016-256 mg/L Fluconazole (Liofilchem REF 921471), 0.002-32 mg/L Caspofungin (Liofilchem REF 921541), or 0.002-32 mg/L Amphotericin B (Liofilchem REF 921531) were placed onto the surface of the agar. Plates were incubated inverted at 37°C for 24 hrs and MICs were determined at the intersection between the zone of inhibition and the MIC test strip gradient.

3.5.14 Statistics and reproducibility

Statistical analyses were carried out using R statistical software (version 4.3) or GraphPad Prism (version 9). Data are presented as means ± standard error of means from biological replicates.

Except where otherwise specified, each experiment was performed in at least three independent biological replicates yielding similar results. Statistical significance among different groups was calculated using one-way ANOVA, with Tukey's or Dunnett's post hoc tests for multiple comparisons, Chi-square test, or Mantel-Cox log rank test. *, $p \leq 0.05$; **, $p \leq 0.01$; ***, $p \leq 0.001$; ns, $p > 0.05$.

3.5.15 Data availability

Data from Illumina sequences used to identify transgene insertion sites are available in the NCBI SRA under BioProject accession number PRJNA722500. Gene sequences for mapping and designing constructs were retrieved from the B8441 genome assembly (NCBI GCA_002759435.2) through fungidb.org.

Strain Name	Alias	Genotype	Source
pTO123	*Agrobacterium tumefaciens* EHA105	Harbors pEHA105 (pTiBo542ΔT-DNA)	[255]
pTO131	*Agrobacterium tumefaciens* EHA105	Harbors pEHA105 + pTO128 (pPZP-NATca)	This Study
AR381	*Candida auris* B11220		[4,229]
AR382	*Candida auris* CDC-0382		[4,229]
AR383	*Candida auris* B11221		[4,229]
AR386	*Candida auris* B11245		[4,229]
AR387	*Candida auris* B8441		[4,229]
CauTO58	*Candida auris* AR382	Tn*CauACE2*	This Study
CauTO112	*Candida auris* AR382	TnB9J08_002252	This Study
CauTO113	*Candida auris* AR382	Tn*CauCHS2*	This Study
CauTO114	*Candida auris* AR382	Tn*CauELM1*	This Study
CauTO115	*Candida auris* AR382	Tn*CauTAO3*	This Study
CauTO180	*Candida auris* AR382	Δ*CauACE2*	This Study
CauTO182	*Candida auris* AR382	Δ*CauELM1*	This Study
	Candida auris AR382	Δ*CauTAO3*	This Study
	Candida auris AR382	Δ*CauFKH2*	This Study
	Candida auris AR381	Δ*CauACE2*	This Study
	Candida auris AR381	Δ*CauELM1*	This Study

Table 3-2 Strains used in this chapter.

Name	Description	Source
pPZP-NEO1	*neoR* in T-DNA region, *kanR*	[253]
pTO128 (pPZP-NATca)	*CaNAT1R* in T-DNA region, *kanR*	This study
pLC49	*FLP-NAT, ampR, natR*	[254]
pLC963	*CaCas9,sgRNA, ampR*	[257]
pLC1047	*RFP-FLP-NAT, natR ampR*	[258]
pUC19	*ampR*	[256]
pTO135	*pENO1-CaCas9-tCyc1, ampR*	This study
pTO136	*pADH1-tRNA-Ala-gRNA-tracrRNA-HDV-tAgTEF2, ampR*	This study
pTO137	*RFP-tADH1-pAgTEF2-NAT1-tAGTEF2,* with targeting arms to tag Eno1 cterminus, *natR ampR*	This study
pTO154	*CauELM1::NAT, ampR natR*	This study
pTO155	*CauACE2::NAT, ampR natR*	This study

Table 3-3 Plasmids used in this chapter.

Name	Sequence	Use
oTO112	ttcgagctcggtaccCCTCTTTGTAGTTCAACTTATG	Generation of pTO135
oTO113	atacttttatccatGATGAAAATTAAGTTTGGATAGG	
oTO114	aacttaattttcatcATGGATAAAAAGTATAGTATTGGTTTAG	
oTO115	gactctagaggatccGTCCCAAAACCTTCTCAAG	
oTO116	agaaggttttgggacGGATCCTCTAGAGTCGAC	
oTO117	tgaactacaaagaggGGTACCGAGCTCGAATTC	
oTO118	ttcgagctcggtaccCGAGATAGATCGAAATACG	Generation of pTO136
oTO119	cgctaccaactacgccacacgcccgagtagGATTTCGTGAAGATTGATTG	
oTO120	gtcgattcgatactaacgccgccatccagtGGATCCTCTAGAGTCGAC	
oTO121	tttcgatctatctcgGGTACCGAGCTCGAATTC	
oTO122	ttcgagctcggtaccGGTGAGCAATTGGCTGAC	Generation of pTO137
oTO123	tgaaacaccaccaccCAAGTTTTGAGCAGCCTTG	
oTO124	gctgctcaaaacttgGGTGGTGGTGTTTCAAAAG	
oTO125	taatcatgctgctacTTATTTATATAATTCATCCATACCACC	
oTO126	gaattatataaataaGTAGCAGCATGATTATGAAC	
oTO127	cgaggcaagcttgatCCTAAACTGCAAACCCATC	
oTO128	ggtttgcagtttaggATCAAGCTTGCCTCGTCC	
oTO129	gtttgaagcgcaaacACTGGATGGCGGCGTTAG	
oTO130	acgccgccatccagtGTTTGCGCTTCAAACCAC	
oTO131	gactctagaggatccGTCTTTGACCCAATCAAC	
oTO132	gattgggtcaaagacGGATCCTCTAGAGTCGAC	
oTO133	agccaattgctcaccGGTACCGAGCTCGAATTC	
oTO317	TGAATTCGAGCTCGGTACCCCGTTTGGATAACAAAAACTCG	Generation of pTO154
oTO318	tactaacgccgccatccagtTGCCCTTTATGTTGCTTTCA	
oTO319	TGAAAGCAACATAAAGGGCAactggatggcggcgttagta	
oTO320	CAGATTCTCACTAAGCCTGCatcaagcttgcctcgtcccc	
oTO321	ggggacgaggcaagcttgatGCAGGCTTAGTGAGAATCTG	
oTO337	AGGTCGACTCTAGAGGATCCCTTTTCTTGAACGGAGGTAAT	
oTO323	TTACCTCCGTTCAAGAAAAGGGATCCTCTAGAGTCGACCT	
oTO324	GAGTTTTTGTTATCCAAACGGGGTACCGAGCTCGAATTCA	
oTO325	GTGAATTCGAGCTCGGTACCCCTTCTCTAGTTCAGGGTCCC	Generation of pTO155
oTO326	tactaacgccgccatccagtAGCGGGCGCTGGTGAAATTT	
oTO327	AAATTTCACCAGCGCCCGCTactggatggcggcgttagta	
oTO328	AAGGAAAAAGAAATGCAACGatcaagcttgcctcgtcccc	
oTO329	ggggacgaggcaagcttgatCGTTGCATTTCTTTTTCCTTT	
oTO330	AGGTCGACTCTAGAGGATCCCCAACTAATCCCAAAGGCCG	
oTO331	CGGCCTTTGGGATTAGTTGGGGATCCTCTAGAGTCGACCT	
oTO332	GGACCCTGAACTAGAGAAGGGGTACCGAGCTCGAATTCAC	
oTO18	CAGGAAACAGCTATGAC	

oTO19	GTAAAACGACGGCCAG	Amplification of transformation cassettes
oTO353	GGAATCACCATTTTTAATCTCCCCTTCAGTAATTCACCTCCTTCT TCCTCTTTTCactggatggcggcgttag	*tao3::NAT* repair cassette
oTO354	GGTAGATATGAGGCCCTGCATAGTCGCGGAGTATAGACA ATTCATGCAGAAAAATGGTTGCAAATTTTCCatcaagcttgcctcgtcc	
oTO367	GTGTTTTCAAATAAAAAAAAGGAGCCCCCTTTCTCGATCTTACTGGCA GTTGCTGTCTTCACAAAGTAAATAactggatggcggcgttag	*fkh2::NAT* repair cassette
oTO368	TTTACAACGTTCAAGTGACTAATGCAAATGTTATCGTGGCGAAGA AATGAAGGAATTTCATGAAGTCGATTTatcaagcttgcctcgtcc	
oTO224	GCTATTACGCCAGCTGG	sgRNA Fusion PCR
oTO225	CGCAATTAATGTGAGTTAGC	
oTO333	GACTAGACATAGAGCTTGATgttttagagctagaaatagcaag	Fusion PCR – *ELM1* gRNA
oTO334	ATCAAGCTCTATGTCTAGTCTGGACGAGTCCGGATTC	
oTO335	CTCAACGAAACCTCGTACACgttttagagctagaaatagcaag	Fusion PCR – *ACE2* gRNA
oTO336	GTGTACGAGGTTTCGTTGAGTGGACGAGTCCGGATTC	
oTO355	TTGGTACAGGGAAACACAATgttttagagctagaaatagcaag	Fusion PCR – *TAO3* gRNA
oTO356	ATTGTGTTTCCCTGTACCAAtggacgagtccggattc	
oTO371	GATTTCCACGCTACAAATTCgttttagagctagaaatagcaag	Fusion PCR – *FKH2* gRNA
oTO372	GAATTTGTAGCGTGGAAATCtggacgagtccggattc	
oTO359	CGTGCTGTGTTCCCATCCAT	*ACT1* qPCR
oTO360	AGCCTCATCACCGACATACG	
oTO361	GAAACGGACGTGCCTGAAAG	*CHS2* qPCR
oTO362	TGCCGCAATGAGTAAAGTGC	
oTO363	GACTTGTCAGTCCAAGGGCA	*CTS1* qPCR
oTO364	AAGGTCTCTCGGAGTCGGAA	
oTO365	CAAGCCTCTTTTGCCACCAC	*B9J08_0022 52* qPCR
oTO366	TCAAGCCTACCGTTCACAGC	
oTO373	GATGCCGTGGGGGAAGATAG	*ACE2* qPCR
oTO374	GGAGTGAATGGCGTAGCAGA	
oTO310	CCGAAACTATCTACATGACCC	
oTO311	CAGTCTCCATTTGCCTCTC	
oTO312	CCGATACACCAACATTGC	

oTO313	GCCATCGTTGCTAATCTTC	AtMT Transgene Insertion Site Mapping
oTO314	CTCCTTTCAGACATGCAAAG	
oTO315	GTGGTGGTCCTAACAGAG	
oTO316	CAACCATTTGTGTCTGTGC	
oTO338	GTTGGACCTCTGATCAGTATC	
oTO339	CTTTGAGGTAGGGTAGGAC	
oTO340	GTAGGAGTATTGGACCTCG	
oTO341	GGCATTGTAACAGTCTGAG	
oTO342	GATTCTCACTAAGCCTGC	
oTO343	GGTGCGCATAGATAAGG	
oTO344	GTGAAGACTACGCAAAGCATG	
oTO6	gactgtcaaggagggtattc	
oTO90	gctttatacgatggtactgc	

Table 3-4 Oligonucleotides used in this chapter.

Chapter 4 A Lineage-Specific Adhesin, Scf1, Governs *Candida auris* Surface Association, Colonization, and Virulence

4.1 Abstract

Candida auris is an emerging fungal pathogen responsible for healthcare-associated outbreaks that arise from persistent surface and skin colonization. We characterized the arsenal of adhesins used by *C. auris* and discovered an uncharacterized adhesin, *Surface Colonization Factor (SCF1)*, and a conserved adhesin, *IFF4109*, that are essential for colonization of inert surfaces and mammalian hosts. *SCF1* is apparently specific to *C. auris* and its expression mediates adhesion to inert and biological surfaces across isolates from all five clades. Unlike canonical fungal adhesins, which function through hydrophobic interactions, *SCF1* relies on exposed cationic residues for surface association. *SCF1* is required for *C. auris* biofilm formation, skin colonization, virulence in systemic infection, and colonization of inserted medical devices.

4.2 Introduction

Since initial reports of its discovery in 2009, the emerging fungal pathogen *Candida auris* has become an increasingly common source of life-threatening infection worldwide[216,266]. *C. auris* is frequently reported in association with nosocomial outbreaks, a characteristic rarely described with other *Candida* species, and is of urgent concern for public health authorities[91,267–270]. *C.*

The data in this chapter has been published in *Science*.

Santana, D.J., Anku, J.A.E., Zhao, G., Zarnowski, R., Johnson, C.J., Hautau, H., Visser, N.D., Ibrahim, A.S., Andes, D., Nett, J.E., Singh, S.S., O'Meara, T.R. (2023). A Candida auris-specific adhesin, Scf1, governs surface association, colonization, and virulence. Science *381*, 1461–1467.

auris outbreaks are characterized by persistent colonization of patient skin and abiotic surfaces, which can remain positive for extensive periods and serve as a source of contaminative transmission[22,32,34–36,44,112]. *C. auris* also colonizes indwelling medical devices, which act as a risk factor for the development of invasive disease[41,46,98,109,271–273]. Lapses in diagnostic screening and infection prevention measures are thought to contribute to the increasing rate of *C. auris* outbreaks[41]. The ability of *C. auris* to robustly colonize a range of living and abiotic substrates is central to its emergence as a global health threat.

Colonization requires the initial physical association and attachment between fungal cells and substrate. For fungal pathogens, attachment is largely mediated by cell surface-exposed adhesin proteins[68]. In *Candida* species, genetic expansion has resulted in the formation of adhesin families containing genes similar in sequence and domain architecture, with adhesive functions that are redundant or specific across family members[75,83]. *C. auris* encodes genes similar to members of the conserved *ALS* and *IFF/HYR* adhesin families found across the genus, although these genes may have expanded independently in *C. auris* and lack clear one-to-one homology with adhesins from well-characterized species. Moreover, their phenotypic importance in *C. auris* is not well understood[82–84].

To interrogate the role of individual *C. auris* adhesins in colonization phenotypes, we measured the adhesion between fungal cells and polymer substrates as a model for surface association. We found that *C. auris* does not primarily rely on conserved adhesins for surface attachment. Instead, we identified *Surface Colonization Factor (SCF1)*, an adhesin specific to *C. auris*. *SCF1* is necessary and sufficient for robust attachment of *C. auris* cells to polymer substrates. *C. auris* isolates from diverse and similar genetic lineages exhibit striking divergence in terms of substrate association, and this phenotypic plasticity is tightly correlated with strain-

specific transcriptional control of *SCF1*. The nonspecific surface association driven by *SCF1* does not occur through canonical hydrophobic interactions, but rather through cation-substrate interactions. To explore the clinical relevance of these findings, we investigated the importance of *SCF1* in long-term colonization models. *SCF1* is critical for biofilm formation *in vitro*, robust colonization of *in vivo* central venous catheters, colonization of both human and murine skin, and virulence in disseminated infection. These findings offer insight into the genetic and molecular mechanisms by which *C. auris* mediates surface association, a trait critical to the increasing disease burden of this emerging pathogen.

4.3 Results

4.3.1 Polymer surface attachment by the adhesin Scf1.

C. auris encodes twelve genes homologous to members of the characterized *ALS* and *IFF/HYR* adhesin families[83,84,274]. We generated individual deletion mutants in the clade I AR0382 background for each adhesin gene to model their impact on surface association. We employed a flow cytometric adhesion assay that measures the ability of cells to attach to dispersed polystyrene microspheres in suspension[275]. Of the twelve adhesin mutants, only deletion of *IFF4109* (B9J08_004109) conferred an adhesive defect, while still failing to completely ablate attachment (Fig. 4-1A). To investigate the possibility that there were occult adhesive factors, we screened a library of 2,560 insertional mutants, prioritizing mutants exhibiting the most significant defects (Fig. 4-1B). The greatest loss of adhesive capacity was observed in *tnSWI1* (B9J08_003460) and *tnBCY1* (B9J08_002818) mutants (Fig. 4-1B, Fig. 4-1C, Fig. 4-2). Compared to the AR0382 parent, the *tnSWI1* mutant exhibited no significant transcriptional dysregulation of the *ALS* or *IFF/HYR* adhesins, suggesting alternative mediators of adhesion (Fig. 4-1D). The strongest, most significantly dysregulated gene in *tnSWI1* was an

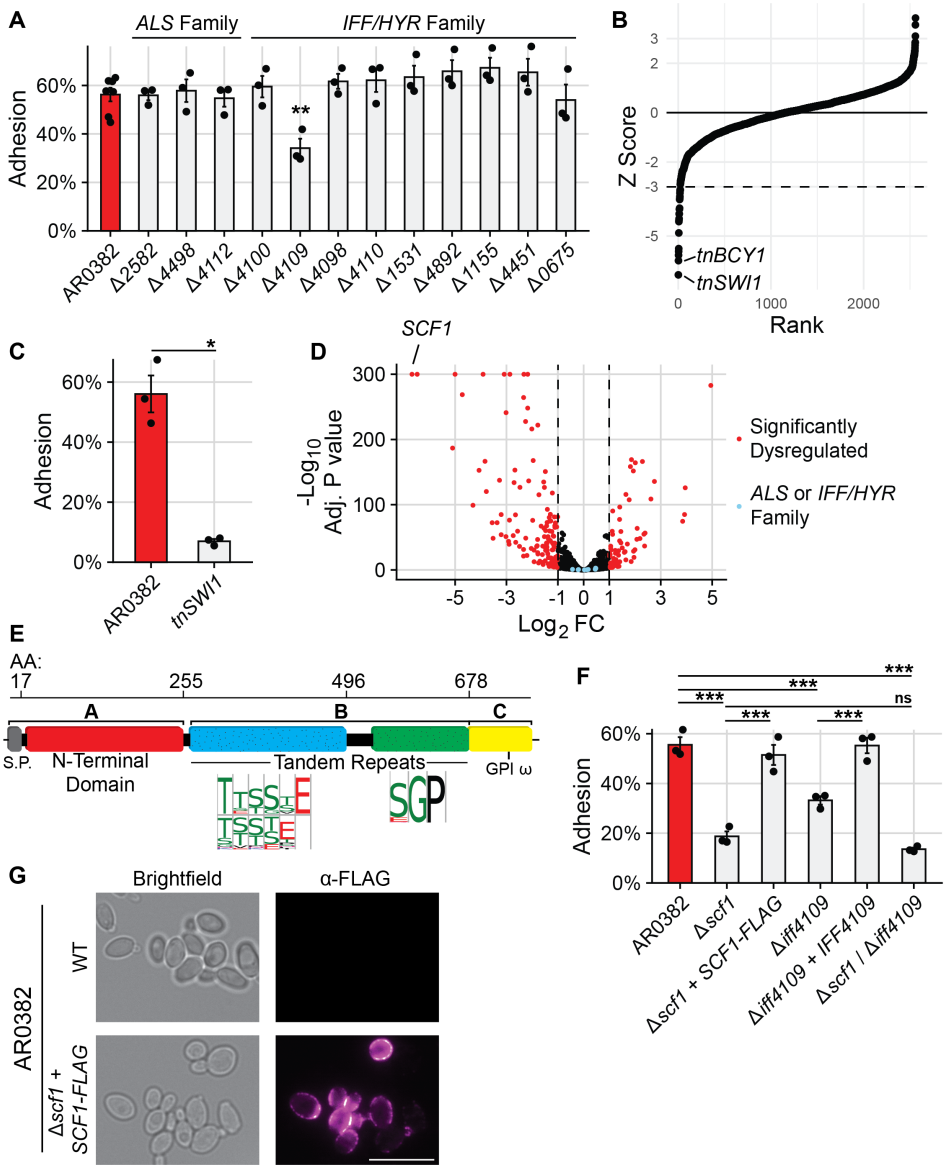

Figure 4-1 Surface Colonization Factor (Scf1) mediates *C. auris* adhesion to polymer surfaces. (A) Adhesion of wild type AR0382 or mutants lacking one of twelve genes from *ALS* or *IFF/HYR* adhesin families. **(B)** 2,560 insertional mutants in the AR0382 strain background were screened for adhesion defects by measuring the proportion of cells able to remain attached to a cyclic olefin polymer surface after 3 washes with PBS. Strains are ordered by Z-score rank. Mutants with a Z-score more negative than -3 were considered to have a significant adhesive defect. **(C)** Adhesion of AR0382 and an insertional *SWI1* mutant. **(D)** RNA-seq comparing the transcriptome of *tnSWI1* to AR0382. *SCF1* (B9J08_001458) is the strongest dysregulated gene. **(E)** Predicted domain architecture of Scf1, based on the clade I primary sequence, is consistent with canonical fungal adhesins. **(F)** Adhesion of adhesin mutants and complements compared to AR0382 **(G)** Immunofluorescence microscopy using an α-FLAG antibody. Representative images shown for WT AR0382 and AR0382 Δ*scf1* + *SCF1-FLAG*. Scale bar = 5 μm. Statistical differences were assessed using one-way ANOVA with Dunnett's post-hoc test (A), student's t-test (C), or one-way ANOVA with Tukey's post-hoc test (G); *p ≤ 0.05; **p ≤ 0.01; ***p ≤ 0.001; ns: p > 0.05.

uncharacterized ORF (B9J08_001458), which had no significant primary sequence homology to characterized genes (Fig. 4-1D). This gene, however, exhibited a putative three-domain architecture consistent with canonical GPI-anchored fungal adhesins (Fig. 4-1E)[75]. Notably, this same gene was also strongly downregulated in the *tnBCY1* mutant while *IFF4109* was not (Fig. 4-2).

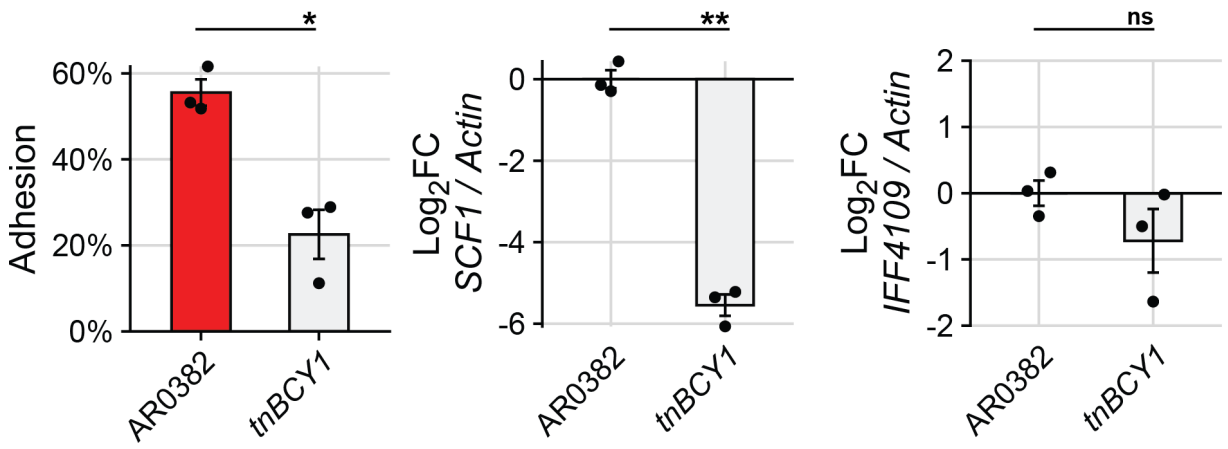

Figure 4-2 A *BCY1* insertional mutant shows reduced adhesion associated with downregulation of *SCF1* but not *IFF4109*. Adhesion to polystyrene microspheres and transcript abundance compared to the parental AR0382 for *SCF1* and *IFF4109*. Statistical differences were assessed using student's t-test; *p ≤ 0.05; **p ≤ 0.01; ***p ≤ 0.001; ns: p > 0.05.

Deletion of the B9J08_001458 ORF in AR0382 conferred a substantial adhesive defect, thus we refer to the gene as *Surface Colonization Factor (SCF1)* (Fig. 4-1F). Complementation with an epitope-tagged *SCF1* allele in the endogenous locus rescued the adhesive defect, and the epitope-tagged Scf1 protein localized to the cell surface, consistent with its role as an adhesin (Fig. 4-1F, Fig. 4-1G). Notably, deletion of *IFF4109* in the Δ*scf1* background did not significantly reduce attachment beyond deletion of *SCF1* alone, suggesting non-additive roles for these adhesins (Fig. 4-1F).

The specific reliance on *SCF1* and *IFF4109* for adhesion despite potential redundancy with other adhesins is reminiscent of other fungal pathogens. For instance, loss of *ALS1* alone reduces *Candida albicans* adhesion, despite the presence of seven other *ALS* genes (Fig. 4-3A)[80]. In *C. auris,* adhesins exhibit structural and transcriptional variation, which may explain their functional specificity (Fig. 4-3B)[82,84]. However, *IFF4892* encodes the entire canonical adhesin architecture and shows similar expression to *IFF4109*, but of the two, only *IFF4109* is required for adhesion, suggesting individual adhesins mediate specific adhesive mechanisms (Fig. 4-1A, Fig. 4-3B)[84]. Such functional specificity is shown by increased flocculation and aggregation

associated with overexpression of *ALS4112*, while these phenotypes are not associated with *SCF1*, despite its transcriptional expression being among the highest 2.5% of all genes in this strain background (Fig. 4-3B, Fig. 4-3C, Fig. 4-3D)[158,174]. These findings suggest functional specificity for surface association for *SCF1* and *IFF4109*.

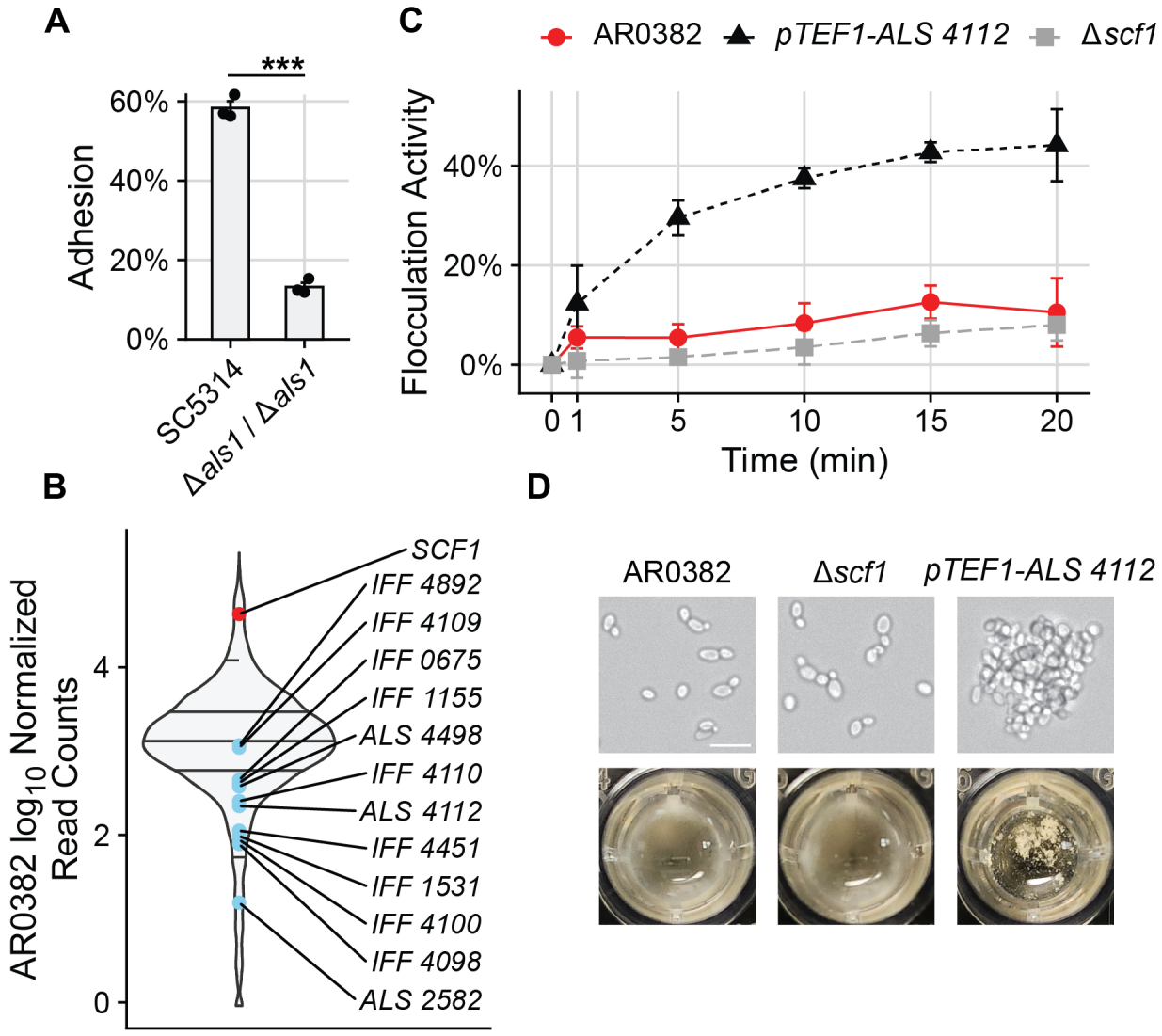

Figure 4-3 Individual adhesin genes exhibit distinct phenotypes. (A) Adhesion to polystyrene microspheres measured for *C. albicans* SC5314 or a mutant lacking *ALS1*. Cells were grown in yeast phase in YPD at 30 °C. **(B)** DESeq-normalized read counts for all ORFs based on AR0382 RNA-seq. Read counts for adhesins are indicated. Horizontal lines mark the 5th, 25th, 50th, 75th, and 95th percentiles among all ORFs. **(C)** Flocculation activity measured over time for wild type AR0382 or mutants lacking *SCF1* or driving *ALS 4112* with the *C. auris TEF1* promoter. Data are mean ± SEM from three replicates. **(D)** Representative brightfield microscopy (top) and photographs of broth culture after 20 minutes of settling (bottom) for the strains assessed in (C). Scale bar = 10 µm. Statistical differences were assessed using student's t-test (A); *p ≤ 0.05; **p ≤ 0.01; ***p ≤ 0.001; ns: p > 0.05.

4.3.2 *C. auris* relies on Scf1 for adhesive plasticity.

While many *Candida* and *Saccharomyces* adhesins belong to conserved gene families, we identified homologs of *SCF1* only in *C. auris* and the closely related *Candida haemulonii* species and not in other members of the *haemulonii* complex (Fig. 4-4A). *SCF1* is encoded in a genomic locus in *C. auris* and *C. haemulonii* that is syntenic, lacking an *SCF1* homolog, even to distantly related species (Fig. 4-4A). Although the *C.*

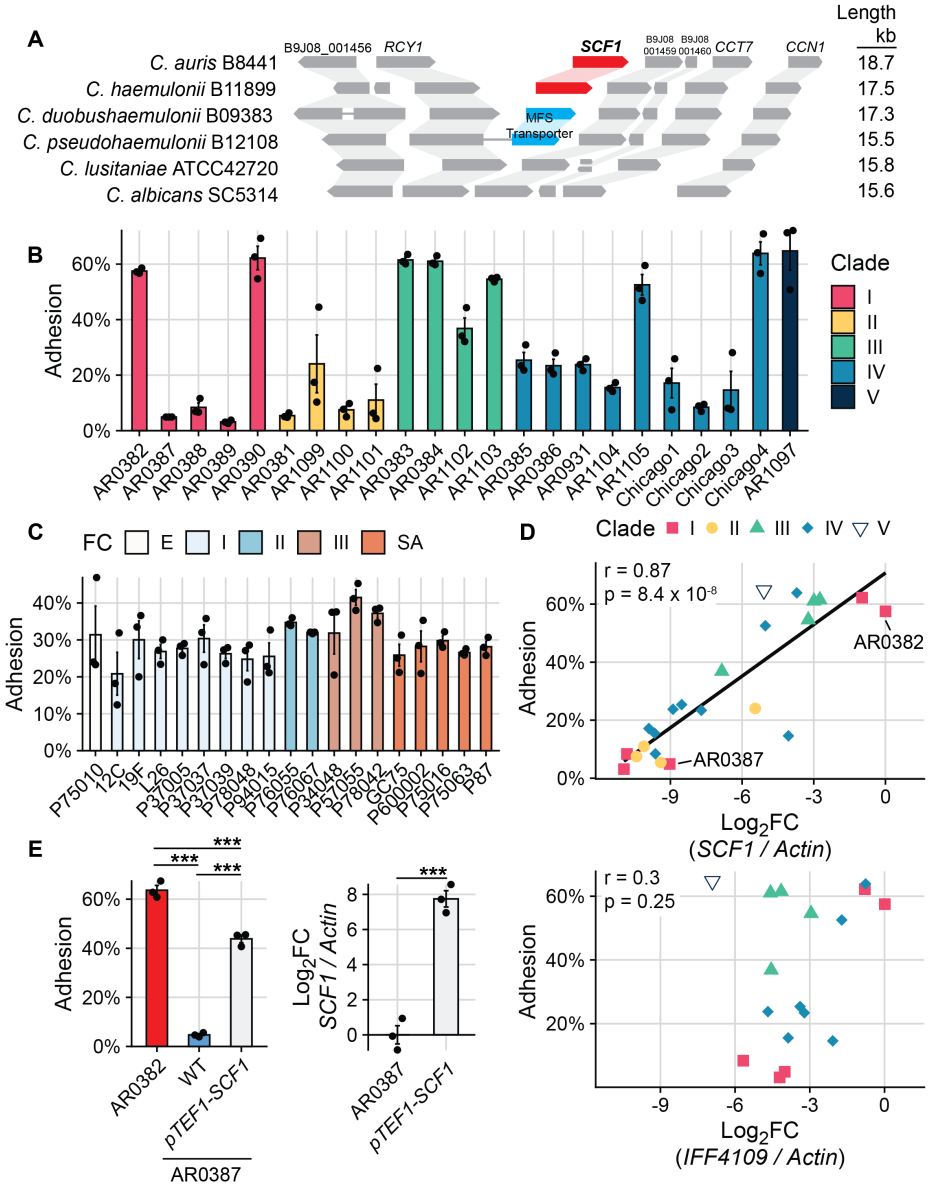

Figure 4-4 *C. auris* uniquely relies on Scf1 for adhesive plasticity. (A) Synteny schema depicting *SCF1* and the conservation and orientation of adjacent ORFs. Genomic loci are shown in comparison to *C. auris*. Putative *SCF1* homologs were only identified in *C. auris* and *C. haemulonii*. **(B)** Adhesion of 23 *C. auris* clinical isolates from all 5 clades. **(C)** Adhesion of 19 *C. albicans* clinical isolates from five clades. FC = Fingerprint Clade. **(D)** *SCF1* transcript abundance (top panel) but not *IFF4109* transcript abundance (bottom panel) is associated with adhesion to polystyrene in the same 23 *C. auris* isolates from (A). Log_2FC are expressed relative to AR0382. Each point signifies the mean of three biological replicates. Pearson correlation coefficient and p-value indicated. Isolates that do not encode *IFF4109* are not indicated in the bottom panel. **(E)** Comparison of adhesion between two Clade I isolates: AR0382 and AR0387. Overexpression of *SCF1* using the strong *TEF1* promoter is sufficient to drive adhesion in the poorly adhesive AR0387 background. Statistical differences were assessed using one-way ANOVA (A) and (B), with Tukey's post-hoc test (D) or student's t-test (D); *p ≤ 0.05; **p ≤ 0.01; ***p ≤ 0.001; ns: p > 0.05.

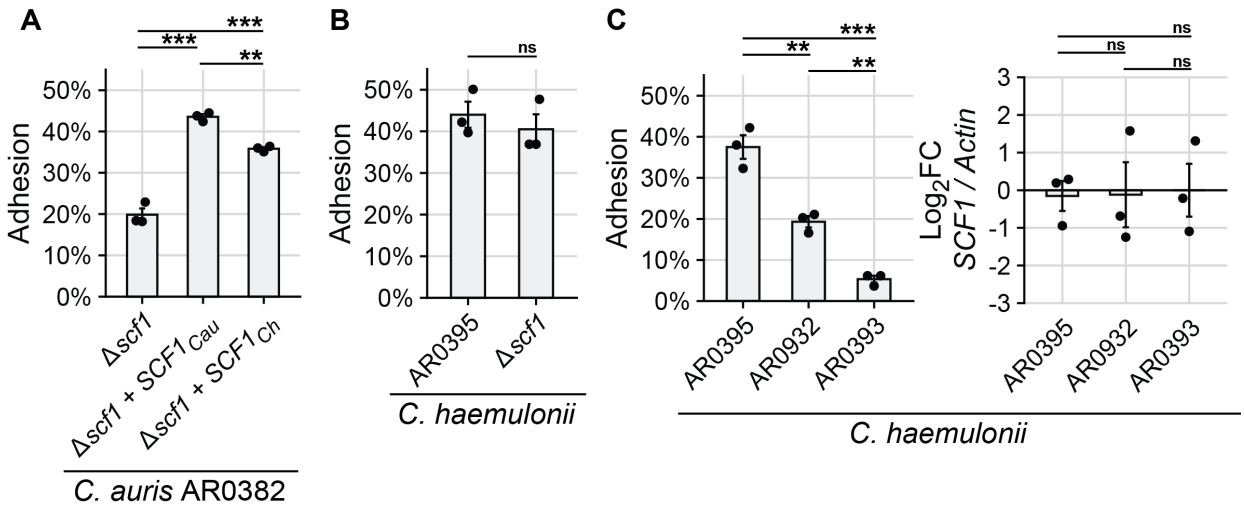

Figure 4-5 *C. haemulonii* does not rely on Scf1 for adhesion. (A) Adhesion of *C. auris* AR0382 Δ*scf1* mutant or the same mutant complemented with the *SCF1* allele from *C. auris* AR0382 or from *C. haemulonii* AR0395. **(B)** Adhesion of *C. haemulonii* AR0395 and a mutant lacking the putative *SCF1* homolog (CXQ85_003100). **(C)** Adhesion of three distinct *C. haemulonii* isolates and *SCF1* expression compared to AR0393. Statistical differences were assessed using student's t-test (B) or one-way ANOVA with Tukey's post-hoc test (A) and (C); *$p \leq 0.05$; **$p \leq 0.01$; ***$p \leq 0.001$; ns: $p > 0.05$.

haemulonii SCF1 homolog functionally complements Δ*scf1* in *C. auris,* it is not essential for adhesion in *C. haemulonii* and shows poor expression across isolates, indicating reliance on *SCF1* for adhesion is specific to *C. auris* (Fig. 4-5).

To investigate the generalizability of the reliance on *SCF1* and the variability between *C. auris* strains, we measured adhesion for 23 *C. auris* isolates representing all five clades and diverse geographic origins of *C. auris*. These strains exhibited substantial adhesive variation, regardless of clade ($p=2x10^{-16}$, F=35.06, one-way ANOVA) (Fig. 4-4B). In contrast, a similar analysis of 19 genetically diverse *C. albicans* clinical isolates showed no significant adhesive variation (p=0.054, F=1.856, one-way ANOVA), indicating the surface association strategies of *C. auris* are more plastic than *C. albicans* (Fig. 4-4C). Interestingly, substantial variation in adhesion was observed even between genetically similar isolates of *C. auris*, e.g., AR0382 and AR0387, which differ by only 206 coding SNPs (Fig. 4-4B). In the poorly adhesive AR0387, *SCF1* was the most down-regulated gene compared to the highly adhesive AR0382, reminiscent

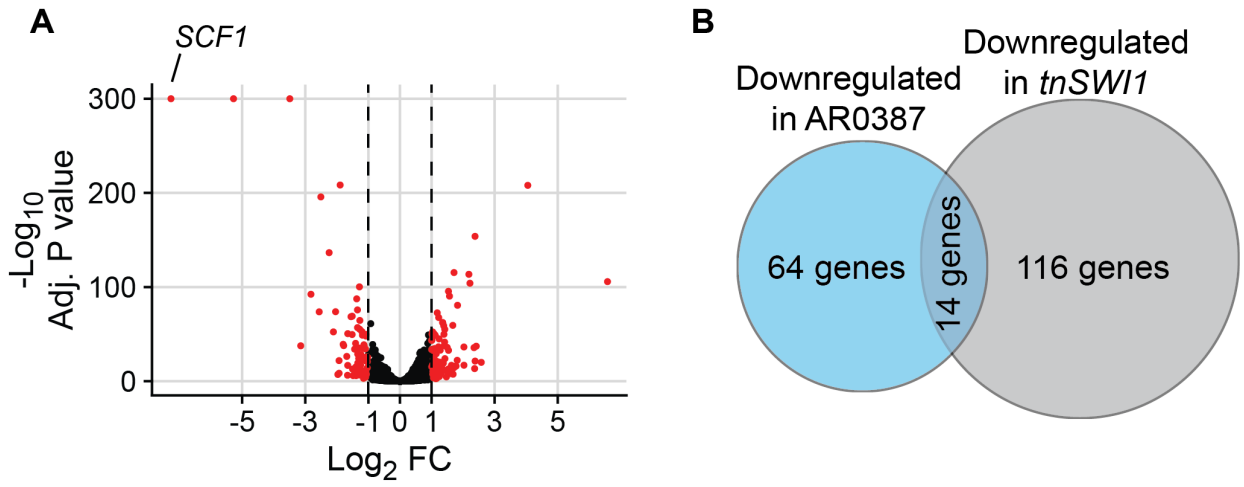

Figure 4-6 *SCF1* is the most strongly dysregulated gene between AR0387 and AR0382. (A) Transcriptome of AR0387 compared to AR0382. Genes in red are significantly dysregulated in AR0387, with *SCF1* being the most strongly and most significantly downregulated gene. **(B)** Comparison of the downregulated transcriptome between two poorly adhesive strains compared to the strongly adhesive AR0382. The regulon of AR0387 and *tnSWI1* overlap by 14 genes.

of the poorly adhesive *tnSWI1* mutant (Fig. 4-6A, Fig. 4-1D). The transcriptome of AR0387 showed little overlap with that of the *tnSWI1* strain, however, indicating dysregulation of *SCF1* in AR0387 is not caused by a *SWI/SNF* complex defect (Fig. 4-6B). Furthermore, we observed no nucleotide variants in the *SCF1* ORF or neighboring intragenic regions between AR0382 and AR0387.

Transcript abundance of *SCF1* was tightly positively correlated with adhesion across isolates, regardless of clade ($r=0.87$, $p=8.4 \times 10^{-8}$) (Fig. 4-4D). In contrast, we observed no association between transcriptional control of *IFF4109* and adhesion ($r=0.3$, $p=0.25$) (Fig. 4-4D). Experimentally, transcriptional overexpression of *SCF1* was sufficient to elevate adhesion in the otherwise poorly adhesive isolate AR0387 (Fig. 4-4E). Importantly, the magnitude of overexpression using the *TEF1* promoter (approximately 2^8-fold increase) was similar to and did not exceed the naturally varying magnitude of expression difference between the two wild type isolates AR0382 and AR0387 (approximately 2^9-fold change) (Fig. 4-4D, Fig. 4-4E). These data

show that adhesive variation between *C. auris* isolates is associated with *SCF1* expression variation.

Strain	Clade	NT Domain % Identity	NT TR Domain Number of Repeats	CT TR Domain Number of Repeats	C Domain % Identity
B8441	I	Ref.	42	46	Ref.
B11220	II	100%	47	31	100%
B11221	III	100%	42	40	92%
B11243	IV	99.6%	42	39	85%
IFRC2087	V	99.6%	35	34	97.7%
B11889	*C. haemulonii*	60.9%			40.6%

Table 4-1 Primary sequence comparison between *SCF1* encoded by *C. auris* strains from each of the five clades and *C. haemulonii*. NT = N-terminal. CT = C-terminal. TR = Tandem Repeat.

In AR0382 and AR0387, the *SCF1* locus is invariant, but other isolates exhibit allelic variation, primarily concentrated in the low complexity tandem repeats (Table 4-1). We tested whether allelic variation also contributed to the adhesive variation among isolates. Overexpression of the native *SCF1* allele in AR0381, a poorly adhesive clade II isolate, was sufficient to increase attachment (Fig. 4-7A). However, overexpression of the clade I *SCF1* allele from AR0382 further elevated adhesion, despite similar levels of overexpression (Fig. 4-7A). Interestingly, in the clade I AR0382

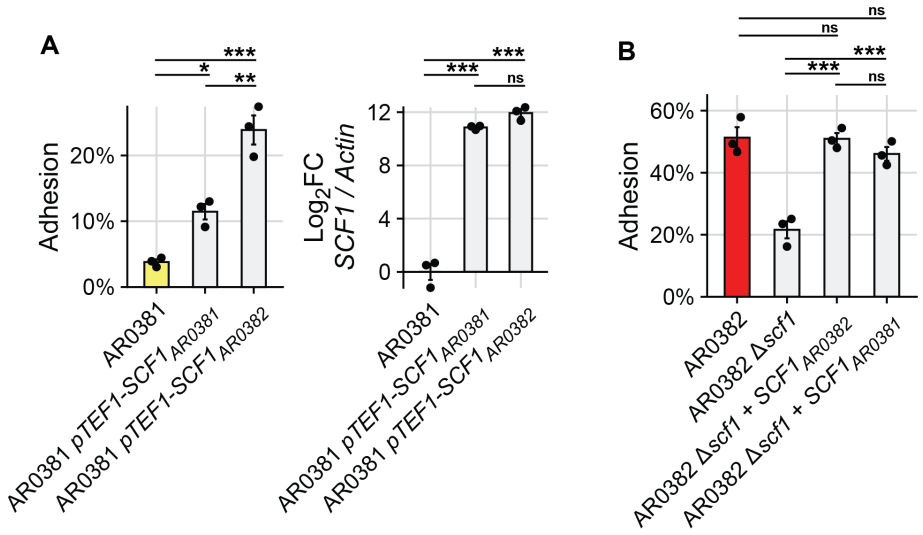

Figure 4-7 Different *SCF1* alleles exhibit different magnitudes of attachment in a strain-dependent manner. (A) Overexpression of the AR0382 (Clade I) *SCF1* allele in AR0381 (Clade II) confers a stronger adhesive phenotype than overexpression of the endogenous AR0381 *SCF1* allele (left panel), despite similar transcript abundance (right panel). **(B)** The AR0382 Δ*scf1* attachment defect is fully rescued by complementation with the *SCF1* allele from either AR0382 or AR0381. Statistical differences were assessed using one-way ANOVA with Tukey's post-hoc test; *$p \leq 0.05$; **$p \leq 0.01$; ***$p \leq 0.001$; ns: $p > 0.05$.

background, which relies strongly on *SCF1* for adhesion, complementation of the Δ*scf1* mutant with either the clade I or the clade II *SCF1* allele resulted in similar levels of rescue of the adhesive phenotype (Fig. 4-7B). These findings show that sequence variation between these two *SCF1* alleles does not intrinsically contribute to functional differences in adhesion, and that other factors may also influence adhesive capacity.

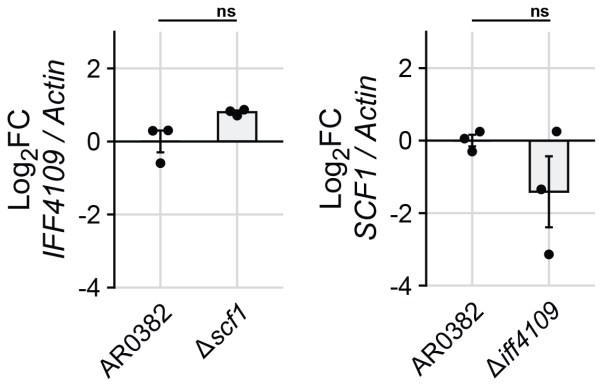

Figure 4-8 Loss of either SCF1 or IFF4109 does not result in transcriptional dysregulation of the other. qPCR comparing transcript abundance for *IFF4109* or *SCF1* in strains lacking *SCF1* or *IFF4109* compared to the parental wild type. Statistical differences were assessed using student's t-test; *p ≤ 0.05; **p ≤ 0.01; ***p ≤ 0.001; ns: p > 0.05.

4.3.3 Scf1 and Iff4109 mediate adhesion through distinct nonspecific mechanisms

The reliance on *SCF1* for surface association is complicated by the genetic interaction with *IFF4109*, where deletion of both does not result in a more severe adhesive defect than deletion of *SCF1* alone (Fig. 4-1F). Loss of one adhesin did not result in dysregulation of the other, suggesting the interaction is not a regulatory one (Fig. 4-8). One possibility is that the two genes contribute to adhesion through distinct but complementary physical mechanisms. For other *Candida* species, adhesion to abiotic substrates is often nonspecific, with adhesins promoting affinity for hydrophobic substrates[57,58,88]. The highly adhesive AR0382 strain exhibited elevated cell surface hydrophobicity compared to the poorly adhesive AR0387 (Fig. 4-9A, Fig. 4-9B). Deletion of the *IFF4109* adhesin in AR0382 reduced cell surface hydrophobicity, which was rescued to wild type levels by complementation (Fig. 4-9A, Fig. 4-9B). In contrast, deletion or

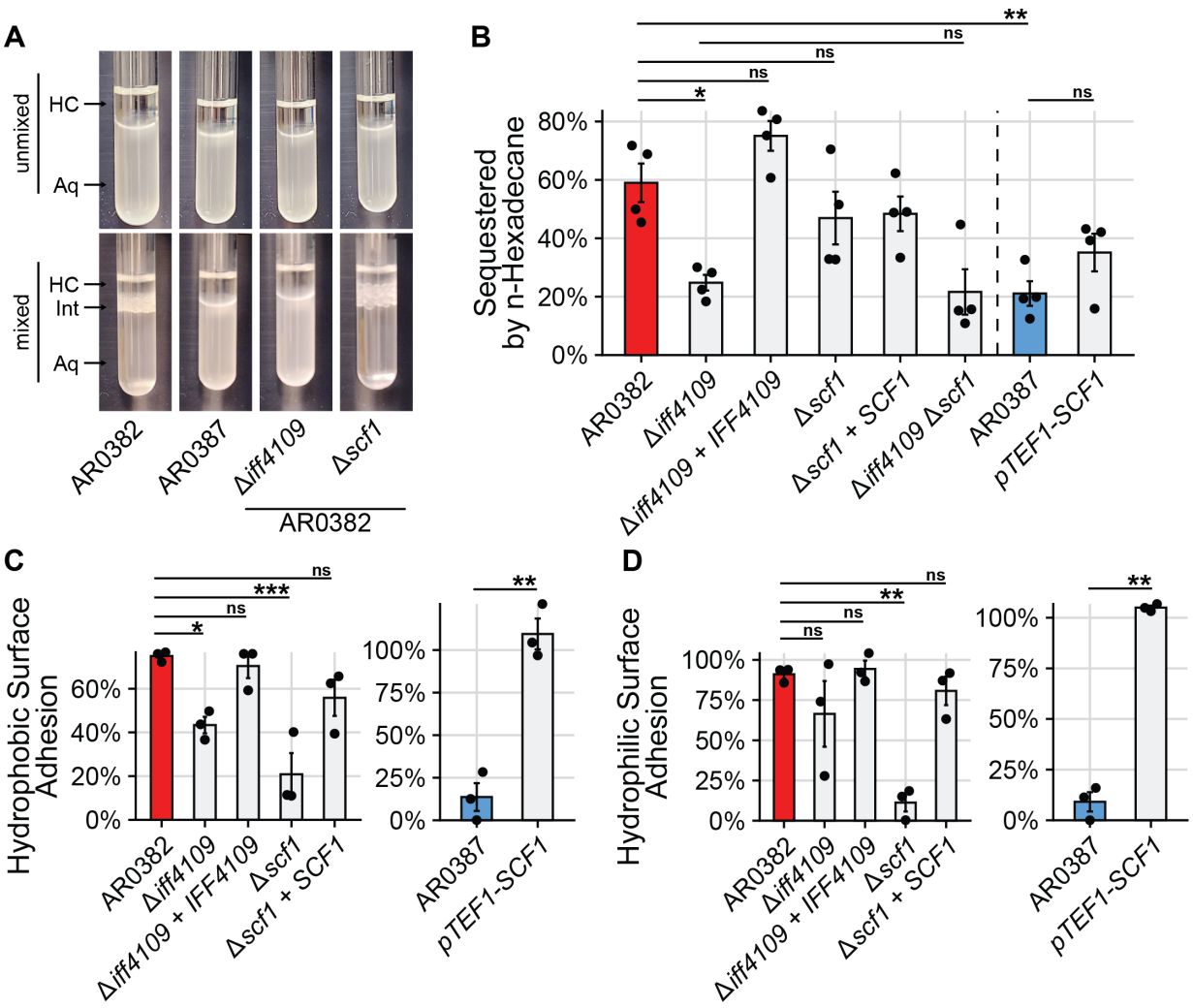

Figure 4-9 Iff4109, but not Scf1, mediates adhesion through cell surface hydrophobicity. (A) Representative images from Microbial Attachment to Hydrocarbons (MATH) assay. Hydrophobic cells are sequestered from the aqueous phase (Aq) to the aqueous-hydrocarbon interface (Int) after mixing with the hydrocarbon phase (HC). **(B)** Proportion of cells sequestered out of the aqueous phase during MATH assay. **(C)**, **(D)** Cells were allowed to attach to a hydrophobic, untreated polystyrene surface (C) or a hydrophilic, vacuum plasma treated polystyrene surface (D) for 1 hour. The surface was washed and the proportion of cells that remained attached after washing was measured. Statistical differences were assessed using one-way ANOVA with Tukey's post-hoc test (B), (C), and (D) or student's t-test (C) and (D); *$p \leq 0.05$; **$p \leq 0.01$; ***$p \leq 0.001$; ns: $p > 0.05$.

overexpression of *SCF1* did not significantly impact cell surface hydrophobicity in either AR0382 or AR0387 (Fig. 4-9A, Fig. 4-9B).

Elevated cell surface hydrophobicity likewise promotes affinity for hydrophobic substrates[58]. We measured the adhesion of *C. auris* isolates to both an untreated hydrophobic polystyrene surface and a polystyrene surface modified using a vacuum plasma treatment to

become strongly hydrophilic. Both *IFF4109* and *SCF1* mediated adhesion to the hydrophobic substrate (Fig. 4-9C). However, only *SCF1* mediated adhesion to the hydrophilic substrate, showing that *SCF1* is not dependent on hydrophobicity (Fig. 4-9D). Notably, AR0382 and

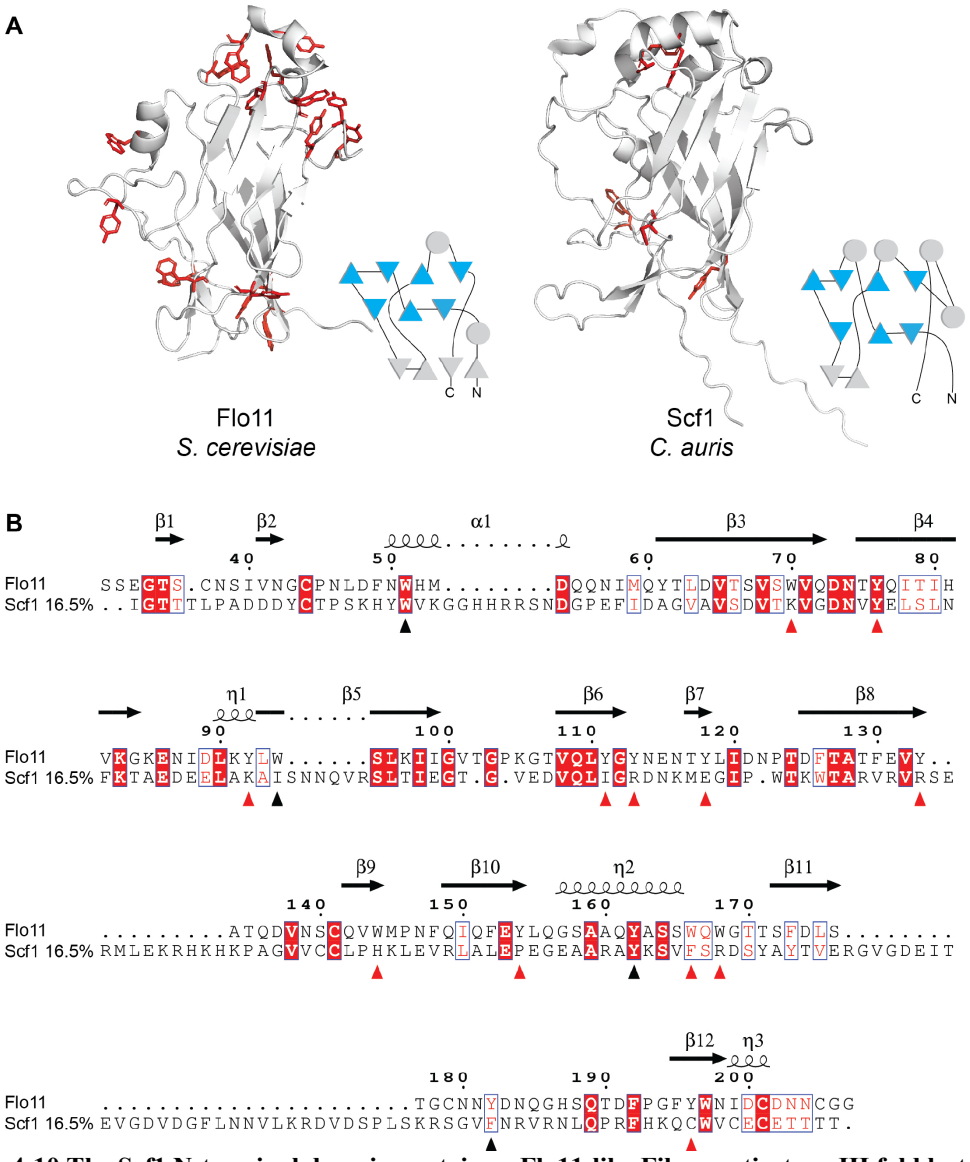

Figure 4-10 The Scf1 N-terminal domain contains a Flo11-like Fibronectin-type III fold but lacks conserved aromatic residues critical to Flo11 function. (A) N-terminal domain models for *S. cerevisiae* Flo11 (crystal structure) and *C. auris* Scf1 (AlphaFold2 predictive model) and membrane topology diagrams. Aromatic bands that are conserved and have functional roles in Flo11 homologues throughout *Ascomycota* are highlighted. The central Fibronectin-type III fold is highlighted in the topology diagrams. **(B)** Primary sequence alignment between *S. cerevisiae* Flo11 N-terminal domain and *C. auris* Scf1 N-terminal domain. Identical residues are boxed in red; similar residues are boxed in white. Inverted triangles indicate the positions of aromatic residues that are conserved from *S. cerevisiae* to Flo11 homologues in other *Ascomycotal* species. Red triangles indicate residues that have demonstrated functional roles in biofilm formation, invasive growth, or homotypic interactions.

AR0387 still exhibited differential adhesion to the hydrophilic surface, indicating hydrophobic interactions are not primarily responsible for the differential strain phenotypes (Fig. 4-9D).

To investigate the mechanism of Scf1 adhesion, we examined the apical N-terminal domain using AlphaFold2, which suggested this domain contains a core Fibronectin-type III fold similar to the *FLO11* family of adhesins characterized in *Saccharomyces cerevisiae* and conserved throughout *Ascomycota* (Fig. 4-10A)[88,89]. However, *SCF1* does not exhibit significant primary sequence homology to *S. cerevisiae FLO11* and lacks conservation of the canonical aromatic bands responsible for adhesive functions in true *FLO11* homologs (Fig. 4-10)[88,89]. Furthermore, model confidence dwindles outside the Fibronectin fold, suggesting substantial variation from Flo11 adhesins (Fig. 4-11). In its primary sequence, the *SCF1* N-terminal domain exhibits an enrichment of arginine and lysine residues compared to other yeast adhesins (Table

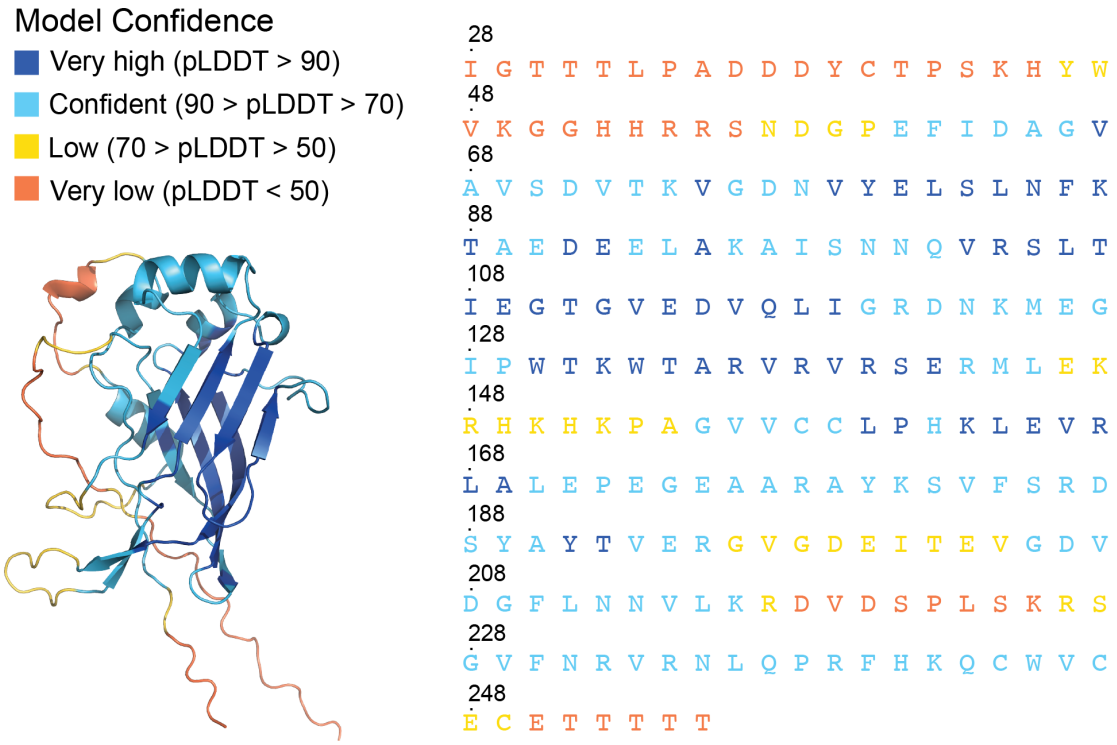

Figure 4-11 Predictive model confidence for the Scf1 N-terminal domain is substantially reduced outside of the Fibronectin-type III fold. N-terminal domain models for *C. auris* Scf1 (AlphaFold2 predictive model) and the domain sequence colored by per-residue pLDDT score. Cutoffs are set according to AlphaFold2 conventions. Numbers indicate amino acid position from the start codon.

4-2). Adhesive systems in many marine organisms rely on similarly cation-rich proteins, which act through displacement of hydrated ions at the surface-liquid interface or direct cation-π interactions with substrates[63–65,67,276]. We reasoned that if Scf1 relied on such interactions, adhesion could be inhibited by a saturating concentration of cations at the substrate interface that could not be competitively displaced by *SCF1*. Consistent with this hypothesis, high concentrations of arginine in solution were sufficient to ablate AR0382 adhesion (Fig. 4-12A). Similar concentrations of NaCl or other non-cationic amino acids did not produce the same

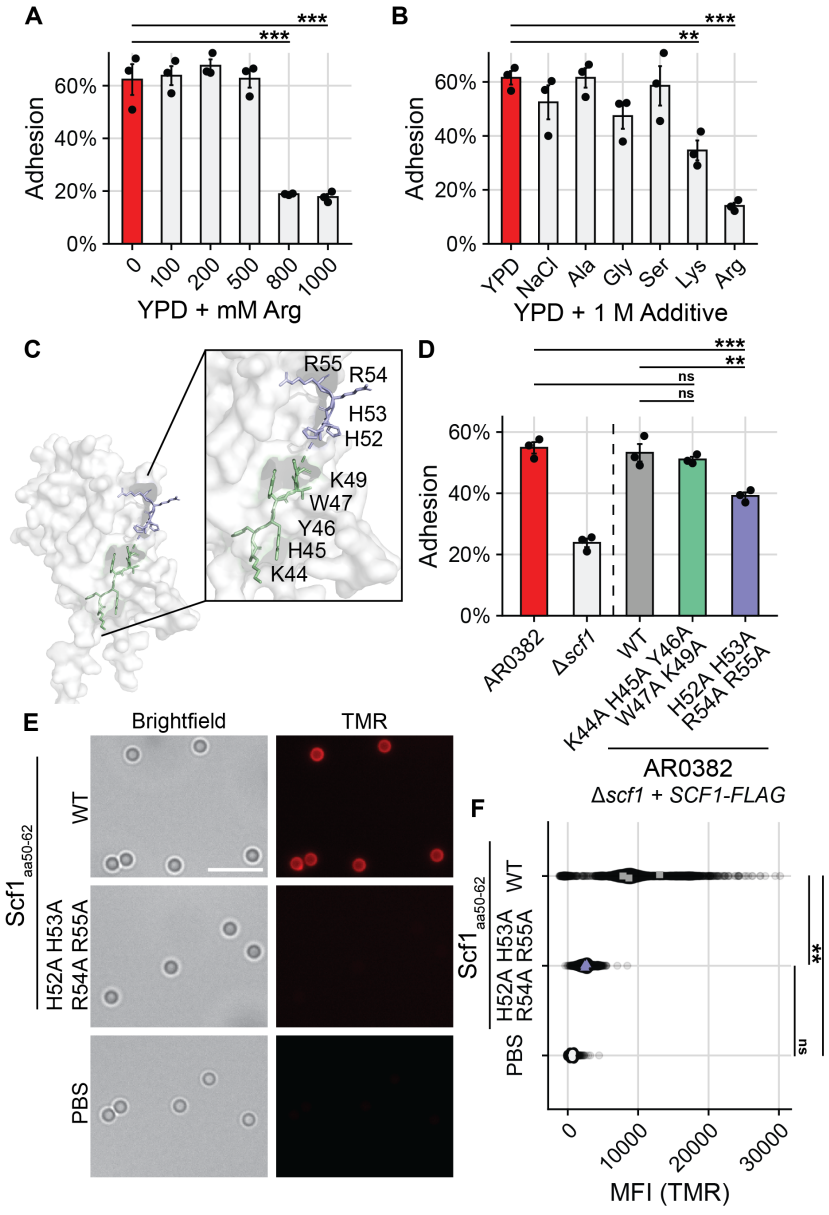

Figure 4-12 Specific cationic residues are critical for Scf1-mediated surface association. (A), (B) WT AR0382 adhesion in the presence of increasing concentrations of arginine (A) or 1 M additives (B). **(C)** Predictive model of the Scf1 N-terminal domain with two neighboring cationic-aromatic clusters highlighted. **(D)** Adhesion of wild type AR0382, a mutant lacking *SCF1*, or AR0382 Δ*scf1* + *SCF1-FLAG* mutants encoding the wild type *SCF1* allele or alleles containing the indicated mutations. **(E)** TMR-labelled 13-amino acid peptides corresponding to the wild type Scf1 sequence (residues 50-62) or the same sequence with the indicated mutations incubated with the same polystyrene microspheres used to measure adhesion in (D). Scale Bar = 5 μm. **(F)** Quantification (MFI) of peptide binding to individual polystyrene microspheres as in (E) measured by TMR epifluorescence, corrected for background fluorescence. Each point represents an individual microsphere. Colored points represent averages of individual experiments, used for statistical analysis. Statistical differences were assessed using one-way ANOVA with Dunnett's post-hoc test (A), (B) or one-way ANOVA with Tukey's post-hoc test (D), (F); *p ≤ 0.05; **p ≤ 0.01; ***p ≤ 0.001; ns: p > 0.05.

effect, while exogenous lysine produced a more modest inhibition of attachment, consistent with lysine's weaker ability to form electrostatic interactions (Fig. 4-12B)[277].

Family	Adhesin	Organism	Uniprot ID	Domain Length	Arg (%)	Arg + Lys (%)
SCF1						
	Scf1	***C. auris***	**A0A2H1A319**	**228**	**18 (7.9%)**	**33 (14.5%)**
FLO11						
	Flo11	*S. cerevisiae*	P08640	177	0 (0%)	5 (2.8%)
	KpFLO11	*K. pastoris*	C4R2D7	171	2 (1.2%)	15 (8.8%)
	Rbt1	*C. albicans*	Q59TP1	278	5 (1.8%)	26 (9.4%)
PA14						
	Flo1	*S. cerevisiae*	P32768	176	0 (0%)	4 (2.3%)
	Flo5	*S. cerevisiae*	P38894	176	0 (0%)	3 (1.7%)
	Flo9	*S. cerevisiae*	P39712	176	0 (0%)	4 (2.3%)
	Flo10	*S. cerevisiae*	P36170	161	2 (1.2%)	11 (6.8%)
	Epa1	*C. glabrata*	Q6FUW5	148	5 (3.4%)	11 (7.4%)
	Epa6	*C. glabrata*	Q6FX55	159	5 (3.1%)	12 (7.5%)
	Epa9	*C. glabrata*	B4UMX2	163	5 (3.1%)	16 (9.8%)
	Pwp7	*C. glabrata*	Q6FQ10	174	4 (2.3%)	12 (6.9%)
	Cea1	*K. pastoris*	A0A1B2J5V1	161	5 (3.1%)	15 (9.3%)
	KpFlo2	*K. pastoris*	A0A1B2JGH2	188	9 (4.8%)	12 (6.4%)
ALS						
	Als1	*C. albicans*	Q5A8T4	247	2 (0.8%)	13 (5.3%)
	Als3	*C. albicans*	Q59L12	247	3 (1.2%)	14 (5.7%)
	Als9	*C. albicans*	A0A1D8PQ86	246	2 (0.8%)	11 (4.5%)
	Sag1	*S. cerevisiae*	P20840	107	1 (0.9%)	2 (1.9%)
	Als2582	*C. auris*	A0A2H0ZWS7	254	7 (2.8%)	13 (5.1%)
	Als4498	*C. auris*	A0A2H0ZFP2	254	7 (2.8%)	18 (7.1%)
	Als4112	*C. auris*	A0A2H0ZHZ9	255	4 (1.6%)	11 (4.3%)
IFF/HYR						
	Hyr1	*C. albicans*	Q5AL03	324	10 (3.1%)	26 (8.0%)
	Iff4	*C. albicans*	Q5AAL9	319	9 (2.8%)	19 (6.0%)
	Iff4109	*C. auris*	A0A2H0ZI42	312	5 (1.6%)	13 (4.2%)
	Iff1531	*C. auris*	A0A2H0ZYK9	315	5 (1.6%)	10 (3.2%)
	Iff4892	*C. auris*	A0A2H0ZGW1	312	3 (1%)	9 (2.9%)

Table 4-2 The Scf1 N-terminal domain is enriched in arginine and lysine residues compared to characterized yeast adhesins. Total residue counts and proportions of arginine and lysine residues from the N-terminal domain of representative adhesins from major yeast adhesin families are shown.

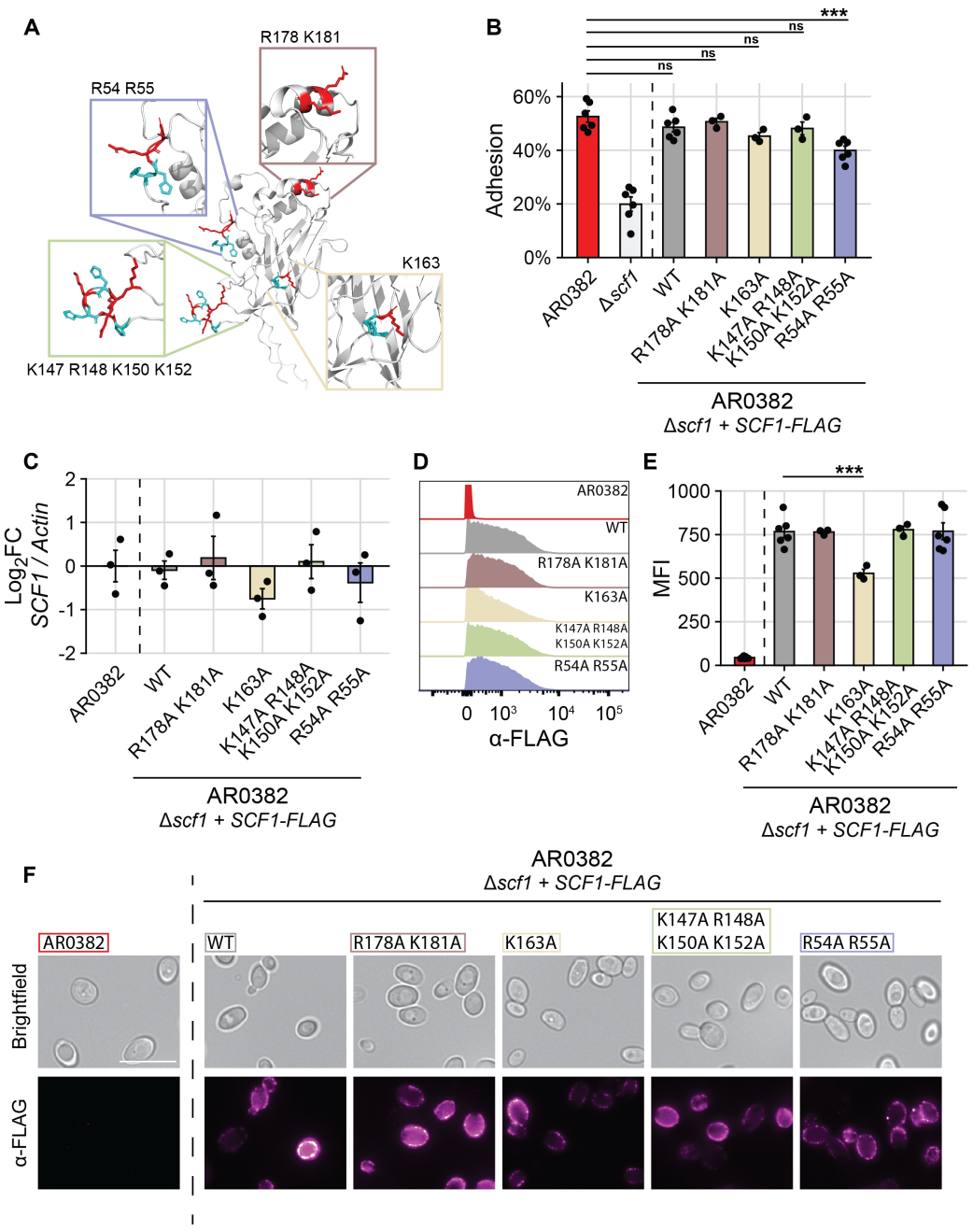

Figure 4-13 Tolerance of mutation of specific cationic residues in the Scf1 N-terminal domain. (A) Predictive model of the Scf1 N-terminal domain with hypothesized critical cationic residues highlighted in red and neighboring aromatic residues highlighted in blue. **(B)** Adhesion to polystyrene microspheres measured for wild type AR0382, a mutant lacking *SCF1*, or AR0382 Δ*scf1 + SCF1-FLAG* mutants encoding the wild type *SCF1* allele or alleles containing the indicated mutations. **(C)** Relative *SCF1* transcript abundance by RT-qPCR compared to wild type AR0382 levels. No significant differences were identified. **(D)** Representative fluorescence intensity of strains labeled with α-FLAG antibody. Each plot represents 50,000 events captured by flow cytometry. **(E)** MFI quantification of replicates from labelled cells as in (B). **(F)** Brightfield and epifluorescent microscopy of cells labeled with α-FLAG antibody. Scale bar = 5 μm. Statistical differences were assessed using one-way ANOVA with Dunnett's post-hoc test using AR0382 as comparator (B), (C) or AR0382 Δ*scf1 + SCF1-FLAG*$_{WT}$ as comparator (E); *p ≤ 0.05; **p ≤ 0.01; ***p ≤ 0.001; ns: p > 0.05.

We next investigated whether specific cationic regions or residues were critical for Scf1 activity. We generated point mutations in cationic residues in different areas of the N-terminal domain, focusing on residues that clustered with aromatic groups, as this pattern potentiates electrostatic adhesion (Fig. 4-13A)[66]. Several mutations had no adhesive impact, but an R54A R55A mutant exhibited a modest adhesive defect, while showing no discernable effect on *SCF1* transcription, protein expression, or localization (Fig. 4-13). Mutating the entire cation-aromatic cluster, H52 H53 R54 R55, resulted in a similar

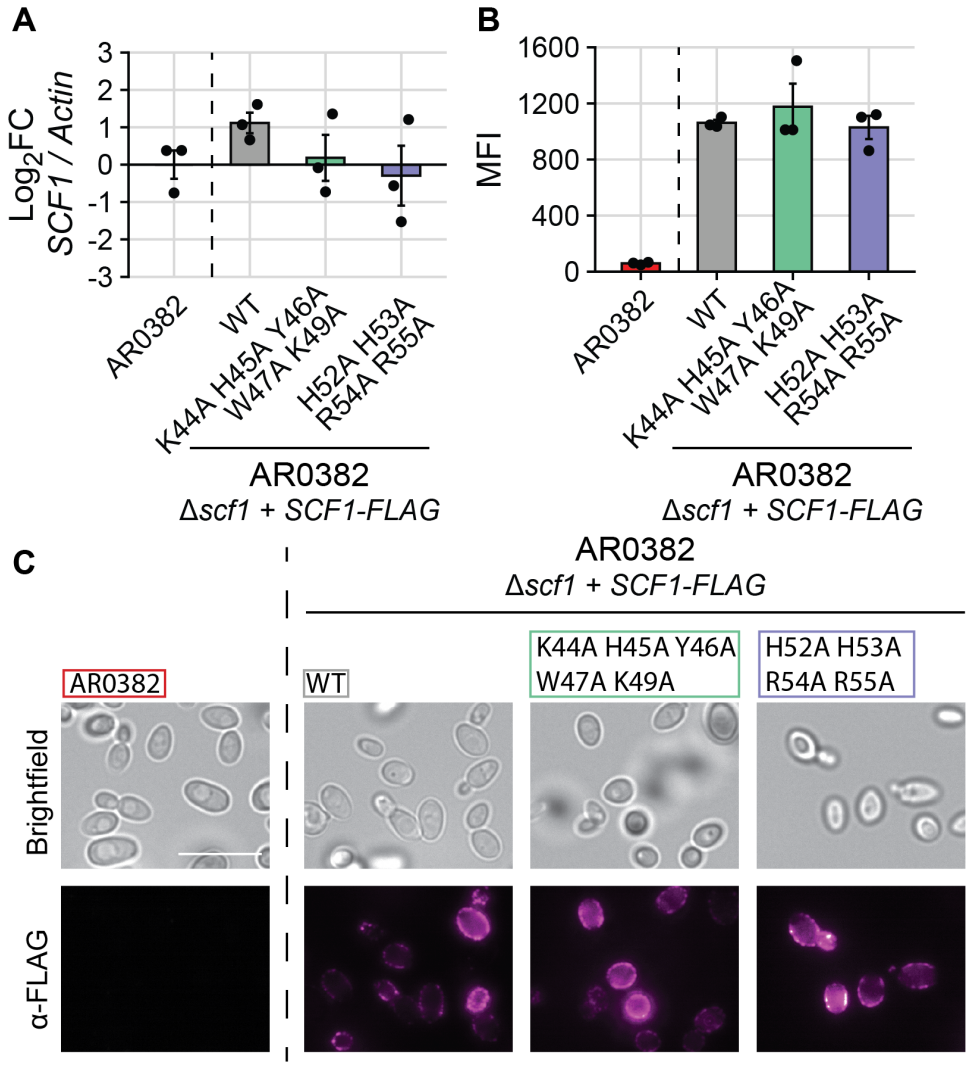

Figure 4-14 Mutation of two adjacent cation-aromatic clusters does not impact Scf1 expression or localization. Measurements are determined for wild type AR0382 or AR0382 Δ*scf1 + SCF1-FLAG* mutants encoding the wild type *SCF1* allele or alleles containing the indicated mutations. **(A)** Relative *SCF1* transcript abundance by RT-qPCR compared to wild type AR0382 levels. No significant differences were identified. **(B)** MFI of cells labelled with α-FLAG antibody collected from 50,000 events. No significant differences were identified among strains encoding the various *SCF1* alleles. **(C)** Brightfield and epifluorescent microscopy of cells labeled with α-FLAG antibody. Scale bar = 5 μm. Statistical differences were assessed using one-way ANOVA with Dunnett's post-hoc test using AR0382 as comparator (A) or AR0382 Δ*scf1 + SCF1-FLAG*$_{WT}$ as comparator (B); *p ≤ 0.05; **p ≤ 0.01; ***p ≤ 0.001; ns: p > 0.05.

adhesive defect (Fig. 4-12C, Fig. 4-12D, Fig. 4-14). Notably, a nearby cation-aromatic cluster, K44-K49, which was modeled to be less surface-exposed, was not required for adhesion (Fig. 4-12C, Fig. 4-12D, Fig. 4-14). To determine whether surface exposure of the HHRR cluster (res. 52-55) would be sufficient to promote adhesion, we synthesized peptides corresponding to Scf1 residues 50-62 with the intact wild-type cluster or the HHRR residues mutated. The wild-type peptide adhered to polystyrene microspheres, but mutation of the HHRR cluster completely ablated this ability (Fig. 4-12E, Fig. 4-12F). Interestingly, similar patterns of cation-aromatic clusters are also abundant in some lipid-binding proteins[67,278]. The wild type Scf1 peptide was similarly able to adhere to

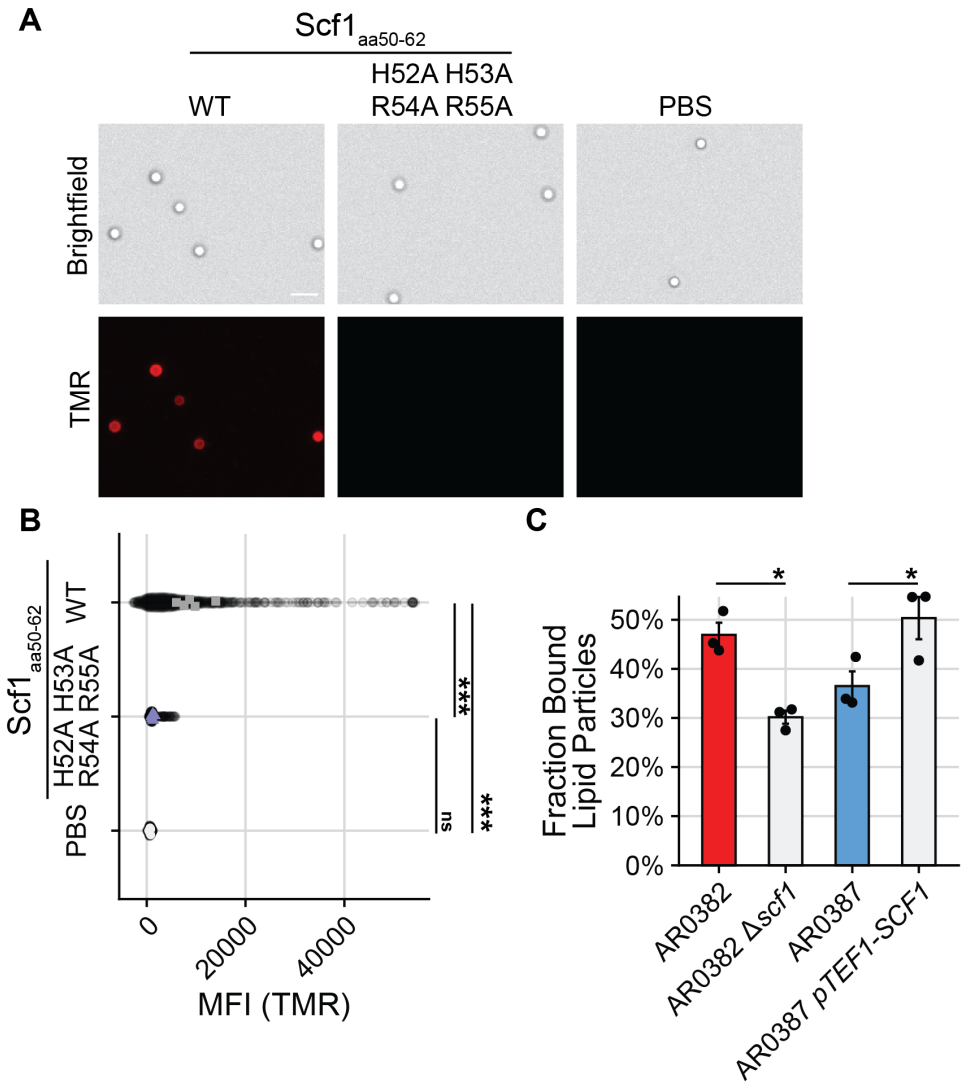

Figure 4-15 Scf1 mediates lipid binding. (A) TMR-labelled 13-amino acid peptides corresponding to Scf1 residues 50-62 or the same sequence with indicated mutations were incubated with phosphotidyl choline (PC) microparticles with exposed phospholipid head groups. Scale bar = 10 μm. **(B)** MFI of PC lipid particles bound by peptides as in (A), normalized to background fluorescence. Each point represents an individual particle. Colored points represent averages from individual experiments, used for statistical analysis. **(C)** Fraction of PC lipid particles bound by cells after incubation with cultures of each of the indicated strains. Statistical differences were assessed using one-way ANOVA with Tukey's post-hoc test; *$p \leq 0.05$; **$p \leq 0.01$; ***$p \leq 0.001$; ns: $p > 0.05$.

phosphotidylcholine microparticles, and *SCF1* expression potentiated lipid particle binding by *C. auris* cells, suggesting *SCF1* may also contribute to association with biotic substrates (Fig. 4-15).

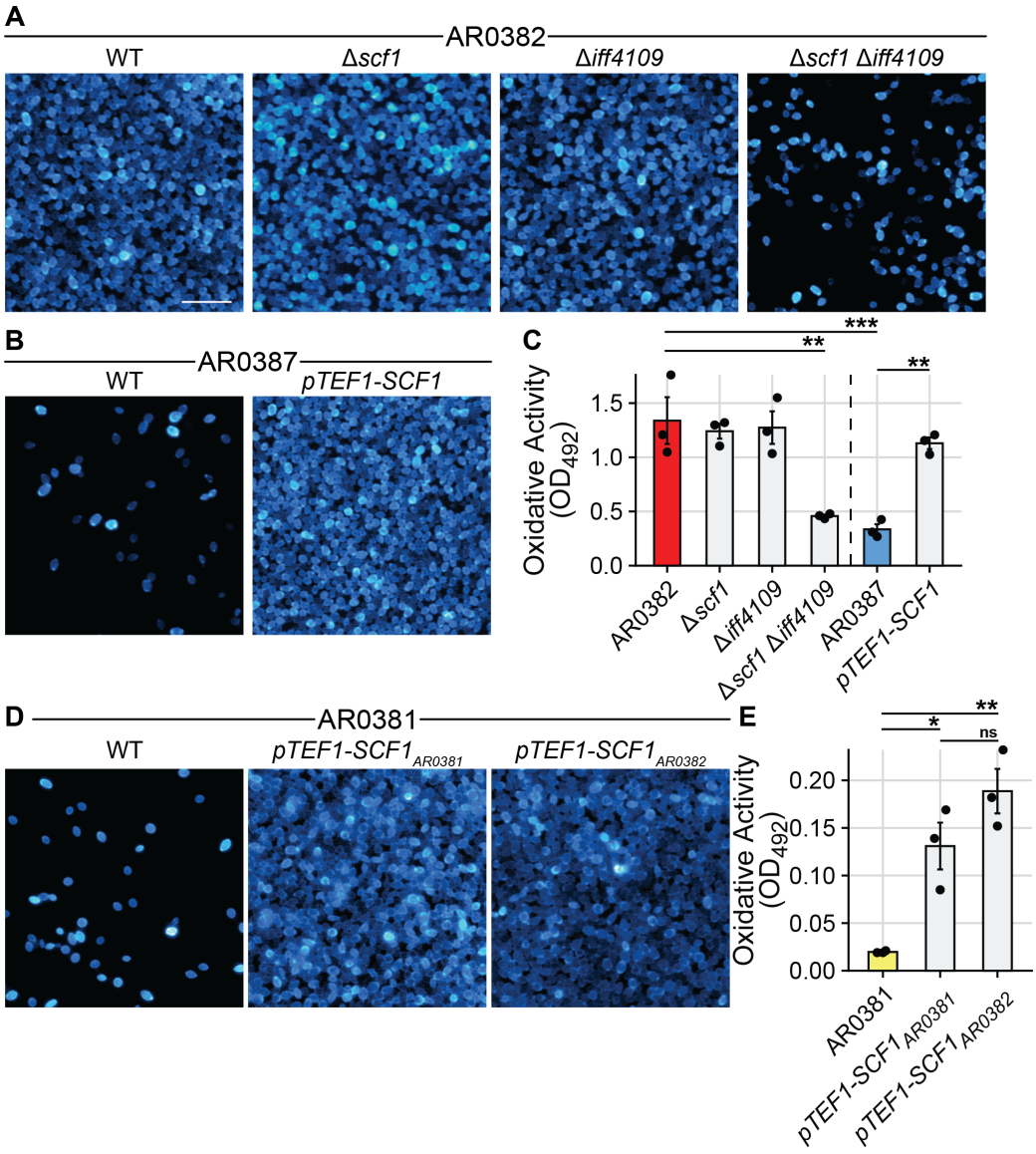

Figure 4-16 Scf1 drives biofilm formation in vitro. Biofilms were grown on polystyrene in RPMI at 37°C and stained with calcofluor white. Representative biofilm images in (A), (B), and (D) are depicted as maximum intensity projections from Z-stacks captured using epifluorescence microscopy. **(A)** Deletion of both *SCF1* and *IFF4109* is required to abrogate biofilm formation in AR0382. **(B)** Overexpression of *SCF1* is sufficient to drive biofilm formation in AR0387. **(C)** Oxidative activity of *in vitro* biofilms was measured using an XTT-reduction assay. **(D)** Expression of *SCF1* in a clade II isolate is sufficient to drive biofilm formation. Representative images of biofilms formed by wild type AR0381 (clade II) or mutants overexpressing either the endogenous AR0381 *SCF1* allele or the clade I *SCF1* allele from AR0382. **(E)** Oxidative activity of clade II biofilms was measured using an XTT-reduction assay. Scale bar = 20 μm. Statistical differences were assessed using one-way ANOVA with Tukey's post-hoc test; *p ≤ 0.05; **p ≤ 0.01; ***p ≤ 0.001; ns: p > 0.05.

4.3.4 Scf1 promotes long term colonization and virulence

We next investigated the impact of *SCF1* and *IFF4109* on other aspects of surface colonization. We measured the importance of these adhesins for biofilm growth, which can promote prolonged environmental persistence[34,202,204,205]. The two adhesins were functionally redundant, and

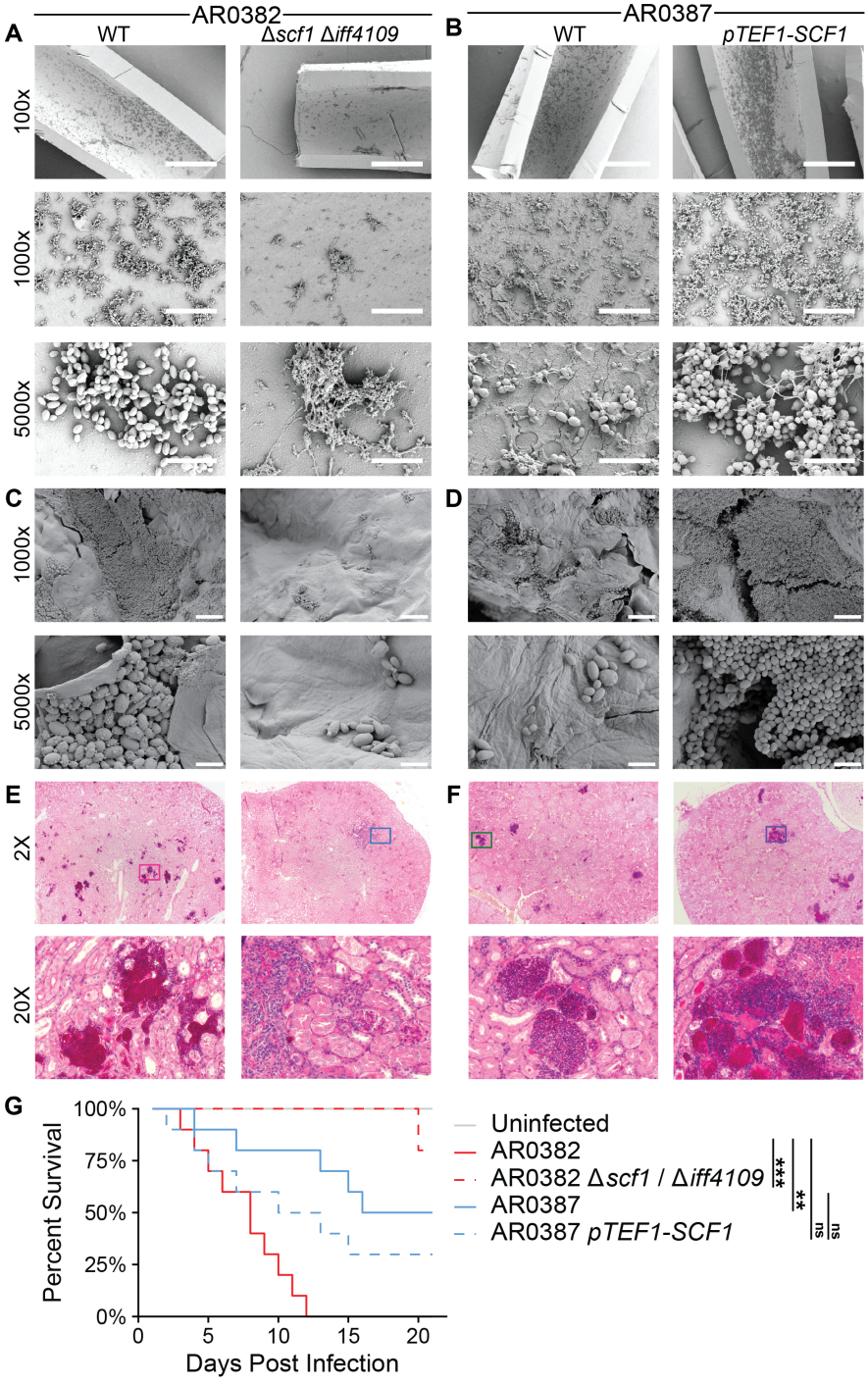

Figure 4-17 Scf1 mediates host colonization and infection phenotypes. (A), (B) Polyethylene central venous catheters were set in rat jugular veins and inoculated intraluminally with *C. auris*. Representative scanning electron microscopy images of the luminal catheter surface are shown from catheters collected 24 hrs after infection. Scale bars: 400 µm (100x), 40 µm (1000x), 5 µm (5000x). **(C), (D)** Full thickness human skin explants were colonized with *C. auris* for 24 hrs before washing to remove unassociated cells. Representative scanning electron microscopy images of the skin surface following washing are shown. Scale bars: 20 µm (1000x), 4 µm (5000x). **(E), (F), (G)** Immunosuppressed mice were infected intravenously (via tail vein injection) with 5 x 10^7 *C. auris* cells. Histopathology sections of the kidneys 7 days post infection (E), (F) were stained with PAS. Magenta color indicates lesion areas. Ten infected mice for each strain were monitored for survival for 21 days (G). Statistical comparisons of overall survival were assessed using the Mantel-Haenszel log-rank test with Benjamini-Hochberg correction. *$p \leq 0.05$; **$p \leq 0.01$; ***$p \leq 0.001$; ns $p > 0.05$.

deletion of both was required to ablate biofilm formation in AR0382, suggesting the partial adhesive contributions of each is sufficient to establish colonization (Fig. 4-16A). Expression of *SCF1* alone in otherwise biofilm-incompetent isolates was sufficient to establish biofilm colonization (Fig. 4-16(B-E)). This pattern continued for *in vivo* biofilms, where loss of *SCF1* and *IFF4109* ablated the ability of AR0382 to colonize the luminal surface of a polyethylene rat central venous catheter, and overexpression of *SCF1* was sufficient to potentiate AR0387 colonization (Fig. 4-17A, Fig. 4-17B).

We then investigated whether biological surface association followed the same reliance on these adhesins. Again, we observed that loss of *SCF1* and *IFF4109* diminished the ability of AR0382 to colonize *ex vivo* human skin explants and *in vivo* murine skin, while overexpression of *SCF1* potentiated skin colonization by AR0387 (Fig. 4-17C, Fig. 4-17D, Fig. 4-18). Given this potential for interaction with host tissues, we also investigated the importance of these adhesins in disseminated infection. Histopathological examination of tissues collected from mice 7 days

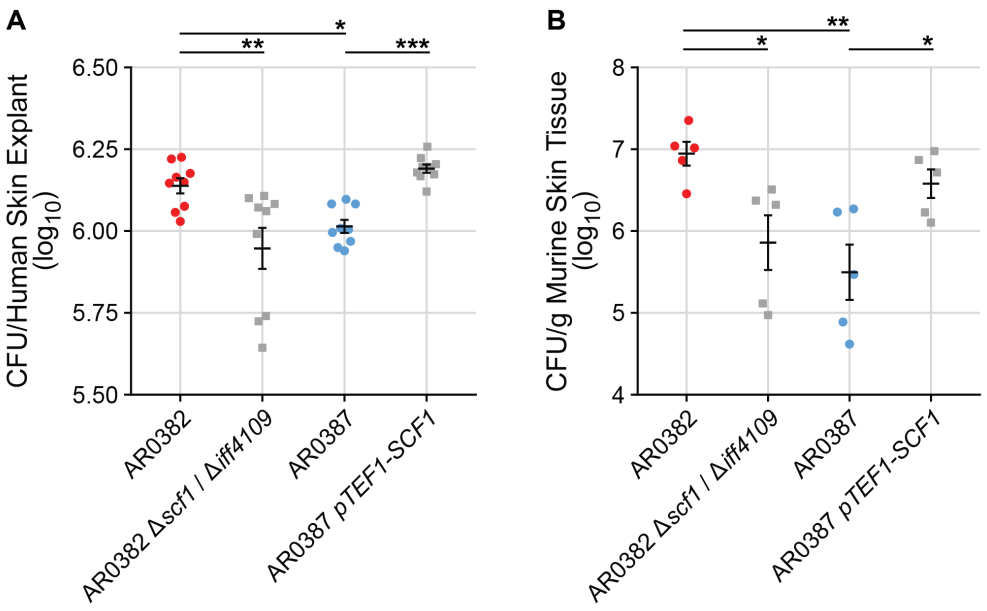

Figure 4-18 Scf1 is critical for skin colonization. (A) *C. auris* cells were incubated on full thickness *ex vivo* human skin samples for 24 hrs before washing and measuring remaining bioburden by colony forming units (CFU). **(B)** Viable burden of *C. auris* after 2 days incubation on murine skin *in vivo*. Data are presented as CFU/g tissue normalized to actual delivered inocula. Statistical differences were assessed using one-way ANOVA with Tukey's post-hoc test; *p ≤ 0.05; **p ≤ 0.01; ***p ≤ 0.001; ns: p > 0.05.

after intravenous *C. auris* infection revealed that loss of *SCF1* and *IFF4109* reduced AR0382 dissemination to the kidneys and heart, while overexpression of *SCF1* in AR0387 was sufficient to increase fungal lesions (Fig. 4-17E, Fig. 4-17F, Fig. 4-19). Loss of *SCF1* and *IFF4109* substantially attenuated the virulence of AR0382, with the wild type causing 100% mortality within 12 days of infection and the mutant causing 20% mortality after 21 days (Fig. 4-17G). Similarly, overexpression of *SCF1* reduced the median survival of mice infected with AR0387 from 18.5 days to 11.5 days and ablated the difference in overall survival between the less virulent AR0387 and the more virulent AR0382 (Fig. 4-17G).

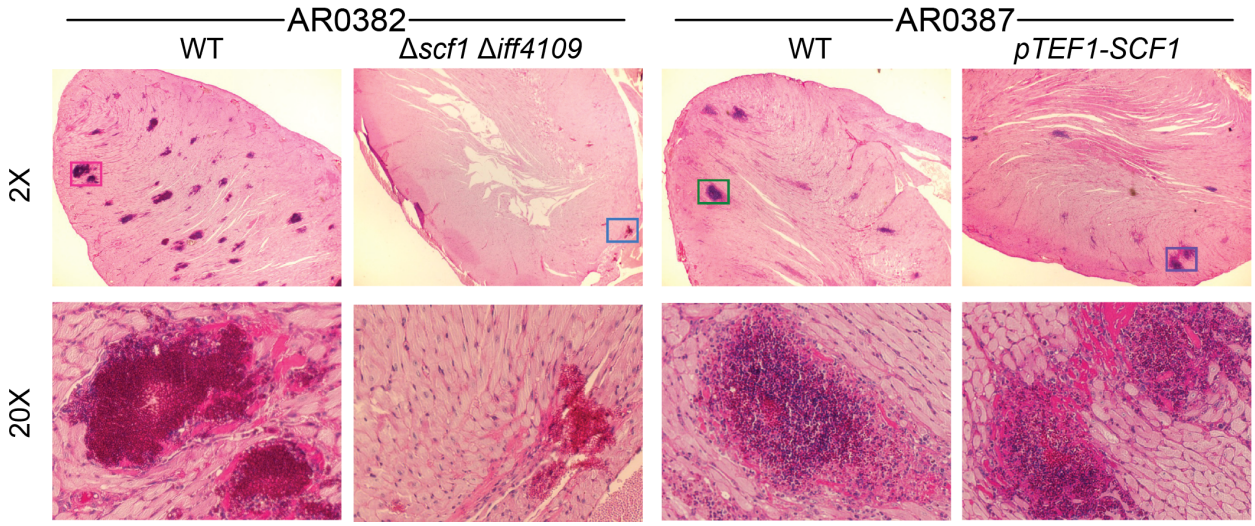

Figure 4-19 Scf1 is critical for dissemination and fungal burden. Histopathology sections of the heart of *C. auris*-infected mice were stained with PAS and imaged at 2X and 20X resolution using Olympus bright field microscopy. Lower panel for each organ represents the magnified area of colored boxes from 2X panel. Magenta color indicates lesion areas.

4.4 Conclusions

C. auris encodes genes similar to the conserved *ALS* and *IFF/HYR* adhesin families, and proposed models suggest differential utilization of these adhesins may contribute to epidemiological differences among isolates[84,274]. Our findings suggest the *C. auris*-specific adhesin *SCF1* and the conserved adhesin *IFF4109* are the principal mediators of association with abiotic surfaces, and additionally contribute substantially to infection and long-term colonization

of both biological and abiotic surfaces. Interestingly, the other conserved adhesin genes appeared to not mediate surface association. Whether this is the product of functional or regulatory divergence remains to be explored. Notably, we observed widespread differential regulation of *SCF1* among *C. auris* isolates regardless of clade, suggesting transcriptional control of this adhesin has adapted more recently than clade separation. The widespread plasticity around a single genetic element responsible for diverse clinically-relevant phenotypes could be problematic in outbreak settings. While *SCF1* and *IFF4109* contribute to host infection and colonization, the mechanisms of their interaction with host systems remain unclear. Understanding how variable adhesion allows *C. auris* to mediate infection is likely to offer therapeutic insights. Prior work suggests vaccination or monoclonal antibody therapy targeting Als or Iff/Hyr adhesins may offer protection against lethal *C. auris* infection[274,279]. Furthermore, the complementary function of *SCF1* and *IFF4109* with divergent mechanisms suggests *C. auris* has evolved the capacity for promiscuous surface association and colonization. Mediation of hydrophobic interactions is largely conserved among fungal adhesins, consistent with the adhesive mechanism of the conserved *IFF4109*[57,58,88]. The cation rich *SCF1*, however, appears to functionally resemble proteins from bivalve, barnacle, and *Vibrio* adhesion systems. For these organisms, cation-dependent surface interactions promote adhesion in aqueous and highly ionic environments[63–65,276]. *C. auris* has been isolated from the coastal wetlands of the Andaman Islands and from a Colombian estuary, suggesting a possible marine natural habitat, and this ecological niche may have conferred similar selective pressures on adhesion mechanisms[13,14]. Development of unique adhesion biology may in part explain the tenacity of this organism on medically-relevant substrates. Still, differential utilization of *SCF1* by different isolates suggests an unknown selective pressure may govern its expression. Understanding this adaptation and its

clinical consequences more fully may offer important insights into the outbreak potential of this pathogen.

Overall, our work characterizes of the adhesin machinery used by *C. auris* for surface association and colonization. The identification of *SCF1* and the characterization of the genetic determinants of adhesion add to the growing understanding of the pathobiology this emerging organism.

4.5 Notable Contributions

Author contributions are as follows: Juliet Anku assisted with cell surface hydrophobicity experiments in Fig. 4-9 and murine skin colonization experiments in Fig. 4-18. Guolei Zhao performed the murine skin colonization experiments in Fig. 4-18 with Juliet Anku. Robert Zarnowski performed the rat catheter colonization experiments in Fig. 4-17, and this line of experimentation was supervised by David Andes. Chad Johnson performed the ex vivo human skin colonization experiments in Fig. 4-17 and Fig. 4-18, and this line of experimentation was supervised by Jeniel Nett. Haley Hautau and Shakti Singh performed the murine intravenous infection experiments in Fig. 4-17 and Fig. 4-19, and this line of experimentation was supervised by Shakti Singh and Ashraf Ibrahim. Noelle Visser assisted with the high throughput adhesion screen in Fig. 4-1.

4.6 Methods

4.6.1 Strains and culture conditions

A list of all strains used in this study is included in Table 4-3. Clinical *C. auris* isolates were obtained through the CDC/FDA Antibiotic Resistant Isolate Bank[229] or from Rush University Medical Center, Chicago, IL (Gift from Mary Hayden). Except where specified, *C. auris* cells

were cultured at 30°C in YPD liquid media (1% yeast extract, 2% peptone, 2% dextrose) with constant agitation. All strains were maintained as frozen stocks of 25% glycerol at -80°C.

4.6.2 Genomic DNA isolation

Genomic DNA was isolated using a PCA extraction method. Briefly, yeast cells were incubated overnight in liquid YPD at 30°C then harvested by centrifugation and resuspended in lysis buffer (2% (v/v) Triton X-100, 1% (w/v) SDS, 100 mM NaCl, 10 mM Tris-Cl, 1 mM EDTA). The cell suspension was disrupted by bead-beating and released DNA was extracted into PCA and then into Chloroform. The resulting DNA was purified by ethanol precipitation and resuspended in water before being treated with RNase A. RNase was heat-inactivated, then extracted DNA was purified by ethanol precipitation and resuspended in water.

4.6.3 Primers and plasmids

A list of all plasmids used in this study is included in Table 4-4. A list of all primers used in this study is included in Table 4-5. Cassettes for transformation of *C. auris* were maintained in the multiple cloning site of the pUC19 cloning vector and assembled from fragments using the NeBuilder HIFI DNA Assembly Master Mix (NEB #E2621) or the Codex DNA Gibson Assembly Ultra Master Mix (Codex DNA #GA1200) according to the manufacturer's instructions.

4.6.4 Plasmid and strain construction

pTO144/CauTO186: The plasmid backbone was amplified from pTO139 using oTO190-oTO191. The NAT cassette was amplified from pTO137 using oTO186-oTO187. The NAT cassette was flanked by approximately 500 bp regions homologous to the regions immediately upstream and downstream of *ALS* (B9J08_002582) amplified from *C. auris* genomic DNA using

oTO184-oTO185 and oTO188-oTO189 respectively. The repair cassette was amplified using oTO18-oTO19 and transformed into AR0382 to generate CauTO186.

pTO167/CauTO187: The plasmid backbone was amplified from pTO139 using oTO410-oTO411. The NAT cassette was amplified from pTO137 using oTO414-oTO415. The NAT cassette was flanked by approximately 500 bp regions homologous to the regions immediately upstream and downstream of *ALS* (B9J08_004498) amplified from *C. auris* genomic DNA using oTO412-oTO413 and oTO416-oTO417 respectively. The repair cassette was amplified using oTO18-oTO19 and transformed into AR0382 to generate CauTO187.

pTO166/CauTO226: The plasmid backbone was amplified from pTO139 using oTO402-oTO403. The NAT cassette was amplified from pTO137 using oTO406-oTO407. The NAT cassette was flanked by approximately 500 bp regions homologous to the regions immediately upstream and downstream of *ALS* (B9J08_004112) amplified from *C. auris* genomic DNA using oTO404-oTO404 and oTO408-oTO409 respectively. The repair cassette was amplified using oTO18-oTO19 and transformed into AR0382 to generate CauTO226.

pTO145/CauTO233: The plasmid backbone was amplified from pTO139 using oTO198-oTO199. The NAT cassette was amplified from pTO137 using oTO194-oTO195. The NAT cassette was flanked by approximately 500 bp regions homologous to the regions immediately upstream and downstream of *IFF* (B9J08_004100) amplified from *C. auris* genomic DNA using oTO192-oTO193 and oTO196-oTO197 respectively. The repair cassette was amplified using oTO18-oTO19 and transformed into AR0382 to generate CauTO233.

pTO148/CauTO234: The plasmid backbone was amplified from pTO139 using oTO222-oTO223. The NAT cassette was amplified from pTO137 using oTO218-oTO219. The NAT cassette was flanked by approximately 500 bp regions homologous to the regions immediately

upstream and downstream of *IFF* (B9J08_004109) amplified from *C. auris* genomic DNA using oTO216-oTO217 and oTO220-oTO221 respectively. The repair cassette was amplified using oTO18-oTO19 and transformed into AR0382 to generate CauTO234.

pTO202/CauTO235: The plasmid backbone was amplified from pTO139 using oTO590-oTO591. The NAT cassette was amplified from pTO137 using oTO788-oTO789. The NAT cassette was flanked by approximately 500 bp regions homologous to the regions immediately upstream and downstream of *IFF* (B9J08_004098) amplified from *C. auris* genomic DNA using oTO786-oTO787 and oTO790-oTO791 respectively. The repair cassette was amplified using oTO18-oTO19 and transformed into AR0382 to generate CauTO235.

pTO188/CauTO236: The plasmid backbone was amplified from pTO139 using oTO590-oTO591. The NEO cassette was amplified from pTO169 using oTO668-oTO669. The NEO cassette was flanked by approximately 500 bp regions homologous to the regions immediately upstream and downstream of *IFF* (B9J08_004110) amplified from *C. auris* genomic DNA using oTO678-oTO679 and oTO680-oTO681 respectively. The repair cassette was amplified using oTO18-oTO19 and transformed into AR0382 to generate CauTO236.

pTO146/CauTO247: The plasmid backbone was amplified from pTO139 using oTO206-oTO207. The NAT cassette was amplified from pTO137 using oTO202-oTO203. The NAT cassette was flanked by approximately 500 bp regions homologous to the regions immediately upstream and downstream of *IFF* (B9J08_001531) amplified from *C. auris* genomic DNA using oTO200-oTO201 and oTO204-oTO205 respectively. The repair cassette was amplified using oTO18-oTO19 and transformed into AR0382 to generate CauTO247.

pTO147/CauTO248: The plasmid backbone was amplified from pTO139 using oTO214-oTO215. The NAT cassette was amplified from pTO137 using oTO210-oTO211. The NAT

cassette was flanked by approximately 500 bp regions homologous to the regions immediately upstream and downstream of *IFF* (B9J08_004892) amplified from *C. auris* genomic DNA using oTO208-oTO209 and oTO212-oTO213 respectively. The repair cassette was amplified using oTO18-oTO19 and transformed into AR0382 to generate CauTO248.

pTO205/CauTO249: The plasmid backbone was amplified from pTO139 using oTO590-oTO591. The NAT cassette was amplified from pTO137 using oTO821-oTO822. The NAT cassette was flanked by approximately 500 bp regions homologous to the regions immediately upstream and downstream of *IFF* (B9J08_001155) amplified from *C. auris* genomic DNA using oTO819-oTO820 and oTO823-oTO824 respectively. The repair cassette was amplified using oTO18-oTO19 and transformed into AR0382 to generate CauTO249.

pTO206/CauTO250: The plasmid backbone was amplified from pTO139 using oTO590-oTO591. The NAT cassette was amplified from pTO137 using oTO827-oTO828. The NAT cassette was flanked by approximately 500 bp regions homologous to the regions immediately upstream and downstream of *IFF* (B9J08_004451) amplified from *C. auris* genomic DNA using oTO825-TO826 and oTO829-oTO830 respectively. The repair cassette was amplified using oTO18-oTO19 and transformed into AR0382 to generate CauTO250.

pTO207/CauTO251: The plasmid backbone was amplified from pTO139 using oTO590-oTO591. The NAT cassette was amplified from pTO137 using oTO833-oTO834. The NAT cassette was flanked by approximately 500 bp regions homologous to the regions immediately upstream and downstream of *IFF* (B9J08_000675) amplified from *C. auris* genomic DNA using oTO831-TO832 and oTO835-oTO836 respectively. The repair cassette was amplified using oTO18-oTO19 and transformed into AR0382 to generate CauTO250.

pTO211/CauTO261: The plasmid backbone was amplified from pTO139 using oTO590-oTO591. The NAT cassette was amplified from pTO137 using oTO668-oTO874. The NAT cassette was flanked by approximately 500 bp regions homologous to the regions immediately upstream and downstream of *SCF1* (B9J08_001458) amplified from *C. auris* genomic DNA using oTO879-TO880 and oTO881-oTO882 respectively. The repair cassette was amplified using oTO18-oTO19 and transformed into AR0382 to generate CauTO261.

CauTO320: A FLAG-tagged *SCF1* complementation cassette was generated using overlap extension PCR to insert a FLAG sequence between domains A and B (between amino acids 250-251). Fragments were amplified from pTO223 using oTO1160-oTO224 and oTO1159-oTO225 and fused with extension primers oTO945-oTO946. The resulting fusion fragment was transformed into CauTO261 to generate CauTO320.

pTO222/CauTO307: The ORF for *IFF* (B9J08_004109) along with approximately 500 bp of upstream sequence was amplified from *C. auris* genomic DNA using oTO937-oTO938. The NEO cassette was amplified from pTO169 using oTO668-oTO669. The plasmid backbone was amplified from pTO139 using oTO943-oTO944. The repair cassette was amplified using oTO947-oTO948 and transformed into CauTO234 to generate CauTO307.

pTO221/CauTO270: The vector including approximately 500 bp regions homologous to the regions immediately upstream and downstream of *IFF* (B9J08_004109) was amplified from pTO148 using oTO927-oTO928. The NEO cassette was amplified from pTO169 using oTO668-oTO669. The repair cassette was amplified using oTO18-oTO19 and transformed into CauTO261 to generate CauTO270.

CaTO227: The *ALS1* deletion cassette with NAT was amplified from pTO100 using oTO652-oTO653. The sgRNA guide was amplified from pTO102 usint oTO6-oTO698 and oTO8-

oTO699, and the fusion was amplified using oTO7-oTO9. Cas9 was amplified from pTO102 using oTO40-oTO41. The three linear pieces of DNA were transformed into SC5314 using a PEG-heat shock transformation, as described previously [257].

pTO288/CauTO436: The plasmid backbone was amplified from pTO139 using oTO590-oTO591. The NAT cassette and pCauTEF1 promoter were amplified from pTO250 using oTO1482-oTO1483. Flanking regions of approximately 500 bp were amplified from *C. auris* genomic DNA using oTO1480-oTO1481 and oTO1484-oTO1485. The repair cassette was amplified using oTO18-19 and transformed into AR0382 to generate CauTO436.

pTO255/ChTO346: The plasmid backbone was amplified from pTO139 using oTO590-oTO591. The NAT cassette was amplified from pTO137 using oTO668-oTO874. The NAT cassette was flanked by approximately 500 bp regions homologous to the regions immediately upstream and downstream of *SCF1* (CXQ85_003100) amplified from *C. haemulonii* genomic DNA using oTO1223-oTO1224 and oTO1225-oTO1226 respectively. The repair cassette was amplified using oTO18-oTO19 and transformed into AR0395 to generate ChTO346.

pTO264/CauTO364: The plasmid backbone was amplified from pTO139 using oTO590-oTO591. *C. haemulonii SCF1* was amplified from AR0395 gDNA using oTO1276-oTO1277. The ADH1 terminator, NEO cassette, and approximately 500 bp of SCF1 downstream intragenic region were amplified from pTO223 using oTO1274-oTO882. Approximately 500 bp *SCF1* upstream flanking region was amplified from *C. auris* gDNA using oTO879-oTO1275. The repair cassette was amplified using oTO945-946 and transformed into CauTO261 to generate CauTO364.

pTO250/CauTO308, CauTO312, CauTO323: The plasmid backbone was amplified from pTO139 using oTO590-oTO591. Approximately 500 bp homologous to the region immediately

upstream of *SCF1* (B9J08_001458) was amplified from *C. auris* genomic DNA using oTO879-oTO1150. The NAT cassette was amplified from pTO137 using oTO668-oTO875. 1000 bp of promoter sequence upstream of *CauTEF1* (B9J08_003610) was amplified from *C. auris* genomic DNA using oTO1151-1152. The first 506 bp of the *SCF1* ORF was amplified using oTO1153-oTO1154. The repair cassette was amplified using oTO945-oTO1161 and transformed into AR0387 to generate CauTO308 and into AR0381 to generate CauTO312. The entire promoter replacement cassette and *SCF1* ORF was amplified from CauTO308 genomic DNA using oTO945-oTO946 and transformed into AR0381 to generate CauTO323.

pTO223/CauTO306: The ORF for *SCF1* (B9J08_001458) along with approximately 500 bp of upstream sequence was amplified from *C. auris* genomic DNA using oTO879-oTO1078. The ADH1 terminator and NEO cassette were amplified from pTO169 using oTO1066-oTO668. Approximately 500 bp homologous to the region immediately downstream of *SCF1* was amplified from *C. auris* genomic DNA using oTO1077-oTO882. The plasmid backbone was amplified from pTO139 using oTO590-oTO591. The repair cassette was amplified using oTO945-oTO946 and transformed into CauTO261 to generate CauTO306.

pTO284/CauTO438: *SCF1* was amplified from AR0381 gDNA using oTO1212-oTO1430 and assembled into the vector amplified from pTO223 using oTO1431-oTO1432. The repair cassette was amplified using oTO945-oTO946 and transformed into CauTO261 to generate CauTO438.

pTO280: The *SCF1* complementation vector was amplified from pTO223 using oTO1159-oTO1160, which incorporate a 1x FLAG tag at the A-B Domain junction. The resultant product was assembled in a single fragment Gibson assembly and used as template for site-directed mutagenesis.

pTO281/CauTO433: The entire pTO280 vector was amplified in two overlapping fragments using overlapping backbone-specific primers oTO1427 and oTO1428 paired with oTO1418 and oTO1417, respectively. oTO1418 and oTO1417 contain overlapping sequence with the point mutations instantiated. The repair cassette was amplified using oTO945-oTO946 and transformed into CauTO261 to generate CauTO433.

pTO282/CauTO434: The entire pTO280 vector was amplified in two overlapping fragments using overlapping backbone-specific primers oTO1427 and oTO1428 paired with oTO1422 and oTO1421, respectively. oTO1422 and oTO1421 contain overlapping sequence with the point mutations instantiated. The repair cassette was amplified using oTO945-oTO946 and transformed into CauTO261 to generate CauTO434.

pTO283/CauTO430: The entire pTO280 vector was amplified in two overlapping fragments using overlapping backbone-specific primers oTO1427 and oTO1428 paired with oTO1426 and oTO1425, respectively. oTO1426 and oTO1425 contain overlapping sequence with the point mutations instantiated. The repair cassette was amplified using oTO945-oTO946 and transformed into CauTO261 to generate CauTO430.

pTO268/CauTO432: The N-terminal domain of *SCF1* was synthesized with the point mutations instantiated and cloned into the PCR product of pTO223 generated from oTO1159-591. The repair cassette was amplified using oTO945-oTO946 and transformed into CauTO261 to generate CauTO430.

pTO292/CauTO453: The entire pTO280 vector was amplified in two overlapping fragments using overlapping backbone-specific primers oTO1427 and oTO1428 paired with oTO1564 and oTO1563, respectively. oTO1563 and oTO1564 contain overlapping sequence with the point

mutations instantiated. The repair cassette was amplified using oTO945-oTO946 and transformed into CauTO261 to generate CauTO453.

pTO293/CauTO455: The entire pTO280 vector was amplified in two overlapping fragments using overlapping backbone-specific primers oTO1427 and oTO1428 paired with oTO1566 and oTO1565, respectively. oTO1566 and oTO1565 contain overlapping sequence with the point mutations instantiated. The repair cassette was amplified using oTO945-oTO946 and transformed into CauTO261 to generate CauTO455.

4.6.5 *C. auris* transformation

C. auris transformation was performed using a transient-Cas9 expression approach as described previously[170]. Briefly, transformation repair cassettes were amplified from assembled plasmids. A Cas9 expression cassette was amplified from pTO135 using oTO143-oTO41. Cassettes for the expression of sgRNA targeting specific loci were amplified from pTO136 using overlap-extension PCR to change the gRNA sequence. All linear PCR products were purified using a Zymo DNA Clean & Concentrator kit (Cat no. D4034, Zymo Research) according to the manufacturer's instructions.

To prepare electro-competent cells, *C. auris* cells were incubated in liquid YPD at 30°C overnight with gentle agitation. Cells were harvested by centrifugation and resuspended in TE buffer with 100 mM Lithium Acetate and incubated at 30°C for 1 hr with constant shaking. DTT was added to the cells at a final concentration of 25 mM before further incubating at 30°C for 30 min. Cells were harvested by centrifugation at 4°C before being washed once with ice-cold water and once with ice-cold 1 M Sorbitol. Harvested cells were resuspended in ice-cold 1M sorbitol and maintained on ice for immediate usage or aliquoted and stored at -80°C for up to several months before transformation.

Electroporation was performed by adding 45 µL competent cells to a pre-chilled 2 mm-gap electro-cuvette along with 500-1000 ng each of the PCR-amplified Cas9, sgRNA, and repair cassettes. Cells were electroporated using a Bio-Rad MicroPulser Electroporator according to the pre-defined *P. pastoris* (PIC) protocol (2.0 kV, 1 pulse). Electroporated cells were recovered in 1 M Sorbitol then resuspended in YPD and allowed 2 hrs of outgrowth at 30°C with constant rotation. Outgrown cells were spread-plated on selective media. For repair cassettes encoding the *NAT* marker, cells were selected on YPD + 200 µg/mL nourseothricin and incubated at 30°C for 2-3 days. For repair cassettes encoding the *NEO* marker, cells were selected on YPD + 1 mg/mL G418 and incubated at 23°C for 4 days or YPD + 1 mg/mL G418 + 1 mg/mL Molybdate^{280} and incubated at 30°C for 2-3 days. Transformant colonies were passaged to isolation and correct incorporation of the repair cassette was confirmed for each by colony PCR using Phire Plant Direct PCR Master Mix (F160; Thermo Fisher Scientific) according to the manufacturer's instructions. Each mutant was confirmed by at least three independent PCR reactions with distinct primer sets specific to the mutation site and compared to parental strains. Deletion mutants were confirmed with gene-specific primers based on absence of amplification from the ORF and integration of the repair cassette at the genetic locus. For mutants encoding site-directed mutations, genomic DNA was isolated and the entire genetic locus spanning the gene and sequence surrounding the integration junctions was PCR-amplified and sequenced to confirm the site-directed mutations were intact and no unintended mutations were present at the locus.

4.6.6 *C. haemulonii* transformation

C. haemulonii transformation was performed similarly to *C. auris* transformation, except the outgrowth was extended to 5 hrs and transformants were selected on YPD + 50 μg/mL nourseothricin at 30°C for 3 days.

4.6.7 *Agrobacterium tumefaciens*-mediated transformation (AtMT)

AtMT was performed as described previously[170]. Briefly, *A. tumefaciens* strain pTO131 (EHA 105 harboring pTO128) was grown overnight at 30°C in liquid LB media containing kanamycin. *A. tumefaciens* cells were harvested by centrifugation, washed once with sterile water, then resuspended at a final OD_{600} of 0.15 in liquid Induction Medium (IM) supplemented with 100 μM acetosyringone 3',5'-dimethoxy-4-hydroxyacetophenone (AS) and incubated at room temperature for 6 hrs with constant agitation. Recipient *C. auris* AR0382 cells were grown overnight at 30°C in YPD and harvested by centrifugation then resuspended in sterile water at a final OD_{600} of 1.0. Prepared *A. tumefaciens* and *C. auris* cells were combined at equal volumes and the mixed culture was incubated on solid IM Agar supplemented with AS at 23°C for 4 days. Cells were harvested into liquid YPD. The resulting suspension was washed three times by low-speed centrifugation to separate fungal cells from bacterial cells and aliquots of the washed culture were spread-plated on YPD + 200 μg/mL nourseothricin + 200 μg/mL cefotaxime. Plates were incubated at 30°C for 2 days. Transformant colonies were manually arrayed into 96 well plates and grown overnight in YPD at 30°C. Each well was overlayed with 50% glycerol and arrayed plates were frozen and stored at -80°C.

4.6.8 AtMT transgene insertion site identification

Identification of transgene insertion sites was performed as described previously[170]. Briefly, genomic DNA was isolated from mutants of interest and sequenced by Illumina sequencing.

Library preparation, quality control, and Whole Genome Sequencing were performed by SeqCenter (Pittsburg, PA, USA). Library preparation was performed based on the Illumina Nextera kit and sequencing performed on the Nextseq 550 platform to generate 150 bp paired-end sequencing reads. Sequencing data was analyzed using the Galaxy web platform public server at *usegalaxy.org*[281]. Read quality was assessed using FastQC and reads were trimmed using Trimmomatic[282] with a Phred quality cutoff of 20. Processed reads were then mapped to a linearized reference sequence of pTO128 (pPZP-Nat) using the Burrows-Wheeler Aligner with maximum exact matches (BWA-MEM)[283] configured with minimum seed length = 50 and band width = 2. Soft clipped read sequence corresponding to genomic DNA neighboring the T-DNA integration junction was extracted from the aligned BAM file using the extractSoftClipped script from SE-MEI (https://github.com/dpryan79/SE-MEI). The resulting sequences were mapped back to the *C. auris* B8441 reference assembly (NCBI GCA_002759435.2) using BWA-MEM with the default configuration to identify integration sites. T-DNA integration loci were confirmed for each sequenced mutant with Sanger sequencing.

4.6.9 RNA extraction

RNA extraction was performed using a formamide extraction method[263]. Briefly, cultured cells were harvested by centrifugation and all media was removed. Dry cell pellets were frozen on dry ice and stored at -80°C before processing. To extract RNA, cell pellets were thawed at room temperature and resuspended in 100 µL FE Buffer (98% formamide, 0.01M EDTA). 50 µL of 500 µm RNAse-free glass beads was added to this suspension and the mixture was homogenized for 30 sec 3 times using a BioSpec Mini-Beadbeater-16 (Biospec Products Inc., Bartlesville, OK, USA). The resulting cell lysate was clarified by centrifugation to remove cell debris. The supernatant was collected as the crude RNA extract. The crude extract was purified using a

Qiagen RNeasy mini kit (ref 74104, Qiagen) according to the manufacturer's instructions. Samples were DNAse treated with Invitrogen DNAse (RNAse free) (Qiagen, cat no. 79254). The integrity and purity of the extracted RNA was confirmed via Nanodrop and agarose gel electrophoresis prior to downstream applications.

4.6.10 RT-qPCR

Purified RNA from cells cultured overnight in YPD at 30°C was used to generate cDNA using the iScript cDNA synthesis kit (cat. 1708890, Bio-Rad Laboratories, Inc., Hercules, CA, USA) according to the manufacturer's instructions. Primers specific to target genes were designed using NCBI primer blast[284] with the *C. auris* B8441 assembly (NCBI GCA_002759435.2) or the *C. haemulonii* B11899 assembly (NCBI GCA_002926055.1) as a reference. Prepared cDNA was used as a template in qPCR reactions with the Power-Up SYBR Green Master Mix (cat. A25741, ThermoFisher Scientific, Waltham, MA, USA) according to the manufacturer's specifications. Cycling was performed using a Bio-Rad CFX Opus 384 Real Time PCR System. For *C. auris*, amplification of *ACT1* was measured using primers oTO359-oTO360, of *SCF1* using primers oTO1251-oTO1252, and of *IFF4109* using primers oTO615-oTO616. For *C. haemulonii*, amplification of *ACT1* was measured using primers oTO1253-oTO1254 and amplification of *SCF1* was measured using primers oTO1229-oTO1230.

4.6.11 RNA-seq

Purified RNA from cells cultured to mid-exponential phase in YPD at 30°C was sequenced by SeqCenter (Pittsburgh, PA, USA). Library preparation was performed using the Stranded total RNA Prep Ligation with Ribo-Zero Plus kit (Illumina, San Diego, CA, USA) and 10bp IDT for Illumina indices. Sequencing was performed using the NextSeq2000 platform to generate 2 x 50

bp reads. Sequencing data was analyzed using the Galaxy web platform public server at *usegalaxy.org*[281]. Read quality was assessed using FastQC and reads were trimmed for quality using Cutadapt[285] with a Phred cutoff score of 20. Reads were then mapped to the *C. auris* B8441 reference assembly (NCBI GCA_002759435.2) using RNA Star[286] with the default parameters. Mapped reads were quantified using featureCounts[287] and differential expression was assessed using DESeq2[288]. Genes with a fold change greater than 2 times upregulated or downregulated and an adjusted p-value less than 0.05 were considered statistically significant.

4.6.12 Dispersed surface flow cytometry adhesion assay

Adhesion to polystyrene was assessed using a previously established flow cytometric assay to measure the proportion of a population of cells able to attach to dispersed polystyrene surfaces in one hour[275]. Cells from overnight culture were suspended in YPD containing green fluorescent polystyrene microspheres (1 μm, F-8823, Molecular Probes) at a ratio of 10 microspheres to 1 cell. For experiments involving additives, cells and microspheres were suspended in YPD containing the appropriate concentration of additive (NaCl or amino acids) and adjusted to neutral pH. This mixture was incubated with continuous inversion at 25 revolutions/min for 1 hour at room temperature. Cells were fixed with 4% formaldehyde for 10 minutes at room temperature, then washed and resuspended in PBS for flow cytometric analysis. Samples were analyzed using an LSRFortessa Flow Cytometer (BD Biosciences, NJ, USA) using a standard filter (FITC, 530/30). Acquisition settings were defined using the green fluorescent polystyrene microsphere samples to adjust the voltage of the fluorescent channel to the fourth logarithmic decade. FSC was used to gate cells from unattached microspheres. Data was collected for 10,000 gated events, which represented two distinct fluorescent populations. The percentage of cells with microspheres attached was determined by assessing the ratio of fluorescent to total events.

4.6.13 High throughput adhesion assay

An automated imaging-based assay was used for high throughput adhesion measurements. A total of 2,560 insertional mutants in the AR0382 strain background were arrayed and individually assayed in 96-well plates. Arrayed mutants were cultured from glycerol stocks on solid YPD agar at 30°C. The resulting colonies were used to seed 200 µL YPD cultures in 96 well plates and grown overnight at 30°C. For the adhesion assay, cells from each well were transferred into 100 µL YPD in a CellCarrier-96 Ultra Microplate with an optical cyclic olefin polymer surface (cat #NC1463153, Perkin Elmer, Waltham, MA, USA) using a 96-well microplate replicator (RePad 96 long pin, REP-001, Singer Instruments, United Kingdom). A single layer of visually distinct cells on the well surface were transferred. Each microplate contained 80 individual wells of mutants and 8 wells each of AR0382 and AR0387 as high adhesion and low adhesion controls, respectively. After adding cells, the plates were centrifuged at 210 x g for 1 minute to settle the cells. Cells were incubated on the surface of the well for 1 hr at room temperature to allow for attachment. Unattached cells were removed by washing each well 3 times with 100 µL PBS and using a vacuum aspirator with 8 channel manifold (BrandTech QuickSip aspirator) to remove media between each wash. Each well was imaged in brightfield using a Yokogawa CellVoyager CQ1 automated microscope before and after washing. Four fields containing an average of approximately 1,000 cells/field were captured in defined positions such that the same four regions were imaged for each well before and after washing. Pre-processing of images was performed in Fiji ImageJ software (version 1.52)[262] using a custom macro that segmented cells in the brightfield images using edge detection and generated a binary mask from the segmented cells. The pre-processed images were quantified using CellProfiler software (version 3.1.9)[289] to generate a cell count for each captured field. A

ratio of adhesive cells was calculated by dividing the count of the attached cells remaining after washing by the count of the input cells for each captured field.

The dynamic range of the assay was determined using a plate containing 48 wells of AR0382 and 48 wells of AR0387 as high and low adhesion controls, respectively. To determine the degree of separation between the two controls, the z-factor for the assay was calculated based on an established formula[290]. Similarly, a z-factor was calculated based on the control wells for each mutant plate tested. The average z-factor for the control-only condition was 0.7167, indicating sufficient separation to detect differences between high and low adhesive strains, where an acceptance criteria of $0.5 < \text{z-factor} < 1.0$ was established for each mutant plate based on the control wells for that plate.

A z-score was assessed for each mutant by subtracting the proportion of adhesive cells from the average proportion of adhesive cells amongst all the mutants and dividing by the standard deviation amongst all the mutants. Mutants with a z-score more negative than -3 were considered to have significantly reduced adhesion.

4.6.14 Flocculation assay

Cells were cultured overnight in YPD at 30°C. Cultures were vortexed to suspension for 10 sec at max speed, then placed upright at room temperature and allowed to settle for 20 min. Immediately after vortexing and at specified timepoints, a 20 μL aliquot was gently removed from the top of the culture and diluted to optical range in a 96 well plate. OD_{600} was measured for each removed aliquot using a BioTek 800 TS absorbance reader. Flocculation activity was calculated as the percent reduction in OD_{600} in aliquots at each timepoint compared to the initial reading.

4.6.15 Immunofluorescence microscopy and flow cytometry

Wild type and Δ*scf1* + *SCF1-FLAG* cells were cultured overnight in YPD at 30°C then harvested by centrifugation and washed in PBS. The cells were fixed with 4% formaldehyde for 10 min at room temperature, then washed and resuspended in PBS. Once fixed, the cells were blocked in 2% BSA for 60 min. The cells were then pelleted and resuspended in 0.1% BSA containing a 1:500 dilution of primary antibody (Rabbit α-FLAG Polyclonal, Sigma F7425) and incubated at room temperature for 3 hrs. The primary antibody was removed, and the cells were resuspended in 0.1% BSA containing a 1:500 dilution of secondary antibody (Goat α-Rabbit Igg, Alexafluor 594, Invitrogen A11037) and incubated at room temperature for 45 min, protected from light. The cells were washed three times in PBS with 0.1% Tween-20 and resuspended in PBS. Microscopy was performed using a Biotek Lionheart FX automated microscope using 100X oil objective (Olympus 1.4NA) and the TexasRed imaging filter cube and LED. Flow Cytometry was performd using an LSRFortessa Flow Cytometer (BD Biosciences, NJ, USA) using a standard filter (PE-Texas Red, 610/20). Data was collected for 50,000 events. Median fluorescence intensity was calculated using FlowJo™ v10.8.2 Software (BD Life Sciences).

4.6.16 Homology search and structural prediction

The genomic and protein sequence for *SCF1* (B9J08_001458) was retrieved from the B8441 reference assembly (NCBI GCA_002759435.2). Protein domain organization was determined based on automatic annotations from the UniProt database. To search for *SCF1* homologs, either the entire sequence or the N-terminal domain sequence was subjected to a BLAST search with an E value cutoff of 0.05. Significant hits that only exhibited homology in low complexity, repetitive regions were disregarded. The only remaining hits found were in *C. auris* or *C.*

haemulonii genomes. Synteny of the *SCF1* locus was evaluated using the annotations available through the FungiDB database[259] and Candida Gene Order Browser database[291].

The N-terminal domain was modeled using AlphaFold2 through the ColabFold platform[292]. The *FLO11*-like Fibronectin-III fold was annotated through UniProt. Searching with Foldseek[293] returned proteins across the domains of life containing Fibronectin-III folds, including *FLO11* homologs. To assess the similarity to *FLO11*, *SCF1* and *FLO11* sequence and N-terminal sequence were cross-blasted against the *S. cerevisiae* or *C. auris* genome, respectively, which returned no significant homology with an E value cutoff of 0.05. The N-terminal domains were aligned to determine percent identity and to compare the positions of functionally critical aromatic bands from Flo11 to the Scf1 sequence.

4.6.17 Microbial attachment to hydrocarbons (MATH) assay

Cell surface hydrophobicity was determined using the microbial adhesion to hydrocarbon (MATH) assay[294], which measures the fraction of cells sequestered out of aqueous suspension by pure hydrocarbon. Overnight cultures were harvested by centrifugation and washed three times in PBS. The cells were standardized to an OD_{600} of 0.4 in PBS using a Bio Tek 800 TS microplate reader. An aliquot of the cell suspension was reserved for an initial OD_{600} reading (A0). 1200 µL of each cell suspension in PBS was transferred into clean, unused borosilicate glass test tubes with a 10 mm diameter. 200 µL n-hexadecane (Sigma-Aldrich, cat no: H6703) was gently overlaid atop the culture suspension in the test tube. The tubes were allowed to rest for 10 minutes at room temperature, then capped and vortexed at max speed for 1 min to mix the hydrocarbon and aqueous phases. The tubes were left for 15 minutes at room temperature to allow for separation of phases, after which an aliquot of the lower aqueous layer was taken for the final OD_{600} reading (A1). The proportion of sequestered cells were calculated by dividing the

final OD_{600} reading (A1) by the initial reading (A0) according to the formula: [1 – (A1/A0)] * 100%.

4.6.18 Plasma-etched polystyrene adhesion

Adhesion of *C. auris* cells to hydrophobic and hydrophilic substrates was modeled using untreated or surface-modified polystyrene multi-well plates (Nest Biotechnology Co., cat. 701311), which were considered to be hydrophobic as untreated[295]. To assess adhesion to a hydrophilic substrate, the surface hydrophobicity of the polystyrene was modified by the addition of free radicals using vacuum plasma treatment. The plate was placed without the lid in a PE-25 plasma cleaner (Plasma Etch Inc, Nevada, USA) and treated for 90 seconds at 400W 50 kHz with 200 mtorr / 27 Pa vacuum pressure. The plate was tested to be fully water-wettable by visual examination of a droplet spreading on the surface and compared to an untreated (hydrophobic) polystyrene plate. *C. auris* cells were cultured overnight in YPD at 30°C and added to either the hydrophobic or hydrophilic polystyrene plates. Cells were centrifuged at 210 x g for 1 min to gently settle a single layer of cells on the polystyrene surface. Plates were incubated for 1 hr at room temperature to allow for attachment. For each well, images of four fields in defined positions were taken in brightfield using a BioTek Lionheart FX automated microscope. Unattached cells were removed by washing 3 times with PBS, and fields in the same defined positions were imaged after washing. Cell counts for each field were determined using image analysis software as described above. The percentage of adherent cells was calculated by dividing the count of the attached cells remaining after washing by the total number of the cells input for each captured field.

4.6.19 Peptide-microparticle binding

13-amino acid peptides corresponding to WT Scf1 residues 50-62 or the same sequence with H52A H53A R54A R55A mutations were synthesized with N-terminal tetramethylrhodamine (TMR) labels (Genscript, NJ, USA). Peptide purity was confirmed to be ~95% or greater by HPLC. Peptides were dissolved in PBS, pH 7.4 (Ref. 10010-023, Gibco). For microsphere binding measurements, peptides were mixed with polystyrene microspheres (1 μm, F-8823, Molecular Probes) or phosphotidylcholine (PC) lipid microparticles (3 μm, P-B1PC, Echelon Biosciences) suspended in YPD and vortexed at max speed for 1 minute. Peptide binding was assessed using a Biotek Lionheart FX automated microscope with the TRITC imaging filter cube and LED. Mean fluorescence intensity of individual particles was measured and corrected for background fluorescence using Gen5 software (version 3.12).

4.6.20 Whole cell lipid particle binding

Cells from overnight culture were suspended in YPD containing green fluorescent PC lipid microparticles (3 μm, P-B1PC, Echelon Biosciences) at a ratio of 1 microparticle to 10 cells. This mixture was incubated with continuous inversion at 25 revolutions/min for 1 hour at room temperature. Aliquots were dispensed into 96-well plates and centrifuged at 210 x g for 1 min to settle cells and lipid particles before imaging using a Biotek Lionheart FX automated microscope with the GFP imaging filter cube and LED. Lipid particles were segmented from the image based on green fluorescence and the fraction of bound particles was calculated by dividing the number of particles colocalizing with cells by the total number of lipid particles.

4.6.21 In vitro biofilm formation

Cells were cultured overnight in YPD at 30°C and resuspended in RPMI-1640 media. Each strain was standardized to a starting OD_{600} of 0.5 in RPMI and seeded in 200 μL in 96-well

plates with a virgin polystyrene surface. The seeded plates were sealed with a breathable membrane and incubated for 90 min at 37°C with shaking at 250 rpm to allow for attachment. After this initial incubation, the media was aspirated and each well was washed with 200 µL PBS before replacing the liquid in each well with fresh RPMI-1640 media. The plates were sealed and biofilms were allowed to form for 24 hrs at 37°C with constant orbital shaking at 250 rpm. After 24 hrs, each well was washed three times with 200 µL PBS. To quantify the oxidative activity of the viable biofilms, a colorimetric XTT reduction assay was performed[296]. A 0.5 mg/mL XTT (XTT sodium salt, cat #AAJ61726MD, Thermo Scientific) solution in PBS was combined with a 0.32 mg/mL PMS (Phenazine Methosulfate, cat #10955, MP Biomedicals) solution in water at a 9:1 XTT:PMS ratio and 100 µL was added to each biofilm. The plate was incubated at 37°C for 30 min before removing the media to a clean 96 well plate and measuring the OD_{492}. To image biofilms, the biofilms were fixed with 4% formaldehyde for 10 minutes at room temperature then washed two times with 200 µL PBS. The fixed biofilms were stained with calcofluor white (cat #18909, Sigma-Aldrich) for 10 minutes then washed three times with 200 µL PBS. Stained biofilms were imaged in Z-stacks using a Biotek Lionheart FX automated microscope at 400x magnification with the DAPI imaging filter cube and LED. Maximum intensity projections were generated using Gen5 software (version 3.12).

4.6.22 Rat catheter biofilm formation

In vivo biofilm testing was performed with a rat external jugular venous catheter model as previously described[297]. Briefly, a 10^6 cells/ml inoculum for each strain was allowed to grow on an internal jugular catheter placed in specific-pathogen-free Sprague–Dawley rats (16-week old, 400 g) for 24 h. After this period, biofilm formation on the intraluminal surface of the catheters was observed by scanning electron microscopy. SEM images were acquired on a ZEISS Gemini

450 scanning electron microscope using an accelerating voltage of 3.0 kV, a working distance of 6 mm, an Everhart-Thornley SE2 detector with optically coupled photomultiplier, and the ZEISS SmartSEM (v. 6.05) software. Procedures were approved by the Institutional Animal Care and Use Committee at the University of Wisconsin, Madison (protocol MV1947).

4.6.23 Ex vivo human skin bioburden

Human skin samples were collected from patients through an IRB-exempt protocol[157]. Full-thickness excised skin samples were placed in 12-well plates containing 3 mL of Dulbecco's Modified Eagle Medium (DMEM) (Lonza, Walkersville, MD, USA), supplemented with 10% FBS (Atlanta Biologicals, Lawrenceville, GA, USA), penicillin (1000 U/mL), and streptomycin (1 mg/mL) [155,157]. After 24 h, samples were washed with DPBS and moved to semi-solid media (6:4 ratio of 1% agarose (BIO-RAD, Hercules, CA, USA) in DPBS and DMEM with 10% FBS). Paraffin wax was applied as a barrier between the epidermal surface and the semi-solid media. *Candida* spp. (10 μL at 10^7 cells/mL) were applied to the skin surface. Skin samples were incubated at 37°C for 24 h, rinsed, and processed for viable burden determination or microscopy. For microscopic analysis, skin samples were fixed overnight (4% formaldehyde, 1% glutaraldehyde, in sodium phosphate buffer), washed with sodium phosphate buffer, stained with 1% osmium tetroxide in DPBS, and dehydrated by ethanol rinsing. Samples were then dried using three changes of Hexamethyldisiazane (1 h each) followed by air desiccation for 48 h. Samples were mounted on aluminum stubs with silver paint applied at the interface. Samples were then platinum sputter coated and imaged by scanning electron microscopy (Zeiss Gemini 450, 3 kV).

4.6.24 Intravenous murine infection

Overnight cultures of *C. auris* were pelleted by centrifugation at 4000 rpm for 10 min at 4°C, followed by washing three times with 1X Dulbecco's Phosphate Buffer Saline (DPBS). The yeast cells were finally suspended in 1X DPBS and counted using a hemocytometer. The yeast cell densities were adjusted at $2.5X10^8$ cells/ml ($5X10^7$ cells/0.2 ml) using 1X DPBS. Infection was performed using an immunosuppressed mouse model of *C. auris* infection with hematogenous dissemination to assess the virulence of various *C. auris* strains *in vivo*. Briefly, outbred ICR CD-1 mice, aged 4-6 weeks (n=10+1/group), were subjected to immunosuppression by intraperitoneal (i.p.) injection of 200 mg/kg cyclophosphamide and subcutaneous injection of 250 mg/kg cortisone acetate on day -2 prior to infection. To prevent bacterial superinfection in the immunosuppressed mice, enrofloxacin was added to the drinking water at a concentration of 50 μg/mL on the day of immunosuppression and continued for two weeks. The mice were then infected with various *C. auris* strains via tail vein injection, using the inoculum of $5x10^7$ yeast cells in 0.2 ml per mouse. The survival of the infected mice was monitored for a duration of 21 days. For histopathological examination of the infected mice, an additional mouse was included in each group. On day 7 post-infection, one mouse from each group was euthanized, and their kidneys and heart were collected for further analysis. The harvested organs were fixed in 10% zinc-buffered formalin, embedded in paraffin, and then sectioned. To visualize the tissue, Periodic Acid Schiff (PAS) stain was applied to the sections. The stained tissue sections were then imaged using Olympus microscopy.

4.6.25 Epicutaneous murine infection

The murine epicutaneous infection was performed as previously described with modifications[298]. Infection was performed using C57BL/6J mice at 7 weeks of age (Jackson Laboratories). Mouse dorsal hairs were shaved one day before infection. For infection, *C. auris*

strains were cultured overnight at 30°C, washed once with PBS, and resuspended at a concentration of $1x10^9$ cells/ml in PBS using a hemocytometer. $2x10^8$ cells of *C. auris* were placed on a patch of sterile gauze and attached to the shaved skin of individual mice with a transparent occlusive plastic dressing (Tegaderm; 3M). The actual inoculum of each *C. auris* culture used for infection was also determined by colony-forming units (CFUs) on YPD+ ampicillin + gentamycin plates. Mice were sacrificed after being exposed to *C. auris* for 2 days through the patch. Dorsal skin tissue underneath the gauze was harvested, weighed, and digested with 0.25 mg/ml liberase in 500 ul PBS for 1 hour and 45 minutes at 37 °C and 5% CO2. Digested dorsal skin tissue was homogenized with a bead beater for 30 seconds x 4 times. The supernatant of each homogenized sample was plated on YPD + ampicillin + gentamycin plates to determine the CFUs recovered from each mouse. The number of CFU was determined after 48 h of incubation at 30°C. The actual fungal burden for each mouse was determined by normalizing the CFUs recovered from each mouse by the weight of the recovered dorsal skin tissue and actual delivered inoculum.

4.6.26 Statistics and reproducibility

Statistical analyses were performed using R statistical software (version 4.0.3) using the DescTools package (version 0.99.49) for ANOVA and the survminer package (version 0.4.9) for survival analysis. Unless otherwise specified, experiments were performed in at least three independent biological replicates and data are presented as means ± standard error of means from biological replicates, with each point representing individual biological replicates. Microscopy and photography images are representative of at least 3 experiments with similar results. Statistically significant differences were calculated using student's t-test or one-way ANOVA with Tukey's or Dunnett's post hoc test for multiple comparisons. Correlation was measured

using Pearson correlation. Differences in survival analysis were determined using a Mantel-Haenszel log-rank test with Benjamini-Hochberg correction. *$p \leq 0.05$; **$p \leq 0.01$; ***$p \leq 0.001$; ns $p > 0.05$.

Strain Name	Alias	Genotype	Source
CauTO33	*C. auris* B11109	AR0382	(*50*)
CauTO186	*C. auris* B11109	AR0382 Δ*als(B9J08_002582)::NAT*	This Study
CauTO187	*C. auris* B11109	AR0382 Δ*als(B9J08_004498)::NAT*	This Study
CauTO226	*C. auris* B11109	AR0382 Δ*als(B9J08_004112)::NAT*	This Study
CauTO233	*C. auris* B11109	AR0382 Δ*iff(B9J08_004100)::NAT*	This Study
CauTO234	*C. auris* B11109	AR0382 Δ*iff(B9J08_004109)::NAT*	This Study
CauTO235	*C. auris* B11109	AR0382 Δ*iff(B9J08_004098)::NAT*	This Study
CauTO236	*C. auris* B11109	AR0382 Δ*iff(B9J08_004110)::NEO*	This Study
CauTO247	*C. auris* B11109	AR0382 Δ*iff(B9J08_001531)::NAT*	This Study
CauTO248	*C. auris* B11109	AR0382 Δ*iff(B9J08_004892)::NAT*	This Study
CauTO249	*C. auris* B11109	AR0382 Δ*iff(B9J08_001155)::NAT*	This Study
CauTO250	*C. auris* B11109	AR0382 Δ*iff(B9J08_004451)::NAT*	This Study
CauTO251	*C. auris* B11109	AR0382 Δ*iff(B9J08_000675)::NAT*	This Study
At pTO131	*Agrobacterium tumefaciens EHA105*	EHA105 harboring pTO128 (pPZP-NAT)	(*52*)
CauTO219	*C. auris* B11109	AR0382 *tnSWI1(B9J08_003460)*	This Study
CauTO322	*C. auris* B11109	AR0382 *tnBCY1(B9J08_002818)*	This Study
CauTO261	*C. auris* B11109	AR0382 Δ*scf1(B9J08_001458)::NAT*	This Study
CauTO320	*C. auris* B11109	AR0382 Δ*scf1(B9J08_001458)::NAT + NAT::SCF1-FLAG NEO*	This Study
CauTO307	*C. auris* B11109	AR0382 Δ*iff(B9J08_004109)::NAT + IFF(B9J08_004109) NEO*	This Study
CauTO270	*C. auris* B11109	AR0382 Δ*scf1(B9J08_001458)::NAT* Δ*iff(B9J08_004109)::NEO*	This Study
CaTO1	*C. albicans* SC5314	SC5314	
CaTO227	*C. albicans* SC5314	SC5314 *als1::FRT/als1::FRT*	This Study
CauTO436	*C. auris* B11109	AR0382 *pTEF1-ALS4112 NAT*	This Study
CauTO32	*C. auris* B11220	AR0381	(*50*)
CauTO34	*C. auris* B11221	AR0383	(*50*)
CauTO35	*C. auris* B11222	AR0384	(*50*)
CauTO36	*C. auris* B11244	AR0385	(*50*)
CauTO37	*C. auris* B11245	AR0386	(*50*)
CauTO38	*C. auris* B8441	AR0387	(*50*)
CauTO39	*C. auris* B11098	AR0388	(*50*)
CauTO40	*C. auris* B11203	AR0389	(*50*)
CauTO41	*C. auris* B11205	AR0390	(*50*)
CauTO52	*C. auris* B11243	AR0931	(*50*)
CauTO53	*C. auris* IFRC2087	AR1097	(*50*)
CauTO325	*C. auris* B14308	AR1099	(*50*)
CauTO326	*C. auris* B13463	AR1100	(*50*)
CauTO327	*C. auris* B18578	AR1101	(*50*)
CauTO328	*C. auris* B17835	AR1102	(*50*)
CauTO329	*C. auris* B18683	AR1103	(*50*)
CauTO330	*C. auris* B18017	AR1104	(*50*)

CauTO331	*C. auris* B11842	AR1105	(*50*)
CauTO315	*C. auris* A.04.TO.Ax.9-ORG1	Chicago-1	(*77*)
CauTO316	*C. auris* A.04.TO.Ax.9-ORG2	Chicago-2	(*77*)
CauTO317	*C. auris* B.02.TO.lc.9-ORG1	Chicago-3	(*77*)
CauTO318	*C. auris* B.06.TO.Ax.9-ORG1	Chicago-4	(*77*)
CaTO380	*C. albicans* P75010	P75010	ATCC
CaTO382	*C. albicans* 12C	12C	ATCC
CaTO381	*C. albicans* 19F	19F	ATCC
CaTO388	*C. albicans* L26	L26	ATCC
CaTO391	*C. albicans* P37005	P37005	ATCC
CaTO383	*C. albicans* P37037	P37037	ATCC
CaTO392	*C. albicans* P37039	P37039	ATCC
CaTO384	*C. albicans* P78048	P78048	ATCC
CaTO377	*C. albicans* P94015	P94015	ATCC
CaTO379	*C. albicans* P76055	P76055	ATCC
CaTO389	*C. albicans* P76067	P76067	ATCC
CaTO378	*C. albicans* P34048	P34048	ATCC
CaTO386	*C. albicans* P57055	P57055	ATCC
CaTO390	*C. albicans* P78042	P78042	ATCC
CaTO375	*C. albicans* GC75	GC75	ATCC
CaTO376	*C. albicans* P600002	P600002	ATCC
CaTO385	*C. albicans* P75016	P75016	ATCC
CaTO387	*C. albicans* P75063	P75063	ATCC
CaTO393	*C. albicans* P87	P87	ATCC
ChTO46	*C. haemulonii* B10441	AR0395	(*50*)
ChTO346	*C. haemulonii* B10441	AR0395 Δ*scf1(CXQ85_003100)::NAT*	This Study
CauTO306	*C. auris* B11109	AR0382 Δ*scf1(B9J08_001458)::NAT + NAT::SCF1 NEO*	This Study
CauTO364	*C. auris* B11109	AR0382 Δ*scf1(B9J08_001458)::NAT + NAT::SCF1*$_{Ch}$ *(CXQ85_003100) NEO*	This Study
ChTO324	*C. haemulonii*	AR0932	(*50*)
ChTO44	*C. haemulonii*	AR0393	(*50*)
CauTO312	*C. auris* B11220	AR0381 *pTEF1-SCF1*$_{AR0381}$ *NAT*	This Study
CauTO323	*C. auris* B11220	AR0381 *pTEF1-SCF1*$_{AR0382}$ *NAT*	This Study
CauTO438	*C. auris* B11220	AR0382 Δ*scf1(B9J08_001458)::NAT + NAT::SCF1*$_{AR0381}$ *(CJI96_0001187) NEO*	This Study
CauTO308	*C. auris* B8441	AR0387 *pTEF1-SCF1 NAT*	This Study
CauTO432	*C. auris* B8441	AR0382 Δ*scf1(B9J08_001458)::NAT + NAT::SCF1-FLAG*$_{R178A\ K181A}$ *NEO*	This Study

CauTO433	*C. auris* B8441	AR0382 Δ*scf1(B9J08_001458)::NAT + NAT::SCF1-FLAG*$_{K163A}$ *NEO*	This Study
CauTO434	*C. auris* B8441	AR0382 Δ*scf1(B9J08_001458)::NAT + NAT::SCF1-FLAG*$_{K147A\ R148A\ K150A\ K152A}$ *NEO*	This Study
CauTO430	*C. auris* B8441	AR0382 Δ*scf1(B9J08_001458)::NAT + NAT::SCF1-FLAG*$_{R54A\ R55A}$ *NEO*	This Study
CauTO453	*C. auris* B8441	AR0382 Δ*scf1(B9J08_001458)::NAT + NAT::SCF1-FLAG*$_{H52A\ H53A\ R54A\ R55A}$ *NEO*	This Study
CauTO455	*C. auris* B8441	AR0382 Δ*scf1(B9J08_001458)::NAT + NAT::SCF1-FLAG*$_{K44A\ H55A\ Y46A\ W47A\ K49A}$ *NEO*	This Study

Table 4-3 Strains used in this chapter.

Name	Description	Source
pTO135	*pENO1-CaCas9-tCyc1, AMP*	(*52*)
pTO136	*pADH1-tRNA-Ala-gRNA-tracrRNA-HDV-tAgTEF2, AMP*	(*52*)
pTO137	*RFP-tADH1-pAgTEF2-NAT1-tAGTEF2, AMP*	(*52*)
pTO169	*ACE2 NEO, AMP*	(*52*)
pTO139	pUC19, *AMP*	(*52*)
pTO144	*als(B9J08_002582)::NAT, AMP*	This Study
pTO167	*als(B9J08_004498)::NAT, AMP*	This Study
pTO166	*als(B9J08_004112)::NAT, AMP*	This Study
pTO145	*iff(B9J08_004100)::NAT, AMP*	This Study
pTO148	*iff(B9J08_004109)::NAT, AMP*	This Study
pTO202	*iff(B9J08_004098)::NAT, AMP*	This Study
pTO188	*iff(B9J08_004110)::NEO, AMP*	This Study
pTO146	*iff(B9J08_001531)::NAT, AMP*	This Study
pTO147	*iff(B9J08_004892)::NAT, AMP*	This Study
pTO205	*iff(B9J08_001155)::NAT, AMP*	This Study
pTO206	*iff(B9J08_004451)::NAT, AMP*	This Study
pTO207	*iff(B9J08_000675)::NAT, AMP*	This Study
pTO222	*IFF(B9J08_004109) NEO, AMP*	This Study
pTO211	*scf1::NAT, AMP*	This Study
pTO221	*iff(B9J08_004109)::NEO, AMP*	This Study
pTO100	pLC49 *C. albicans NAT flp*	(*51*)
pTO102	pLC953 *C. albicans* Cas9 sgRNA	(*51*)
pTO288	*pTEF1-ALS(B9J08_004112), NAT, AMP*	This Study
pTO255	*scf1(CXQ85_003100)::NAT, AMP*	This Study
pTO264	$SCF1_{Ch}$ *(CXQ85_003100) NEO*	This Study
pTO250	*pTEF1-SCF1 NAT, AMP*	This Study
pTO223	*SCF1 NEO, AMP*	This Study
pTO284	$SCF1_{AR0381}$ *(CJI96_0001187) NEO, AMP*	This Study
pTO280	*SCF1-FLAG NEO, AMP*	This Study
pTO281	$SCF1\text{-}FLAG_{K163A}$ *NEO, AMP*	This Study
pTO282	$SCF1\text{-}FLAG_{K147A\ R148A\ K150A\ K152A}$ *NEO, AMP*	This Study
pTO283	$SCF1\text{-}FLAG_{R54A\ R55A}$ *NEO, AMP*	This Study
pTO268	$SCF1\text{-}FLAG_{R178A\ K181A}$ *NEO*	This Study
pTO292	$SCF1\text{-}FLAG_{H52A\ H53A\ R54A\ R55A}$ *NEO*	This Study
pTO293	$SCF1\text{-}FLAG_{K44A\ H55A\ Y46A\ W47A\ K49A}$ *NEO*	This Study

Table 4-4 Plasmids used in this chapter.

Name	Sequence	Purpose
qPCR Primers		
oTO359	CGTGCTGTGTTCCCATCCAT	*C. auris ACT1*
oTO360	AGCCTCATCACCGACATACG	
oTO1251	GTGAGAGTGAGGTCGGAACG	*C. auris SCF1*
oTO1252	CAGCTTCTCCTTCTGGCTCC	
oTO615	GGGAGACACCTTGACGCTTT	*IFF* (B9J08_004109)
oTO616	GTTGGCTCAGGGAAGTCGAA	
oTO1253	TGAGAGATTTAGAGCCGCCG	*C. haemulonii ACT1*
oTO1254	TACGCTCTGCAATACCTGGG	
oTO1229	TTGGTGAAGGAGCAACCGAG	*C. haemulonii SCF1*
oTO1230	GGGGCTTCAAGTGTCTGACT	
Amplification of transformation cassettes		
oTO143	CCTCTTTGTAGTTCAACTTATGC	Amplification of Cas9 Cassette
oTO41	GTCCCAAAACCTTCTCAAGC	
oTO18	CAGGAAACAGCTATGAC	Amplification of Repair Cassettes
oTO19	GTAAAACGACGGCCAG	
oTO1159	gactacaaggacgacgatgacaagACAACCACCACTACTTCG	Overlap Extension PCR for *SCF1-FLAG* Cassette
oTO1160	cttgtcatcgtcgtccttgtagtcTTCACACTCACACACCCAAC	
oTO224	GCTATTACGCCAGCTGG	
oTO225	CGCAATTAATGTGAGTTAGC	
oTO945	CAGTGGAGCGGAAACTC	
oTO946	GTGGACCTGATTTGACTGG	
oTO947	CCTGAATCTCTCAACGAAG	pTO222 Repair Cassette
oTO948	GTGGTGTAAGCGATTGTG	
oTO1161	GCAAGACGAACCTCCAAC	pTO250 Repair Cassette
Amplification of plasmid fragments for Gibson Assembly		
oTO590	GGATCCTCTAGAGTCGAC	Amplification of pUC19 backbone
oTO591	GGTACCGAGCTCGAATTC	
oTO668	ACTGGATGGCGGCGTTAG	Amplification of NEO cassette
oTO669	CGACATGGAGGCCCAGAATAC	
oTO874	ATCAAGCTTGCCTCGTCC	Amplification of NAT cassette
oTO184	ttcgagctcggtaccGTACTCATCAGAGTATACGATGC	
oTO185	acgccgccatccagtGAGCAGTCGATGCTTCAAATTAAATC	
oTO186	aagcatcgactgctcACTGGATGGCGGCGTTAG	
oTO187	gagaacctaaaaattATCAAGCTTGCCTCGTCC	

oTO188	cgaggcaagcttgatAATTTTTAGGTTCTCTAGCC	Assembly of pTO144
oTO189	gactctagaggatccCGGAGTGTCACATTTCTTTC	
oTO190	aaatgtgacactccgGGATCCTCTAGAGTCGAC	
oTO191	tactctgatgagtacGGTACCGAGCTCGAATTC	
oTO410	TAGCCTTGATTTGAGCAACCGGATCCTCTAGAGTCGACCT	Assembly of pTO167
oTO411	TACAAATAGCAGTTATCAGCGGTACCGAGCTCGAATTCAC	
oTO412	GTGAATTCGAGCTCGGTACCGCTGATAACTGCTATTTGTATACA	
oTO413	tactaacgccgccatccagtTGATAAATGGAAAGTAGAGAAACAT	
oTO414	TCTCTACTTTCCATTTATCAactggatggcggcgttagta	
oTO415	AAATAATAATTGAGTAGGCCatcaagcttgcctcgtcc	
oTO416	ggacgaggcaagcttgatGGCCTACTCAATTATTATTTAATTTTTTT	
oTO417	AGGTCGACTCTAGAGGATCCGGTTGCTCAAATCAAGGCTA	
oTO402	GACTATCCTGAAAACGCTTGGGATCCTCTAGAGTCGACCT	Assembly of pTO166
oTO403	GCGTTTACGGCGATTGCACCGGTACCGAGCTCGAATTCAC	
oTO404	GTGAATTCGAGCTCGGTACCGGTGCAATCGCCGTAAACGC	
oTO405	tactaacgccgccatccagtGAAAGATGATGGGAAACAAGGTGA	
oTO406	CTTGTTTCCCATCATCTTTCactggatggcggcgttagta	
oTO407	GGTATCATAAAAGCTCACGTatcaagcttgcctcgtcc	
oTO408	ggacgaggcaagcttgatACGTGAGCTTTTATGATACCT	
oTO409	AGGTCGACTCTAGAGGATCCCAAGCGTTTTCAGGATAGTC	
oTO192	ttcgagctcggtaccCCTTCTCGAGTTACTCTG	Assembly of pTO145
oTO193	acgccgccatccagtTGGATAAAGCAAGTGAAAAAG	
oTO194	cacttgctttatccaACTGGATGGCGGCGTTAG	
oTO195	agtgggtatatggtcATCAAGCTTGCCTCGTCC	
oTO196	cgaggcaagcttgatGACCATATACCCACTCGC	
oTO197	gactctagaggatccCGCCACTTTACTTGCCAAC	
oTO198	gcaagtaaagtggcgGGATCCTCTAGAGTCGAC	
oTO199	agtaactcgagaaggGGTACCGAGCTCGAATTC	
oTO216	ttcgagctcggtaccCAGACATCTTTTGTGCAAG	Assembly of pTO148
oTO217	acgccgccatccagtTTGTTGATGGGGAACTAC	
oTO218	gttccccatcaacaaACTGGATGGCGGCGTTAG	
oTO219	aaagtgacaccgtcaATCAAGCTTGCCTCGTCC	
oTO220	cgaggcaagcttgatTGACGGTGTCACTTTCGAG	

oTO221	gactctagaggatccGTGGTGTAAGCGATTGTG	
oTO222	aatcgcttacaccacGGATCCTCTAGAGTCGAC	
oTO223	cacaaaagatgtctgGGTACCGAGCTCGAATTC	
oTO786	acgacggccagtgaattcgagctcggtaccCGTATTCTCGAGCTCTTAAAG	Assembly of pTO202
oTO787	acgccgccatccagtAATGGTTGATTAACAAAAGAAAAAAAAAAAAAG	
oTO788	tgttaatcaaccattACTGGATGGCGGCGTTAG	
oTO789	gctaggaaaaattgcATCAAGCTTGCCTCGTCC	
oTO790	cgaggcaagcttgatGCAATTTTTCCTAGCCTTTATTTTTTC	
oTO791	gcatgcctgcaggtcgactctagaggatccCTACCAAAAGTTGACGTG	
oTO678	ggccagtgaattcgagctcggtaccGCAAACGTCAGTCTACCG	Assembly of pTO188
oTO679	ttcgatactaacgccgccatccagtGATGGAATGGATGGAGAG	
oTO680	gagggtattctgggcctccatgtcgCTTTAAAATCGTTTTATTTAGTTCTG	
oTO681	cctgcaggtcgactctagaggatccGTACAGCTTACACAACTAATAAAAAC	
oTO200	ttcgagctcggtaccGGTCTTGTTAACATGGCC	Assembly of pTO146
oTO201	acgccgccatccagtGATGCTCAATAGCTGAAG	
oTO202	cagctattgagcatcACTGGATGGCGGCGTTAG	
oTO203	aattggtacgttaggATCAAGCTTGCCTCGTCC	
oTO204	cgaggcaagcttgatCCTAACGTACCAATTCTC	
oTO205	gactctagaggatccCCAAAAATATGAAGACGAGAG	
oTO206	tcttcatatttttggGGATCCTCTAGAGTCGAC	
oTO207	catgttaacaagaccGGTACCGAGCTCGAATTC	
oTO208	ttcgagctcggtaccGCAGCTGCATTGGTACATATG	Assembly of pTO147
oTO209	acgccgccatccagtGTGGAGCAGGTTGGGTTAG	
oTO210	cccaacctgctccacACTGGATGGCGGCGTTAG	
oTO211	tttgtgcatttaagtATCAAGCTTGCCTCGTCC	
oTO212	cgaggcaagcttgatACTTAAATGCACAAAACGC	
oTO213	gactctagaggatccGGACTACAGCTTCTTTGG	
oTO214	aagaagctgtagtccGGATCCTCTAGAGTCGAC	
oTO215	taccaatgcagctgcGGTACCGAGCTCGAATTC	
oTO819	acgttgtaaaacgacggccagtgaattcgagctcggtaccCAAAGTAGCCACACACTTG	Assembly of pTO205
oTO820	tactaacgccgccatccagtATTTGGCAGAGAGTAGAATG	
oTO821	cattctactctctgccaaatACTGGATGGCGGCGTTAG	
oTO822	tgtgcagccttgtatcaacaATCAAGCTTGCCTCGTCC	
oTO823	ggggacgaggcaagcttgatTGTTGATACAAGGCTGCAC	
oTO824	cgccaagcttgcatgcctgcaggtcgactctagaggatccCTTCGTCCTCGTGCTTGG	
oTO825	acgttgtaaaacgacggccagtgaattcgagctcggtaccGAACGCAACAACTTAAGC	Assembly of pTO206
oTO826	tactaacgccgccatccagtGCGTTTGTGTTTGATGGAG	
oTO827	tctccatcaaacacaaacgcACTGGATGGCGGCGTTAG	

oTO828	ataaaggtttcgtcttttgtATCAAGCTTGCCTCGTCC	
oTO829	ggggacgaggcaagcttgatACAAAAGACGAAACCTTTATATAAC	
oTO830	aagcttgcatgcctgcaggtcgactctagaggatccCCTAAGATATTCAAGAGGAAATC	
oTO831	gttgtaaaacgacggccagtgaattcgagctcggtaccGGTACCAGAATGTGGGCTTTC	Assembly of pTO207
oTO832	tactaacgccgccatccagtCGTGAGGCGAGGCAGATC	
oTO833	aagatctgcctcgcctcacgACTGGATGGCGGCGTTAG	
oTO834	caaagggaccgtggctgcatATCAAGCTTGCCTCGTCC	
oTO835	ggggacgaggcaagcttgatATGCAGCCACGGTCCCTT	
oTO836	gcttgcatgcctgcaggtcgactctagaggatccGGTTTACGTTGCCACACTATTCTG	
oTO879	acgttgtaaaacgacggccagtgaattcgagctcggtaccCAGTGGAGCGGAAACTCTTC	Assembly of pTO211
oTO880	actgctgtcgattcgatactaacgccgccatccagtTGTGGAGGTGAAGTTTTAAGATAG	
oTO881	ctggccgggtgacccggcggggacgaggcaagcttgatTTCTAATGACTGATACTCATAC	
oTO882	cgccaagcttgcatgcctgcaggtcgactctagaggatccGTGGACCTGATTTGACTG	
oTO937	gtgaattcgagctcggtaccCCTGAATCTCTCAACGAAG	Assembly of pTO222
oTO938	tactaacgccgccatccagtTCAGAACATGGCAAATAATG	
oTO943	accacaatcgcttacaccacGGATCCTCTAGAGTCGAC	
oTO944	tcttcgttgagagattcaggGGTACCGAGCTCGAATTC	
oTO927	tatactgctgtcgattcgatactaacgccgccatccagtTGACGGTGTCACTTTCGAG	Assembly of pTO221
oTO928	gtcaagactgtcaaggagggtattctgggcctccatgtcgTTGTTGATGGGGAACTAC	
oTO6	gactgtcaaggagggtattc	Generation of CaTO227
oTO7	CCGCaagtgattagacttag	
oTO8	gaataccacttgtttaccgg	
oTO9	GGTGGCGGCAAAACTAATTC	
oTO40	CGCTATATCCTTCTTGGTCG	
oTO41	gtcccaaaaccttctcaagc	
oTO652	CATCAGAATTGTTCAAACAACTACCAATTGTTAATATCAGggaaacagctatgaccatg	
oTO653	GAACTAGATCAAGCCAAAAAGGTGATCATAACAATATAGTCAgtaaaacgacggccag	
oTO698	CCTGGTGGTGCAGTTACAGTcaaattaaaaatagtttacgcaagtc	
oTO699	gACTGTAACTGCACCACCAGGgttttagagctagaaatagcaag	
oTO1480	acgttgtaaaacgacggccagtgaattcgagctcggtacccagataactcaccacgag	
oTO1481	ggggacgaggcaagcttgatgaaagatgatgggaaacaag	
oTO1482	cttgtttcccatcatctttcatcaagcttgcctcgtcc	

oTO1483	gcaagcgaagcaagtttcatttttgttagtttttgaggtgatacag	Assembly of pTO288
oTO1484	cacctcaaaaactaacaaaaatgaaacttgcttcgcttg	
oTO1485	cgccaagcttgcatgcctgcaggtcgactctagaggatccgtctacagtggttgagaac	
oTO1274	ccggtcttcttttgctctaaGTAGCAGCATGATTATGAAC	Assembly of pTO264
oTO1275	agaagaagactgtatttcatTGTGGAGGTGAAGTTTTAAG	
oTO1276	cttaaaacttcacctccacaATGAAATACAGTCTTCTTCTTC	
oTO1277	gttcataatcatgctgctacTTAGAGCAAAAGAAGACC	
oTO1150	ggccgggtgacccggcggggacgaggcaagcttgatTGTGGAGGTGAA GTTTTAAGATAG	Assembly of pTO250
oTO1151	ctatactgctgtcgattcgatactaacgccgccatccagtCACATGGGCTCC GTTTCTG	
oTO1152	agaagtaaagagaatctcatTTTTGTTAGTTTTTGAGGTGATACA GAAAAAG	
oTO1153	cacctcaaaaactaacaaaaATGAGATTCTCTTTACTTCTTGC	
oTO1154	cgccaagcttgcatgcctgcaggtcgactctagaggatccGCAAGACGAAC CTCCAAC	
oTO1078	tcgttaactgtgtattacctgttcataatcatgctgctacTTAAAGCAACAAG GCAGC	Assembly of pTO223
oTO1066	GTAGCAGCATGATTATGAACAGG	
oTO1077	tgctgtcgattcgatactaacgccgccatccagtTTCTAATGACTGATAC TCATACTTTC	
oTO1430	TTAAAGCAACAAGGCAGC	Assembly of pTO284
oTO1431	TACACCTGCAAGAAGTAAAGAGAATCTCATTGTGGA GGTGAAGTTTTAAG	
oTO1432	CTTTGCTTGCTGCTGCCTTGTTGCTTTAAGTAGCAGC ATGATTATGAAC	
oTO1159	gactacaaggacgacgatgacaagACAACCACCACTACTTCG	Assembly of pTO280
oTO1160	cttgtcatcgtcgtccttgtagtcTTCACACTCACACACCCAAC	
oTO1427	CAGTTAATAGTTTGCGCAACG	Assembly of pTO281
oTO1428	CTGTAGCAATGGCAACAAC	
oTO1417	CCGGCGTTGTGTGCTGTCTCCCACATGCTTTGGAGGT TCGTCTTGCTTTGGAGCCAG	
oTO1418	GAACCTCCAAAGCATGTGGGAGACAGCACACAACGC CGGCTGGTTTGTGCTTGTGTCTC	
oTO1421	AACGGATGCTCGAGGCTGCTCACGCTCACGCTCCAG CCGGCGTTGTGTGCTGTCTCCCAC	Assembly of pTO282
oTO1422	CCGGCTGGAGCGTGAGCGTGAGCAGCCTCGAGCATC CGTTCCGACCTCACTCTCACTCTG	
oTO1425	GCCATCATGCTGCTTCCAACGATGGCCCCGAGTTTAT CGATGCGGGAG	Assembly of pTO283
oTO1426	GGGGCCATCGTTGGAAGCAGCATGATGGCCACCTTT CACCCAGTAGTG	
oTO1563	GCGCTGCTGCTGCTTCCAACGATGGCCCCGAGTTTAT CGATGCGGGAG	Assembly of pTO292

oTO1564	GGGGCCATCGTTGGAAGCAGCAGCAGCGCCACCTTTCACCCAGTAGTG	
oTO1565	TGCTGCTGCTGCTGTGGCTGGTGGCCATCATCGTCGTTCCAAC	Assembly of pTO293
oTO1566	GCCACCAGCCACAGCAGCAGCAGCAGAAGGTGTACAGTAGTCGTC	

Table 4-5 Oligonucleotides used in this chapter.

Chapter 5 Discussion

5.1 Overview

In many ways, *Candida auris* represents an unprecedented clinical and public health challenge among other fungal pathogens and other *Candida* species. High rates of antifungal and multidrug resistance coupled with outbreak potential and interpersonal transmission may be the hallmarks of a new era of *Candida* pathogens, reflecting adaptations more similar to healthcare associated bacterial pathogens of substantial concern[29]. Although cases and outbreaks are continually increasing, the global burden of *C. auris* remains comparatively low[41]. Even with low case counts compared to other pathogens of high concerns, public health authorities have elevated *C. auris* to maximal research and clinical priorities[91,270]. *C. auris* is one of only six pathogens recognized by the CDC as an urgent antimicrobial resistance threat, and the first fungal pathogen to reach this designation. It also tops the WHO fungal pathogen priority list in the critical designation, along with other pathogens with exponentially greater global case counts. This concern around *C. auris* reflects challenges in preventing and treating infection, but also perhaps apprehension around witnessing the emergence of a human pathogen with enigmatic virulence traits compared to its better studied model counterparts. Seemingly simultaneously, multiple genetic lineages around the world have transitioned from an unknown environmental origin to a pathogenic human-associated lifestyle, driving antifungal resistant infections through transmissible colonization and tenacious outbreaks that can escalate towards endemic spread[4]. Despite the decade of surveillance, sequencing, public health practice, and basic science research

since *C. auris'* emergence, scientific efforts have only just begun to explain the enigmatic behavior of this emerging pathogen.

At the time of writing, the *Candida* Genome Database recognizes functional verification of only 23 open reading frames in the *C. auris* genome, leaving a staggering 99.58% of the genome uncharacterized[299]. This paucity of experimental evidence for molecular explanations of *C. auris* behaviors reflects a number of factors. Early substantial research efforts were heavily biased towards surveillance and sequencing initiatives, which have powerfully described the scope of the global emergence of *C. auris* and produced comprehensive collections of genetic data from diverse lineages but have frequently lacked functional application[4,48]. Phenotypic characterizations and surveillance efforts have definitively demonstrated elevated rates of transmissibility and acquired drug resistance in *C. auris* relative to other *Candida* species[5]. Combining insights from these efforts, a logical and often cited approach to understanding *C. auris* biology is to examine its genetic commonality with characterized species. For instance, conservation of the *ALS* and *IFF/HYR* adhesin families in *C. auris* has been proposed as a mechanism for colonization and outbreak potentiation[84]. As we have demonstrated in this dissertation, however, this approach fails to appreciate the contribution of lineage-specific elements, such as *SCF1*. A seminal analysis described hundreds of predicted genes entirely unique to the multidrug-resistant clade comprising *C. auris* and the related *haemulonii* complex, including enrichment in genes with clinically relevant potential putatively encoding GPI-anchored cell surface proteins, oligopeptide and ABC transporters, and secreted lipases[48]. Of these, *SCF1* is the first with functional characterization[95]. Poor genetic tractability has perhaps contributed to slow progress in molecular experimentation, but our work and the work of others in developing technologies and methodologies for genetic manipulation have effectively

overcome this impediment, to the present point where manipulation in diverse strain backgrounds is accessible and straightforward, in stark contrast to the challenges faced only a few years ago[170,219,222,280,300,301].

In this way, the findings detailed in this dissertation and the associated published manuscripts represent critical and substantial contributions to the scientific understanding of *C. auris* pathobiology. We have developed facile methodologies for efficient forward and reverse genetic manipulation of *C. auris* isolates from diverse genetic, geographic, and clinical origins. Using these techniques, we have explored one mechanism of multicellularity in *C. auris* related to the conserved RAM cell separation pathway and described the impact of perturbation of this pathway on virulence and drug resistance phenotypes. We have also probed the adhesin landscape in *C. auris* to identify the dominant effectors in substrate association and colonization as Iff4109 from the conserved but differentially expanded *IFF/HYR* family of GPI-anchored proteins and the lineage-specific Scf1. In our characterization of these adhesins, we provide the first functional description of an Iff/Hyr adhesin as a hydrophobin and the first described fungal example of clustered cation-aromatic adhesion in Scf1. We show that adhesive plasticity is widespread in *C. auris* at single strain resolution, and that adaptation around regulatory control of the lineage-specific virulence factor Scf1 is a key driver for this plasticity. In modeling colonization and infection dynamics, we demonstrate the potential for substantial clinical impact related to Iff4109 and Scf1 utilization as critical factors in colonization of abiotic surfaces, inserted medical equipment, and host skin as well as virulence during disseminated infection, providing important insights towards a fuller understanding of the biology driving *C. auris* outbreak dynamics.

5.2 Future studies and implications

Characterization of Scf1 and Iff4109 as dominant adhesins governing surface association and colonization represents a major advance in *C. auris* biology and understanding outbreak potential, but our description of widespread adhesive plasticity among *C. auris* strains leaves open vital questions around the place for these adhesins in the scope of *C. auris* evolution and adaptation in response to changing environments in nature and in clinical settings. Biomedical science is inundated with a pervasive "more is more" mentality – more adhesion leads to more bioburden in colonization models, more Scf1 expression leads to more surface contamination, or more adhesin expression means more virulence. This is perhaps the fundamental message I have portrayed by rounding out our adhesion characterization with colonization and infection models, but this effort to produce digestible and interpretable conclusions fails to examine intricate realities that will become critical as we more carefully explore the dynamics of *C. auris* outbreak biology.

Despite any apparent advantages around more adhesin expression, more colonization, and more virulence, a snapshot sampling of two dozen clinical isolates of *C. auris* from different outbreaks and different lineages reveals remarkable differences in adhesion capacity and adhesin expression with few obvious connections to differential clinical or outbreak histories (Fig. 4-4). This observation suggests the selective advantages for adhesive plasticity are more complex than simply adapting towards the most virulent and adhesive phenotype, meriting further consideration in future exploration of *C. auris* outbreak dynamics. As a model for this investigation and a hypothesis to explain *C. auris* adhesive plasticity, I will discuss the scope and scale of adhesive adaptation among clinical and outbreak isolates, a potential selective advantage for tuning adhesion to strike a balance between colonization and transmission, and a narrative for

a possible environmental pressure for the evolution of adhesive adaptability and the connection of this evolution to the emergence of *C. auris* as a global human pathogen.

5.2.1 Real time adaptation of adhesion in outbreak settings

In Chapter 4, I discussed the adhesive variation associated with adaptations in *SCF1* expression among disparate clinical isolates of *C. auris* (Fig. 4-4). Importantly, this variation did not segregate by genetic lineage, suggesting adaptation is occurring more recently than clade separation. This observation raises the question as to whether adhesive adaptation occurred prior to clinical manifestation or actively during outbreak settings, with the underlying assumption that some pressure in either preclinical or clinical environments has selected for the divergent phenotypes. Understanding this selective pressure is likely to be central to understanding the influence of adhesive adaptation on outbreak progression. Of note, each of these isolates was recovered from patients, suggesting host association or infection does not necessarily predict adhesive phenotype.

Where only a handful of proposed environmental *C. auris* isolates have been described, investigating adhesive adaptation in a preclinical context is unrealistic. Conversely, deep hospital sampling is often performed in response to *C. auris* outbreaks, such that collections of outbreak isolates are readily available. One hypothesis for the plasticity is that adaptation is occurring in real time during outbreaks. A functional model would hold that during clonal expansion and dissemination, a pioneer lineage diverges to produce progeny lineages with altered or adapted adhesive capacity, and some selective advantage for a specific adhesive profile might lead to a dominant phenotype among the population over time. A stochastic model might be that the heritable adaptation is effectively independent from selective pressures faced in the outbreak setting, and adaptation occurring as a result of some unexplored mechanism results in variability

within the outbreak population. In either case, the result would be rapid divergence within a semi-clonal population. If a single isolate were recovered in the midst of that divergence, it could exhibit its own adhesive profile without necessarily reflecting the adhesive capacity of the entire outbreak population. This model potentially explains the variability observed in Fig. 4-4, where each strain has been independently isolated from individual cases or outbreaks.

To test whether this adaptation is active within the time scale of a single outbreak, we investigated the adhesion capacity for a sample of isolates from a clonally distributed outbreak. *C. auris* began spreading in post-acute care facilities in metropolitan Chicago in 2016 and continues in ongoing, quasi-endemic spread[30]. We measured the adhesion for 32 outbreak isolates collected between November 2021 and September 2023, including invasive isolates from 9 infected patients or skin colonizing isolates from two patients, with matched isolates sampled from environmental surfaces near these patients (Fig. 5-1). Despite the clonal history of the

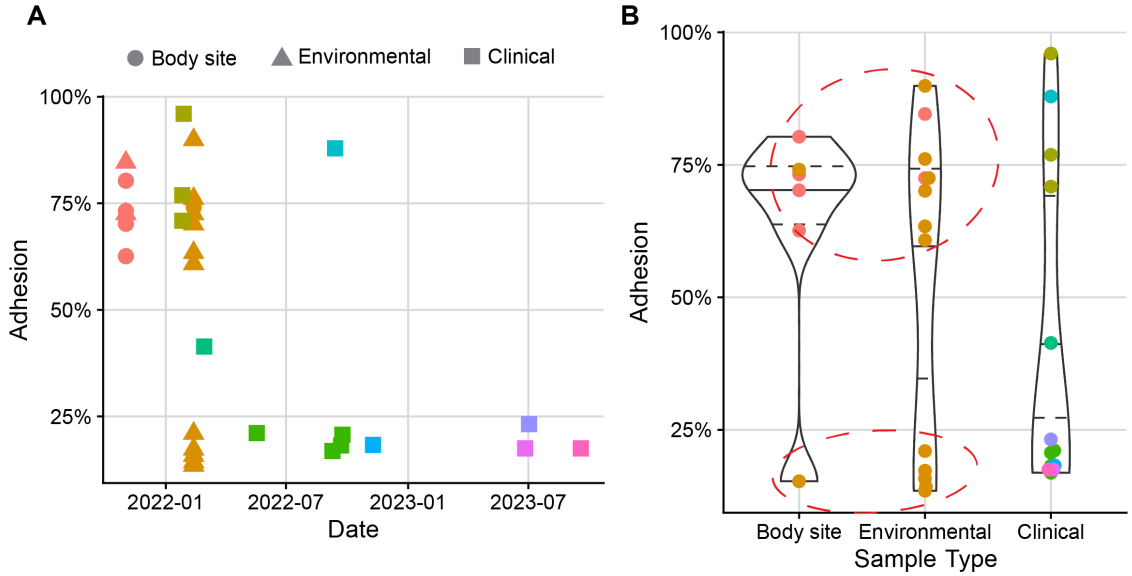

Figure 5-1 Adhesive variability is widespread among isolates within an individual clonal outbreak. Adhesion was measured using flow cytometry adhesion assay described in Chapter 4 for 32 clinical isolates recovered from an ongoing outbreak in metropolitan Chicago. **(A)** Adhesion is plotted against isolate collection date. Shapes designate isolates as colonizing, environmental, or clinical, with colors corresponding to individual patients. **(B)** Adhesion segregated based on sample type, with colors corresponding to individual patients. Circles highlight linked clusters in brown, with a single patient colonized by both high and low adherence isolates, each having matched environmental samples.

outbreak, we observed populations of highly adherent and poorly adherent isolates, suggesting adhesive adaptation has occurred within the timescale of this outbreak (Fig. 5-1). While this sample size is insufficient to draw conclusions around outbreak progression, it is notable that a greater number of patients were clinically infected with less adhesive isolates across the sampling timeframe (Fig. 5-1A). Potentially, a less adherent phenotype may more readily contribute to transmission from colonized substrates; in this case, a comprehensive sample of outbreak isolates might reveal a selective adaptation towards less adhesion over time. Interestingly, a single patient in this sample was colonized with both a highly adhesive and a poorly adhesive isolate, and both isolates have linked clusters of environmental contaminants (Fig. 5-1B). This observation suggests transmission and colonization are both possible regardless of adhesive capacity, although it cannot explain whether advantages in these phenotypes are related to adhesive states. Identifying a weak selective advantage would again require comprehensive sampling. It is also interesting that colonization and infection isolates demonstrate the full gamut of adhesion. Comparing an analysis of adhesive adaptation with clinical outcomes of infected patients could reveal whether the shift in adhesion corresponds with changes in virulence, as might be suggested by infection data in Fig. 4-17 and Fig. 4-19. Together, these findings demonstrate adhesive adaptation occurs within clinical outbreaks, and provides justification for future investigation to understand the selective pressures and clinical manifestations associated with differential adhesion in closely related isolates.

5.2.2 Selective advantages for adhesive plasticity in nosocomial transmission and persistence

Our data in Chapter 4 suggests highly adhesive isolates form higher burden biofilms, grow more biomass on skin, and exhibit greater cell loads on colonized medical devices. These models fail,

however, to account for dissemination away from colonized substrates. Contact transmission requires an adhesive or cohesive failure for some or all of a colony to spread between objects; transmission under fluid flow in colonized catheters or central lines might be increased if cells lift under sheer stress; airborne transmission from colonized skin may be related to shedding of associated skin cells or may be the result of direct shedding of fungal cells. On a molecular level, these transmission events are essentially unstudied for *C. auris*, but transmission itself is likely to be a strong selective pressure for expanding outbreaks. Based on our data, it is difficult to reconcile the trade-off between transmission and colonization. Adhesion is necessary for establishing colonization but may in turn slow transmission. In this regard, a selective advantage around adhesive adaptation may actually reflect a tuning of adhesion towards a population state that favors the optimal potential for both colonization and transmission.

The flow cytometric adhesion assay featured in this dissertation provides what may be an important clue for understanding adhesion tuning in *C. auris*. In this assay, cells are incubated with microparticles and the frequency of irreversible association is reported as a percentage of the population able to attach in a given timeframe. In a uniform population, this percentage would reflect the probability of irreversible adhesion given some number of collision events between cells and microparticles. However, we have observed that a pure culture of the highly adhesive AR0382 isolate contains a heterogenous population with non-uniform expression of the adhesin Scf1 (Fig. 5-2A, B). Even in this genetic background, which exhibits very strong bulk expression of *SCF1* (Fig. 4-3B), individual cells can demonstrate little to no detectable adhesin expression with levels varying along a continuum in the bulk population regardless of cell size

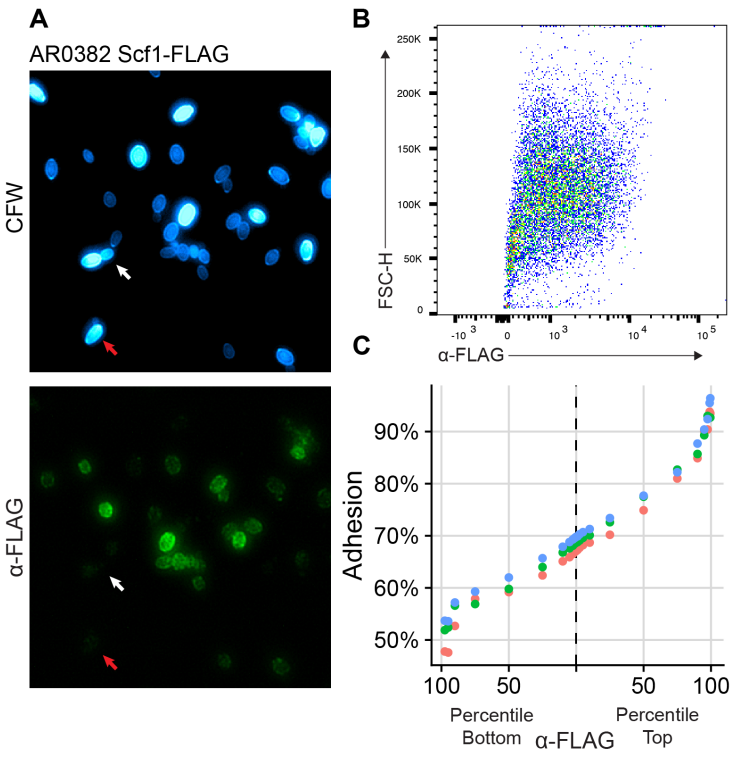

Figure 5-2 The highly adhesive isolate AR0382 exhibits heterogenous Scf1 expression associated with subpopulation variation in adhesion. (A) Pure culture of AR0382 in stationary phase. Total cells were visualized with calcofluor white (CFW), while Scf1-FLAG expression was visualized with immunofluorescence. Variability in Scf1 fluorescent intensity is evident, with arrows indicating cells that show little detectable expression. **(B)** Representation of the population heterogeneity in Scf1 expression by flow cytometry. FSC-H used as a proxy for cell size, indicating heterogeneity is apparent even in newly budded cells, represented by events at the lowest FSC-H values. **(C)** The bulk population was subset into percentiles of Scf1 expression and adhesion was measured for each subpopulation. Different colors represent experimental replicates.

(Fig. 5-2A, B). Since we have proposed that Scf1 directly mediates substrate adhesion, the frequency of irreversible adhesion events should be directly proportional to Scf1 abundance in subpopulations. By segmenting the bulk population based on percentiles of Scf1 expression, we see that this is in fact the case, with adhesion percentages correlating to Scf1 expression subgroups (Fig. 5-2C). This suggests that even within a highly adherent isolate, poorly adherent cells may represent a subpopulation more competent for transmission. Adhesive heterogeneity is evident even in events of small size, which likely reflect young budded cells separated during sample preparation, and variability exists between cells connected at bud sites, suggesting adhesive cells can produce less adhesive cells and vice versa (Fig. 5-2A, B). Transmitted cells, including those with less adhesive capacity, may then be able to propagate populations with highly adhesive cells, competent for stable colonization of substrates after transmission.

Adhesive tuning, then, may mechanistically reflect tuning of subpopulation adhesin expression frequencies. In Fig. 4-17B, the wild type, poorly adhesive isolate AR0387 exhibits scant colonization of an indwelling central line, suggesting the majority of the population has failed to remain surface associated under relevant shear stress. Perhaps importantly, though, the catheter is still colonized, if only by a small number of cells, suggesting some subpopulation is more prone to colonization, while the bulk of the population is more prone to separation and transmission. By expressing an epitope-tagged Scf1 allele in this strain background, which shows a bulk 2^9 transcriptional downregulation of *SCF1* compared to its highly adhesive counterpart AR0382 (Fig. 4-4), we observe a small subpopulation of cells exhibiting higher expression of Scf1 (Fig. 5-3A, B). Stratifying the population by percentiles of Scf1 expression demonstrates a precipitous increase in adhesion capacity for the topmost expressors, achieving an order of magnitude greater frequency of adhesion over the bulk population (Fig. 5-3C). This suggests that even poorly adhesive isolates comprise adhesive subpopulations, with cells competent to

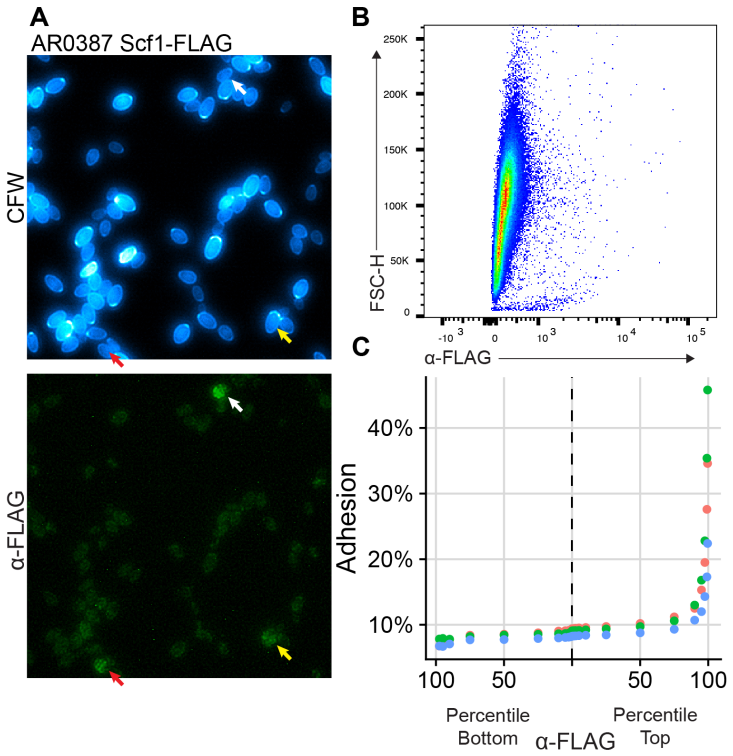

Figure 5-3 The poorly adhesive isolate AR0387 exhibits a small subpopulation of high Scf1-expressing cells exhibiting a precipitous increase in adhesion. (A) Pure culture of AR0387 in stationary phase. Total cells were visualized with calcofluor white (CFW), while Scf1-FLAG expression was visualized with immunofluorescence. Variability in Scf1 fluorescent intensity is evident, with arrows indicating cells that show increased Scf1 expression compared to the bulk population. **(B)** Representation of the population heterogeneity in Scf1 expression by flow cytometry. **(C)** The bulk population was subset into percentiles of Scf1 expression and adhesion was measured for each subpopulation. Different colors represent experimental replicates.

stably colonize substrates, such as those remaining attached to the catheter in Fig. 4-4, and cells that may be more likely to disperse and transmit. Potentially, a lower adhesion frequency might favor development of invasive disease after colonization of an indwelling medical device, which may be related to our observation that poorly adhesive isolates are highly represented in patients with invasive infection during an outbreak (Fig. 5-1).

Modeling transmission experimentally can be challenging, and exploring selective advantages associated with adhesion tuning is likely to require careful experimental design. Transmission from a catheter surface is perhaps physically distinct from transmission from the skin or from a dry abiotic surface, and the selective pressures in each case may be different. This might explain why higher adhesive and lower adhesive isolates are evident in the Chicago outbreak even after 6 years of opportunities for selection. To fully understand the importance of adhesive tuning in outbreak dynamics will require concerted evaluation of clinical data and experimental modeling. From a biological perspective, tuning of adhesive population frequencies between strains is mechanistically interesting and remains effectively unexplained. We have demonstrated that highly and poorly adhesive isolates have distinct subpopulation compositions, but what regulatory mechanisms could lead to changes in single cell frequencies is unknown. The magnitude of the contribution of Scf1 to subpopulation adhesion is also unclear, and further work is needed to investigate what other elements are coordinately regulated at the single cell level.

5.2.3 Marine microplastics as a potential reservoir for *C. auris* emergence and adhesive evolution

One critical question remains unanswered: why has *C. auris* evolved such distinctive adhesive mechanisms? As suggested by our findings, evolution of a unique adhesin, atypical adhesive

plasticity, and enigmatic heterogenous adhesive regulation likely have substantial implications for the nosocomial life cycle of the pathogen, but *C. auris* has only been associated with humans and healthcare settings for at most a few decades. *SCF1* is encoded by all lineages and the close relative *Candida haemulonii*, suggesting the evolution around adhesion is much more ancient. Without more evidence for an environmental reservoir, it is difficult to determine what advantages adhesive evolution would provide *C. auris* in a context isolated from human activity. The prevailing hypothesis holds that *C. auris* emerged from a marine niche based on its high halotolerance and natural isolation from coastal environments[13,37]. Some environmental shift in the past century must have contributed to adaptation towards previously unrealized tolerance of the human host environment, geographic trafficking to promote greater exposure to humans, or increased environment presence to improve the likelihood of becoming encountered. Moreover, this shift would not be a single rare event, such as development of a mutation to change host tropism in a lineage exposed to humans, because the emergence of *C. auris* has occurred at least six times independently at distinct geographic locations all over the world. Because a global change represents the only plausible mechanism, the major hypothesis posits that *C. auris* became pathogenic due to thermal adaptation in response to global warming[302]. However, this hypothesis largely neglects other substantial ecological shifts that have co-occurred with thermal changes connected with climate change, which may have similarly contributed to the global emergence of *C. auris* as a human pathogen.

Industrial production of plastics began in 1950 and has continually increased since; recent estimates suggest over 300 million tons of plastic waste are generated annually, of which 79% is ultimately discharged into the environment[303]. Discharge from coastal countries represents up to 13 million tons annually of plastic waste globally that can be trafficked to marine environments

by wind and river currents[304]. Plastic waste represents a substantial source of marine pollution; one report surveyed 37 sampling sites around the world and found 70% of garbage collected was made up of plastics[305]. The hydrophobic surfaces of plastic waste provides a substrate for microbial colonization in otherwise sparse environments, harboring communities that are known to harbor bacteria, archaea, fungi, and other unicellular eukaryotes[306]. Plastisphere habitats exhibit specific selectivity, with microbial communities distinct from surrounding environments, suggesting an ecological pressure selecting for amenable phenotypes[307]. Solid plastic surfaces or microplastics can in turn serve as both a reservoir and a vector for transmission of microbes, potentially trafficking adherent communities over long distances by wind, currents, and waves[308]. Evolution of adhesion mechanisms that function at hydrophobic interfaces or under aqueous conditions with high ionic strength could theoretically produce an ecological advantage for a marine *C. auris*. In this scenario, globally increasing marine plastic waste could potentially have increased available reservoirs for *C. auris* propagation or trafficked *C. auris* to new environments, creating the opportunity for human exposure. In turn, the evolution of adhesive regulatory mechanisms may have contributed to the outbreak potential and rapid spread of *C. auris* after initial introduction, resulting in wider emergence and global concern.

While this proposal is largely speculative, others have considered the possibility, with a recent publication experimentally modeling survival of *C. auris* isolates on plastic substrates in saltwater and sand environments[309]. Stronger evidence of environmental *C. auris* absent human association would be required to lend credence to the model. However, a further biological argument can be made. With the increasing influx of plastic waste products into the environment, substantial research efforts have characterized microbes with enzymatic capacity for hydrolysis of different plastic compounds. Terrestrial origins represent the most frequent report of plastic-

degrading microbes, but marine and aquatic environments are highly represented[310]. Notably, there may be a selective pressure for plastic-degrading microbes in plastisphere colonization, as sampling of marine plastic contaminants frequently identifies microbes with the capacity for polymer hydrolysis, and experimental enrichment of oceanic water samples with plastic surfaces concurrently enriches for species with plastic degrading activity[311,312]. The most commonly recognized substrate for microbial plastic biodegradation is polycaprolactone (PCL), a linear aliphatic polyester used industrially as an impact-modifying additive for plastics or a binder or adhesive in molding[310,313]. PCL-degrading microorganisms have been isolated from a wide range of marine environments and frequently demonstrate other adaptations consistent with their oceanic niche, such as high halotolerance or psychrophilia[313]. Upon growing *C. auris* isolates on agar plates infused with emulsified PCL, we observed zones of clearing emerging beginning at 4 days of incubation around the colonies, suggesting secreted PCL hydrolytic activity (Fig. 5-4A). No clearing was observed for *C. albicans* in the same assay, however, suggesting some level of distinction in the evolutionary trajectory of this phenotype in *C. auris* (Fig. 5-4A). Macroscopic PCL flakes were also bioavailable, and these were degraded at a rate of ~0.75mg after one week's incubation in liquid *C. auris* culture

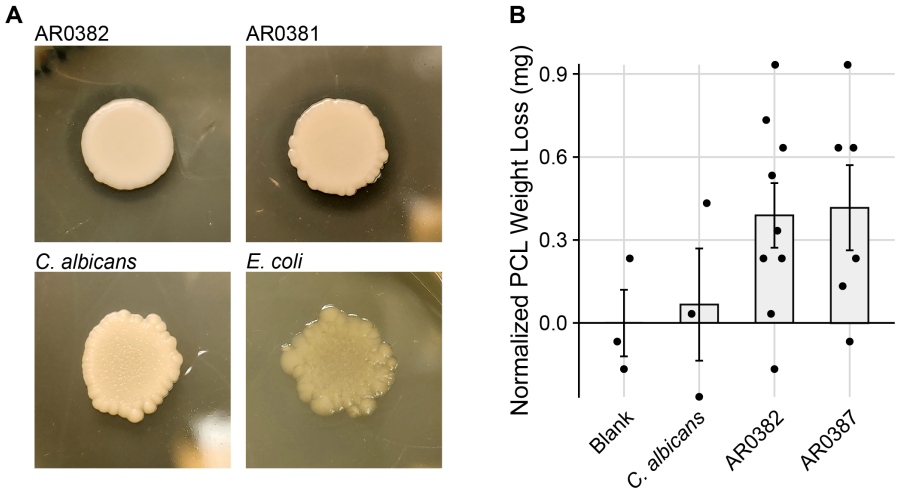

Figure 5-4 *C. auris* can biodegrade polycaprolactone (PCL). (A) Representative colonies of *C. auris* (top – AR0382 or AR0381) or *C. albicans* (SC5314) or *E. coli* grown on LB agar plates supplemented with 1% emulsified PCL. Zones of clearing around *C. auris* colonies indicate biodegradation of the polyester. **(B)** Total weight loss of ~50mg macroscopic PCL flakes after 1 week of incubation in LB broth or broth containing *C. albicans* (SC5314) or *C. auris* (AR0382, AR0387). Normalized to average weight loss of the cell-free Blank condition.

(Fig. 5-4B). These preliminary observations suggest *C. auris* has evolved in an environment that might have selected for the capacity for plastic polymer hydrolysis.

The selective advantage for marine plastic association could represent a number of mechanisms. From this data, it is unclear whether *C. auris* has the capacity for mineralization of decomposed polymer products and assimilation into biomass, although some microorganisms do have the capacity to catabolize hydrolyzed plastics[312]. Access to nutrients through cross-feeding in communities represents another nutritional advantage, and microbial carbon and nitrogen cycle dynamics are known to shift in plastisphere microcommunities[314]. Close-knit communities could realistically provide other advantages, a prominent example being the facilitation of exchange of genetic material[315]. Association of *C. auris* with a continually increasing plastisphere could feasibly have other connections to its pathobiology. As mentioned, selection for adhesive regulation may have contributed to *C. auris* outbreak potential, but virulence and drug resistance could similarly be impacted. Microplastic particles are regularly taken up by various vertebrate and invertebrate species, potentially promoting adaptation towards a host-associated state[316]. Hydrophobic plastics in aqueous environments are also known to concentrate hydrophobic organic chemicals, which might introduce associated microbial communities to contaminating chemical runoff from human activity, such as antifungal azoles used in agriculture[317]. Such a scenario may introduce pressure for development of acquired resistance, which is uniquely frequent in *C. auris*.

This model is of course highly hypothetical, coincidental, and circumstantial. To substantiate the central hypothesis, more definitive characterization of *C. auris* natural reservoirs must take place. A targeted search for a specific marine organism bears its own challenges given the vastness of the oceans, and most publicly available sequence data of marine or plastisphere

communities were not designed to search for fungal or eukaryotic genetic material. Experimentally, genetic characterization of the PCL degrading enzymatic activity in *C. auris* could be straightforward and may offer insights into the evolutionary history of this organism. Wider phenotypic characterization of plastic degrading capacities would also be interesting, as would investigating the conservation of these mechanisms in related lineages. Conspicuously, plastic contaminants themselves are much less ancient than the evolutionary timescale differentiating *C. auris* lineages. Many plastic hydrolyzing enzymes originated as cutinases or lipases that allow microbes to associate with waxes in the cuticular layer on the surface of plants. Evolution of plastic biodegradation activity in *C. auris* may represent an ancient association with plants, not unlike the closely related *Candida ruelliae*[20]. Perhaps, in one last great coincidence, such an evolutionary trajectory has even influenced the tropism with waxy cerumen-lined ear canals from which *C. auris* draws its name and original isolation.

5.3 Conclusion

C. auris is a pathogen that fits within the unique niche of having captured global public health and clinical concern without the millions of case counts cited for most high-profile infectious agents. Its emergence has broken down our conceptions of how a fungal pathogen behaves and how to respond to fungal infection. Seemingly at every turn, clinical control of *C. auris* has faced substantial hurdles: treatment is complicated by high rates of acquired resistance, widespread colonization and transmission drives and prolongs disseminated outbreaks, and decontamination efforts are hindered by recalcitrance towards disinfectant and antiseptic regimes. A decade into the emergence of this organism as a human pathogen has only reinforced the notion that we are largely unprepared for this specific challenge, as cases and outbreaks increase at exponential rates year over year. What is clear is that combatting this new threat requires new approaches.

The same can be said for our search for answers. To know this enemy, the scientific community is in the midst of a concerted epidemiological, clinical, and biological effort effectively unparalleled in the history of fungal pathogens. *C. auris* is truly a pathogen for the modern age, and the response has been a show of force where sequencing and surveillance data informs basic science research which reforms clinical practice, which in turn revises the public health and surveillance practice all over again. To play a role in this integrated response has been empowering, and even in the recent four years of research covered by this dissertation, the medical and scientific community has learned so much and heavily refined perspectives around this organism. And yet, there is much to learn about its origins, its behavior, its emergence. Maybe *C. auris* emerged as a pathogen due to increasing global temperatures, maybe because of plastic pollution, maybe due to agricultural antifungal usage. Our best approximations suggest this is a new human pathogen because of human activity within the past century. Now, on a stage the size of the entire world, we are beginning to recognize how *C. auris* has evolved to become the perfect storm of a healthcare associated pathogen.

Bibliography

1. Satoh, K., Makimura, K., Hasumi, Y., Nishiyama, Y., Uchida, K., and Yamaguchi, H. (2009). *Candida auris* sp. nov., a novel ascomycetous yeast isolated from the external ear canal of an inpatient in a Japanese hospital. Microbiol. Immunol. *53*, 41–44.

2. Kwon, Y.J., Shin, J.H., Byun, S.A., Choi, M.J., Won, E.J., Lee, D., Lee, S.Y., Chun, S., Lee, J.H., Choi, H.J., et al. (2019). *Candida auris* Clinical Isolates from South Korea: Identification, Antifungal Susceptibility, and Genotyping. J. Clin. Microbiol. *57*. 10.1128/JCM.01624-18.

3. Welsh, R.M., Sexton, D.J., Forsberg, K., Vallabhaneni, S., and Litvintseva, A. (2019). Insights into the Unique Nature of the East Asian Clade of the Emerging Pathogenic Yeast *Candida auris*. J. Clin. Microbiol. *57*. 10.1128/JCM.00007-19.

4. Lockhart, S.R., Etienne, K.A., Vallabhaneni, S., Farooqi, J., Chowdhary, A., Govender, N.P., Colombo, A.L., Calvo, B., Cuomo, C.A., Desjardins, C.A., et al. (2017). Simultaneous Emergence of Multidrug-Resistant *Candida auris* on 3 Continents Confirmed by Whole-Genome Sequencing and Epidemiological Analyses. Clin. Infect. Dis. *64*, 134–140.

5. Chow, N.A., Muñoz, J.F., Gade, L., Berkow, E.L., Li, X., Welsh, R.M., Forsberg, K., Lockhart, S.R., Adam, R., Alanio, A., et al. (2020). Tracing the Evolutionary History and Global Expansion of *Candida auris* Using Population Genomic Analyses. MBio *11*, e03364-19.

6. Chen, J., Tian, S., Han, X., Chu, Y., Wang, Q., Zhou, B., and Shang, H. (2020). Is the superbug fungus really so scary? A systematic review and meta-analysis of global epidemiology and mortality of *Candida auris*. BMC Infect. Dis. *20*, 827.

7. Chow, N.A., de Groot, T., Badali, H., Abastabar, M., Chiller, T.M., and Meis, J.F. (2019). Potential Fifth Clade of *Candida auris*, Iran, 2018. Emerg. Infect. Dis. *25*, 1780–1781.

8. Spruijtenburg, B., Badali, H., Abastabar, M., Mirhendi, H., Khodavaisy, S., Sharifisooraki, J., Armaki, M.T., de Groot, T., and Meis, J.F. (2022). Confirmation of fifth *Candida auris* clade by whole genome sequencing. Emerg. Microbes Infect., 1–15.

9. Suphavilai, C., Ko, K.K.K., Lim, K.M., Tan, M.G., Boonsimma, P., Keat Chu, J.J., Goh, S.S., Rajandran, P., Lee, L.C., Tan, K.Y., et al. (2023). Discovery of the sixth *Candida auris* clade in Singapore. bioRxiv. 10.1101/2023.08.01.23293435.

10. Lee, W.G., Shin, J.H., Uh, Y., Kang, M.G., Kim, S.H., Park, K.H., and Jang, H.-C. (2011). First three reported cases of nosocomial fungemia caused by *Candida auris*. J. Clin. Microbiol. *49*, 3139–3142.

11. Wang, Y., and Xu, J. (2022). Population genomic analyses reveal evidence for limited recombination in the superbug *Candida auris* in nature. Comput. Struct. Biotechnol. J. *20*, 3030–3040.

12. Wasi, M., Khandelwal, N.K., Moorhouse, A.J., Nair, R., Vishwakarma, P., Bravo Ruiz, G., Ross, Z.K., Lorenz, A., Rudramurthy, S.M., Chakrabarti, A., et al. (2019). ABC Transporter Genes Show Upregulated Expression in Drug-Resistant Clinical Isolates of *Candida auris*: A Genome-Wide Characterization of ATP-Binding Cassette (ABC) Transporter Genes. Front. Microbiol. *10*, 1445.

13. Arora, P., Singh, P., Wang, Y., Yadav, A., Pawar, K., Singh, A., Padmavati, G., Xu, J., and Chowdhary, A. (2021). Environmental Isolation of *Candida auris* from the Coastal Wetlands of Andaman Islands, India. MBio *12*. 10.1128/mBio.03181-20.

14. Escandón, P. (2022). Novel Environmental Niches for *Candida auris*: Isolation from a Coastal Habitat in Colombia. J Fungi (Basel) *8*. 10.3390/jof8070748.

15. Wang, X., Bing, J., Zheng, Q., Zhang, F., Liu, J., Yue, H., Tao, L., Du, H., Wang, Y., Wang, H., et al. (2018). The first isolate of *Candida auris* in China: clinical and biological aspects. Emerg. Microbes Infect. *7*, 93.

16. Welsh, R.M., Bentz, M.L., Shams, A., Houston, H., Lyons, A., Rose, L.J., and Litvintseva, A.P. (2017). Survival, Persistence, and Isolation of the Emerging Multidrug-Resistant Pathogenic Yeast *Candida auris* on a Plastic Health Care Surface. J. Clin. Microbiol. *55*, 2996–3005.

17. Yadav, A., Wang, Y., Jain, K., Panwar, V.A.R., Kaur, H., Kasana, V., Xu, J., and Chowdhary, A. (2023). *Candida auris* in Dog Ears. J Fungi (Basel) *9*. 10.3390/jof9070720.

18. Yadav, A., Jain, K., Wang, Y., Pawar, K., Kaur, H., Sharma, K.K., Tripathy, V., Singh, A., Xu, J., and Chowdhary, A. (2022). *Candida auris* on Apples: Diversity and Clinical Significance. MBio, e0051822.

19. Geronikou, A., Larsen, N., Lillevang, S.K., and Jespersen, L. (2022). Occurrence and identification of yeasts in production of white-brined cheese. Microorganisms *10*, 1079.

20. Saluja, P., and Prasad, G.S. (2008). *Candida ruelliae* sp. nov., a novel yeast species isolated from flowers of Ruellia sp. (Acanthaceae). FEMS Yeast Res. *8*, 660–666.

21. Martínez, A., and Maicas, S. (2021). Cutinases: Characteristics and insights in industrial production. Catalysts *11*, 1194.

22. Proctor, D.M., Dangana, T., Sexton, D.J., Fukuda, C., Yelin, R.D., Stanley, M., Bell, P.B., Baskaran, S., Deming, C., Chen, Q., et al. (2021). Integrated genomic, epidemiologic

investigation of *Candida auris* skin colonization in a skilled nursing facility. Nat. Med. *27*, 1401–1409.

23. Dias, V. (2020). *Candida* species in the urinary tract: is it a fungal infection or not? Future Microbiol. *15*, 81–83.

24. Henriques, J., Mixão, V., Cabrita, J., Duarte, T.I., Sequeira, T., Cardoso, S., Germano, N., Dias, L., Bento, L., Duarte, S., et al. (2023). *Candida auris* in intensive care setting: The first case reported in Portugal. J. Fungi (Basel) *9*. 10.3390/jof9080837.

25. Schelenz, S., Hagen, F., Rhodes, J.L., Abdolrasouli, A., Chowdhary, A., Hall, A., Ryan, L., Shackleton, J., Trimlett, R., Meis, J.F., et al. (2016). First hospital outbreak of the globally emerging *Candida auris* in a European hospital. Antimicrob. Resist. Infect. Control *5*, 35.

26. Ruiz-Gaitán, A., Moret, A.M., Tasias-Pitarch, M., Aleixandre-López, A.I., Martínez-Morel, H., Calabuig, E., Salavert-Lletí, M., Ramírez, P., López-Hontangas, J.L., Hagen, F., et al. (2018). An outbreak due to *Candida auris* with prolonged colonisation and candidaemia in a tertiary care European hospital. Mycoses *61*, 498–505.

27. Biswal, M., Rudramurthy, S.M., Jain, N., Shamanth, A.S., Sharma, D., Jain, K., Yaddanapudi, L.N., and Chakrabarti, A. (2017). Controlling a possible outbreak of *Candida auris* infection: lessons learnt from multiple interventions. J. Hosp. Infect. *97*, 363–370.

28. Huang, X., Hurabielle, C., Drummond, R.A., Bouladoux, N., Desai, J.V., Sim, C.K., Belkaid, Y., Lionakis, M.S., and Segre, J.A. (2020). Murine model of colonization with fungal pathogen *Candida auris* to explore skin tropism, host risk factors and therapeutic strategies. Cell Host Microbe. 10.1016/j.chom.2020.12.002.

29. Lockhart, S.R., Chowdhary, A., and Gold, J.A.W. (2023). The rapid emergence of antifungal-resistant human-pathogenic fungi. Nat. Rev. Microbiol. 10.1038/s41579-023-00960-9.

30. Pacilli, M., Kerins, J.L., Clegg, W.J., Walblay, K.A., Adil, H., Kemble, S.K., Xydis, S., McPherson, T.D., Lin, M.Y., Hayden, M.K., et al. (2020). Regional Emergence of *Candida auris* in Chicago and Lessons Learned From Intensive Follow-up at 1 Ventilator-Capable Skilled Nursing Facility. Clin. Infect. Dis. *71*, e718–e725.

31. Walits, E., and Schaefer, S. (2023). Outcome of *Candida auris* Contact Investigations Conducted in a Six Month Period at a New York City Hospital. Am. J. Infect. Control. 10.1016/j.ajic.2023.10.005.

32. Sexton, D.J., Bentz, M.L., Welsh, R.M., Derado, G., Furin, W., Rose, L.J., Noble-Wang, J., Pacilli, M., McPherson, T.D., Black, S., et al. (2021). Positive Correlation Between *Candida auris* Skin-Colonization Burden and Environmental Contamination at a Ventilator-Capable Skilled Nursing Facility in Chicago. Clin. Infect. Dis. *73*, 1142–1148.

33. Sansom, S.E., Gussin, G.M., Schoeny, M., Singh, R.D., Adil, H., Bell, P., Benson, E.C., Bittencourt, C.E., Black, S., Del Mar Villanueva Guzman, M., et al. (2023). Rapid

Environmental Contamination with *Candida auris* and Multidrug-Resistant Bacterial Pathogens Near Colonized Patients. Clin. Infect. Dis. 10.1093/cid/ciad752.

34. Dire, O., Ahmad, A., Duze, S., and Patel, M. (2023). Survival of *Candida auris* on environmental surface materials and low-level resistance to disinfectant. J. Hosp. Infect. *137*, 17–23.

35. Patterson, C.A., Wyncoll, D., Patel, A., Ceesay, Y., Newsholme, W., Chand, M., Mitchell, H., Tan, M., and Edgeworth, J.D. (2021). Cloth Lanyards as a Source of Intermittent Transmission of *Candida auris* on an ICU. Crit. Care Med. *49*, 697–701.

36. Eyre, D.W., Sheppard, A.E., Madder, H., Moir, I., Moroney, R., Quan, T.P., Griffiths, D., George, S., Butcher, L., Morgan, M., et al. (2018). A *Candida auris* Outbreak and Its Control in an Intensive Care Setting. N. Engl. J. Med. *379*, 1322–1331.

37. Allert, S., Schulz, D., Kämmer, P., Großmann, P., Wolf, T., Schäuble, S., Panagiotou, G., Brunke, S., and Hube, B. (2022). From environmental adaptation to host survival: Attributes that mediate pathogenicity of *Candida auris*. Virulence *13*, 191–214.

38. Aldejohann, A.M., Wiese-Posselt, M., Gastmeier, P., and Kurzai, O. (2022). Expert recommendations for prevention and management of *Candida auris* transmission. Mycoses. 10.1111/myc.13445.

39. Haq, M.F., Pearlmutter, B.S., Cadnum, J.L., and Donskey, C.J. (2023). Efficacy of 23 commonly used liquid disinfectants against *Candida auris* isolates from the 4 major clades. Infect. Control Hosp. Epidemiol., 1–5.

40. Didik, T., Pak-Yuen Yau, A., Leong Cheung, H., Suet-Yi, L., Nga-Han, C., Yuen-Ting, W.A.H., Kam-Hei Luk, H., Kwan-Yue Choi, G., Hua-Yin Cheng, N., Tse, H., et al. (2023). Long-range air dispersion of *Candida auris* in a Cardiothoracic unit outbreak in Hong Kong. J. Hosp. Infect. 10.1016/j.jhin.2023.09.019.

41. Lyman, M., Forsberg, K., Sexton, D.J., Chow, N.A., Lockhart, S.R., Jackson, B.R., and Chiller, T. (2023). Worsening Spread of *Candida auris* in the United States, 2019 to 2021. Ann. Intern. Med. *176*, 489–495.

42. Kohlenberg, A., Monnet, D.L., Plachouras, D., *Candida auris* survey collaborative group, and Candida auris survey collaborative group includes the following national experts (2022). Increasing number of cases and outbreaks caused by *Candida auris* in the EU/EEA, 2020 to 2021. Euro Surveill. *27*. 10.2807/1560-7917.ES.2022.27.46.2200846.

43. Chakrabarti, A., and Singh, S. (2020). Multidrug-resistant *Candida auris*: an epidemiological review. Expert Rev. Anti. Infect. Ther. *18*, 551–562.

44. Adams, E., Quinn, M., Tsay, S., Poirot, E., Chaturvedi, S., Southwick, K., Greenko, J., Fernandez, R., Kallen, A., Vallabhaneni, S., et al. (2018). *Candida auris* in Healthcare Facilities, New York, USA, 2013-2017. Emerg. Infect. Dis. *24*, 1816–1824.

45. Briano, F., Magnasco, L., Sepulcri, C., Dettori, S., Dentone, C., Mikulska, M., Ball, L., Vena, A., Robba, C., Patroniti, N., et al. (2022). *Candida auris* Candidemia in Critically Ill, Colonized Patients: Cumulative Incidence and Risk Factors. Infect Dis Ther. 10.1007/s40121-022-00625-9.

46. Mulet Bayona, J.V., Tormo Palop, N., Salvador García, C., Guna Serrano, M.D.R., and Gimeno Cardona, C. (2023). *Candida auris* from colonisation to candidemia: A four-year study. Mycoses. 10.1111/myc.13626.

47. Chowdhary, A., Jain, K., and Chauhan, N. (2023). *Candida auris* Genetics and Emergence. Annu. Rev. Microbiol. 10.1146/annurev-micro-032521-015858.

48. Muñoz, J.F., Gade, L., Chow, N.A., Loparev, V.N., Juieng, P., Berkow, E.L., Farrer, R.A., Litvintseva, A.P., and Cuomo, C.A. (2018). Genomic insights into multidrug-resistance, mating and virulence in *Candida auris* and related emerging species. Nat. Commun. *9*, 5346.

49. Lamoth, F., Lockhart, S.R., Berkow, E.L., and Calandra, T. (2018). Changes in the epidemiological landscape of invasive candidiasis. J. Antimicrob. Chemother. *73*, i4–i13.

50. Lyman, M., Forsberg, K., Reuben, J., Dang, T., Free, R., Seagle, E.E., Sexton, D.J., Soda, E., Jones, H., Hawkins, D., et al. (2021). Notes from the Field: Transmission of Pan-Resistant and Echinocandin-Resistant *Candida auris* in Health Care Facilities - Texas and the District of Columbia, January-April 2021. MMWR Morb. Mortal. Wkly. Rep. *70*, 1022–1023.

51. Fisher, M.C., Hawkins, N.J., Sanglard, D., and Gurr, S.J. (2018). Worldwide emergence of resistance to antifungal drugs challenges human health and food security. Science *360*, 739–742.

52. Berne, C., Ellison, C.K., Ducret, A., and Brun, Y.V. (2018). Bacterial adhesion at the single-cell level. Nat. Rev. Microbiol. *16*, 616–627.

53. Gusnaniar, N., van der Mei, H.C., Qu, W., Nuryastuti, T., Hooymans, J.M.M., Sjollema, J., and Busscher, H.J. (2017). Physico-chemistry of bacterial transmission versus adhesion. Adv. Colloid Interface Sci. *250*, 15–24.

54. Zheng, S., Bawazir, M., Dhall, A., Kim, H.-E., He, L., Heo, J., and Hwang, G. (2021). Implication of Surface Properties, Bacterial Motility, and Hydrodynamic Conditions on Bacterial Surface Sensing and Their Initial Adhesion. Front Bioeng Biotechnol *9*, 643722.

55. Agmo Hernández, V. (2023). An overview of surface forces and the DLVO theory. ChemTexts *9*. 10.1007/s40828-023-00182-9.

56. van Oss, C.J., Absolom, D.R., and Neumann, A.W. (1980). The “hydrophobic effect”: Essentially a van der Waals interaction. Colloid Polym. Sci. *258*, 424–427.

57. Valotteau, C., Prystopiuk, V., Cormack, B.P., and Dufrêne, Y.F. (2019). Atomic Force Microscopy Demonstrates that *Candida glabrata* Uses Three Epa Proteins To Mediate Adhesion to Abiotic Surfaces. mSphere *4*. 10.1128/mSphere.00277-19.

58. El-Kirat-Chatel, S., Beaussart, A., Derclaye, S., Alsteens, D., Kucharíková, S., Van Dijck, P., and Dufrêne, Y.F. (2015). Force Nanoscopy of Hydrophobic Interactions in the Fungal Pathogen *Candida glabrata*. ACS Nano *9*, 1648–1655. 10.1021/nn506370f.

59. Wang, X.-T., Deng, X., Zhang, T.-D., Zhang, J., Chen, L.-L., Wang, Y.-F., Cao, X., Zhang, Y.-Z., Zheng, X., and Yin, D.-C. (2022). A versatile hydrophilic and antifouling coating based on dopamine modified four-arm polyethylene glycol by one-step synthesis method. ACS Macro Lett. *11*, 805–812.

60. Israelachvili, J.N. (2011). Intermolecular and Surface Forces (Elsevier).

61. Miyake, Y., Tsunoda, T., Minagi, S., Akagawa, Y., Tsuru, H., and Suginaka, H. (1990). Antifungal drugs effect adherence of *Candida albicans* to acrylic surfaces by changing the zeta-potential of fungal cells. FEMS Microbiol. Lett. *69*, 211–214.

62. Thonart, P., Custinne, M., and Paquot, M. (1982). Zeta potential of yeast cells: application in cell immobilization. Enzyme Microb. Technol. *4*, 191–194.

63. Maier, G.P., Rapp, M.V., Waite, J.H., Israelachvili, J.N., and Butler, A. (2015). BIOLOGICAL ADHESIVES. Adaptive synergy between catechol and lysine promotes wet adhesion by surface salt displacement. Science *349*, 628–632.

64. Kim, S., Yoo, H.Y., Huang, J., Lee, Y., Park, S., Park, Y., Jin, S., Jung, Y.M., Zeng, H., Hwang, D.S., et al. (2017). Salt Triggers the Simple Coacervation of an Underwater Adhesive When Cations Meet Aromatic π Electrons in Seawater. ACS Nano *11*, 6764–6772.

65. Li, Y., Liang, C., Gao, L., Li, S., Zhang, Y., Zhang, J., and Cao, Y. (2017). Hidden complexity of synergistic roles of Dopa and lysine for strong wet adhesion. Mater. Chem. Front. *1*, 2664–2668.

66. Fan, H., Wang, J., Tao, Z., Huang, J., Rao, P., Kurokawa, T., and Gong, J.P. (2019). Adjacent cationic-aromatic sequences yield strong electrostatic adhesion of hydrogels in seawater. Nat. Commun. *10*, 5127.

67. Huang, X., Nero, T., Weerasekera, R., Matej, K.H., Hinbest, A., Jiang, Z., Lee, R.F., Wu, L., Chak, C., Nijjer, J., et al. (2023). *Vibrio cholerae* biofilms use modular adhesins with glycan-targeting and nonspecific surface binding domains for colonization. Nat. Commun. *14*, 2104.

68. de Groot, P.W.J., Bader, O., de Boer, A.D., Weig, M., and Chauhan, N. (2013). Adhesins in human fungal pathogens: glue with plenty of stick. Eukaryot. Cell *12*, 470–481.

69. Li, F., and Palecek, S.P. (2008). Distinct domains of the *Candida albicans* adhesin Eap1p mediate cell--cell and cell--substrate interactions. Microbiology *154*, 1193–1203.

70. Frank, A.T., Ramsook, C.B., Otoo, H.N., Tan, C., Soybelman, G., Rauceo, J.M., Gaur, N.K., Klotz, S.A., and Lipke, P.N. (2010). Structure and function of glycosylated tandem repeats from *Candida albicans* Als adhesins. Eukaryot. Cell *9*, 405–414.

71. Oh, S.-H., Cheng, G., Nuessen, J.A., Jajko, R., Yeater, K.M., Zhao, X., Pujol, C., Soll, D.R., and Hoyer, L.L. (2005). Functional specificity of *Candida albicans* Als3p proteins and clade specificity of ALS3 alleles discriminated by the number of copies of the tandem repeat sequence in the central domain. Microbiology *151*, 673–681. 10.1099/mic.0.27680-0.

72. Beaussart, A., Alsteens, D., El-Kirat-Chatel, S., Lipke, P.N., Kucharíková, S., Van Dijck, P., and Dufrêne, Y.F. (2012). Single-molecule imaging and functional analysis of Als adhesins and mannans during *Candida albicans* morphogenesis. ACS Nano *6*, 10950–10964.

73. Golan, N., Schwartz-Perov, S., Landau, M., and Lipke, P.N. (2022). Structure and Conservation of Amyloid Spines From the *Candida albicans* Als5 Adhesin. Front Mol Biosci *9*, 926959.

74. Ramshaw, J.A., Shah, N.K., and Brodsky, B. (1998). Gly-X-Y tripeptide frequencies in collagen: a context for host-guest triple-helical peptides. J. Struct. Biol. *122*, 86–91.

75. Essen, L.-O., Vogt, M.S., and Mösch, H.-U. (2020). Diversity of GPI-anchored fungal adhesins. Biol. Chem. *401*, 1389–1405.

76. Hoyer, L.L., and Cota, E. (2016). *Candida albicans* Agglutinin-Like Sequence (Als) Family Vignettes: A Review of Als Protein Structure and Function. Front. Microbiol. *7*, 280.

77. Lin, J., Oh, S.-H., Jones, R., Garnett, J.A., Salgado, P.S., Rusnakova, S., Matthews, S.J., Hoyer, L.L., and Cota, E. (2014). The Peptide-binding Cavity Is Essential for Als3-mediated Adhesion of *Candida albicans* to Human Cells. Journal of Biological Chemistry *289*, 18401–18412. 10.1074/jbc.m114.547877.

78. Donohue, D.S., Ielasi, F.S., Goossens, K.V.Y., and Willaert, R.G. (2011). The N-terminal part of Als1 protein from *Candida albicans* specifically binds fucose-containing glycans. Mol. Microbiol. *80*, 1667–1679.

79. Nobile, C.J., Schneider, H.A., Nett, J.E., Sheppard, D.C., Filler, S.G., Andes, D.R., and Mitchell, A.P. (2008). Complementary adhesin function in *C. albicans* biofilm formation. Curr. Biol. *18*, 1017–1024.

80. Finkel, J.S., Xu, W., Huang, D., Hill, E.M., Desai, J.V., Woolford, C.A., Nett, J.E., Taff, H., Norice, C.T., Andes, D.R., et al. (2012). Portrait of *Candida albicans* adherence regulators. PLoS Pathog. *8*, e1002525.

81. Lipke, P.N., Mathelié-Guinlet, M., Viljoen, A., and Dufrêne, Y.F. (2021). A New Function for Amyloid-Like Interactions: Cross-Beta Aggregates of Adhesins form Cell-to-Cell Bonds. Pathogens *10*. 10.3390/pathogens10081013.

82. Oh, S.-H., Schliep, K., Isenhower, A., Rodriguez-Bobadilla, R., Vuong, V.M., Fields, C.J., Hernandez, A.G., and Hoyer, L.L. (2021). Using Genomics to Shape the Definition of the Agglutinin-Like Sequence (ALS) Family in the Saccharomycetales. Front. Cell. Infect. Microbiol. *11*, 794529.

83. Smoak, R.A., Snyder, L.F., Fassler, J.S., and He, B.Z. (2023). Parallel expansion and divergence of an adhesin family in pathogenic yeasts. Genetics *223*. 10.1093/genetics/iyad024.

84. Muñoz, J.F., Welsh, R.M., Shea, T., Batra, D., Gade, L., Howard, D., Rowe, L.A., Meis, J.F., Litvintseva, A.P., and Cuomo, C.A. (2021). Clade-specific chromosomal rearrangements and loss of subtelomeric adhesins in *Candida auris*. Genetics *218*. 10.1093/genetics/iyab029.

85. Fu, Y., Luo, G., Spellberg, B.J., Edwards, J.E., Jr, and Ibrahim, A.S. (2008). Gene overexpression/suppression analysis of candidate virulence factors of *Candida albicans*. Eukaryot. Cell *7*, 483–492.

86. Kempf, M., Cottin, J., Licznar, P., Lefrançois, C., Robert, R., and Apaire-Marchais, V. (2009). Disruption of the GPI protein-encoding gene *IFF4* of *Candida albicans* results in decreased adherence and virulence. Mycopathologia *168*, 73–77.

87. Bates, S., de la Rosa, J.M., MacCallum, D.M., Brown, A.J.P., Gow, N.A.R., and Odds, F.C. (2007). *Candida albicans* Iff11, a secreted protein required for cell wall structure and virulence. Infect. Immun. *75*, 2922–2928.

88. Kraushaar, T., Brückner, S., Veelders, M., Rhinow, D., Schreiner, F., Birke, R., Pagenstecher, A., Mösch, H.-U., and Essen, L.-O. (2015). Interactions by the Fungal Flo11 Adhesin Depend on a Fibronectin Type III-like Adhesin Domain Girdled by Aromatic Bands. Structure *23*, 1005–1017.

89. Brückner, S., Schubert, R., Kraushaar, T., Hartmann, R., Hoffmann, D., Jelli, E., Drescher, K., Müller, D.J., Oliver Essen, L., and Mösch, H.-U. (2020). Kin discrimination in social yeast is mediated by cell surface receptors of the Flo11 adhesin family. Elife *9*. 10.7554/eLife.55587.

90. Denning, D.W. (2024). Global incidence and mortality of severe fungal disease. Lancet Infect. Dis. 10.1016/S1473-3099(23)00692-8.

91. WHO fungal priority pathogens list to guide research, development and public health action. Geneva: World Health Organization (2022).

92. Alvarez-Moreno, C.A., Morales-López, S., Rodriguez, G.J., Rodriguez, J.Y., Robert, E., Picot, C., Ceballos-Garzon, A., Parra-Giraldo, C.M., and Le Pape, P. (2023). The Mortality

Attributable to Candidemia in *C. auris* Is Higher than That in Other Candida Species: Myth or Reality? J Fungi (Basel) *9*. 10.3390/jof9040430.

93. Bravo Ruiz, G., Ross, Z.K., Holmes, E., Schelenz, S., Gow, N.A.R., and Lorenz, A. (2019). Rapid and extensive karyotype diversification in haploid clinical *Candida auris* isolates. Curr. Genet. *65*, 1217–1228.

94. Narayanan, A., Vadnala, R.N., Ganguly, P., Selvakumar, P., Rudramurthy, S.M., Prasad, R., Chakrabarti, A., Siddharthan, R., and Sanyal, K. (2021). Functional and Comparative Analysis of Centromeres Reveals Clade-Specific Genome Rearrangements in *Candida auris* and a Chromosome Number Change in Related Species. MBio *12*. 10.1128/mBio.00905-21.

95. Santana, D.J., Anku, J.A.E., Zhao, G., Zarnowski, R., Johnson, C.J., Hautau, H., Visser, N.D., Ibrahim, A.S., Andes, D., Nett, J.E., et al. (2023). A *Candida auris*-specific adhesin, Scf1, governs surface association, colonization, and virulence. Science *381*, 1461–1467.

96. Muñoz, J.E., Ramirez, L.M., dos Santos Dias, L., Rivas, L.A., Ramos, L.S., Santos, A.L.S., Taborda, C.P., and Parra-Giraldo, C.M. (2020). Pathogenicity Levels of Colombian Strains of *Candida auris* and Brazilian Strains of *Candida haemulonii* Species Complex in Both Murine and Galleria mellonella Experimental Models. Journal of Fungi *6*, 104. 10.3390/jof6030104.

97. Carvajal, S.K., Alvarado, M., Rodríguez, Y.M., Parra-Giraldo, C.M., Varón, C., Morales-López, S.E., Rodríguez, J.Y., Gómez, B.L., and Escandón, P. (2021). Pathogenicity Assessment of Colombian Strains of *Candida auris* in the Galleria mellonella Invertebrate Model. J Fungi (Basel) *7*. 10.3390/jof7060401.

98. Vila, T., Montelongo-Jauregui, D., Ahmed, H., Puthran, T., Sultan, A.S., and Jabra-Rizk, M.A. (2020). Comparative Evaluations of the Pathogenesis of *Candida auris* Phenotypes and *Candida albicans* Using Clinically Relevant Murine Models of Infections. mSphere *5*. 10.1128/mSphere.00760-20.

99. Kurakado, S., Matsumoto, Y., and Sugita, T. (2023). Comparing the virulence of four major clades of *Candida auris* strains using a silkworm infection model: Clade IV isolates had higher virulence than the other clades. Med. Mycol. 10.1093/mmy/myad108.

100. Forgács, L., Borman, A.M., Prépost, E., Tóth, Z., Kardos, G., Kovács, R., Szekely, A., Nagy, F., Kovacs, I., and Majoros, L. (2020). Comparison of in vivo pathogenicity of four *Candida auris* clades in a neutropenic bloodstream infection murine model. Emerg. Microbes Infect. *9*, 1160–1169.

101. Szekely, A., Borman, A.M., and Johnson, E.M. (2019). *Candida auris* Isolates of the Southern Asian and South African Lineages Exhibit Different Phenotypic and Antifungal Susceptibility Profiles In Vitro. J. Clin. Microbiol. *57*. 10.1128/JCM.02055-18.

102. Haq, M.F., Cadnum, J.L., Pearlmutter, B.S., Jencson, A.L., and Donskey, C.J. (2023). Effectiveness of a novel 1-step cleaner and disinfectant against *Candida auris*. Infect. Control Hosp. Epidemiol. *44*, 837–839.

103. Müller, P., Tan, C.K., Ißleib, U., Paßvogel, L., Eilts, B., and Steinhauer, K. (2020). Investigation of the susceptibility of *Candida auris* and *Candida albicans* to chemical disinfectants using European Standards EN 13624 and EN 16615. J. Hosp. Infect. *105*, 648–656.

104. Brandt, P., Mirhakkak, M.H., Wagner, L., Driesch, D., Möslinger, A., Fänder, P., Schäuble, S., Panagiotou, G., and Vylkova, S. (2023). High-Throughput Profiling of *Candida auris* Isolates Reveals Clade-Specific Metabolic Differences. Microbiol Spectr, e0049823.

105. Clark, J., Glasziou, P., Del Mar, C., Bannach-Brown, A., Stehlik, P., and Scott, A.M. (2020). A full systematic review was completed in 2 weeks using automation tools: a case study. J. Clin. Epidemiol. *121*, 81–90.

106. Simon, S.P., Li, R., Silver, M., Andrade, J., Tharian, B., Fu, L., Villanueva, D., Abascal, D.G., Mayer, A., Truong, J., et al. (2022). Comparative Outcomes of *Candida auris* Bloodstream Infections: A Multicenter Retrospective Case-control Study. Clin. Infect. Dis., ciac735.

107. Koleri, J., Petkar, H.M., Rahman S Al Soub, H.A., and Rahman S AlMaslamani, M.A. (2023). *Candida auris* Blood stream infection- a descriptive study from Qatar. BMC Infect. Dis. *23*, 513.

108. Prayag, P.S., Patwardhan, S., Panchakshari, S., Rajhans, P.A., and Prayag, A. (2022). The Dominance of *Candida auris*: A Single-center Experience of 79 Episodes of Candidemia from Western India. Indian J. Crit. Care Med. *26*, 560–563.

109. Allaw, F., Haddad, S.F., Habib, N., Moukarzel, P., Naji, N.S., Kanafani, Z.A., Ibrahim, A., Zahreddine, N.K., Spernovasilis, N., Poulakou, G., et al. (2022). COVID-19 and *C. auris*: A Case-Control Study from a Tertiary Care Center in Lebanon. Microorganisms *10*. 10.3390/microorganisms10051011.

110. Asadzadeh, M., Mokaddas, E., Ahmad, S., Abdullah, A.A., de Groot, T., Meis, J.F., and Shetty, S.A. (2021). Molecular characterization of *Candida auris* isolates from immunocompromised patients in a tertiary-care hospital in Kuwait reveals a novel mutation in FKS1 conferring reduced susceptibility to echinocandins. Mycoses. 10.1111/myc.13419.

111. Umamaheshwari, S., Neelambike, S.M., Shankarnarayan, S.A., Kumarswamy, K.S., Gopal, S., Prakash, H., and Rudramurthy, S.M. (2021). Clinical profile, antifungal susceptibility, and molecular characterization of *Candida auris* isolated from patients in a South Indian surgical ICU. J. Mycol. Med. *31*, 101176.

112. Nobrega de Almeida, J., Jr, Brandão, I.B., Francisco, E.C., de Almeida, S.L.R., de Oliveira Dias, P., Pereira, F.M., Santos Ferreira, F., de Andrade, T.S., de Miranda Costa, M.M., de Souza Jordão, R.T., et al. (2021). Axillary Digital Thermometers uplifted a multidrug-susceptible *Candida auris* outbreak among COVID-19 patients in Brazil. Mycoses *64*, 1062–1072.

113. Di Pilato, V., Codda, G., Ball, L., Giacobbe, D.R., Willison, E., Mikulska, M., Magnasco, L., Crea, F., Vena, A., Pelosi, P., et al. (2021). Molecular Epidemiological Investigation of a Nosocomial Cluster of *C. auris*: Evidence of Recent Emergence in Italy and Ease of Transmission during the COVID-19 Pandemic. J Fungi (Basel) *7*. 10.3390/jof7020140.

114. Levy, Y., Miltgen, G., Rousseau, A., Lugagne, N., Teysseyre, L., Traversier, N., Desnos-Ollivier, M., Allou, N., and Allyn, J. (2020). Case Report: Emergence of *Candida auris* in the Indian Ocean Region. Am. J. Trop. Med. Hyg. *104*, 739–743.

115. Alfouzan, W., Ahmad, S., Dhar, R., Asadzadeh, M., Almerdasi, N., Abdo, N.M., Joseph, L., de Groot, T., Alali, W.Q., Khan, Z., et al. (2020). Molecular Epidemiology of *Candida Auris* Outbreak in a Major Secondary-Care Hospital in Kuwait. J Fungi (Basel) *6*. 10.3390/jof6040307.

116. Farooqi, J.Q., Soomro, A.S., Baig, M.A., Sajjad, S.F., Hamid, K., Jabeen, K., Naqvi, M.F., Nasir, N., Roshan, R., Mahmood, S.F., et al. (2020). Outbreak investigation of *Candida auris* at a tertiary care hospital in Karachi, Pakistan. J. Infect. Prev. *21*, 189–195.

117. Mohsin, J., Weerakoon, S., Ahmed, S., Puts, Y., Al Balushi, Z., Meis, J.F., and Al-Hatmi, A.M.S. (2020). A Cluster of *Candida auris* Blood Stream Infections in a Tertiary Care Hospital in Oman from 2016 to 2019. Antibiotics (Basel) *9*. 10.3390/antibiotics9100638.

118. Theodoropoulos, N.M., Bolstorff, B., Bozorgzadeh, A., Brandeburg, C., Cumming, M., Daly, J.S., Ellison, R.T., 3rd, Forsberg, K., Gade, L., Gibson, L., et al. (2020). *Candida auris* outbreak involving liver transplant recipients in a surgical intensive care unit. Am. J. Transplant *20*, 3673–3679.

119. Almaghrabi, R.S., Albalawi, R., Mutabagani, M., Atienza, E., Aljumaah, S., Gade, L., Forsberg, K., Litvintseva, A., and Althawadi, S. (2020). Molecular characterisation and clinical outcomes of *Candida auris* infection: Single-centre experience in Saudi Arabia. Mycoses *63*, 452–460.

120. Shastri, P.S., Shankarnarayan, S.A., Oberoi, J., Rudramurthy, S.M., Wattal, C., and Chakrabarti, A. (2020). *Candida auris* candidaemia in an intensive care unit - Prospective observational study to evaluate epidemiology, risk factors, and outcome. J. Crit. Care *57*, 42–48.

121. Katoch, O., Bajpai, V., Khurana, S., Katyal, S., and Mathur, P. (2020). Clinical Epidemiology and Risk Factors of *Candida auris* Bloodstream Infection in Trauma Patients. Infect. Control Hosp. Epidemiol. *41*, s168–s168.

122. Al Maani, A., Paul, H., Al-Rashdi, A., Wahaibi, A.A., Al-Jardani, A., Al Abri, A.M.A., AlBalushi, M.A.H., Al-Abri, S., Al Reesi, M., Al Maqbali, A., et al. (2019). Ongoing Challenges with Healthcare-Associated *Candida auris* Outbreaks in Oman. J Fungi (Basel) *5*. 10.3390/jof5040101.

123. Taori, S.K., Khonyongwa, K., Hayden, I., Athukorala, G.D.A., Letters, A., Fife, A., Desai, N., and Borman, A.M. (2019). *Candida auris* outbreak: Mortality, interventions and cost of sustaining control. J. Infect. *79*, 601–611.

124. Barantsevich, N.E., Orlova, O.E., Shlyakhto, E.V., Johnson, E.M., Woodford, N., Lass-Floerl, C., Churkina, I.V., Mitrokhin, S.D., Shkoda, A.S., and Barantsevich, E.P. (2019). Emergence of *Candida auris* in Russia. J. Hosp. Infect. *102*, 445–448.

125. Abdalhamid, B., Almaghrabi, R., Althawadi, S., and Omrani, A. (2018). First report of *Candida auris* infections from Saudi Arabia. J. Infect. Public Health *11*, 598–599.

126. Rudramurthy, S.M., Chakrabarti, A., Paul, R.A., Sood, P., Kaur, H., Capoor, M.R., Kindo, A.J., Marak, R.S.K., Arora, A., Sardana, R., et al. (2017). *Candida auris* candidaemia in Indian ICUs: analysis of risk factors. J. Antimicrob. Chemother. *72*, 1794–1801.

127. Vallabhaneni, S., Kallen, A., Tsay, S., Chow, N., Welsh, R., Kerins, J., Kemble, S.K., Pacilli, M., Black, S.R., Landon, E., et al. (2017). Investigation of the First Seven Reported Cases of *Candida auris*, a Globally Emerging Invasive, Multidrug-Resistant Fungus-United States, May 2013-August 2016. Am. J. Transplant *17*, 296–299.

128. Chowdhary, A., Anil Kumar, V., Sharma, C., Prakash, A., Agarwal, K., Babu, R., Dinesh, K.R., Karim, S., Singh, S.K., Hagen, F., et al. (2014). Multidrug-resistant endemic clonal strain of *Candida auris* in India. Eur. J. Clin. Microbiol. Infect. Dis. *33*, 919–926.

129. de St Maurice, A., Parti, U., Anikst, V.E., Harper, T., Mirasol, R., Dayo, A.J., Garner, O.B., Prabaker, K.K., and Yang, S. (2022). Clinical, microbiological, and genomic characteristics of clade-III *Candida auris* colonization and infection in southern California, 2019-2022. Infect. Control Hosp. Epidemiol., 1–9.

130. Parak, A., Stacey, S.L., and Chibabhai, V. (2022). Clinical and laboratory features of patients with *Candida auris* cultures, compared to other Candida, at a South African Hospital. J. Infect. Dev. Ctries. *16*, 213–221.

131. Karmarkar, E.N., O'Donnell, K., Prestel, C., Forsberg, K., Gade, L., Jain, S., Schan, D., Chow, N., McDermott, D., Rossow, J., et al. (2021). Rapid Assessment and Containment of *Candida auris* Transmission in Postacute Care Settings-Orange County, California, 2019. Ann. Intern. Med. 10.7326/M21-2013.

132. Hanson, B.M., Dinh, A.Q., Tran, T.T., Arenas, S., Pronty, D., Gershengorn, H.B., Ferreira, T., Arias, C.A., and Shukla, B.S. (2021). *Candida auris* Invasive Infections during a COVID-19 Case Surge. Antimicrob. Agents Chemother. *65*, e0114621.

133. van Schalkwyk, E., Mpembe, R.S., Thomas, J., Shuping, L., Ismail, H., Lowman, W., Karstaedt, A.S., Chibabhai, V., Wadula, J., Avenant, T., et al. (2019). Epidemiologic Shift in Candidemia Driven by *Candida auris*, South Africa, 2016-20171. Emerg. Infect. Dis. *25*, 1698–1707.

134. Adam, R.D., Revathi, G., Okinda, N., Fontaine, M., Shah, J., Kagotho, E., Castanheira, M., Pfaller, M.A., and Maina, D. (2019). Analysis of *Candida auris* fungemia at a single facility in Kenya. Int. J. Infect. Dis. *85*, 182–187.

135. de Melo, C.C., de Sousa, B.R., da Costa, G.L., Oliveira, M.M.E., and de Lima-Neto, R.G. (2023). Colonized patients by *Candida auris*: Third and largest outbreak in Brazil and impact of biofilm formation. Front. Cell. Infect. Microbiol. *13*, 1033707.

136. Villanueva-Lozano, H., Treviño-Rangel, R. de J., González, G.M., Ramírez-Elizondo, M.T., Lara-Medrano, R., Aleman-Bocanegra, M.C., Guajardo-Lara, C.E., Gaona-Chávez, N., Castilleja-Leal, F., Torre-Amione, G., et al. (2021). Outbreak of *Candida auris* infection in a COVID-19 hospital in Mexico. Clin. Microbiol. Infect. 10.1016/j.cmi.2020.12.030.

137. Armstrong, P.A., Rivera, S.M., Escandon, P., Caceres, D.H., Chow, N., Stuckey, M.J., Díaz, J., Gomez, A., Vélez, N., Espinosa-Bode, A., et al. (2019). Hospital-Associated Multicenter Outbreak of Emerging Fungus *Candida auris*, Colombia, 2016. Emerg. Infect. Dis. *25*, 1339–1346.

138. Araúz, A.B., Caceres, D.H., Santiago, E., Armstrong, P., Arosemena, S., Ramos, C., Espinosa-Bode, A., Borace, J., Hayer, L., Cedeño, I., et al. (2018). Isolation of *Candida auris* from 9 patients in Central America: Importance of accurate diagnosis and susceptibility testing. Mycoses *61*, 44–47.

139. Ben-Ami, R., Berman, J., Novikov, A., Bash, E., Shachor-Meyouhas, Y., Zakin, S., Maor, Y., Tarabia, J., Schechner, V., Adler, A., et al. (2017). Multidrug-Resistant *Candida haemulonii* and *C. auris*, Tel Aviv, Israel. Emerg. Infect. Dis. *23*. 10.3201/eid2302.161486.

140. Calvo, B., Melo, A.S.A., Perozo-Mena, A., Hernandez, M., Francisco, E.C., Hagen, F., Meis, J.F., and Colombo, A.L. (2016). First report of *Candida auris* in America: Clinical and microbiological aspects of 18 episodes of candidemia. J. Infect. *73*, 369–374.

141. Forgács, L., Borman, A.M., Kovács, R., Balázsi, D., Tóth, Z., Balázs, B., Chun-Ju, C., Kardos, G., Kovacs, I., and Majoros, L. (2022). In Vivo Efficacy of Amphotericin B against Four *Candida auris* Clades. J Fungi (Basel) *8*. 10.3390/jof8050499.

142. Abe, M., Katano, H., Nagi, M., Higashi, Y., Sato, Y., Kikuchi, K., Hasegawa, H., and Miyazaki, Y. (2020). Potency of gastrointestinal colonization and virulence of *Candida auris* in a murine endogenous candidiasis. PLoS One *15*, e0243223.

143. Fan, S., Zhan, P., Bing, J., Jiang, N., Huang, Y., Chen, D., Hu, T., Du, H., and Huang, G. (2021). A biological and genomic comparison of a drug-resistant and a drug-susceptible strain of *Candida auris* isolated from Beijing, China. Virulence *12*, 1388–1399.

144. Spettel, K., Kriz, R., Wu, C., Achter, L., Schmid, S., Galazka, S., Selitsch, B., Camp, I., Makristathis, A., Lagler, H., et al. (2023). *Candida auris* in Austria-What Is New and What Is Different. J Fungi (Basel) *9*. 10.3390/jof9020129.

145. Wurster, S., Bandi, A., Beyda, N.D., Albert, N.D., Raman, N.M., Raad, I.I., and Kontoyiannis, D.P. (2019). *Drosophila melanogaster* as a model to study virulence and azole treatment of the emerging pathogen *Candida auris*. J. Antimicrob. Chemother. *74*, 1904–1910.

146. Romera, D., Aguilera-Correa, J.-J., García-Coca, M., Mahillo-Fernández, I., Viñuela-Sandoval, L., García-Rodríguez, J., and Esteban, J. (2020). The *Galleria mellonella* infection model as a system to investigate the virulence of *Candida auris* strains. Pathog. Dis. *78*. 10.1093/femspd/ftaa067.

147. Hernando-Ortiz, A., Mateo, E., Perez-Rodriguez, A., de Groot, P.W.J., Quindós, G., and Eraso, E. (2021). Virulence of *Candida auris* from different clinical origins in *Caenorhabditis elegans* and *Galleria mellonella* host models. Virulence *12*, 1063–1075.

148. Garcia-Bustos, V., Ruiz-Saurí, A., Ruiz-Gaitán, A., Sigona-Giangreco, I.A., Cabañero-Navalon, M.D., Sabalza-Baztán, O., Salavert-Lletí, M., Tormo, M.Á., and Pemán, J. (2021). Characterization of the Differential Pathogenicity of *Candida auris* in a *Galleria mellonella* Infection Model. Microbiol Spectr *9*, e0001321.

149. White, T.C., Esquivel, B.D., Rouse Salcido, E.M., Schweiker, A.M., Dos Santos, A.R., Gade, L., Petro, E., KuKanich, B., and KuKanich, K.S. (2024). *Candida auris* detected in the oral cavity of a dog in Kansas. MBio, e0308023.

150. Lone, S.A., and Ahmad, A. (2019). *Candida auris*-the growing menace to global health. Mycoses *62*, 620–637.

151. Mario-Vasquez, J.E., Bagal, U.R., Lowe, E., Morgulis, A., Phan, J., Sexton, D.J., Shiryev, S., Slatkevičius, R., Welsh, R., Litvintseva, A.P., et al. (2024). Finding *Candida auris* in public metagenomic repositories. PLoS One *19*, e0291406.

152. Ferrer Gómez, C., Solís Albamonte, P., Delgado Navarro, C., Salvador García, C., Tormo Palop, N., and Andrés Ibáñez, J.A. (2021). Analysis of *Candida auris* candidemia cases in an Intensive Care Unit of a tertiary hospital. Rev. Esp. Anestesiol. Reanim. *68*, 431–436.

153. Garcia-Bustos, V., Salavert, M., Ruiz-Gaitán, A.C., Cabañero-Navalon, M.D., Sigona-Giangreco, I.A., and Pemán, J. (2020). A clinical predictive model of candidaemia by *Candida auris* in previously colonized critically ill patients. Clin. Microbiol. Infect. *26*, 1507–1513.

154. Cortegiani, A., Misseri, G., Fasciana, T., Giammanco, A., Giarratano, A., and Chowdhary, A. (2018). Epidemiology, clinical characteristics, resistance, and treatment of infections by *Candida auris*. J. Intensive Care Med. *6*, 69.

155. Horton, M.V., Johnson, C.J., Kernien, J.F., Patel, T.D., Lam, B.C., Cheong, J.Z.A., Meudt, J.J., Shanmuganayagam, D., Kalan, L.R., and Nett, J.E. (2020). *Candida auris* Forms High-Burden Biofilms in Skin Niche Conditions and on Porcine Skin. mSphere *5*. 10.1128/mSphere.00910-19.

156. Krauke, Y., and Sychrova, H. (2010). Four pathogenic *Candida* species differ in salt tolerance. Curr. Microbiol. *61*, 335–339.

157. Eix, E.F., Johnson, C.J., Wartman, K.M., Kernien, J.F., Meudt, J.J., Shanmuganayagam, D., Gibson, A.L.F., and Nett, J.E. (2022). Ex Vivo Human and Porcine Skin Effectively Model *Candida auris* Colonization, Differentiating Robust and Poor Fungal Colonizers. J. Infect. Dis. *225*, 1791–1795.

158. Bing, J., Guan, Z., Zheng, T., Zhang, Z., Fan, S., Ennis, C.L., Nobile, C.J., and Huang, G. (2023). Clinical isolates of *Candida auris* with enhanced adherence and biofilm formation due to genomic amplification of ALS4. PLoS Pathog. *19*, e1011239.

159. Datta, A., Das, D., Nett, J.E., Vyas, J.M., Lionakis, M.S., and Thangamani, S. (2023). Differential skin immune responses in mice intradermally infected with *Candida auris* and *Candida albicans*. Microbiol Spectr, e0221523.

160. Bitschar, K., Sauer, B., Focken, J., Dehmer, H., Moos, S., Konnerth, M., Schilling, N.A., Grond, S., Kalbacher, H., Kurschus, F.C., et al. (2019). Lugdunin amplifies innate immune responses in the skin in synergy with host- and microbiota-derived factors. Nat. Commun. *10*, 2730.

161. Rather, I.A., Sabir, J.S.M., Asseri, A.H., and Ali, S. (2022). Antifungal Activity of Human Cathelicidin LL-37, a Membrane Disrupting Peptide, by Triggering Oxidative Stress and Cell Cycle Arrest in *Candida auris*. J Fungi (Basel) *8*. 10.3390/jof8020204.

162. Zhu, Y., O'Brien, B., Leach, L., Clarke, A., Bates, M., Adams, E., Ostrowsky, B., Quinn, M., Dufort, E., Southwick, K., et al. (2020). Laboratory Analysis of an Outbreak of *Candida auris* in New York from 2016 to 2018: Impact and Lessons Learned. J. Clin. Microbiol. *58*. 10.1128/JCM.01503-19.

163. Stenzaly-Achtert, S., Schölermann, A., Schreiber, J., Diec, K.H., Rippke, F., and Bielfeldt, S. (2000). Axillary pH and influence of deodorants. Skin Res. Technol. *6*, 87–91.

164. Manus, M.B., Kuthyar, S., Perroni-Marañón, A.G., de la Mora, A.N.-, and Amato, K.R. (2022). Comparing different sample collection and storage methods for field-based skin microbiome research. Am. J. Hum. Biol. *34*, e23584.

165. Rybak, J.M., Cuomo, C.A., and David Rogers, P. (2022). The molecular and genetic basis of antifungal resistance in the emerging fungal pathogen *Candida auris*. Curr. Opin. Microbiol. *70*, 102208.

166. Carolus, H., Pierson, S., Muñoz, J.F., Subotić, A., Cruz, R.B., Cuomo, C.A., and Van Dijck, P. (2021). Genome-Wide Analysis of Experimentally Evolved *Candida auris* Reveals Multiple Novel Mechanisms of Multidrug Resistance. MBio *12*. 10.1128/mBio.03333-20.

167. Carolus, H., Sofras, D., Boccarella, G., Sephton-Clark, P., Romero, C.L., Vergauwen, R., Yazdani, S., Pierson, S., Jacobs, S., Vandecruys, P., et al. (2023). Acquired amphotericin B resistance and fitness trade-off compensation in *Candida auris*.

168. Rybak, J.M., Barker, K.S., Muñoz, J.F., Parker, J.E., Ahmad, S., Mokaddas, E., Abdullah, A., Elhagracy, R.S., Kelly, S.L., Cuomo, C.A., et al. (2021). In vivo emergence of high-level resistance during treatment reveals the first identified mechanism of amphotericin B resistance in *Candida auris*. Clin. Microbiol. Infect. 10.1016/j.cmi.2021.11.024.

169. Borman, A.M., Szekely, A., and Johnson, E.M. (2016). Comparative Pathogenicity of United Kingdom Isolates of the Emerging Pathogen *Candida auris* and Other Key Pathogenic *Candida* Species. mSphere *1*, e00189-16.

170. Santana, D.J., and O'Meara, T.R. (2021). Forward and reverse genetic dissection of morphogenesis identifies filament-competent *Candida auris* strains. Nat. Commun. *12*, 7197.

171. Oud, B., Guadalupe-Medina, V., Nijkamp, J.F., de Ridder, D., Pronk, J.T., van Maris, A.J.A., and Daran, J.-M. (2013). Genome duplication and mutations in *ACE2* cause multicellular, fast-sedimenting phenotypes in evolved *Saccharomyces cerevisiae*. Proc. Natl. Acad. Sci. U. S. A. *110*, E4223-31.

172. Ratcliff, W.C., Fankhauser, J.D., Rogers, D.W., Greig, D., and Travisano, M. (2015). Origins of multicellular evolvability in snowflake yeast. Nat. Commun. *6*, 6102.

173. Tian, S., Bing, J., Chu, Y., Li, H., Wang, Q., Cheng, S., Chen, J., and Shang, H. (2023). Phenotypic and genetic features of a novel clinically isolated rough morphotype *Candida auris*. Front. Microbiol. *14*, 1174878.

174. Pelletier, C., Brown, A.J.P., and Lorenz, A. (2023). *Candida auris* undergoes adhesin-dependent and -independent cellular aggregation. bioRxiv, 2023.04.21.537817. 10.1101/2023.04.21.537817.

175. Malavia-Jones, D., Farrer, R.A., Stappers, M.H.T., Edmondson, M.B., Borman, A.M., Johnson, E.M., Lipke, P.N., and Gow, N.A.R. (2023). Strain and temperature dependent aggregation of *Candida auris* is attenuated by inhibition of surface amyloid proteins. Cell Surf *10*, 100110.

176. Ramos, L.S., Parra-Giraldo, C.M., Branquinha, M.H., and Santos, A.L.S. (2023). Cell Aggregation Capability of Clinical Isolates from *Candida auris* and *Candida haemulonii* Species Complex. Trop Med Infect Dis *8*. 10.3390/tropicalmed8080382.

177. Lipke, P.N. (2018). What We Do Not Know about Fungal Cell Adhesion Molecules. J Fungi (Basel) *4*. 10.3390/jof4020059.

178. Fayed, B., Jayakumar, M.N., and Soliman, S.S.M. (2021). Caspofungin-resistance in *Candida auris* is cell wall-dependent phenotype and potential prevention by zinc oxide nanoparticles. Med. Mycol. *59*, 1243–1256.

179. Zamith-Miranda, D., Amatuzzi, R.F., Munhoz da Rocha, I.F., Martins, S.T., Lucena, A.C.R., Vieira, A.Z., Trentin, G., Almeida, F., Rodrigues, M.L., Nakayasu, E.S., et al.

(2021). Transcriptional and translational landscape of *Candida auris* in response to caspofungin. Comput. Struct. Biotechnol. J. *19*, 5264–5277.

180. Gregori, C., Glaser, W., Frohner, I.E., Reinoso-Martín, C., Rupp, S., Schüller, C., and Kuchler, K. (2011). Efg1 Controls caspofungin-induced cell aggregation of *Candida albicans* through the adhesin Als1. Eukaryot. Cell *10*, 1694–1704.

181. Saputo, S., Chabrier-Rosello, Y., Luca, F.C., Kumar, A., and Krysan, D.J. (2012). The RAM network in pathogenic fungi. Eukaryot. Cell *11*, 708–717.

182. King, L., and Butler, G. (1998). Ace2p, a regulator of *CTS1* (chitinase) expression, affects pseudohyphal production in *Saccharomyces cerevisiae*. Curr. Genet. *34*, 183–191.

183. Nelson, B., Kurischko, C., Horecka, J., Mody, M., Nair, P., Pratt, L., Zougman, A., McBroom, L.D.B., Hughes, T.R., Boone, C., et al. (2003). RAM: a conserved signaling network that regulates Ace2p transcriptional activity and polarized morphogenesis. Mol. Biol. Cell *14*, 3782–3803.

184. Fan, S., Yue, H., Zheng, Q., Bing, J., Tian, S., Chen, J., Ennis, C.L., Nobile, C.J., Huang, G., and Du, H. (2021). Filamentous growth is a general feature of *Candida auris* clinical isolates. Med. Mycol. 10.1093/mmy/myaa116.

185. Yue, H., Bing, J., Zheng, Q., Zhang, Y., Hu, T., Du, H., Wang, H., and Huang, G. (2018). Filamentation in Candida auris, an emerging fungal pathogen of humans: passage through the mammalian body induces a heritable phenotypic switch. Emerg. Microbes Infect. *7*, 188.

186. Brown, J.L., Delaney, C., Short, B., Butcher, M.C., McKloud, E., Williams, C., Kean, R., and Ramage, G. (2020). *Candida auris* Phenotypic Heterogeneity Determines Pathogenicity In Vitro. mSphere *5*, e00371-20.

187. Sexton, D.J., Welsh, R.M., Bentz, M.L., Forsberg, K., Jackson, B., Berkow, E.L., and Litvintseva, A.P. (2020). Evaluation of nine surface disinfectants against *Candida auris* using a quantitative disk carrier method: EPA SOP-MB-35. Infect. Control Hosp. Epidemiol. *41*, 1219–1221.

188. Bragg, R., Jansen, A., Coetzee, M., van der Westhuizen, W., and Boucher, C. (2014). Bacterial resistance to Quaternary Ammonium Compounds (QAC) disinfectants. Adv. Exp. Med. Biol. *808*, 1–13.

189. Zatorska, B., Moser, D., Diab-Elschahawi, M., Ebner, J., Lusignani, L.S., and Presterl, E. (2021). The effectiveness of surface disinfectants and a micellic H2O2 based water disinfectant on *Candida auris*. J. Mycol. Med. *31*, 101178.

190. Lemons, A.R., McClelland, T.L., Martin, S.B., Jr, Lindsley, W.G., and Green, B.J. (2020). Inactivation of the multi-drug resistant pathogen *Candida auris* using ultraviolet germicidal irradiation (UVGI). J. Hosp. Infect. 10.1016/j.jhin.2020.04.011.

191. de Groot, T., Chowdhary, A., Meis, J.F., and Voss, A. (2019). Killing of *Candida auris* by UV-C: Importance of exposure time and distance. Mycoses *62*, 408–412.

192. Pearlmutter, B.S., Haq, M.F., Cadnum, J.L., Jencson, A.L., Carlisle, M., and Donskey, C.J. (2022). Efficacy of relatively low-cost ultraviolet-C light devices against *Candida auris*. Infect. Control Hosp. Epidemiol. *43*, 747–751.

193. Rutala, W.A., Kanamori, H., Gergen, M.F., Sickbert-Bennett, E.E., and Weber, D.J. (2022). Inactivation of *Candida auris* and *Candida albicans* by ultraviolet-C. Infect. Control Hosp. Epidemiol. *43*, 1495–1497.

194. Memic, S., Osborne, A.O., Cadnum, J.L., and Donskey, C.J. (2023). Efficacy of a far-ultraviolet-C light technology for continuous decontamination of air and surfaces. Infect. Control Hosp. Epidemiol., 1–3.

195. Chatterjee, P., Choi, H., Ochoa, B., Garmon, G., Coppin, J.D., Allton, Y., Lukey, J., Williams, M.D., Navarathna, D., and Jinadatha, C. (2020). Clade-specific variation in susceptibility of *Candida auris* to broad-spectrum ultraviolet C light (UV-C). Infect. Control Hosp. Epidemiol. *41*, 1384–1387.

196. Astrid, F., Beata, Z., Van den Nest Miriam, Julia, E., Elisabeth, P., and Magda, D.-E. (2021). The use of a UV-C disinfection robot in the routine cleaning process: a field study in an Academic hospital. Antimicrob. Resist. Infect. Control *10*, 84.

197. Hinrichs, C., Wiese-Posselt, M., Graf, B., Geffers, C., Weikert, B., Enghard, P., Aldejohann, A., Schrauder, A., Knaust, A., Eckardt, K.-U., et al. (2022). Successful control of *Candida auris* transmission in a German COVID-19 intensive care unit. Mycoses. 10.1111/myc.13443.

198. Vogelzang, E.H., Weersink, A.J.L., van Mansfeld, R., Chow, N.A., Meis, J.F., and van Dijk, K. (2019). The first two cases of *candida auris* in The Netherlands. J. Fungi (Basel) *5*, 91.

199. Sayeed, M.A., Farooqi, J., Jabeen, K., and Mahmood, S.F. (2020). Comparison of risk factors and outcomes of *Candida auris* candidemia with non-*Candida auris* candidemia: A retrospective study from Pakistan. Med. Mycol. *58*, 721–729.

200. Meyer, D., Martin, E.K., Madad, S., Dhagat, P., and Nuzzo, J.B. (2021). Preparedness and response to an emerging health threat-Lessons learned from *Candida auris* outbreaks in the United States. Infect. Control Hosp. Epidemiol., 1–6.

201. Lesho, E.P., Bronstein, M.Z., McGann, P., Stam, J., Kwak, Y., Maybank, R., McNamara, J., Callahan, M., Campbell, J., Hinkle, M.K., et al. (2018). Importation, Mitigation, and Genomic Epidemiology of *Candida auris* at a Large Teaching Hospital. Infect. Control Hosp. Epidemiol. *39*, 53–57.

202. Short, B., Brown, J., Delaney, C., Sherry, L., Williams, C., Ramage, G., and Kean, R. (2019). *Candida auris* exhibits resilient biofilm characteristics in vitro: implications for environmental persistence. J. Hosp. Infect. *103*, 92–96.

203. Jabeen, K., Mal, P.B., Tharwani, A., Hashmi, M., and Farooqi, J. (2020). Persistence of *Candida auris* on latex and nitrile gloves with transmission to sterile urinary catheters‡. Med. Mycol. *58*, 128–132.

204. Kean, R., McKloud, E., Townsend, E.M., Sherry, L., Delaney, C., Jones, B.L., Williams, C., and Ramage, G. (2018). The comparative efficacy of antiseptics against *Candida auris* biofilms. Int. J. Antimicrob. Agents *52*, 673–677.

205. Kean, R., Delaney, C., Sherry, L., Borman, A., Johnson, E.M., Richardson, M.D., Rautemaa-Richardson, R., Williams, C., and Ramage, G. (2018). Transcriptome Assembly and Profiling of *Candida auris* Reveals Novel Insights into Biofilm-Mediated Resistance. mSphere *3*. 10.1128/mSphere.00334-18.

206. Kumar, J., Eilertson, B., Cadnum, J.L., Whitlow, C.S., Jencson, A.L., Safdar, N., Krein, S.L., Tanner, W.D., Mayer, J., Samore, M.H., et al. (2019). Environmental Contamination with *Candida* Species in Multiple Hospitals Including a Tertiary Care Hospital with a *Candida auris* Outbreak. Pathog Immun *4*, 260–270.

207. Vargas-Cruz, N., Reitzel, R.A., Rosenblatt, J., Chaftari, A.-M., Wilson Dib, R., Hachem, R., Kontoyiannis, D.P., and Raad, I.I. (2019). Nitroglycerin-Citrate-Ethanol Catheter Lock Solution Is Highly Effective for In Vitro Eradication of *Candida auris* Biofilm. Antimicrob. Agents Chemother. *63*. 10.1128/AAC.00299-19.

208. Sherry, L., Ramage, G., Kean, R., Borman, A., Johnson, E.M., Richardson, M.D., and Rautemaa-Richardson, R. (2017). Biofilm-Forming Capability of Highly Virulent, Multidrug-Resistant *Candida auris*. Emerg. Infect. Dis. *23*, 328–331.

209. Chatzimoschou, A., Giampani, A., Meis, J.F., and Roilides, E. (2021). Activities of nine antifungal agents against *Candida auris* biofilms. Mycoses *64*, 381–384.

210. Dominguez, E.G., Zarnowski, R., Choy, H.L., Zhao, M., Sanchez, H., Nett, J.E., and Andes, D.R. (2019). Conserved Role for Biofilm Matrix Polysaccharides in *Candida auris* Drug Resistance. mSphere *4*. 10.1128/mSphereDirect.00680-18.

211. Anderson, F.M., Visser, N.D., Amses, K.R., Hodgins-Davis, A., Weber, A.M., Metzner, K.M., McFadden, M.J., Mills, R.E., O'Meara, M.J., James, T.Y., et al. (2023). *Candida albicans* selection for human commensalism results in substantial within-host diversity without decreasing fitness for invasive disease. PLoS Biol. *21*, e3001822.

212. McDonough, L.D., Mishra, A.A., Tosini, N., Kakade, P., Penumutchu, S., Liang, S.-H., Maufrais, C., Zhai, B., Taur, Y., Belenky, P., et al. (2021). *Candida albicans* isolates 529L and CHN1 exhibit stable colonization of the Murine gastrointestinal tract. MBio, e0287821.

213. Bazzi, M., Nawrocki, K., Brown, C., Falkowski, N., Stark, K., and Huffnagle, G. (2021). The microbial ecology of *Candida albicans* strains CHN1 and SC5314 in mice. Access Microbiol. *3*. 10.1099/acmi.cc2021.po0097.

214. Glazier, V.E., Kramara, J., Ollinger, T., Solis, N.V., Zarnowski, R., Wakade, R.S., Kim, M.-J., Weigel, G.J., Liang, S.-H., Bennett, R.J., et al. (2023). The *Candida albicans* reference strain SC5314 contains a rare, dominant allele of the transcription factor Rob1 that modulates filamentation, biofilm formation, and oral commensalism. MBio, e0152123.

215. Huang, M.Y., Woolford, C.A., May, G., McManus, C.J., and Mitchell, A.P. (2019). Circuit diversification in a biofilm regulatory network. PLoS Pathog. *15*, e1007787.

216. Chakrabarti, A., and Sood, P. (2021). On the emergence, spread and resistance of *Candida auris*: host, pathogen and environmental tipping points. J. Med. Microbiol. *70*. 10.1099/jmm.0.001318.

217. Kim, S.H., Iyer, K.R., Pardeshi, L., Muñoz, J.F., Robbins, N., Cuomo, C.A., Wong, K.H., and Cowen, L.E. (2019). Genetic Analysis of *Candida auris* Implicates Hsp90 in Morphogenesis and Azole Tolerance and Cdr1 in Azole Resistance. MBio *10*, e02529-18.

218. Bravo Ruiz, G., Ross, Z.K., Gow, N.A.R., and Lorenz, A. (2020). Pseudohyphal Growth of the Emerging Pathogen *Candida auris* Is Triggered by Genotoxic Stress through the S Phase Checkpoint. mSphere *5*, e00151-20.

219. Gao, J., Chow, E.W.L., Wang, H., Xu, X., Cai, C., Song, Y., Wang, J., and Wang, Y. (2021). LncRNA DINOR is a virulence factor and global regulator of stress responses in *Candida auris*. Nat Microbiol. 10.1038/s41564-021-00915-x.

220. Mayr, E.-M., Ramírez-Zavala, B., Krüger, I., and Morschhäuser, J. (2020). A Zinc Cluster Transcription Factor Contributes to the Intrinsic Fluconazole Resistance of *Candida auris*. mSphere *5*, e00279-20.

221. Grahl, N., Demers, E.G., Crocker, A.W., and Hogan, D.A. (2017). Use of RNA-Protein Complexes for Genome Editing in Non-albicans *Candida* Species. mSphere *2*, e00218-17.

222. Rybak, J.M., Doorley, L.A., Nishimoto, A.T., Barker, K.S., Palmer, G.E., and Rogers, P.D. (2019). Abrogation of Triazole Resistance upon Deletion of CDR1 in a Clinical Isolate of *Candida auris*. Antimicrob. Agents Chemother. *63*, e00057-19.

223. Min, K., Ichikawa, Y., Woolford, C.A., and Mitchell, A.P. (2016). *Candida albicans* Gene Deletion with a Transient CRISPR-Cas9 System. mSphere *1*, e00130-16.

224. Fan, Y., and Lin, X. (2018). Multiple Applications of a Transient CRISPR-Cas9 Coupled with Electroporation (TRACE) System in the *Cryptococcus neoformans* Species Complex. Genetics *208*, 1357–1372.

225. Soltani, J., van Heusden, G.P.H., and Hooykaas, P.J.J. (2008). Agrobacterium-Mediated Transformation of Non-Plant Organisms. In Agrobacterium: From Biology to Biotechnology, T. Tzfira and V. Citovsky, eds. (Springer New York), pp. 649–675.

226. Cleene, M.D., De Cleene, M., and De Ley, J. (1976). The host range of crown gall. The Botanical Review *42*, 389–466. 10.1007/bf02860827.

227. Michielse, C.B., Hooykaas, P.J.J., van den Hondel, C.A.M.J.J., and Ram, A.F.J. (2005). *Agrobacterium*-mediated transformation as a tool for functional genomics in fungi. Curr. Genet. *48*, 1–17.

228. Hooykaas, P.J.J., van Heusden, G.P.H., Niu, X., Reza Roushan, M., Soltani, J., Zhang, X., and van der Zaal, B.J. (2018). *Agrobacterium*-Mediated Transformation of Yeast and Fungi. Curr. Top. Microbiol. Immunol. *418*, 349–374.

229. Lutgring, J.D., Machado, M.-J., Benahmed, F.H., Conville, P., Shawar, R.M., Patel, J., and Brown, A.C. (2018). FDA-CDC Antimicrobial Resistance Isolate Bank: a Publicly Available Resource To Support Research, Development, and Regulatory Requirements. J. Clin. Microbiol. *56*, e01415-17.

230. McClelland, C.M., Chang, Y.C., and Kwon-Chung, K.J. (2005). High frequency transformation of *Cryptococcus neoformans* and *Cryptococcus gattii* by *Agrobacterium* tumefaciens. Fungal Genet. Biol. *42*, 904–913.

231. Bundock, P., den Dulk-Ras, A., Beijersbergen, A., and Hooykaas, P.J. (1995). Trans-kingdom T-DNA transfer from *Agrobacterium tumefaciens* to *Saccharomyces cerevisiae*. EMBO J. *14*, 3206–3214.

232. Park, D., Park, S.-H., Ban, Y.W., Kim, Y.S., Park, K.-C., Kim, N.-S., Kim, J.-K., and Choi, I.-Y. (2017). A bioinformatics approach for identifying transgene insertion sites using whole genome sequencing data. BMC Biotechnol. *17*, 67.

233. O'Meara, T.R., and O'Meara, M.J. (2021). DeORFanizing *Candida albicans* Genes using Coexpression. mSphere *6*, e01245-20.

234. Ng, H., and Dean, N. (2017). Dramatic Improvement of CRISPR/Cas9 Editing in *Candida albicans* by Increased Single Guide RNA Expression. mSphere *2*, e00385-16.

235. Schiffer, S., Rösch, S., and Marchfelder, A. (2002). Assigning a function to a conserved group of proteins: the tRNA 3'-processing enzymes. EMBO J. *21*, 2769–2777.

236. Gao, Y., and Zhao, Y. (2014). Self-processing of ribozyme-flanked RNAs into guide RNAs in vitro and in vivo for CRISPR-mediated genome editing. J. Integr. Plant Biol. *56*, 343–349.

237. Kelly, M.T., MacCallum, D.M., Clancy, S.D., Odds, F.C., Brown, A.J.P., and Butler, G. (2004). The *Candida albicans CaACE2* gene affects morphogenesis, adherence and virulence. Mol. Microbiol. *53*, 969–983.

238. Calderón-Noreña, D.M., González-Novo, A., Orellana-Muñoz, S., Gutiérrez-Escribano, P., Arnáiz-Pita, Y., Dueñas-Santero, E., Suárez, M.B., Bougnoux, M.-E., Del Rey, F., Sherlock, G., et al. (2015). A single nucleotide polymorphism uncovers a novel function for the transcription factor Ace2 during *Candida albicans* hyphal development. PLoS Genet. *11*, e1005152.

239. Riquelme, M., and Sánchez-León, E. (2014). The Spitzenkörper: a choreographer of fungal growth and morphogenesis. Curr. Opin. Microbiol. *20*, 27–33.

240. Rybak, J.M., Muñoz, J.F., Barker, K.S., Parker, J.E., Esquivel, B.D., Berkow, E.L., Lockhart, S.R., Gade, L., Palmer, G.E., White, T.C., et al. (2020). Mutations in TAC1B: a Novel Genetic Determinant of Clinical Fluconazole Resistance in *Candida auris*. MBio *11*, e00365-20.

241. Du, L.-L., and Novick, P. (2002). Pag1p, a Novel Protein Associated with Protein Kinase Cbk1p, Is Required for Cell Morphogenesis and Proliferation inSaccharomyces cerevisiae. MBoC *13*, 503–514.

242. Dünkler, A., Walther, A., Specht, C.A., and Wendland, J. (2005). *Candida albicans* CHT3 encodes the functional homolog of the Cts1 chitinase of *Saccharomyces cerevisiae*. Fungal Genet. Biol. *42*, 935–947.

243. Kuranda, M.J., and Robbins, P.W. (1991). Chitinase is required for cell separation during growth of *Saccharomyces cerevisiae*. J. Biol. Chem. *266*, 19758–19767.

244. Koehler, C.M., and Myers, A.M. (1997). Serine-threonine protein kinase activity of Elm1p, a regulator of morphologic differentiation in *Saccharomyces cerevisiae*. FEBS Lett. *408*, 109–114.

245. Sreenivasan, A., and Kellogg, D. (1999). The elm1 kinase functions in a mitotic signaling network in budding yeast. Mol. Cell. Biol. *19*, 7983–7994.

246. Ito, Y., Miyazaki, T., Tanaka, Y., Suematsu, T., Nakayama, H., Morita, A., Hirayama, T., Tashiro, M., Takazono, T., Saijo, T., et al. (2020). Roles of Elm1 in antifungal susceptibility and virulence in *Candida glabrata*. Sci. Rep. *10*, 9789.

247. Sutherland, C.M., Hawley, S.A., McCartney, R.R., Leech, A., Stark, M.J.R., Schmidt, M.C., and Hardie, D.G. (2003). Elm1p is one of three upstream kinases for the *Saccharomyces cerevisiae* SNF1 complex. Curr. Biol. *13*, 1299–1305.

248. McCreath, K.J., Specht, C.A., and Robbins, P.W. (1995). Molecular cloning and characterization of chitinase genes from *Candida albicans*. Proc. Natl. Acad. Sci. U. S. A. *92*, 2544–2548.

249. Selvaggini, S., Munro, C.A., Paschoud, S., Sanglard, D., and Gow, N.A.R. (2004). Independent regulation of chitin synthase and chitinase activity in *Candida albicans* and *Saccharomyces cerevisiae*. Microbiology *150*, 921–928.

250. Song, Y., Cheon, S.A., Lee, K.E., Lee, S.-Y., Lee, B.-K., Oh, D.-B., Kang, H.A., and Kim, J.-Y. (2008). Role of the RAM network in cell polarity and hyphal morphogenesis in *Candida albicans*. Mol. Biol. Cell *19*, 5456–5477.

251. Homann, O.R., Dea, J., Noble, S.M., and Johnson, A.D. (2009). A phenotypic profile of the *Candida albicans* regulatory network. PLoS Genet. *5*, e1000783.

252. Shen, J., Guo, W., and Köhler, J.R. (2005). CaNAT1, a heterologous dominant selectable marker for transformation of *Candida albicans* and other pathogenic *Candida* species. Infect. Immun. *73*, 1239–1242.

253. Walton, F.J., Idnurm, A., and Heitman, J. (2005). Novel gene functions required for melanization of the human pathogen *Cryptococcus neoformans*. Mol. Microbiol. *57*, 1381–1396.

254. Cowen, L.E., Singh, S.D., Köhler, J.R., Collins, C., Zaas, A.K., Schell, W.A., Aziz, H., Mylonakis, E., Perfect, J.R., Whitesell, L., et al. (2009). Harnessing Hsp90 function as a powerful, broadly effective therapeutic strategy for fungal infectious disease. Proc. Natl. Acad. Sci. U. S. A. *106*, 2818–2823.

255. Hood, E.E., Gelvin, S.B., Melchers, L.S., and Hoekema, A. (1993). New *Agrobacterium* helper plasmids for gene transfer to plants. Transgenic Res. *2*, 208–218.

256. Norrander, J., Kempe, T., and Messing, J. (1983). Construction of improved M13 vectors using oligodeoxynucleotide-directed mutagenesis. Gene *26*, 101–106. 10.1016/0378-1119(83)90040-9.

257. Veri, A.O., Miao, Z., Shapiro, R.S., Tebbji, F., O'Meara, T.R., Kim, S.H., Colazo, J., Tan, K., Vyas, V.K., Whiteway, M., et al. (2018). Tuning Hsf1 levels drives distinct fungal morphogenetic programs with depletion impairing Hsp90 function and overexpression expanding the target space. PLoS Genet. *14*, e1007270.

258. O'Meara, T.R., O'Meara, M.J., Polvi, E.J., Pourhaghighi, M.R., Liston, S.D., Lin, Z.-Y., Veri, A.O., Emili, A., Gingras, A.-C., and Cowen, L.E. (2019). Global proteomic analyses define an environmentally contingent Hsp90 interactome and reveal chaperone-dependent regulation of stress granule proteins and the R2TP complex in a fungal pathogen. PLoS Biol. *17*, e3000358.

259. Basenko, E.Y., Pulman, J.A., Shanmugasundram, A., Harb, O.S., Crouch, K., Starns, D., Warrenfeltz, S., Aurrecoechea, C., Stoeckert, C.J., Jr, Kissinger, J.C., et al. (2018). FungiDB: An Integrated Bioinformatic Resource for Fungi and Oomycetes. J Fungi (Basel) *4*. 10.3390/jof4010039.

260. Esher, S.K., Granek, J.A., and Alspaugh, J.A. (2015). Rapid mapping of insertional mutations to probe cell wall regulation in *Cryptococcus neoformans*. Fungal Genet. Biol. *82*, 9–21.

261. Robinson, J.T., Thorvaldsdóttir, H., Winckler, W., Guttman, M., Lander, E.S., Getz, G., and Mesirov, J.P. (2011). Integrative genomics viewer. Nat. Biotechnol. *29*, 24–26.

262. Schindelin, J., Arganda-Carreras, I., Frise, E., Kaynig, V., Longair, M., Pietzsch, T., Preibisch, S., Rueden, C., Saalfeld, S., Schmid, B., et al. (2012). Fiji: an open-source platform for biological-image analysis. Nat. Methods *9*, 676–682.

263. Lee, D.W., Hong, C.P., and Kang, H.A. (2019). An effective and rapid method for RNA preparation from non-conventional yeast species. Anal. Biochem. *586*, 113408.

264. Aranda, P.S., LaJoie, D.M., and Jorcyk, C.L. (2012). Bleach gel: a simple agarose gel for analyzing RNA quality. Electrophoresis *33*, 366–369.

265. Fuchs, B.B., O'Brien, E., Khoury, J.B.E., and Mylonakis, E. (2010). Methods for using *Galleria mellonella* as a model host to study fungal pathogenesis. Virulence *1*, 475–482.

266. Akinbobola, A.B., Kean, R., Hanifi, S.M.A., and Quilliam, R.S. (2023). Environmental reservoirs of the drug-resistant pathogenic yeast *Candida auris*. PLoS Pathog. *19*, e1011268.

267. Ashkenazi-Hoffnung, L., and Rosenberg Danziger, C. (2023). Navigating the New Reality: A Review of the Epidemiological, Clinical, and Microbiological Characteristics of *Candida auris*, with a Focus on Children. J Fungi (Basel) *9*. 10.3390/jof9020176.

268. Chow, N.A., Gade, L., Tsay, S.V., Forsberg, K., Greenko, J.A., Southwick, K.L., Barrett, P.M., Kerins, J.L., Lockhart, S.R., Chiller, T.M., et al. (2018). Multiple introductions and subsequent transmission of multidrug-resistant *Candida auris* in the USA: a molecular epidemiological survey. Lancet Infect. Dis. *18*, 1377–1384.

269. Roberts, S.C., Zembower, T.R., Ozer, E.A., and Qi, C. (2021). Genetic Evaluation of Nosocomial *Candida auris* Transmission. J. Clin. Microbiol. *59*. 10.1128/JCM.02252-20.

270. Vallabhaneni, S., Kallen, A., Tsay, S., Chow, N., Welsh, R., Kerins, J., Kemble, S.K., Pacilli, M., Black, S.R., Landon, E., et al. (2016). Investigation of the First Seven Reported Cases of *Candida auris*, a Globally Emerging Invasive, Multidrug-Resistant Fungus - United States, May 2013-August 2016. MMWR Morb. Mortal. Wkly. Rep. *65*, 1234–1237.

271. Vinayagamoorthy, K., Pentapati, K.C., and Prakash, H. (2022). Prevalence, risk factors, treatment and outcome of multidrug resistance *Candida auris* infections in Coronavirus disease (COVID-19) patients: A systematic review. Mycoses *65*, 613–624.

272. Rajni, E., Jain, A., Gupta, S., Jangid, Y., and Vohra, R. (2022). Risk Factors for Candidemia in Intensive Care Unit: A Matched Case Control Study from North-Western India. Acta Medica *65*, 83–88.

273. Benedict, K., Forsberg, K., Gold, J.A.W., Baggs, J., and Lyman, M. (2023). *Candida auris*–Associated Hospitalizations, United States, 2017-2022. Emerg. Infect. Dis. *29*, 1485–1487.

274. Singh, S., Uppuluri, P., Mamouei, Z., Alqarihi, A., Elhassan, H., French, S., Lockhart, S.R., Chiller, T., Edwards, J.E., Jr, and Ibrahim, A.S. (2019). The NDV-3A vaccine protects mice from multidrug resistant *Candida auris* infection. PLoS Pathog. *15*, e1007460.

275. Silva-Dias, A., Miranda, I.M., Rocha, R., Monteiro-Soares, M., Salvador, A., Rodrigues, A.G., and Pina-Vaz, C. (2012). A novel flow cytometric protocol for assessment of yeast cell adhesion. Cytometry A *81*, 265–270.

276. Liang, C., Strickland, J., Ye, Z., Wu, W., Hu, B., and Rittschof, D. (2019). Biochemistry of Barnacle Adhesion: An Updated Review. Frontiers in Marine Science *6*. 10.3389/fmars.2019.00565.

277. Sokalingam, S., Raghunathan, G., Soundrarajan, N., and Lee, S.-G. (2012). A study on the effect of surface lysine to arginine mutagenesis on protein stability and structure using green fluorescent protein. PLoS One *7*, e40410.

278. McLaughlin, S., Wang, J., Gambhir, A., and Murray, D. (2002). PIP(2) and proteins: interactions, organization, and information flow. Annu. Rev. Biophys. Biomol. Struct. *31*, 151–175.

279. Singh, S., Barbarino, A., Youssef, E.G., Coleman, D., Gebremariam, T., and Ibrahim, A.S. (2023). Protective Efficacy of Anti-Hyr1p Monoclonal Antibody against Systemic Candidiasis Due to Multi-Drug-Resistant *Candida auris*. J Fungi (Basel) *9*. 10.3390/jof9010103.

280. Park, S.O., Frazer, C., and Bennett, R.J. (2022). An Adjuvant-Based Approach Enables the Use of Dominant HYG and KAN Selectable Markers in *Candida albicans*. mSphere *7*, e0034722.

281. Afgan, E., Baker, D., Batut, B., van den Beek, M., Bouvier, D., Cech, M., Chilton, J., Clements, D., Coraor, N., Grüning, B.A., et al. (2018). The Galaxy platform for accessible, reproducible and collaborative biomedical analyses: 2018 update. Nucleic Acids Res. *46*, W537–W544.

282. Bolger, A.M., Lohse, M., and Usadel, B. (2014). Trimmomatic: a flexible trimmer for Illumina sequence data. Bioinformatics *30*, 2114–2120.

283. Li, H., and Durbin, R. (2009). Fast and accurate short read alignment with Burrows-Wheeler transform. Bioinformatics *25*, 1754–1760. 10.1093/bioinformatics/btp324.

284. Ye, J., Coulouris, G., Zaretskaya, I., Cutcutache, I., Rozen, S., and Madden, T.L. (2012). Primer-BLAST: a tool to design target-specific primers for polymerase chain reaction. BMC Bioinformatics *13*, 134.

285. Martin, M. (2011). Cutadapt removes adapter sequences from high-throughput sequencing reads. EMBnet.journal *17*, 10–12.

286. Dobin, A., Davis, C.A., Schlesinger, F., Drenkow, J., Zaleski, C., Jha, S., Batut, P., Chaisson, M., and Gingeras, T.R. (2013). STAR: ultrafast universal RNA-seq aligner. Bioinformatics *29*, 15–21.

287. Liao, Y., Smyth, G.K., and Shi, W. (2014). featureCounts: an efficient general purpose program for assigning sequence reads to genomic features. Bioinformatics *30*, 923–930.

288. Love, M.I., Huber, W., and Anders, S. (2014). Moderated estimation of fold change and dispersion for RNA-seq data with DESeq2. Genome Biol. *15*, 550.

289. Lamprecht, M.R., Sabatini, D.M., and Carpenter, A.E. (2007). CellProfiler™: free, versatile software for automated biological image analysis. Biotechniques *42*, 71–75.

290. Bray, M.-A., Carpenter, A., and Imaging Platform, Broad Institute of MIT and Harvard (2017). Advanced Assay Development Guidelines for Image-Based High Content Screening and Analysis. In Assay Guidance Manual, S. Markossian, G. S. Sittampalam, A. Grossman, K. Brimacombe, M. Arkin, D. Auld, C. P. Austin, J. Baell, J. M. M. Caaveiro, T. D. Y. Chung, et al., eds. (Eli Lilly & Company and the National Center for AdvancingTranslational Sciences).

291. Maguire, S.L., ÓhÉigeartaigh, S.S., Byrne, K.P., Schröder, M.S., O'Gaora, P., Wolfe, K.H., and Butler, G. (2013). Comparative genome analysis and gene finding in *Candida* species using CGOB. Mol. Biol. Evol. *30*, 1281–1291.

292. Mirdita, M., Schütze, K., Moriwaki, Y., Heo, L., Ovchinnikov, S., and Steinegger, M. (2022). ColabFold: making protein folding accessible to all. Nat. Methods *19*, 679–682.

293. van Kempen, M., Kim, S.S., Tumescheit, C., Mirdita, M., Lee, J., Gilchrist, C.L.M., Söding, J., and Steinegger, M. (2023). Fast and accurate protein structure search with Foldseek. Nat. Biotechnol. 10.1038/s41587-023-01773-0.

294. Rosenberg, M., Gutnick, D., and Rosenberg, E. (1980). Adherence of bacteria to hydrocarbons: A simple method for measuring cell-surface hydrophobicity. FEMS Microbiol. Lett. *9*, 29–33.

295. Li, Y., Pham, J.Q., Johnston, K.P., and Green, P.F. (2007). Contact angle of water on polystyrene thin films: effects of CO(2) environment and film thickness. Langmuir *23*, 9785–9793.

296. Gulati, M., Lohse, M.B., Ennis, C.L., Gonzalez, R.E., Perry, A.M., Bapat, P., Arevalo, A.V., Rodriguez, D.L., and Nobile, C.J. (2018). In Vitro Culturing and Screening of *Candida albicans* Biofilms. Curr. Protoc. Microbiol. *50*, e60.

297. Andes, D., Nett, J., Oschel, P., Albrecht, R., Marchillo, K., and Pitula, A. (2004). Development and characterization of an in vivo central venous catheter *Candida albicans* biofilm model. Infect. Immun. *72*, 6023–6031.

298. Nakamura, Y., Oscherwitz, J., Cease, K.B., Chan, S.M., Muñoz-Planillo, R., Hasegawa, M., Villaruz, A.E., Cheung, G.Y.C., McGavin, M.J., Travers, J.B., et al. (2013). *Staphylococcus* δ-toxin induces allergic skin disease by activating mast cells. Nature *503*, 397–401.

299. Skrzypek, M.S., Binkley, J., Binkley, G., Miyasato, S.R., Simison, M., and Sherlock, G. (2017). The Candida Genome Database (CGD): incorporation of Assembly 22, systematic identifiers and visualization of high throughput sequencing data. Nucleic Acids Res. *45*, D592–D596.

300. Ennis, C.L., Hernday, A.D., and Nobile, C.J. (2021). A Markerless CRISPR-Mediated System for Genome Editing in *Candida auris* Reveals a Conserved Role for Cas5 in the Caspofungin Response. Microbiol Spectr, e0182021.

301. Gregor, J.B., Gutierrez-Schultz, V.A., Hoda, S., Baker, K.M., Saha, D., Burghaze, M.G., Vazquez, C., Burgei, K.E., and Briggs, S.D. (2023). An expanded toolkit of drug resistance cassettes for *Candida glabrata*, *Candida auris*, and *Candida albicans* leads to new insights into the ergosterol pathway. mSphere, e0031123.

302. Casadevall, A., Kontoyiannis, D.P., and Robert, V. (2021). Environmental *Candida auris* and the Global Warming Emergence Hypothesis. MBio *12*. 10.1128/mBio.00360-21.

303. Geyer, R., Jambeck, J.R., and Law, K.L. (2017). Production, use, and fate of all plastics ever made. Sci. Adv. *3*. 10.1126/sciadv.1700782.

304. Jambeck, J.R., Geyer, R., Wilcox, C., Siegler, T.R., Perryman, M., Andrady, A., Narayan, R., and Law, K.L. (2015). Plastic waste inputs from land into the ocean. Science *347*, 768–771.

305. Derraik, J.G.B. (2002). The pollution of the marine environment by plastic debris: a review. Mar. Pollut. Bull. *44*, 842–852.

306. Li, C., Wang, L., Ji, S., Chang, M., Wang, L., Gan, Y., and Liu, J. (2021). The ecology of the plastisphere: Microbial composition, function, assembly, and network in the freshwater and seawater ecosystems. Water Res. *202*, 117428.

307. Oberbeckmann, S., Osborn, A.M., and Duhaime, M.B. (2016). Microbes on a bottle: Substrate, season and geography influence community composition of microbes colonizing marine plastic debris. PLoS One *11*, e0159289.

308. Casabianca, S., Capellacci, S., Giacobbe, M.G., Dell'Aversano, C., Tartaglione, L., Varriale, F., Narizzano, R., Risso, F., Moretto, P., Dagnino, A., et al. (2019). Plastic-associated harmful microalgal assemblages in marine environment. Environ. Pollut. *244*, 617–626.

309. Akinbobola, A., Kean, R., and Quilliam, R.S. (2023). Plastic pollution as a novel reservoir for the environmental survival of the drug resistant fungal pathogen *Candida auris*. Mar. Pollut. Bull. *198*, 115841.

310. Gambarini, V., Pantos, O., Kingsbury, J.M., Weaver, L., Handley, K.M., and Lear, G. (2021). Phylogenetic Distribution of Plastic-Degrading Microorganisms. mSystems *6*. 10.1128/mSystems.01112-20.

311. Kim, S.H., Lee, J.W., Kim, J.S., Lee, W., Park, M.S., and Lim, Y.W. (2022). Plastic-inhabiting fungi in marine environments and PCL degradation activity. Antonie Van Leeuwenhoek *115*, 1379–1392.

312. Howard, S.A., Carr, C.M., Sbahtu, H.I., Onwukwe, U., López, M.J., Dobson, A.D.W., and McCarthy, R.R. (2023). Enrichment of native plastic-associated biofilm communities to enhance polyester degrading activity. Environ. Microbiol. *25*, 2698–2718.

313. Suzuki, M., Tachibana, Y., and Kasuya, K.-I. (2020). Biodegradability of poly(3-hydroxyalkanoate) and poly(ε-caprolactone) via biological carbon cycles in marine environments. Polym. J. *53*, 47–66.

314. Hartmann, N.B., Hüffer, T., Thompson, R.C., Hassellöv, M., Verschoor, A., Daugaard, A.E., Rist, S., Karlsson, T., Brennholt, N., Cole, M., et al. (2019). Are we speaking the same language? Recommendations for a definition and categorization framework for plastic debris. Environ. Sci. Technol. *53*, 1039–1047.

315. Arias-Andres, M., Klümper, U., Rojas-Jimenez, K., and Grossart, H.-P. (2018). Microplastic pollution increases gene exchange in aquatic ecosystems. Environ. Pollut. *237*, 253–261.

316. Jâms, I.B., Windsor, F.M., Poudevigne-Durance, T., Ormerod, S.J., and Durance, I. (2020). Estimating the size distribution of plastics ingested by animals. Nat. Commun. *11*, 1594.

317. Diepens, N.J., and Koelmans, A.A. (2018). Accumulation of Plastic Debris and Associated Contaminants in Aquatic Food Webs. Environ. Sci. Technol. *52*, 8510–8520.